Departamento de Química
Universidad de La Laguna

MONITORING OF EMERGING CONTAMINANTS IN WATERS USING NOVEL MICROEXTRACTIVE TECHNIQUES

MONITORIZACIÓN DE CONTAMINANTES EMERGENTES EN AGUAS HACIENDO USO DE NOVEDOSAS TÉCNICAS MICROEXTRACTIVAS

PROVIDENCIA GONZÁLEZ HERNÁNDEZ
Febrero 2020

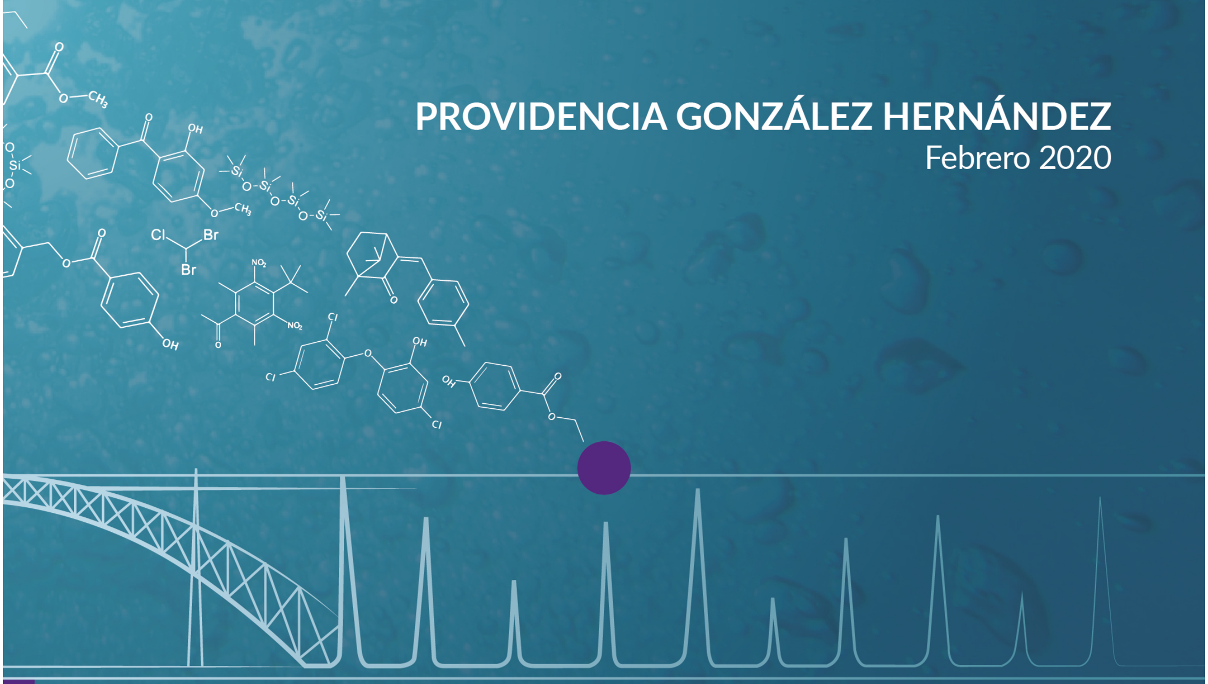

Director: Dr. Juan H. Ayala Díaz
Co-directora y tutora: Dr. Verónica Pino Estévez

Departamento de Química
Universidad de La Laguna

Dr. D. Juan Ayala Díaz y Dra. Dña. Verónica Pino Estévez, Profesores Titulares en el Departamento de Química, Unidad Departamental de Química Analítica, de la Universidad de La Laguna,

AUTORIZAN:

La presentación de la Tesis Doctoral titulada “MONITORIZACIÓN DE CONTAMINANTES EMERGENTES EN AGUAS HACIENDO USO DE NOVEDOSAS TÉCNICAS MICROEXTRACTIVAS”, realizada por Dña. María Providencia González Hernández, para optar al Título de Doctora en Química por la Universidad de La Laguna.

Y para que conste y surta los efectos oportunos, firman la presente en La Laguna, a treinta de enero de dos mil veinte.

Fdo:	Fdo:
El Director de la Tesis	La Co-directora de la Tesis
Dr. Juan H. Ayala Díaz	Dra. Verónica Pino Estévez

Lo más valioso de la vida no lo conquistas, lo recibes. Y yo he recibido tanto durante este período de formación, que nunca podré encontrar la forma adecuada de mostrar mi agradecimiento. Sin embargo, quisiera mostrar mis más sinceras palabras hacia aquellas personas que, de alguna forma u otra, siento que han hecho posible la realización de esta Tesis Doctoral.

A mis directores de Tesis, el Dr. Juan H. Ayala y la Dra. Verónica Pino, por haberle dado forma y sentido al trabajo realizado durante estos años. Juan, gracias por confiar en mí desde el principio, gracias por tu dedicación, por darme siempre el empujón y la serenidad que necesitaba, cada día con esa sonrisa que te caracteriza. Gracias por valorarme tal cual soy. Y, cómo no, por tener el don de la reparación instrumental. Vero, gracias por todo lo que has hecho por mí, por tirar del carro más que nadie, por llevar al máximo nivel los trabajos, por corregirme y hacerme ver siempre la positividad en las dificultades. Tu sacrificio, tu dedicación y tu trabajo han sembrado en mí una de mis mayores ambiciones: ser cada día mejor personal y profesionalmente.

En segundo lugar, quiero agradecer a las dos personas que, aunque no se encuentren en activo, para mí dan un sentido original a cualquier trabajo realizado en el Grupo de Investigación de Química Analítica Agroalimentaria y Medioambiental (GIN-QAAMA). Al fundador del grupo, el Catedrático Venerando González, por acogerme desde el principio con gran cariño, y por transmitirme que tan importante es el trabajo como las relaciones personales, para que ese trabajo lleve consigo una calidad excepcional. A la Catedrática Ana M. Afonso, porque sin ella yo no estaría escribiendo estas palabras hoy. Ana, has sido mi pilar y un gran ejemplo para mí. Gracias por cuidarme, gracias por haber estado desde el principio hasta el final batallando, gracias por coger la toalla cuando ya yo la había tirado y darme motivos para seguir, gracias por todo lo que me has enseñado, gracias por corregirme cuando era necesario desde el afecto, pero, sobre todo, gracias por aportar todo tu conocimiento en cada trabajo. Siempre habrá algo nuevo que aprender contigo.

A todos los compañeros del grupo de investigación con los que he tenido el placer de compartir esta etapa de mi vida. A María José, mi mentora, gracias por estar conmigo cuando empecé y enseñarme las buenas prácticas del laboratorio; eres un gran ejemplo para mí. A

Priscilla, gracias por tu paciencia, tu inagotable alegría, y por transmitirnos tu motivación para hacer investigación. A Arturo, gracias por tus enseñanzas y los buenos momentos compartidos. A mis dos grandes amigos Idaira y Adrián, gracias por el trabajo compartido, el cual siempre es doblemente satisfactorio, gracias por su ayuda tanto personal como profesional, por ayudarme siempre a ver con objetividad las cosas, y gracias por haberme hecho sentir la compañera más afortunada del mundo. A mis chicos Iván, Raúl y Diego, por todo el ánimo, la ayuda y la afectividad recibida en tan poco tiempo; han sido el broche de oro de esta etapa. A aquellos estudiantes internacionales que también han formado parte de esta historia, que han sido motivo de grandes alegrías y, al mismo tiempo, despedidas dolorosas, con los que he aprendido que, a pesar de las diferencias culturales, el corazón humano está hecho de la misma materia para todos: Meriem, Giulia, Kristina y Jakub, cuatro corazones que siempre llevaré en el mío. Quisiera hacer mención también a todos aquellos estudiantes de Grado, Máster y colaboraciones con los que he compartido trabajo, especialmente a Juanfra, María y Manu.

A todos los miembros que han formado parte del Grupo de Investigación Laboratorio de Rayos X y Materiales Moleculares (MATMOL), especialmente a la Catedrática Catalina Ruíz, el Dr. Jorge Pasán, y la Dra. Ana B. Lago. Gracias a la Catedrática Catalina Ruíz por emprender su colaboración con nuestro grupo, que ha dado la razón del carácter multidisciplinar de esta Tesis Doctoral. Gracias infinitas Jorge por tu investigación, tu ayuda, y tu dedicación hacia mi trabajo, gracias por hacerme pensar y no dar nada por descontado. Gracias Ana también por tu trabajo, tu ayuda incondicional, por cuidar cada pequeño detalle, y hacerme creer en mí misma un poquito más.

Al Dr. Francisco Conde, por tu gran apoyo profesional y tu atención personalizada. No solo has estado siempre disponible para arreglar lo que no funcionaba o iba mal, sino que, además, me has ensañado tanto de forma desinteresada que no tengo palabras de agradecimiento. Gracias por esos días largos buscando soluciones y por tu inagotable motivación profesional.

Al Dr. Nuno Ratola, del Grupo de Investigación *Environmental Sciences and Technologies* de la Facultad de Ingeniería de la Universidad de Porto (Portugal), por permitirme realizar mi estancia predoctoral bajo su dirección. Gracias infinitas por todo Nuno, por permitirme vivir esta experiencia, por la formación recibida durante mi estancia, por tu apoyo, por tu confianza ciega en mí para acogerme en tu laboratorio, y por ayudarme tantísimo. Gracias también a la Dra. Vera Homem sin la cual el trabajo no hubiera sido el mismo. Gracias por tu ayuda desinteresada y por la colaboración inicial. Al resto de miembros del MIA201, especialmente Mónica, Idalina, Filippa, y José Avelino. Pero sin duda, quisiera mostrar mi más sincero agradecimiento al mejor compañero de laboratorio que jamás pude imaginar. Fabio fuiste el mayor regalo inesperado, hiciste que mi estancia, dura de por sí por las circunstancias personales, fuera de las mejores experiencias de mi vida. Me fui dejando a mi familia atrás, y regresé dejando un trocito de corazón allá. Gracias.

A los miembros del Grupo de Investigación Química Analítica Aplicada (AChem) de la Universidad de La Laguna, al Dr. Javier Hernández Borges, el Dr. Javier González Sálamo, y sus estudiantes Diana y Cecilia. Al profesor Javier gracias por tu gran profesionalidad, tu valor humano y tu apoyo. A mi gran amigo Javi, que cariñosamente llamo mi marido científico, gracias porque has formado parte de mi tesis de una forma muy especial y característica, independientemente de las circunstancias.

Asimismo, quisiera dar las gracias a todos los miembros de la Unidad Departamental de Química Analítica de la Universidad de La Laguna, tanto profesores como técnicos e investigadores. Quisiera hacer una mención especial a los profesores Francisco Jiménez y Ana I. Jiménez por su cercanía y su apoyo.

A todas aquellas instituciones públicas que han dado apoyo científico y económico para la realización de esta Tesis Doctoral:

- Al Servicio de Medio Ambiente de la Universidad de La Laguna (SEMALL)
- Al Servicio General de Apoyo a la Investigación de la Universidad de La Laguna (SEGAI)
- Al Proyecto de Investigación AGUA05 de la Fundación CajaCanarias por el contrato a cargo de proyecto disfrutado durante 2014 y 2015
- A la Fundación ULL-Caixa por el contrato predoctoral disfrutado durante 2016 y 2018
- A la Agencia Canaria de Investigación, Innovación y Sociedad de la Información (ACIISI) por el contrato predoctoral disfrutado desde 2018 hasta la fecha
- A los Proyectos de Investigación MAT2013-43101-R, MAT2014-57465-R y MAT2017-89207-R por financiar las investigaciones desarrolladas

A mis compañeros y amigos del Grado de Química que también han formado parte de lo que hoy soy: Pilar, Elba, Adrián, Pedro, Javi y Nilde. Especialmente gracias Elba y Pilar por haber sido un apoyo fundamental durante estos años, por ver crecer nuestra amistad a pesar de la distancia y por apoyarme en cada momento.

A todos mis amigos que han tratado de entender mi trabajo durante estos años, por escucharme, por aconsejarme y guiarme de la mejor forma posible, por no olvidarse de mí y rescatarme cuando me hacía falta: Miguel Ángel, Jorge, Esther Loro, Alejandro, Inma, Josito, Iván y Sarai. Gracias también a Bego, Amala, Vicente, Ana, Karen, Rafa, Isa y Héctor. Gracias a Juan Carlos por su especial apoyo. Es bello el camino para quien camina, para quien sabe a dónde ir, pero sobre todo por la compañía.

Gracias a toda mi familia por su apoyo incondicional. A mis padres, mi hermana Yasmina y mi tía Mariluz, por su preocupación y por sentirse orgullosos de mis logros. A mis suegros, Paco y Fátima, por ser de los ejemplos más grande que tengo en la vida, porque sin ustedes no hubiera podido trabajar en las mismas condiciones y no hubiera podida realizar mi estancia predoctoral. Gracias por cuidar de mi hijo cuando yo no estaba y estar siempre disponible a ello.

A mi hijo Marcos, por ser mi razón de esfuerzo, de sacrificio, y por ser la mayor de las recompensas.

A mi compañero, mi vida, mi marido Jero. Gracias por todos estos años, gracias por hacerme lo mujer más feliz y afortunada del mundo, gracias por tu apoyo, por tu comprensión, por compartir mis alegrías, mis frustraciones y mis tristezas, gracias por nunca soltarme de la mano.

En definitiva, gracias a todos y cada una de las personas aquí nombradas por apoyarme y dar sentido humano a mi trayectoria científica.

¡Gracias inifinitas!

Scientia potentia est.

Francis Bacon

El éxito de una investigación es una gracia. Cada vez que la ciencia da un paso es gracias a algo que no depende de ella. Tan cierto es esto que cuando uno hace un descubrimiento siente una enorme gratitud, experimenta una sorpresa, porque nada está inerte, todo vive, todo es un acto de agradecimiento.

Luigi Giussani

A la memoria de Catalina Ruíz Pérez

ABSTRACT

This Doctoral Thesis focuses on the development of analytical methods under the Green Analytical Chemistry (GAC) requirements for the monitoring of two important group of emerging contaminants in environmental water samples: personal care products (PCPs) and disinfection by-products (DBPs). The developed methods are based on the use of microextraction techniques: liquid-phase microextraction (LPME), dispersive miniaturized solid-phase extraction (D-µSPE), and solid-phase microextraction (SPME). Novel strategies are also explored within the extraction step to improve the performance of the methods following current trends in the Analytical Chemistry research field. Furthermore, novel metal-organic frameworks (MOFs) specifically designed to be successful as sorbents in D-µSPE and SPME are completely characterized, and included successfully in monitoring methods for PCPs. All these methods are combined with gas or liquid chromatography (GC or LC) with different detectors to validate and apply the methodologies to the analysis of real samples.

This Doctoral Thesis is divided in five Chapters: I) Introduction, II) Hypothesis and Objectives, III) Experimental, IV) Results and Discussion, and V) Conclusions.

General considerations about the importance and current state of the monitoring of emerging contaminants in environmental samples are presented in Chapter I. Next sections in this Chapter deal with the description of the main microextraction approaches, together with the improvements proposed within this topic according to the guidelines of GAC. In this sense, the incorporation of novel materials in microextraction methods are outlined, highlighting the use of MOFs, and the applications of these microextraction advances for the determination of emerging contaminants are detailed.

Chapter II describes the main and partial objectives of this Doctoral Thesis. Chapter III includes the experimental section, including the analytes, materials, and instrumentation used in this Doctoral Thesis, together with a description of the optimum procedures and the samples analyzed. In Chapter IV, the results obtained are presented and discussed, while Chapter V includes the summary of the most relevant conclusions derived from Chapter IV.

Section 1 of Chapter IV includes the first research line of this Doctoral Thesis, specifically the application of a LPME approach in combination with ultra-high-performance LC (UHPLC) and UV detection for the determination of non-volatiles PCPs in water samples. The vortex-assisted emulsification microextraction method (VAEME) proposed in this study is mainly characterized by its simplicity, good extraction efficiencies, low consumption of organic solvents and short analysis time. VAEME does not require the utilization of any type of organic solvent as dispersive solvent, and it is used for the first time in the monitoring of PCPs.

Section 2 of Chapter IV includes the second research line of this Doctoral Thesis: the use of sorbent-based microextraction strategies coupled with chromatographic techniques for the determination of emerging compounds in waters. It is divided in D-µSPE (Section 2.1.) and SPME (Section 2.2.) sub-sections according to the type of microextraction method employed.

In Section 2.1., traditional and well-known MOFs (HKUST-1(Cu), MIL-53(Al), and UiO-66(Zr)) are synthesized and prepared (to be further used in a comparison study), while novel MOFs based on pillared-layer structures (named CIM-80s and CIM-90s) are designed to ensure better desorption ability when used in D-µSPE, synthesized and properly characterized. For these new MOFs, adsorption/release, kinetics and computational studies are also carried out in order to gain a better understanding on the nature of interactions established between the target analytes and the MOF, while evaluating the presence of preferential adsorption sites. All these MOFs are applied as sorbents in D-µSPE for the monitoring of several groups of PCPs (UV-filters, preservatives, disinfectants, and insect repellents) in environmental water samples. With the aim of covering a wide range of PCPs with different chemical structures and characteristics, the D-µSPE method is combined first with UHPLC (non-volatile PCPs) and then with GC techniques (semi-volatile and volatile PCPs). Therefore, two analytical methodologies (D-µSPE-UHPLC-UV and D-µSPE-GC-mass spectrometry (MS)) are developed and characterized by the incorporation of new tailorable materials, such as MOFs.

Section 2.2. is focused on SPME applications in headspace mode (HS-SPME) using both commercial and MOF-based fibers. Commercial fibers are employed for the extraction and preconcentration of DBPs in treated water samples. The proposed method (HS-SPME-GC-flame ionization detection (FID)) presents proper sensitivity for the monitoring of these emerging contaminants using a fully solvent-free microextraction technique, with good precision and short analysis times. Finally, a MOF-based SPME fiber is evaluated for the monitoring of PCPs (methylsiloxanes and musk fragrances). With this simple HS-SPME-GC-MS method, it was possible to cover in the same extraction method two groups of volatile PCPs with quite different chemical nature for the analysis of several environmental waters. Furthermore, the latter approach not only reports the use of a novel MOF-based stationary phase for this specific analytical application, but also deals with a difficult analytical determination: that of methylsiloxanes (considering their wide presence in the environment and in the laboratory materials, and thus involving high risks of contaminations even when using blanks).

All the analytical methods are properly optimized (in most cases using experimental designs). They are also validated in terms of accuracy, precision, sensitivity, and possible matrix effects depending on the type of water sample.

INDEX

CHAPTER I - Introduction...1

I.1. Emerging contaminants in waters...3

  1.1. Types of emerging contaminants...5

    1.1.1. Personal care products (PCPs)...6

    1.1.2. Disinfection by-products (DBPs)...13

  1.2. Regulations regarding emerging contaminants...17

  1.3. Reported contents of emerging contaminants in environmental waters...22

  1.4. Analytical methodologies for the environmental monitoring of emerging contaminants in waters...24

I.2. Green Analytical Chemistry...26

I.3. Microextraction techniques...30

  3.1. Liquid-based microextraction techniques...33

    3.1.1. SDME...33

    3.1.2. HF-LPME...37

    3.1.3. DLLME...39

  3.2. Sorbent-based microextraction techniques...41

    3.2.1. µSPE...41

    3.2.2. SPME...45

    3.2.3. Novel materials in sorbent-based microextraction techniques for water samples...52

  3.3. Microextraction techniques for the monitoring of PCPs and DBPs in waters...67

CHAPTER II - Hypothesis and objectives...99

CHAPTER III - Experimental **107**

III.1. Analytes 109

III.2. Solvents, reagents and solutions 116

  2.1. Reagents for the synthesis of MOFs 117

  2.2. Standards solutions 117

III.3. Materials and apparatus 117

III.4. Cleaning protocols 118

III.5. Instrumentation and software 119

  5.1. Chromatographic equipment 119

  5.2. Instrumentation for the characterization of MOFs 120

  5.3. Statistical analysis 121

III.6. Procedures 122

  6.1. Synthesis of MOFs 122

  6.2. Analytical microextraction procedures 128

  6.3. Adsorption isotherm studies 131

III.7. Sample collection 132

CHAPTER IV - Results and discussion **135**

Section IV.1. Liquid-phase microextraction applications **137**

1.1. A step forward with liquid-phase microextraction 139

  1.1.1. A simplified vortex-assisted emulsification microextraction method for determining personal care products in environmental water samples by ultra-high-performance liquid chromatography 143

Section IV.2. Sorbent-based microextraction applications **165**

2.1. A step forward with dispersive miniaturized solid-phase extraction 167

  2.1.1. Characterization of MOFs intended for microextraction 171

2.1.2. Adsorption isothermal studies of CIM-81(Zn) 193

2.1.3. Application of a pillared-layer Zn-triazolate metal-organic framework in the dispersive miniaturized solid-phase extraction of personal care products from wastewater samples 213

2.1.4. Dispersive miniaturized solid-phase extraction using the CIM-81(Zn) metal-organic framework and gas chromatography–mass spectrometry to determine personal care products in waters 235

2.2. A step forward with solid-phase microextraction 251

2.2.1. Monitoring trihalomethanes and nitrogenous disinfection by-products in blending desalinated waters using solid-phase microextraction and gas chromatography 255

2.2.2. Solid-phase microextraction based on the metal-organic framework CIM-80(Al) to determine volatile methylsiloxanes and musk fragrances in aqueous samples using gas chromatography 283

CHAPTER V - CONCLUSIONS 309

GLOSARY 319

CHAPTER I

Introduction

1. Emerging contaminants in waters

Water is undoubtedly essential for the life on Earth [1]. From a total estimated amount of ~$1.26{\cdot}10^{21}$ L of water, only 0.007% of water in the world is edible for human consumption, and recent climatic problems are even distorting this percentage [2]. To sum up, worldwide societies are facing problems arising from the high population, with the prevision of the United Nations pointing out to 9.6 billion in 2050 [3] and, subsequently, increasing the existing difficulties associated to easy access to quality water. Furthermore, there is not only a problem in the freshwater accessibility in adequate amounts, but contamination of natural resources is worsening the situation [4].

Groundwater is the main resource of fresh water for human consumption, although recently desalination constitutes another reliable source [5]. The groundwater sources cyclically replenish by rainfall but, at the same time, they are subject to contamination issues. Many pollutants are introduced into surface and ground waters due to natural and mainly anthropogenic sources through water cyclic of the ecosystem. Consequently, they are incorporated to drinking water [6], causing a direct or indirect potential risk for all living organisms. Seawaters also act as sink for contaminants, and thus their contamination levels must be set before ensuring desalination quality. Clearly, wastewaters are everyday increased with a plethora of contaminants that, despite controls, will eventually find their way to environmental waters. The main human activities linked to contamination are the industry, the agriculture, and the urban lifestyle. Thus, drinking waters can be contaminated with a growing number of pollutants, which is a risk for human health despite being present at trace levels [7].

The concept of environmental contaminants is due to Rachel Carson in 1962, [8], who established the potential risk that pesticides could exert in the environment and, consequently, to human health. Nowadays, the term **emerging contaminants** [9] (distinguishing itself from that of conventional contaminants, such as polycyclic aromatic hydrocarbons, heavy metals, pesticides, polybrominated diphenyl ethers, volatile organic compounds or aliphatic hydrocarbons) only refers to chemical substances recently categorized as hazardous or that can cause a risk for the human health and the environment, or at least labelled as having a suspected toxicity [10,11], but their presence in the environment is not necessarily new.

Most emerging contaminants have an anthropogenic origin [6], and many of the compounds already termed as emerging contaminants have been also recognized to present an endocrine disrupting activity [6,11,12]. Some of them cannot be metabolized easily and thus accumulate in living organisms; whereas others transform into metabolites or even suffer abiotic transformation in aquatic systems [10]. Sometimes, these secondary pollutants can be more persistent and/or more toxic than their origin compounds. Thus, the environmental risk of emerging contaminants also embraces the formation of metabolites, their environmental fate, their bioactivity, and their high persistence in some cases.

The introduction of emerging contaminants in the environment is not so different to the entry of other conventional contaminants (Figure I.1.). It can occur by different routes, including their direct discharge in the environment, or through treated wastewaters coming from urban, hospital, and industrial wastewater treatment plants (WWTPs) [13]. The increasing presence of emerging hazardous substances in environmental matrices can be also attributed to runoff water from urban or agricultural areas [14]. Among all the mentioned sources for emerging contaminants, WWTPs receive particular attention, due to the continuous inputs (significant amounts of emerging contaminants are introduced by the influents) and outputs (their discharge by the effluents) [13]. There is a number of secondary treatments at WWTPs, aimed to remove significant amounts of organic contaminants, such as the activated sludge processes [7]. However, these treatments are not enough to ensure the complete elimination of unwanted organic substances. Additional post water treatments have been implemented progressively, such as advanced oxidation processes, reverse osmosis, membrane bioreactors, activated carbon, and nanofiltration [7]. These treatments have shown to be effective for the removal of both hydrophilic and persistent emerging contaminants. Despite this, the growth of the global population, together with the increasing demand of consumption of certain chemicals, have contributed to increase highly the levels of these contaminants entering WWTPs, thus overloading the capacity of the most efficient systems. Thus, emerging contaminants are frequently detected in raw effluents [15] despite these post-treatment procedures in WWTPs.

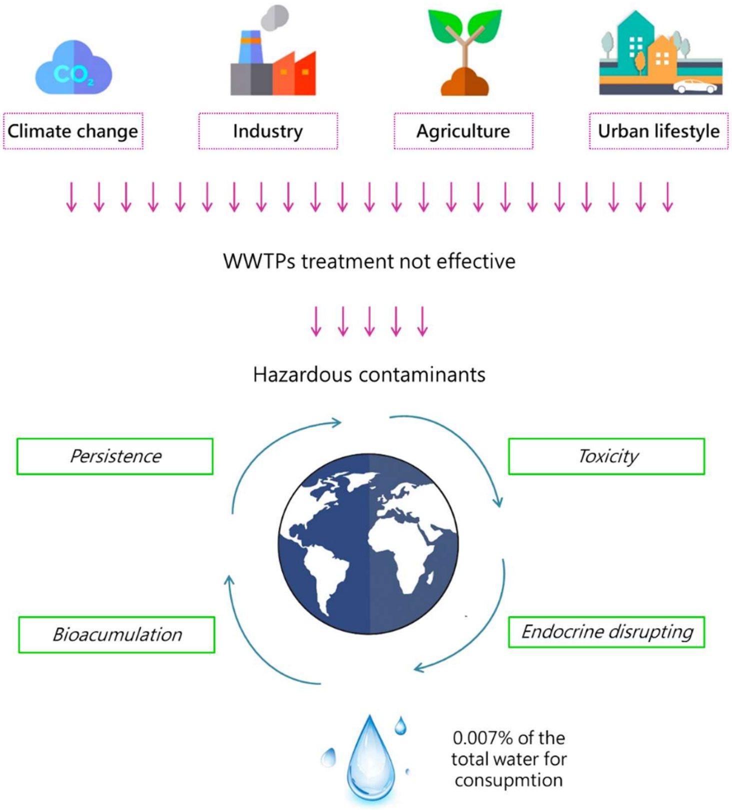

Figure I.1. Decreasing quality of drinking waters and consequent risk of exposure to emerging contaminants due to the water cycle.

1.1. Types of emerging contaminants

Currently, the most frequent chemical compounds labelled as emerging contaminants [8,15,16], grouped by families include: disinfection by-products, drugs of abuse, flame retardants, hormones, inorganic and organic nanomaterials, microplastics, perfluorinated substances, pharmaceuticals and personal care products (PPCPs), plasticizers, and surfactants, among others.

This Doctoral Thesis pays attention to personal care products and disinfection by-products, and thus a detailed description of these two types of emerging contaminants is included.

1.1.1. Personal care products (PCPs)

Personal care products constitute a subgroup of the PPCPs family [17]. PCPs refer to those substances used as cosmetics and in personal cleaning products (creams, gels, fragrances, shampoo, sunscreens…). The potential risk of PCPs relates with their extensive use by the population, thus increasing its contents in the environment on a daily basis, and in some cases (depending on the PCP nature) it relates with their persistence, bioaccumulation, and relatively low biodegradability [17,18].

Once PCPs-containing products are used, they can be absorbed by the body and excreted, or directly released to the environment after its personal application (i.e. a shower removing shampoo…) to sewage waters [19]. Giving their intense and growing use, it is evident that significant amounts of these compounds and their metabolites end up to WWTPs, where they are treated. As it has been mentioned previously, the secondary and ternary treatments are not enough for their complete elimination, and finally they incorporate to aquatic systems [18].

PCPs can be mainly classified according to their use: UV-filters, preservatives, fragrances, disinfectants, insect repellents, and siloxanes. Siloxanes are the only subgroup of PCPs that are classified by their structures.

UV-filters

UV-filters, also named sunscreens, are divided into the organic or chemical UV-filters, which can absorb the UV radiation, and the inorganic UV filters, which reflect the UV radiation. The risk associated to the use of organic UV-filters is much higher than that of inorganic. Organic UV-filters are chemical compounds formed in general by one or more conjugated benzene rings and/or carbonyl groups, presenting a high molar absorptivity at the ultraviolet electromagnetic region. Benzophenones, *p*-aminobenzoates, salicylates, cinnamates, benzotriazoles, benzimidazoles, camphor derivatives, and triazines, are compounds widely used for the UV protection [20]. They are added to sun products and to cosmetics (makeup, moisturizers, shampoos…), in order to prevent or minimize the adverse effects of the UV sun radiation [21,22]. These substances are also used in industrial applications to prevent photodegradation of polymers and pigments. Sometimes, several types of UV-filters are mixed in the same commercial product in order to cover a broad spectrum of wavelengths. Figure I.2. shows the most frequent UV-filters used and permitted by European regulations. It has been reported that UV-filters present high hydrophobicity and poor biodegradability [23]; and thus they have been frequently detected in sewage sludge [24], sediments [25], and biota [26]. Several studies have demonstrated that UV-filters can alter the endocrine system [27].

benzophenone-3
(BP3)

4-methylbenzylidene camphor
(MBC)

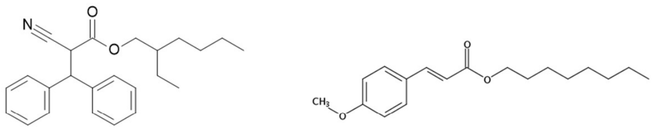

octocrylene
(OCR)

octyl 4-methoxycinnamate
(HMS)

2-ethyl-hexyl-4-trimethoxycinnamate
(EHMC)

2-phenylbenzimidazole-5-sulfonic acid
(PBSA)

Figure I.2. Representative UV-filters.

Preservatives

Preservatives are chemical substances added to increase the shelf life of the personal care and cleaning products. Preservatives prevent bacterial and fungal growth and oxidation. Furthermore, they inhibit the natural ripening of fruits and vegetables, being also applied in the food industry. The chemical compounds most used as preservatives are *p*-hydroxybenzoate esters, also known as parabens.

They have properties that *a priori* make them ideal for human use, like neutral pH, odorless, colorless, and they do not cause discoloration or hardening of the final product [18]. Its low production cost explains its popular use in industrial applications [17]. The fabrication and commercialization of parabens started around 1920s, and since then they have been widely used. Nowadays, only seven parabens are permitted: methyl-, ethyl-, propyl-, isopropyl-, butyl-, isobuthyl-, and benzylparaben, whose structure are shown in Figure I.3. Methylparaben and propylparaben are those most commonly used together, typically to increase their preservative effect [28]. Until quite recently, they have been considered of little toxicity, inert, and biodegradable. Concerns related to their risks to human health have only appeared in the last decade [29]. Thus, at the beginning of 2000s, several studies suggested that parabens could be hazardous substances [30], but results on their endocrine activity are still inconclusive [29].

In any case, the monitoring of parabens and their metabolites in biological human samples indicated a high human exposition to them. Thus, parabens have been detected in urine [31], breast milk [32,33], and tumor cells [34-36].

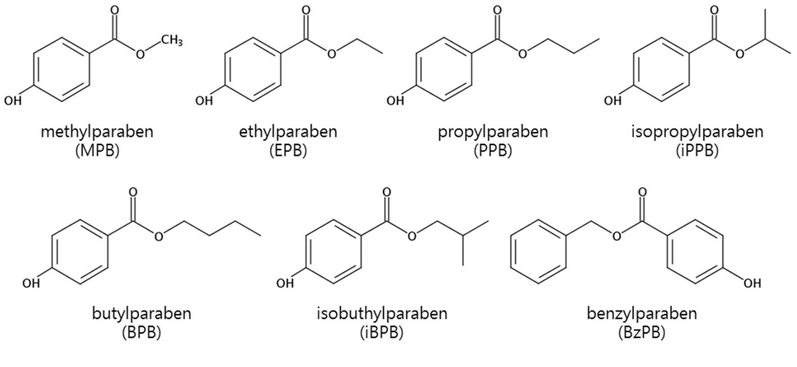

Figure I.3. Representative preservatives.

Musk fragrances

Fragrances are used in soaps, deodorants, detergents, makeup, and perfumes, with the objective to give odor and pleasant scent to them. Natural fragrances taken from floral and animal extracts have been used since antiquity. Synthetic musk fragrances arose to replace expensive natural fragrances [37]. Musk fragrances can be classified according to their chemical structure in nitro, polycyclic, macrocyclic, and alicyclic musk, as it is shown in Figure I.4.

Nitro musk fragrances were the first synthetic musk introduced in the late 1800s. They are dinitro- or trinitrobenzene derivatives with additional alkyl, keto or methoxy groups [37]. The most frequently used are musk xylene (MX) and musk ketone (MK), and less frequently musk ambrette (MA) and musk moskene (MM). Nitro musk fragrances have demonstrated to be transformed in the WWTPs in metabolites with higher toxicity and higher disrupting activity [37]. These problems, together with their high persistence and potential toxicity in aquatic system, justify that nitro musk has been gradually replaced by polycyclic musk.

Polycyclic musk fragrances are a class of highly alkylated tetralin or indane substitutes [18]. They were synthesized and commercialized around 1950s, and high amounts of them are still being used. Typical polycyclic musks are celestolide (ADBI), galaxolide (HHCB), tonalide (AHTN), chasmeran (DPMI), and phantolide (AHMI). Both nitro and polycyclic musk are soluble in water but presenting high octanol-water coefficients that explain their easy bioaccumulation in the aquatic biota [17].

Macrocyclic musk fragrances are formed by 15- or 17-membered ring systems [37]. Among them it is possible to cite musk muscone (MM), ethylene brassylate, globalide, and thibetolide. They have not been used as polycyclic musk due to their expensive synthesis. However, macrocyclic musk presents proper properties (stability, fixation, great odors…), that with a decreasing cost of their synthesis could replace completely the polycyclic musk in industrial applications. The scent of macrocyclic musk is more intense respect to polycyclic musk, which is a great advantage from an industrial point of view.

Ultimately, alicyclic musk is considered the last generation of musk fragrances, and they are characterized by having linear chains in their structure [37], like romandolide and helvetolide [38].

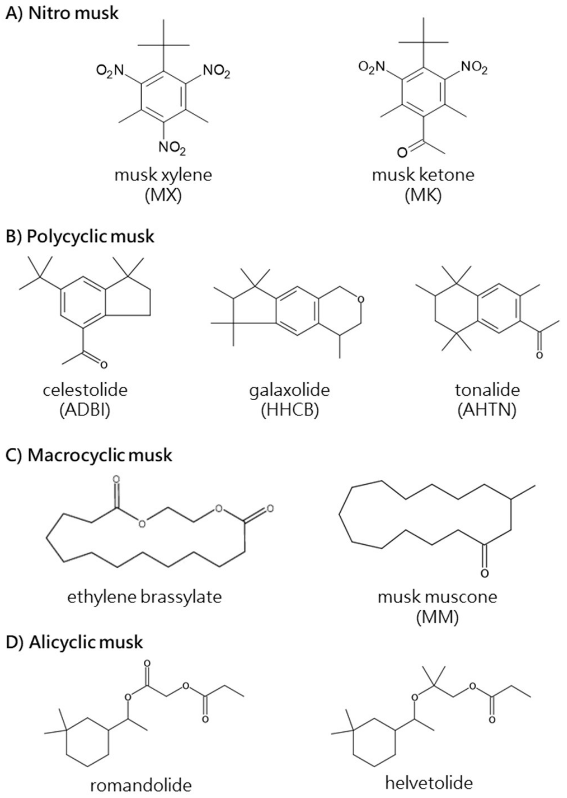

Figure I.4. Representative **A)** nitro musk, **B)** polycyclic musk, **C)** macrocyclic musk, and **D)** alicyclic musk fragrances.

Disinfectants

Disinfectant or antiseptic compounds are extensively used in daily activities for antimicrobial purposes. The main function of these substances is the prevention of the microbial activity of bacteria, viruses, fungi or protozoa. The most commonly used are benzotriazole (BZ), triclosan (TCS), and triclocarban (TCC), whose structures are shown in Figure I.5. It has been speculated that these compounds may be involved in antimicrobial resistance [39,40].

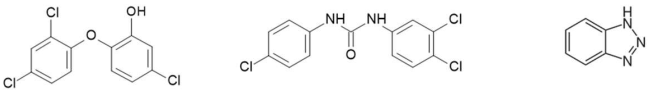

triclosan (TCS) triclocarban (TCB) benzotriazole (BZ)

Figure I.5. Representative disinfectants.

BZ is a versatile heterocyclic compound used for its biocide properties in numerous industrial applications. In addition to the biocidal function, BZ presents anticorrosion properties. Given its low hydrophobicity, the technological treatments in WWTPs for their removal are not effective, and thus BZ has been detected at high levels in sewage and sludge [41]. It has been reported in bacteria assays that the methyl metabolites of BZ are more toxic than the BZ, and some *in vitro* and *in vivo* studies have demonstrated its potential endocrine activity [42].

TCS and TCC are biphenyl ethers mainly used in soaps, deodorants, skin creams, and toothpaste. TCS is easily degraded to more persistent and toxic compounds by photochemical reactions, chlorination, or ozonelysis [43,44], forming chlorinated or methyl metabolites, like the 2,8-dichlorodibenzo-*p*-dioxin (2,8-DCDD) and the methyl-TCS, respectively [18]. TCS and TCC show certain tendency to accumulate in wastewater sludge and sediments due to their hydrophobic properties [39]. Furthermore, TCS has been reported as endocrine disruptor, causing interference in the thyroid gland [45].

Insect repellents

Insect repellents are chemical compounds whose surface application avoid the approaching of insects. Their use is quite widespread in tropical regions. They are critical in the protection of some diseases when other forms are not available, like in underdeveloped countries. There is little information about their real effects, because this has been the group of PCPs less studied. Some studies about their toxicity are not conclusive, and up-to-date there is not confirmation of their endocrine effects [46].

Insect repellents include *N,N*-diethyl-m-toluamide (DEET), piperonyl butoxide (PBO), and Bayrepel (1-piperidinecarboxylic acid, 2-(2-hydroxyethyl)) [18], whose structures are shown in Figure I.6. DEET is the most common chemical used as insect repellent. This compound was developed and registered for commercial use in the 1940s [47]. There is limited toxicity data about it, but DEET has reported to be slightly toxic in some small living vertebrates [48], with some reported adverse effects as rashes and urticaria [49]. Furthermore, it presents quite persistency in the aquatic environment [50].

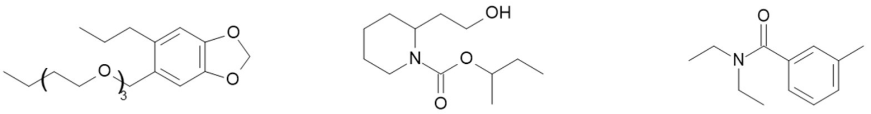

piperonyl butoxide
(PBO)

1-piperidinecarboxylic acid, 2-(2-hydroxyethyl)
(Bayrepel)

N,N-diethyl-m-toluamide
(DEET)

Figure I.6. Representative insect repellents.

Siloxanes

Siloxanes, also known as volatile methyl siloxanes (VMSs), are also categorized as PCPs by their chemical structure, but not by their use as the previous PCPs. Their structure is formed by polymeric organic chains, alternating silicon and oxygen atoms, with methyl groups or organic chains attached to the silicon atoms [18]. They can be classified as linear or cyclic siloxanes, and Figure I.7. summarizes some representative examples. These highly hydrophobic substances provide softness, smoothness, and moistness to the cosmetic and cleaning products. Octamethylcyclotetrasiloxane (D4), decamethylcyclopentasiloxane (D5), and dodecamethylcyclohexasiloxane (D6), are the cyclic siloxanes most widely used. Their use has been extended to industrial applications including production of polymers, dry cleaning solvents, and industrial cleaning fluids.

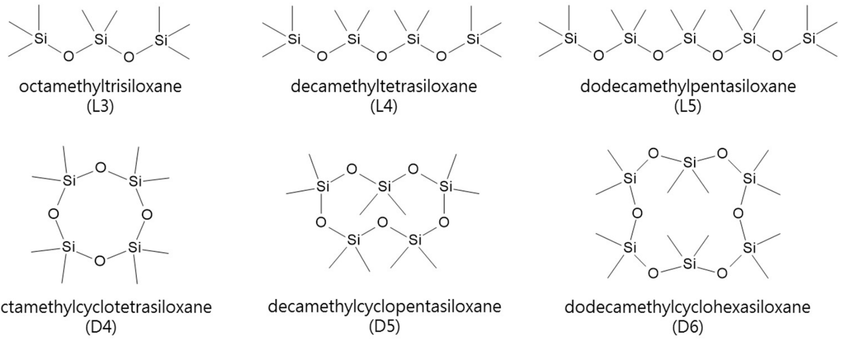

Figure I.7. Representative siloxanes.

Regarding their presence in the environment, siloxanes have been frequently quantified in WWTPs influents, sewage sludge, sediment, and marine vegetation [51-53]. Some studies have demonstrated their possible toxicity issues [54], and their relationship with carcinogenic effects [55].

1.1.2. Disinfection by-products (DBPs)

Disinfection of waters is essential to inactivate and remove microbial activity in distribution systems of tap water, desalination plants, and swimming pools [29]. Free chlorine (Cl_2) is the most commonly used disinfectant for pre-treatment steps as well as in the final disinfection, due to its low cost, availability, efficiency, and high stability in the distribution network. Chlorine is added typically in a concentration level of 0.5-2.0 $mg{\cdot}L^{-1}$ in the treatment of water, intending a residual level of 0.25-0.5 $mg{\cdot}L^{-1}$ after the initial treatment [1,29]. Despite its important action to ensure quality waters for human consumption, chlorine is also able to react with natural organic matter (NOM), such as humic and fulvic acids present in natural waters, forming a wide variety of halogenated compounds, a type of hazardous pollutants known as DBPs [56]. Concerns related to the toxicity of DBPs were raised since 1970s [57], and thus the formation of such by-products entails a risk for the human health and the environmental ecosystems. Other precursors of DBPs include body fluids (urine and sweat), and PCPs present in the aqueous media such as UV-filters [58]. Until now, around 700 DBPs have been identified in drinking waters, wastewaters, desalinated waters, and pool waters [29,59,60]. The nature and the concentration of formed DBPs depend on several factors, such as the amount of disinfectant used, the contact time, the type of organic and inorganic substances present in the water sample, the temperature, and the pH. Humans are exposed to DBPs mainly by three pathways [58]: i) inhalation of volatile DBPs, ii) skin absorption of DBPs, and iii) direct ingestion of tap water containing DBPs.

Among all the chlorinated and brominated derivatives of DBPs, mainly formed by chlorination of waters, trihalomethanes (THMs) and haloacetic acids (HAAs) have been the most commonly studied; the brominated DBPs, in general, are more carcinogenic than their chlorinated analogues [61]. The main route of formation of THMs and HAAs is shown in Figure I.8.

Nowadays, these DBPs (THMs and HAAs) are strictly regulated, and other disinfectants for water have been investigated to avoid the formation of these DBPs. This way, chloramines, ozone, and chlorine dioxide are substances that have been considered as an alternative to chlorine, in order to inactive residual pathogenic microorganisms [62]. Sometimes, the chlorination treatment is mixed with one or more methods to obtain a synergic effect [63] intending the minimization of DBPs formation. Thus, it is well known that ozone reduces considerably the formation of THMs and HAAs, but this alternative disinfectant has important issues because it forms bromate with waters containing high levels of bromide, and bromate is a potential carcinogenic substance [29]. On the other hand, chloramine forms other types of DBPs, including nitrogenous-based DBPs, such as nitrosamines, haloacetonitriles (HANs), and halonitromethanes (HNMs), or iodinated-based DBPs, such as I-THMs and I-HAAs. Although nitrogenous and

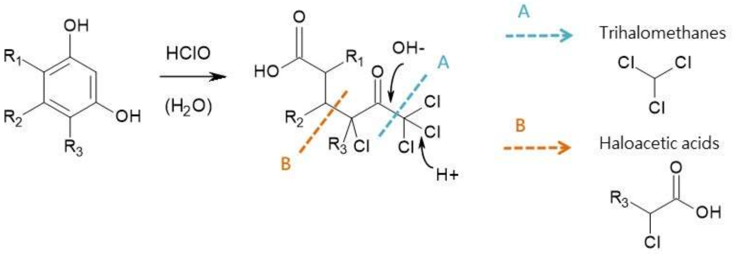

Figure I.8. Formation of THMs and HAAs as by-products during the chlorination of drinking water.

iodinated DBPs are not regulated by competent bodies, some of them have been claimed to be much more cytotoxic and genotoxic than the brominated and chlorinated analogues [64,65]. High amounts of bromide or iodide in waters are precursors of brominated and iodinated DBPs, respectively. Other DBPs detected in drinking water include haloketones (HKs), chloral hydrate, bromate, and chorite.

There are some discrepancies in epidemiological and toxicological studies nowadays regarding DBPs [66,67], due to the limited research data. It must be considered that there are around 700 DBPs identified, and comparatively, a relatively small number of publications on the quantitative occurrence and health effects of them. Indeed, it is calculated that only ~10% of DBPs have been subjected to toxicological studies [67,68]. In any case, carcinogenic and mutagenic effects, together with alterations to the nervous system, have been reported for THMs, and several HAAs and HANs [59,69].

Trihalomethanes (THMs)

THMs are formulated as CHX_3, where X represents chlorine or bromine. Commonly, THMs refer to four compounds: trichloromethane (TCM), bromodichloromethane (BDCM), dibromochloromethane (DBCM) and tribromomethane (TBM). Figure I.9. shows their structures. If THMs contain iodine atoms, the compounds are named as I-THMs, whose growing interest in the scientific community is due to the higher toxicity when compared with their chlorinated and brominated analogues [70]. In general, toxicity issues of THMs can be ordered as: I-THMs, brominated-THMs, and chlorinated THMs [63]. THMs are formed easily during the chlorination treatment of drinking waters. Furthermore, they are also by-products of the degradation of others DBPs such as HAAs [71].

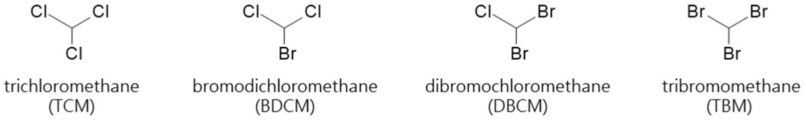

Figure I.9. Chemical structures of THMs.

Haloacetic acids (HAAs)

HAAs are carboxylic acids in which a hydrogen atom in the acetic acid has been replaced by a halogen atom. The five HAAs most commonly studied are monochloroacetic acid (MCAA), dichloroacetic acid (DCAA), trichloroacetic acid (TCAA), monobromoacetic acid (MBAA), and dibromoacetic acid (DBAA), whose structures are shown in Figure I.10. Unlike THMs, HAAs are highly polar and present low volatility. They can be easily degraded at high values of temperature and pH, and HAAs have been described as precursor of THMs. Thus, treated waters with chlorination present high amounts of THMs not only coming from the chlorination itself but from the degradation of HAAs [63].

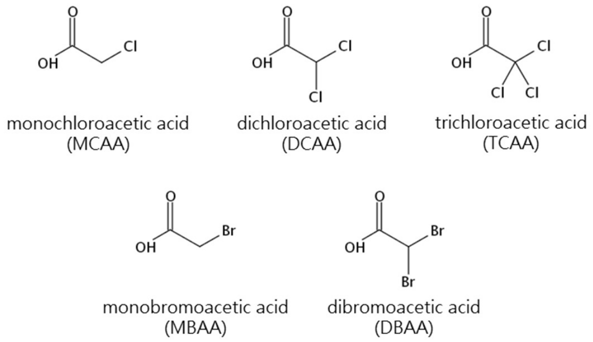

monochloroacetic acid (MCAA)
dichloroacetic acid (DCAA)
trichloroacetic acid (TCAA)
monobromoacetic acid (MBAA)
dibromoacetic acid (DBAA)

Figure I.10. Chemical structures of several representative HAAs.

Haloacetonitriles (HANs)

The nitrogenous DBPs most commonly formed are: dichloroacetonitrile (DCAN), trichloroacetonitile (TCAN), bromochloroacetonitrile (BCAN) and dibromoacetontrile (DBAN). Their structures are shown in Figure I.11. These DBPs are formed in the presence of amines, which have as precursors amino acids present in waters [63]. It has been pointed out that the use of higher amounts of ozone as water treatment ensures lower content of haloacetonitriles [72].

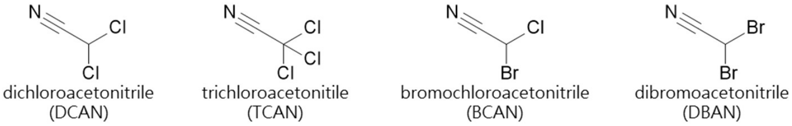

Figure I.11. Chemical structures of several representative HANs.

Halonitromethanes (HNMs)

HNMs are structurally different to THMs only by one nitro group. The most common substances are trichloronitromethane (TCNM) and tribromomitromethane (TBNM), shown in Figure I.12. The HNMs formation depends directly on the amount of nitrogen in the treated water, mainly in those waters treated with chloramines. There is evidence about their health effects [63], and thus its determination in treated waters is advisable.

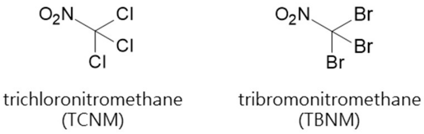

Figure I.12. Chemical structures of several representative HNMs.

1.2. Regulations regarding emerging contaminants in waters

The awareness of the potential contamination of surface and ground waters (which are the main sources of edible water) has encouraged both scientific and political communities to adopt new strategies to reduce the production and consumption of certain chemical products [15]. Additionally, the requirements established by the different institutions worldwide to ensure the quality of the waters have been updated over the years to adapt to the current state of water resources, as it is shown in Table I.1.

In the European Union (EU), the creation of the Water Framework Directive in 2000 [73] led to an increasing concern on the assurance of the standards of both environmental waters and drinking water. Specific legislations within water policy were also established and are continuously reviewed in order to adapt them to current technological progress and scientific knowledge, as well as a preventive strategy.

Regarding environmental waters, including surface and ground waters, the European Parliament and Council created a list of priority and hazardous substances taking into account their persistence, bioaccumulation and toxicity properties [74]. This list was updated in 2013 [75], and now includes a total of 45 compounds (and, in some cases, their derivatives), which is a small number considering the wide range of hazardous chemical substances that are commonly released into the environment. Indeed, among the emerging contaminants studied in this Doctoral Thesis (PCPs and DBPs), only TCM is considered in this list, and any of the other compounds are neither regulated nor considered as potential hazardous substances. This Directive does not set a maximum concentration value for these compounds in environmental waters, but it includes an annual average concentration of 2.5 $\mu g \cdot L^{-1}$ for TCM as a preventive value that ensures meeting the environmental quality standards of surface waters. The musk fragrance MX (covered in this Doctoral Thesis) now appears in the list of substances that will be subjected to review as a potential hazardous compound. Thus, many compounds labelled as emerging contaminants and covered in this Thesis are not included in the EU list for surface and ground waters, but they have been or are currently considered as possible inclusions.

Regarding the increasing regulations of the EU to ensure the quality of water intended for human consumption, the Directive 98/83/EC was amended by the Directive 2015/1787 to come down the levels for some contaminants, while including the water used in food industry within the drinking water policy [76]. Regarding emerging contaminants, this regulation establishes a parametric value of 100 $\mu g \cdot L^{-1}$ for THMs, as the sum of concentrations of TCM, TBM, DBCM, BDCM, while the remaining substances considered in this Doctoral Thesis are not included. Nevertheless, thanks to an initiative proposed by European citizens in 2019, the European Council undertook a revision of the current quality standards of drinking water in order to improve the accessibility to safe and clean water and to facilitate the access to useful information on water quality for consumers [77]. The proposal was reviewed, and despite the definitive Directive will be introduced in Spring 2020, the preliminary document is already available [78]. Thus, this new Directive will set for the first time a parametric value for HAAs in drinking waters, with a maximum concentration of 60 μg·L^{-1} as the sum of MCAA, DCAA, TCAA, MBAA, and DBAA. Furthermore, a watch list of substances or compounds of emerging concern (with endocrine disrupting characteristics) and with a potential presence in water intended for human consumption will be implemented. The substances included in this list will be carefully monitored and the list will be actively updated to cover all those compounds that may have a significant risk for human health to identify possible priority substances.

In the United States, the Environmental Protection Agency (US-EPA) establishes the laws to ensure the safety and quality of the water, while providing the guidelines to prevent the contamination of this natural resource and the support for the treatment of wastewaters [79].

The Clean Water Act is the program in charge of the control of federal water pollution and regulates the quality of surface waters to ensure the protection of the environment and human health. As in the EU, there is not a maximum concentration level for any of the PCPs or DBPs covered in this Thesis according to the environmental waters US-EPA regulation [80]. However, three out of the THMs (TCM, TBM and DCBM) are considered priority toxic pollutants within the water quality criteria in some UN states, including California and Washington.

The Safe Drinking Water Act is the program responsible to ensure the quality of drinking water in the United States [81]. It has set a maximum of allowed concentrations for 90 chemical compounds, to be considered as hazardous substances. Among the DBPs, the regulation establishes a limit value of 80 μg·L^{-1} for the sum of concentrations of the four THMs, and 60 μg·L^{-1} for the sum of most common HAAs: MCAA, DCAA, TCAA, MBAA, and DBAA [82]. While PCPs are not included within the current drinking water quality requirements imposed by the US-EPA, it is important to mention that the US-EPA is actively evaluating the presence and health risks of drinking water contaminants by updating the Contaminant Candidate List every five years. This update is possible thanks to the data reported by research studies all over the world [83]. This list includes those emerging substances that are not yet regulated by this agency but are known to occur in drinking water and, therefore, should be considered to update the current regulation.

The World Health Organization (WHO) tries to coordinate all issues on international health by promoting some guidelines within different topics, including drinking water quality, to ensure safe and affordable access to clean water worldwide [84]. In this sense, the WHO publishes the "Guidelines for drinking-water quality" with the aim of providing tools and basic information that will help the different national governments or international institutions to set the quality standards within water policy. In the last edition of 2017, PCPs were not labelled among the chemical contaminants, but the guide set recommended maximum values for some DBPs: 300 $\mu g \cdot L^{-1}$ for TCM, 100 $\mu g \cdot L^{-1}$ for DBCM and TBM, 60 $\mu g \cdot L^{-1}$ for BDCM, 70 $\mu g \cdot L^{-1}$ for DBAN, and 20 $\mu g \cdot L^{-1}$ for DCAN [1].

It is interesting to mention that, despite PCPs are not considered neither in environmental nor in drinking water regulations, several institutions have become more aware of their abusive use in the cosmetic industry, which may have an important impact in the environment given their toxicity and unavoidable incorporation to wastewaters due to bathing and washing human activities [26]. In this sense, the European Regulation 1223/2009 on cosmetic products set a list of authorized UV filters and banned the use of the preservatives iPPB, iBPB, BzPB, penthylparaben and phenylparaben, and the musk MA. It also specifies maximum concentrations for some preservatives in cosmetic products, including parabens with a maximum level of 0.4% for single ester and 0.8% for mixtures of esters, and a value of 0.2% or 0.3% for TCS depending on the cosmetic product [85]. In the case of the United States, the Food and Drug Administration (US-FDA) manages the regulations on food, drug and cosmetic products under the Federal Food, Drug, and Cosmetic Act [86]. This institution applies less strict criteria than the EU regarding the composition of cosmetic products before going to the market, but it emphasizes on the correct labelling of the products (including all the information on their adequate use and ingredients for consumers). Nevertheless, several US states have set additional requirements for cosmetic products, including a list of prohibited substances or priority chemicals, as the Proposition 65 of California [87].

Table I.1. PCPs and DBPs identified as priority contaminants and their maximum allowable concentrations in different waters, according to the regulations established by different institutions worldwide.

Institution/organization	Environmental water	Drinking water
PCPs		
EU	Musk MX[a]	–
US-EPA	–	–
WHO	–	–
DBPs		
EU	TCM[b]: 2.5 μg·L^{-1}	*Total THMs*: 100 μg·L^{-1} (TCM, TBM, DBCM and BDCM) *Total HAAs*[d]: 60 μg·L^{-1} (MCAA, DCAA, TCAA, MBAA and DBAA)
US-EPA	TCM, TBM and DCBM[c]	*Total THMs*: 80 μg·L^{-1} (TCM, TBM, DBCM and BDCM) *Total HAAs*: 60 μg·L^{-1} (MCAA, DCAA, TCAA, MBAA and DBAA)
WHO	–	TCM: 300 μg·L^{-1} TBM and DBCM: 100 μg·L^{-1} BDCM: 60 μg·L^{-1} DBAN: 70 μg·L^{-1} DCAN: 20 μg·L^{-1}

[a] Included in the list of substances to be reviewed as possible priority hazardous substance
[b] Annual average environmental quality standard value established as a priority and hazardous substance
[c] Included in the list of priority toxic pollutants within water quality policy in several US states
[d] Preliminary maximum parametric values that will be adopted in the new Directive from 2020

1.3. Reported contents of emerging contaminants in environmental waters

In the last decades, given the existing regulations and concerns, there is a large number of publications on the occurrence, the fate, and the presence of emerging contaminants in environmental water samples [7,88]. A current overview of contamination levels is summarized in Table I.2. It can be observed that the concentration levels in water samples ranged from low ng·L^{-1} to µg·L^{-1}, thus representing in general quite low amounts, but causing a risk even at those levels due to constant exposure.

Regarding PCPs, they have been mainly monitored in WWTPs [20,37,89,90], in surface waters [20,37,89,90], and also in ground waters [90]. Several groups have been detected their presence in drinking water and swimming pool waters, due to their high use in social activities [91]. Among all PCPs, the compounds more widely reported include HHCB, AHTN, ADBI, and AHM as musk fragrances; TCS and TCC as disinfectants; DEET as insect repellents; and BP-3 as UV-filters [90]. Obviously, the concentration levels found of PCPs in wastewater is frequently higher than in surface water, and in surface water higher than in ground water. However, there is still a lack of definitive studies establishing relationships on their occurrence in the aquatic environment and their toxicological effects.

Regarding DBPs, they have been monitored essentially in drinking water [59] and swimming pool water [58,66], due to concerns on their potential toxicity and human exposure after chlorination and other disinfection strategies. Furthermore, DBPs formation and occurrence have been studied in blending [29] and recycled waters [63]. In some cases, the concentrations of DBPs observed in recycled waters seem to be higher than those in drinking water [63]. Thus, a study on human exposure to HAAs in pool water has found that the half-lives of HAAs is much higher than the half-lives of THMs [92], which increases their potential risk. Regarding their determination, slightly higher concentration levels of HAAs have been found in tap water (up to 10 µg·L^{-1}) than in commercial drinking water [93]; while concentration levels reported in wastewater samples have been higher than those of drinking water [94].

Table I.2. Overview of concentration levels of emerging contaminants in environmental waters.

Emerging contaminants (number)	Type of water sample	Conc. levels found ($ng \cdot L^{-1}$)	Ref.
plasticizers (7)	tap, river and canal	1-2000	[95]
musk fragrances (5)	river	11.7-18.7	[96]
pharmaceuticals (3), hormones (7), plasticizers (2) and flame retardants (1)	river	80-4200	[97]
drugs (4)	river and lake	149-264	[98]
drugs (2)	seawater	8.2-203.6	[99]
per- and poly-fluoroalkyl substances (PFASs) (29)	seawater	2-12	[100]
pharmaceuticals (32), illicit drugs (2), PCPs (5), perfluorinated compounds (2), anthropogenic markers (2), and plasticizers (3),	river	10-120	[101]
pharmaceuticals (2), pesticides (3), and hormones (2)	river, lake, reservoir, and well	0.05-1.85	[102]
flame retardants (10)	river	20-800	[103]
EU "Watch" list (17)	river water and WWTP	0.9-109	[104]
pesticides (15), drugs (5), PCPs (3), and industrial chemicals (4)	surface and wastewaters	30-68870	[105]
drugs (2)	river, wastewater and tap	1500	[106]

1.4. Analytical methodologies for the environmental monitoring of emerging contaminants in waters

Together with political strategies, the science holds a crucial role to stand up to chemical pollution. The challenge of the scientists focuses on two main points: to generate and to analyze adequate information on the emerging contaminants content in environmental samples. Thus, the society needs to know the concentration of a substance that presents a risk, what is the real risk, how it affects to the human health or to the ecosystems, and what are the concentration levels linked to exposure. This task is undoubtedly multidisciplinary, comprising fields such as toxicology, medicine, engineering, sociology, and chemistry. Particularly, analytical chemists play an important role in the development of adequate analytical methods to ensure proper monitoring. Two main challenges are being addressed:

1. The huge and growing number of compounds present in the environment, with great diversity regarding their physical-chemical composition. Multi-residue and multiclass methodologies have been proposed to cover entire groups of emerging contaminants, or at least several groups of them.
2. The presence or these compounds at very low content, causing a risk even at those levels, in complex matrices with a number of co-existing interfering components. The ongoing development of sophisticated instrumentation and, consequently, the improvement in analytical methodologies is being undertaken.

These two challenges for analytical chemists are combined to perform target or non-target analysis [107,108]. In the case of target analysis, the methodologies are based on the identification and quantification of known compounds, generally at trace levels in samples with high complexity [109,110]. The methodology is mainly selected according to the nature of the target compounds. These methods normally require a previous step of enrichment/preconcentration to achieve the expected sensitivity. Non-targeted analysis focused mainly on the identification quantification of all the organic compounds present in a sample [111]. This kind of analyses are not limited to the determination of regulated compounds, and in general implies chromatographic separation techniques in combination with mass spectrometry.

Current analytical methods to monitor emerging contaminants, particularly for PCPs and DBPs in waters, utilize chromatographic techniques, with gas chromatography (GC) being devoted to volatile or semi-volatile contaminants, such as UV-filters [112,113], musk fragrances

[112-114], siloxanes [115-117], THMs [118-120], HANs [117,121], and HNMs [117,120]. On the other side, liquid chromatography (LC) is frequently used for the determination of non-volatile and polar contaminants, such as certain UV-filters [112,123,124], preservatives [124,125], disinfectants [124,126], and HAAs [127,128].

To achieve a proper sensitivity (quite necessary considering the levels in environmental samples, Table I.2. of the Section I.1.3.), preconcentration and clean-up strategies most commonly used include liquid-liquid extraction [112,117-119,125,124,127], and solid-based extraction [113-116,120,122,123,126].

There is only one official method for the analytical determination of DBPs in waters, and official methods for PCPs are still required (pending on their inclusion in the regulations). The official method for the determination of DBPs in drinking water is the US-EPA Method 551.1, proposed by US-EPA for the determination of several THMs (TCM, DCBM, BDCM, and TBM), HANs (BCAN, DBAN, DCAN, and TCAN), and other DBPs (chloral hydrate, chlorocipin, 1,1-dichloro-2-propanone, and 1,1,1-trichloro-2-propanone) [129]. The method requires liquid-liquid extraction (LLE) followed by GC analysis and electron capture detection (ECD). For 50 mL of water sample, the LLE method uses 3 mL of methyl tert-butyl ether as the first extractant solvent, with 5 mL of pentane offered as second optional extractant solvent. If it is considered that only 2 microliters of the total extractant volume is finally injected in the GC, the method generated an important amount of wastes per sample.

Despite the success in terms of analytical performance of the methods mentioned before for DBPs and PCPs, they cannot be considered in all cases environmental-friendly. Furthermore, many reported analytical methods are focused on one exclusive group of PCPs [115,123,125,130,131] or DBPs [116,118,128,]. The multiclass analysis of these emerging contaminants should be considered to reduce the analysis time and the costs for their monitoring. Clearly, more efficient methodologies for PCPs and DBPs are still required.

2. Green Analytical Chemistry

The concept of **Green Chemistry** was defined by P. Anastas and J.C. Warner in 1998, as "the movement toward pursuing chemistry with the knowledge that the consequences of synthesis and the use of reagents do not stop with the properties of the target molecule or the efficacy of a particular reagent. The impact of the chemistry designed by the chemists is felt by the people that come in contact with the substances that they make and use, and by the environment" [108]. The goal of the Green Chemistry is therefore to minimize the environmental and occupational risks inherent to industrial activities that link directly to chemical issues. This necessarily implies a direct cooperation between chemists and society, and it must accomplish the integration of efficacy, efficiency, and economic criteria in all the chemical activities to ensure the reduction of their environmental impact. Consequently, Anastas and Warner postulated a set of recommendations and guidelines, summarized in these well-known 12 principles [132]:

1. Prevent waste in order to avoid the need of cleaning or decontamination procedures
2. Design safer chemical and products to avoid their risks or toxic effects
3. Design less hazardous chemicals synthesis for both humans and environment
4. Use renewable feedstock to replace depleting feedstock media for fossil fuel
5. Use catalysts, not stoichiometric reagent to reduce the amount of reagent used through the world
6. Avoid chemical derivatization to reduce once again the amounts of reagent to be used
7. Maximize atom economy in order to reduce wastes and to improve the synthesis yield
8. Use safer solvents and reaction conditions to improve the use of water or eco-friendly solvents that do not contribute to smog formation or ozone layer depletion
9. Increase energy efficiency working, as possible at room temperature
10. Design chemicals and products to degrade after use, in order to avoid reagent accumulation in the environment and to assure that employed chemicals degrade to innocuous final products
11. Analyze in real time to prevent pollution thus involving in-field analysis and real time monitoring of processes

12. Minimize the potential for accidents like explosions, fires, and releases to the environment

Green Chemistry is today understood as a multidimensional approach, despite being initially limited to chemical aspects, such as improving the chemical economy, the chemical synthesis, the catalytic method, the use of renewable feedstocks, and the environmental side effects of the chemical activities [110].

The compiling of the Green Chemistry principles undoubtedly requires the development of new and sustainable analytical methodologies. Under these principles, it would be contradictory that methods used to monitor hazardous substances could have a higher risk than the analytes that are going to be determinate. In this context, trends in Analytical Chemistry moved to the research on eco-friendly processes. Thus, Galuszka, Migaszewski and Namiesnki adapted in 2013 the 12 principles of the Green Chemistry to analytical procedures, thus generating the concept of **Green Analytical Chemistry** (GAC) [133]. The four priorities of GAC are:

1. Elimination or reduction of consumption of reagents and organic solvents in the analytical procedures
2. Reduction of emission of vapors and gases, as well as the generation of solid wastes, in the analytical laboratories
3. Elimination of reagents displaying high toxicity and/or ecotoxicity from the analytical procedures
4. Reduction of labor and energy consumption of the analytical procedures

Following these priorities, GAC has promoted the development of environmental-friendly instrumentation and methodologies. According to M. de la Guardia and S. Armenta [108], these basic strategies for GAC have been considered in recent analytical efforts, and can be grouped mainly in the following trends: the elimination and reduction of reagents (i-iv), and the reduction of energy requirements (v-vi):

i. *Direct analysis*, by in-field analysis of untreated samples
ii. *Alternative treatment*, using alternative, less energy-consuming, and less reagent-consumption sample treatments
iii. *Miniaturization* of the analytical methodologies
iv. *Automation* of the analytical methodologies

v. *Energy saving*, by the assessment of energy consumption and the labor consumption of analytical procedures
vi. *Consumable saving*, searching for alternative reagents
vii. *Online waste treatment*, to reduce and to eliminate the ecotoxicity of the wastes generated that, together with the miniaturization and automation, it implies an accreditation of value for such treatment of wastes

Additionally, several efforts have been devoted to evaluate the real greenness of the analytical methodologies proposed. Thus, the National Environmental Methods Index (NEMI) was the first proposed tool to evaluate the greenness of methods [134]; and then Raynie and Driver included the energy consumption [135]. Later, Garrigues and De la Guardia introduced a three-color scale (from red to yellow) to modify the NEMI pictogram [136]. In 2012, the Eco-scale was introduced by Galuszka *et al.* for the evaluation of analytical procedures by the introduction of penalty points [137]. Then, the Green Certificate concept was proposed in 2016 by De la Guardia and coworkers, as a modification of the previous Eco-scale, based on colors code and letters [138]. The most recent proposal is the Green Analytical Procedure Index (GAPI), based on the NEMI and the Analytical Eco-Scale, and evaluates the greenness of the methods through a three-level category of colors: green, yellow, and red [139].

However, it is very difficult to establish a unique consensus for the evaluation of the green scale of the analytical procedures, because they imply several approaches. Figure I.13. shows the most significant events, concepts, and features since 1940s regarding environmental and analytical issues. In any case, nowadays the common agreement among authors is the effort for developing environmental-friendly procedures, increasingly "green".

In order to obtain a complete green analytical procedure, an ideal methodology would imply the direct analyses of samples, obtaining the maximum information with minimum costs and times [140]. However, due to the complexity of the samples or the purpose of performing a multi-component analysis, the analytical procedures normally require multiple steps, particularly in the pretreatment of the samples [110]. The analytical sample preparation approaches probably constitute the less green part of any analytical method [141]. Main challenges to ensure real green analytical methodologies focus on different strategies: the minimization of consumption of reagents, sorbents and/or solvents, if it is possible, with environmental-friendly features, and the miniaturization and, it is also if possible, automation of the procedures.

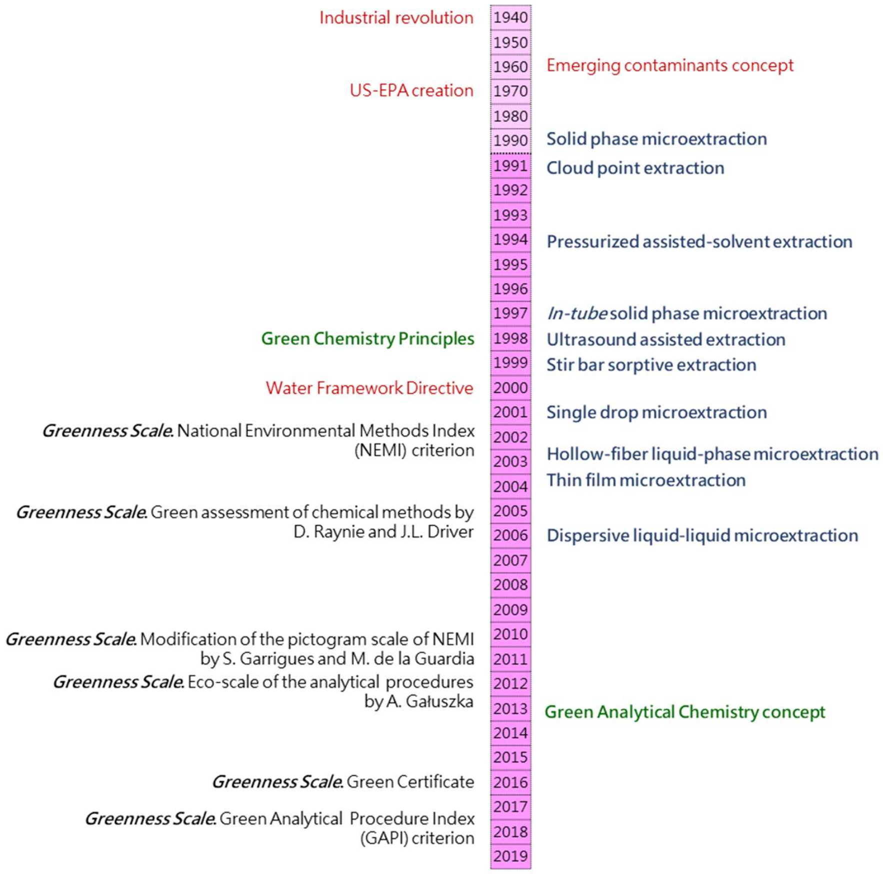

Figure I.13. Historic evaluation of main events related to Green Chemistry (adapted from [108]). Terms highlighted in blue correspond to analytical method development, with an increasing presence of liquid-based and sorbent-based miniaturized methods. Terms highlighted in green relate to concepts, and terms highlighted in red correspond to important historic features and regulations. The different scales proposed to somehow measure the greenness of a method are also included.

3. Microextraction techniques

The monitoring of emerging pollutants implies necessarily a step of sample preparation due to their low concentration levels (Section I.1.3.), and particularly considering the complexity of the environmental sample matrices. The analytical sample preparation intends: i) the selective (as selective as possible) extraction of target analytes, ii) the analyte enrichment to increase the sensitivity of the overall method, and iii) a sample clean-up to minimize interferences coming from the sample matrix and to avoid damage to the further analytical instrument used for detection.

Attending to the physical state of the sample, it is possible to classify the extraction procedures in three main types:

1. Extraction methods for solid samples
2. Extraction methods for liquid samples
3. Extraction methods for volatile compounds, by the generation or measurement of the vapor phase from the sample

Regarding solid samples, the extraction of target compounds is accomplished traditionally using Soxhlet, and it is still an official method [142]. Despite outstanding analytical performance, this method cannot be considered green (long times, high energy requirements, and high consumption of toxic organic solvents per sample). Several techniques have been proposed to improve the greenness in the extraction of solid samples, such as the solid-phase extraction (SPE), microwave-assisted extraction (MAE), ultrasound-assisted extraction (UAE), pressurized-liquid extraction (PLE), and supercritical-fluid extraction (SFE) [143-146]. Despite the clear environmental advantages over Soxhlet, these techniques still imply relatively large amounts of solvent or acids, expensive equipment in some cases, or additional steps such as clean-up procedures and/or evaporation/reconstitution stages.

Regarding the analysis of liquid samples, LLE is the conventional approach. Traditionally, organic solvents are added to the liquid sample (generally of aqueous nature), and the partition of the target analytes between organic and aqueous phases is facilitated by shaking. Then, both phases are properly separated and the organic phase is collected. Additional preconcentration steps are carried out in order to increase the sensitivity, like the evaporation of the organic solvent, and then followed of the direct injection to the chromatographic system.

Regarding the extraction of volatile or semivolatile compounds from both solid or liquid samples, or the direct sampling of gases, most frequent techniques include systems of headspace and purge-and-trap followed by GC separation. The generation of this vapor phase provides a green technique based on an easy and fast extraction procedure, followed by its direct injection. Nevertheless, the expected sensitivity is not always attained with these methods, and quantification/calibration is always complex.

Recent advances in analytical sample preparation shift to meet the requirements of GAC, while maintaining adequately analytical performance and compiling with current regulations [109,147,148]. Within this context, there has been an increasing number of studies on the development of miniaturized methodologies or in the research of new and green solvent and/or sorbent materials [109,147]. Undoubtedly, the miniaturization of conventional extraction methodologies based on solvents and/or on sorbents, while keeping good enrichment factors, precision and efficiency, constitute a scientific challenge [109].

As it has been mentioned before, the most classic sample preparation procedures include LLE, Soxhlet extraction, and SPE. Microextraction techniques arise as environmental-friendly alternatives that have been proposed to solve two great disadvantages in LLE and SPE, such as the long time required and the requirement of large amounts of toxic organic solvents [109]. In this sense, the use of low volumes of solvents (normally less than 500 µL) gives rise to liquid-phase microextraction (LPME) and their sub-modes: mainly single drop microextraction (SDME), hollow-fiber liquid-phase microextraction (HF-LPME), and dispersive liquid-liquid microextraction (DLLME). With regard to the miniaturized versions of SPE (also implying low amounts of solid sorbent, normally less than 500 mg), it is possible to distinguish the miniaturized sorbent-based microextraction method, which can be performed under static mode (static µSPE), under dispersive mode (D-µSPE), or using magnetic materials (M-D-µSPE); and the solid-phase microextraction (SPME) method, including the latter its main variants: *in-tube* solid-phase microextraction (*in-tube* SPME), stir-bar sorptive extraction (SBSE), and thin-film microextraction (TFME).

A simple search on databases shows the potential and increasing number of applications reported regarding both liquid-based and sorbent-based microextraction approaches. Figure I.14.(A) summarizes the total number of articles reported with these techniques, according to the Scopus® database. Furthermore, Figure I.14.(B) shows the percentage of the articles regarding each sub-mode for each technique. It can be noticed that the number of analytical applications of µSPE and SPME is much higher than that of LPME applications.

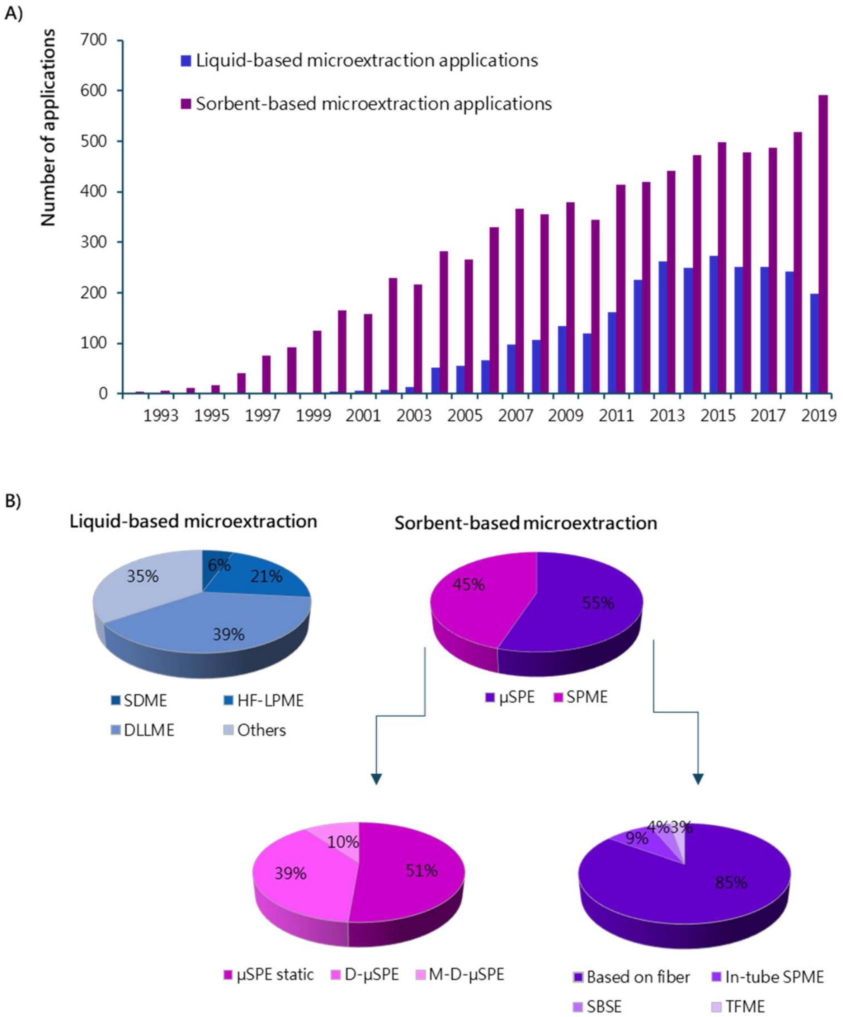

Figure I.14. **A)** Historic evaluation of the total articles reported about LPME and sorbent-based microextraction applications, and **B)** the amount of sub-modes in each type.

3.1. Liquid-based microextraction techniques

3.1.1. SDME

SDME was the first LPME mode developed. It was presented by two independent research groups. Liu and Dasgupta [149] were the first to report in 1995 a device for the measurement of gaseous NH_3 using as extractant a microdroplet suspended from a microsyringe needle. The next year, the same authors published a system [150] for the determination of sodium dodecyl sulfate extracted as an ion pair. The system permitted the submersion of a microdroplet of chloroform (~1.3 µL) in the aqueous sample which was pumped continuously. The sample was supplied by the upper part of the system, and aspirated with a tube that was located at the bottom. Concurrently, Jeannot and Cantwell [151], reported a new modality of SDME that consisted in the suspension of a microdroplet (~1.3 µL) of n-octane, containing n-dodecane as internal standard, at the end of a hollow Teflon rod. The application was the measure of equilibrium distribution isotherm of 4-methylacetophenone in aqueous sample. The rod was introduced in the aqueous sample with continuous stirring using a stir bar. The same authors described afterwards a similar method [152], suspending 1 µL of n-octane at the tip of a microsyringe needle for the study of the amount extracted of 4-methylacetophenone as a function of the time. In SDME, the typical volumes used (from 1 to 10 µL) permitted to attain high enrichment factors, given the high sample volume – droplet volume ratio, but requiring extraction times around 1 hour. Decreases in the extraction time can be accomplished using a dynamic mode (flowing the sample through the droplet) [153]. Furthermore, stirring the solution and the increase of the extraction temperature facilitate the migration of the analytes from the aqueous sample to the organic solvent, which also decrease the extraction times [153]. In most cases, the microdroplet containing extracted analytes can be injected directly in the analytical detection system, but in some cases clean-up or solvent-exchange steps are necessary.

SDME can be carried out in two modes: dipping the drop directly into the sample matrix (DI-SDME), or keeping it in the headspace (HS-SDME). It is obvious that in the first case, the extractant solvent should be immiscible with the sample matrix (most frequently, an aqueous matrix). Figure I.15. shows a representative scheme of both modes (DI- and HS-SDME), and a scheme of the dynamic mode.

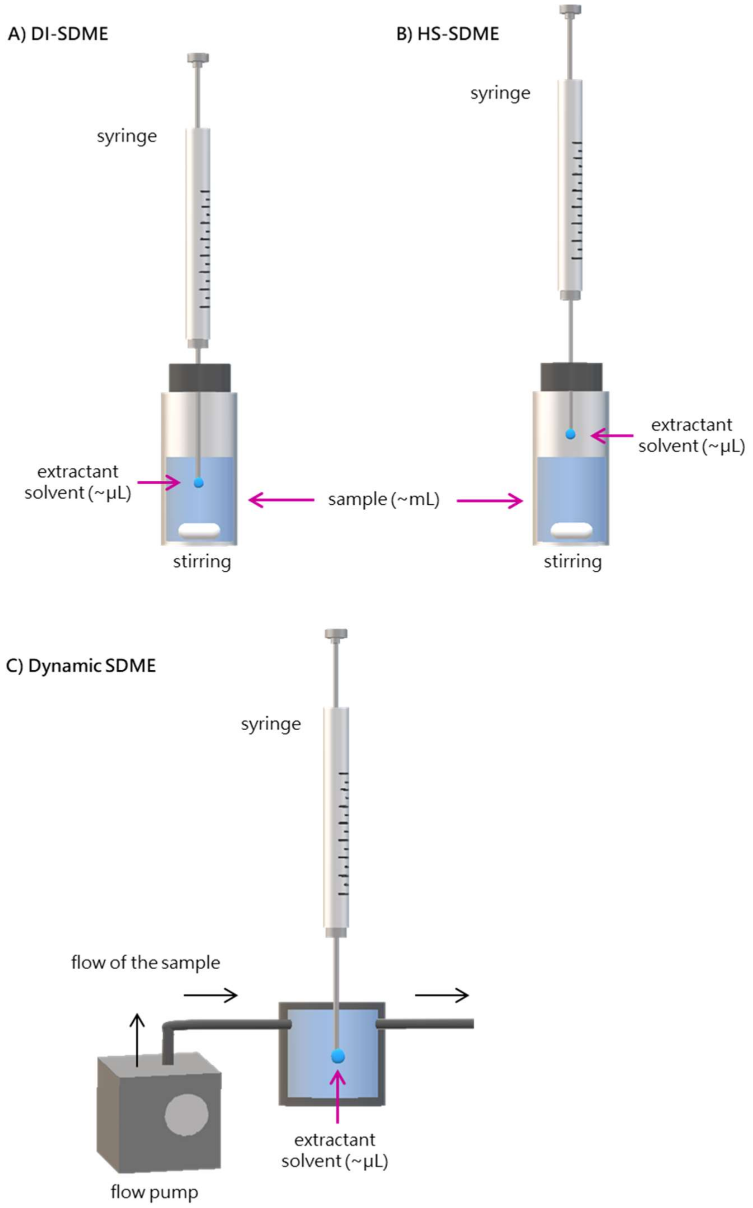

Figure I.15. Scheme of the operational sub-modes of SDME.

Like any liquid-liquid system, the analyte in organic and aqueous phases suffers an equilibrium distribution. In the case in DI-SDME, the equilibrium distribution constant, k, is defined as:

$$C_{\text{aqueous phase}} \leftrightarrow C_{\text{organic phase}} \qquad k=\frac{C_o}{C_a} \qquad \text{Equation I.1.}$$

where C_o and C_a represent concentrations of the analyte in the organic and aqueous phases, respectively. If the condition of mass balance is taken into account, for an initial amount of analyte:

$$C_{0a}V_a=C_aV_a+C_oV_o \qquad \text{Equation I.2.}$$

where C_{0a} is the initial concentration, V_a the volume of the aqueous phase, and V_o the volume of the organic phase. The equilibrium concentration in the organic phase, C_o, as function of the initial analyte concentration in the aqueous sample can be obtained by the following equation:

$$C_o=\frac{kC_{0a}}{1+k\frac{V_0}{V_a}} \qquad \text{Equation I.3.}$$

In the case in HS-SDME there are three phases, and two equilibrium distribution coefficients are involved:

$$C_{\text{aqueous phase}} \leftrightarrow C_{\text{headspace}} \qquad k_{ah}=\frac{C_h}{C_a} \qquad \text{Equation I.4.}$$

$$C_{\text{headspace}} \leftrightarrow C_{\text{organic phase}} \qquad k_{ho}=\frac{C_o}{C_h} \qquad \text{Equation I.5.}$$

$$C_{0a}V_a=C_aV_a+C_hV_h+C_oV_o \qquad \text{Equation I.6.}$$

where k_{ah} and k_{ho} are the headspace-aqueous phase and organic-headspace distribution coefficients, respectively, and C_h the concentration of the analyte in the headspace, and V_h the volume of the headspace. The concentration of the analyte in the organic phase for HS-SDME is given for the following equation:

$$C_o=\frac{K_{ao}C_{0a}}{1+K_{ah}\frac{V_h}{V_a}+K_{ow}\frac{V_o}{V_h}} \qquad \text{Equation I.7.}$$

The extraction time exerts the distribution of the analyte between the aqueous and the organic phases. In general, equilibrium conditions in LPME required prolonged extraction times. For this, proper analytical efficiencies under suitable extraction times are typically performed in non-equilibrium conditions [148]. The general kinetic equation in LPME that relates the concentration of the analyte in the organic phase with the extraction time was proposed by Jeannot and Cantwell [151]:

$$C_o = C_{o,eq}(1-e^{-Kt}) \qquad \text{Equation I.8.}$$

where $C_{o,eq}$ is the concentration of the analyte in the organic phase in the equilibrium, and K a constant expressed by the following equation:

$$K = \frac{A_i}{V_0}\beta_0\left(k\frac{V_0}{V_a}+1\right) \qquad \text{Equation I.9.}$$

being A_i the interfacial area between the phases, and β_0 the overall mass transfer coefficient for the organic phase. In this sense, it can clearly be observed that the extraction time could be minimized by increasing the interfacial area between the aqueous sample and the organic extractant.

SDME presents the following advantages compared to other microextraction techniques:

- Reduction of extraction times when using the dynamic extraction
- Quite high enrichment factors (until 1000 or more)
- Operational simplicity and few steps required
- Absence of carry over effects, since for each extraction the extractant solvent is replaced (a new microdroplet)
- Easily automated

Among the disadvantages, it can be cited that the microdroplet can fall during the extraction procedure, and low stirring rates must be used to avoid it (thus increasing the extraction time because the diffusion is slow). Furthermore, the surface of the microdroplet is too low to ensure the efficient diffusion of the compounds between the matrix sample and the extractant solvent. In addition, when highly volatile organic solvents are used as extractant, they can evaporate producing irreproducibility in the method performance. In HS-SDME, when heating the sample to favor a higher number of volatiles in the HS, the solvent of the microdroplet can also evaporate. It can be highlighted that some improvements in SDME have been reported in order to facilitate the collection of low-density extractant solvents [154,155]. For example, the solidified floating organic drop microextraction (SFOME) consists in the solidification of the organic solvent by the introduction of the sample in an ice bath. In addition, other research groups have designed a system that gets a better collection of the microdroplet [156-158].

3.1.2. HF-LPME

HF-LPME is considered a membrane-protected mode of the LPME, developed by Pedersen-Bjergaard and Rassmussen in 1999 [159]. The technique is based on the use of a porous polypropylene hollow fiber, usually sealed and containing few microliters of extractant solvent. The volume of the extractant solvent used is higher than that of SDME, due to the internal capacity of the membrane (typically between 4 and 20 µL). The membrane protects the extractant solvent from the matrix effects or possible contamination issues. Thus, HF-LPME is the most suitable LPME technique for complex matrix samples.

Attending to the number of phases involved in the procedure, the HF-LPME can be classified in two modalities:

- Two phases system (HF(2)LPME). The HF is filled with an organic solvent, impregnating also the membrane. The extraction system is composed by a donor phase (the sample), and an acceptor phase (the extractant solvent). This mode is useful for aqueous samples with a high content of suspended solids or other matrix interferences [153].
- Three phases system (HF(3)LPME). In this case, the membrane is impregnated with the extractant solvent, and the lumen of the HF contains an aqueous phase. The acceptor phase (the aqueous phase in the HF lumen) should have a different pH value respect to the sample, in order to generate a pH gradient, thus facilitating the diffusion of the target ionizable compounds [153].

The procedure can also be carried out in static or dynamic mode [153]. In the first case, the fiber impregnated with the extractant solvent is exposed in the headspace of the sample (HS-HF-LPME), or immersed directly in it (DI-HF-LPME), while the sample is being stirred. In the second case, the HF is immersed in the sample and the extractant solvent is pumped repeatedly. The dynamic mode improves the diffusion of the target analytes from the donor phase to the acceptor phase, increasing the extractive efficiency. As in the case of SDME, the extraction times are improved if the extraction procedure is combined with stirring of the sample and an increase of temperatures [153]. HF-LPME Figure I.16. shows a representative scheme of the different HF-LPME configurations as a function of the number of phases involved.

The advantage of the HF-LPME compared to the other LPME techniques relies on its applicability to complex matrix samples, especially biological samples. On the other hand, better extraction efficiencies are obtained compared with the SDME given the higher amount of extractant phase. To sum up, better stability of the extractant solvent is ensured, due to the HF support. However, the main limitation of the HF-LPME links to difficulties in its automation, which is accompanied by certain lack of reproducibility.

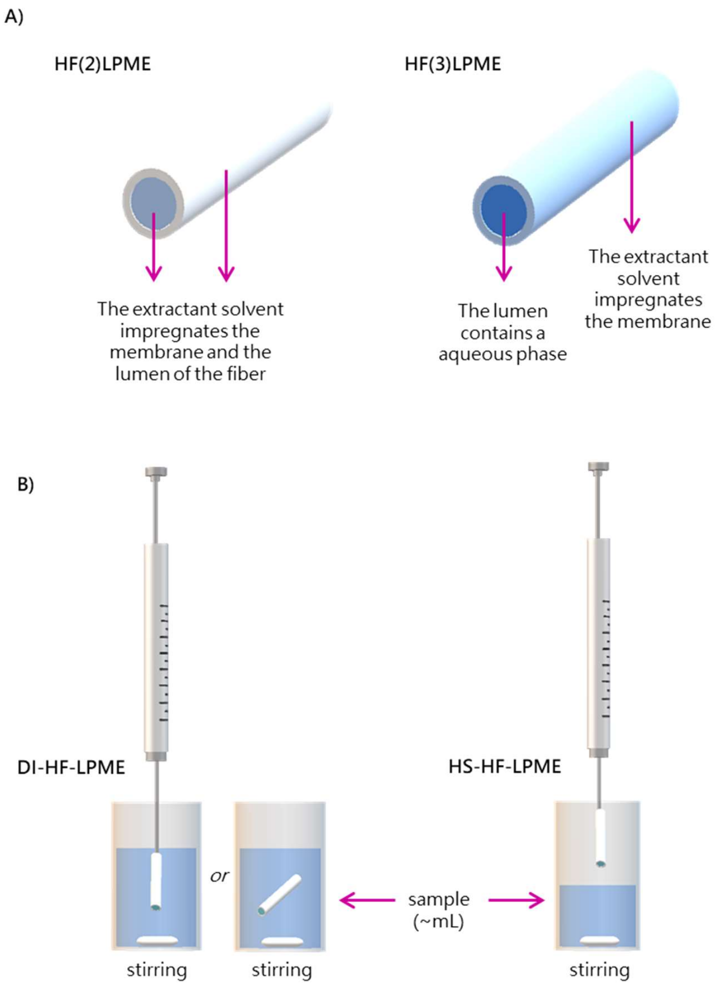

Figure I.16. Scheme of the different HF-LPME modalities. **A)** Modes according with the number of phases involved. **B)** Direct (DI-HF-LPME) and headspace (HS-HF-LPME) mode in static.

3.1.3. DLLME

In 2006, Rezaee *et al.* [160] reported a novel LPME technique based on the generation of an emulsification in an aqueous sample under the presence of two different solvents: an aqueous immiscible organic solvent (the extractant solvent) and an aqueous miscible solvent (the dispersive solvent, also miscible with the extractant solvent). The dispersive solvent is added in order to increase the interaction between the donor phase (aqueous sample) and the acceptor phase (extractant solvent), and consequently to improve diffusion of the target analytes to the solvent. Furthermore, the DLLME technique allows the use of higher volumes of extractant solvent compared to SDME and HF-LPME, thus ensuring higher extraction efficiencies. These volumes usually range between 20 and 250 µL for the extractant solvent, and between 0.1 and 2 mL in the case of the dispersive solvent. With regard to the nature of the solvents, the extractant solvents most commonly used are organic solvents highly non-polar, and the dispersive solvents are normally acetonitrile, acetone, methanol, or ethanol. The aqueous sample to perform DLLME is in the order of several mL: frequently between 4 and 20 mL. Such mixture of solvents in DLLME ensures the formation of many microdroplets due to the emulsion. The next step of the procedure consists in the obtaining of a final microdroplet formed by the extractant solvent and containing the preconcentrated analytes, which can be separated from the aqueous phase by centrifugation in most cases. Figure I.17. shows a representative scheme of the procedure.

In some cases, the microdroplet is formed quickly (few seconds) and it separates by gravity, without need to apply centrifugation [148,155]. Depending on the nature of the extractant solvent, the microdroplet will form on the top (if non-halogenated solvents are used) or the bottom (if halogenated solvents are used) of the tube. The organic phase (the microdroplet) is finally sampled with a syringe and injected directly in a GC, or re-dissolved in a compatible solvent and injected in a LC. Combinations of the droplets with spectroscopic techniques are also common, and the droplets can be aspirated, and the analytes measured by atomic absorption spectroscopy (AAS) [153].

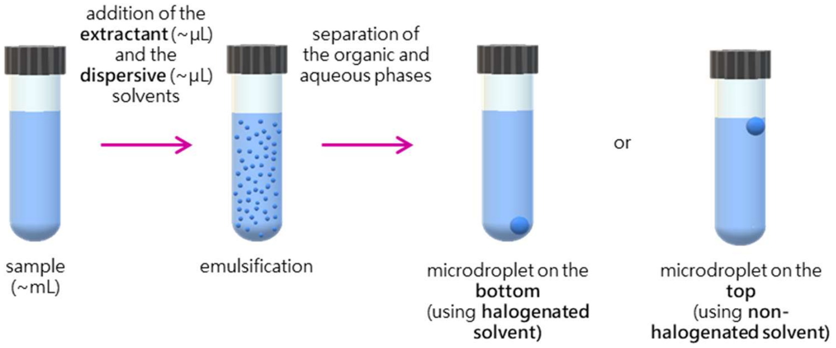

Figure I.17. Scheme of the DLLME procedure.

Among all the LPME modes, DLLME is the most successful given its advantages:

- Fastness, implying analysis times lower than several minutes, due to the easy diffusion of the target analytes into the emulsion generated
- Quantitative recoveries obtained in most cases (SDME and HF-LPME are non-exhaustive extraction techniques)
- Simplicity of the entire procedure (simple mixing of solvents)
- Low cost required and the absence of any special device to proceed
- Easily compatible with both GC and LC

Its limitations include the difficulty of the handling of the final microdroplet formed, and that its automation requires advanced and expensive instrumentation. In addition, the extractant solvent can be partially dissolved in the aqueous sample because the dispersive solvent increases its solubility in it, and thus there are consequently losses of enrichment factor. When intending the applicability of the technique to highly polar analytes, previous derivatization steps are required (steps that are against GAC principles). Undoubtedly, another disadvantage of the DLLME is the low selectivity of the conventional extractant solvents used. Finally, DLLME is not recommended for the monitoring of analytes in complex samples, since there is a direct contact between the extractant and the sample, which increases the contamination given the presence of undesirable interferences.

3.2. Sorbent-based microextraction techniques

3.2.1. µSPE

SPE is the most popular extraction and clean-up technique worldwide due to its high efficiency and simplicity, having its principles based on LC partitioning [153]. In its more conventional mode, the aqueous sample is passed through the solid sorbent previously conditioned, which is packed in a cartridge. Then, the sorbent is washed to remove the undesired components, and finally the analytes which were successfully retained in the sorbent are eluted using an organic solvent and subjected to determination. The first application of its miniaturized version (µSPE) was introduced in 2006 [161]. This static mode of µSPE implies the use of sorbent amounts lower than 500 mg, ensuring in this way a further consumption decrease of organic solvents in the elution step of the compounds retained. New µSPE formats, such as micro-disks and micro-columns, are able to support in many cases high sample flows, and consequently the analysis time decreases highly. Figure I.18. shows typical supports used in the static µSPE mode.

Additional versions of µSPE have been developed in order to improve the analytical performance [162]. The dispersive version of the µSPE (D-µSPE) is particularly useful because it allows an efficient diffusion of the target compounds between the sample and the sorbent material, and in addition drawbacks related to the packaging are solved. Nowadays, there are a large number of D-µSPE due to the good extraction efficiency that it can be obtained by this technique, becoming one of the most useful procedures used in microextraction approaches. This dispersion can be assisted by different forms: magnetic stirring, manual shaking, vortex, and ultrasounds. Nevertheless, vortex and ultrasounds can cause degradation of the target analytes or even that of the extractant sorbent. Magnetic materials as sorbents have been introduced, and the resulting extraction technique is named magnetic and dispersive based µSPE (M-D-µSPE). The use of magnetic sorbents clearly facilitates the separation of the sorbents containing the analytes extracted from the aqueous samples, by simple use of an external magnetic field (a strong magnet placed in the outer part of the extraction recipient). This way, centrifugation and/or filtration steps are avoided, permitting a high decrease of the analysis times while decreasing sources of errors. Figure I.19. shows the general scheme of the three different dispersive modes of µSPE.

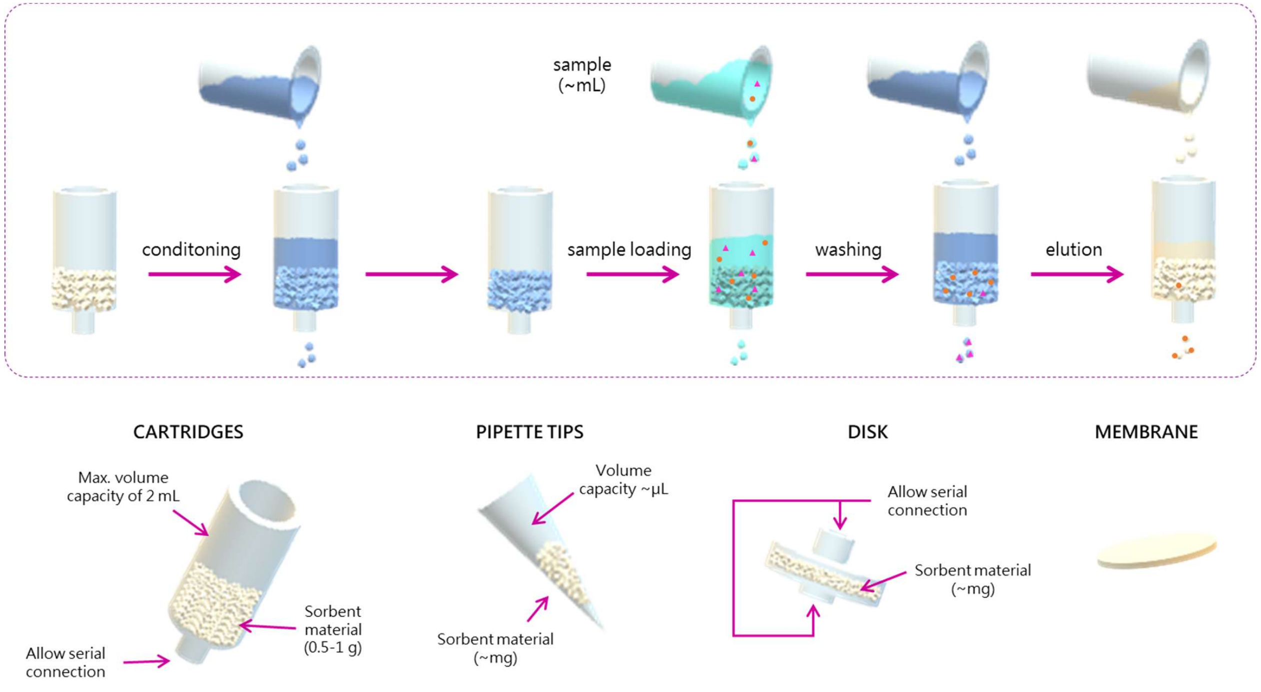

Figure I.18. General procedure of SPE totally applicable to µSPE and supports used in static µSPE approaches.

The main advantages of µSPE *versus* other sorbent-based microextraction techniques are:

- The effectiveness in the extraction of target analytes in complex matrix that contains suspensions or semisolids, which imply that preliminary filtration steps can be eliminated
- High enrichment factors
- Reduction of costs given the minimization of reagents required (sorbent and elution/desorption solvents)
- Possibility of reuse of the extractant sorbent
- Easiness of the procedure (particularly in the magnetic version)
- Reduction of the analysis times

Satisfactory analytical performances have been obtained in all the miniaturized versions of SPE, and at the same time compiling the requirements of the GAC principles. Among its disadvantages, irreversible adsorption in the extractant sorbent of some compounds can occur.

An important improvement in µSPE has been the emerging of lab-on-chip and microfluidics instrumentation [108]. Online µSPE previous to chromatographic analysis, which allows the use of nanoliter volumes of both samples and solvents [108], thus allowing truly GAC conditions.

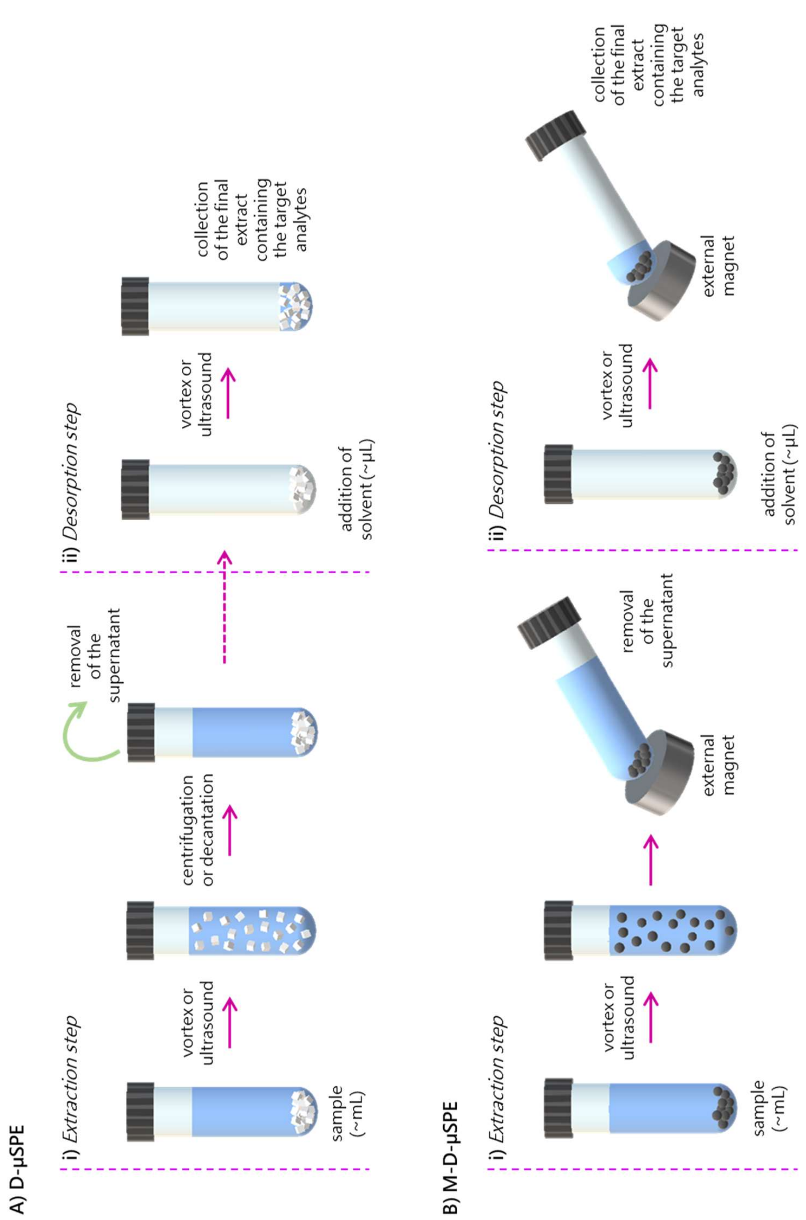

Figure I.19. Scheme of the different dispersive modes of the µSPE technique. The sorbent (few mg) is represented as squares in D-µSPE and as circles in M-D-µSPE.

3.2.2. SPME

SPME is a non-exhaustive extraction technique developed by Pawliszyn and coworkers in 1990 [163], based on the use of fused silica or metal fibers with 100 or 250 μm and coated with a sorbent of 1 cm of length and few μm of thickness. The technique is based on the distribution equilibrium of the analyte between the sample matrix to the sorbent. Operationally, the technique can be carried out in two modes according to the type of extraction: by direct immersion of the fiber into the aqueous sample (DI-SPME), or by exposing the fiber to the headspace (HS-SPME). The second step of the technique, the desorption of the analytes adsorbed in the fiber coating, is accomplished thermally in the injection port of a GC, or by desorption using low volumes of organic solvent. This last option generally involves further combination with LC. In order to increase the lifetime of fibers, the sub-mode based on membranes protecting raised in 2009 [164], being called hollow-fiber SPME (HF-SPME). Figure I.20. shows the general scheme of the different modalities of SPME using fibers.

When the partition of the analyte to the sorbent relies on an **absorption** mechanism in the DI-SPME mode, the distribution of the amount of one analyte A between the sample matrix (A_{matrix}) and the fiber coating ($A_{fiber\ coating}$) can be expressed by the following equation:

$$A_{matrix} \leftrightarrow A_{fiber\ coating} \qquad K_{mf} = \frac{C_f}{C_m}$$ Equation I.10.

where K_{mf} is the distribution constant of the analyte A between the sample matrix and the fiber, C_f is the concentration of the analyte A in the fiber coating, and C_m is the concentration of the compound A in the sample matrix. In the equilibrium, the amount of the analyte is constant in each phase, and can be described by the following equation:

$$n = \frac{C_0 V_m V_f K_{mf}}{V_m + V_f K_{mf}}$$ Equation I.11.

where n is the total amount of the analyte A extracted by the fiber coating, C_o is the initial concentration of the analyte A in the sample matrix, V_m is the volume of the matrix, and V_f is the volume of the fiber coating.

If the extraction relies on an absorption mechanism but in HS-SPME mode, two distribution equilibrium of the analyte A are considered: between the sample matrix and the headspace, and between the headspace and the fiber coating. The distributions of the amount of the analyte A in the sample matrix (A_{matrix}), the headspace ($A_{headspace}$), and the fiber coating ($A_{fiber\ coating}$) can be expressed by the following equations:

$A_{matrix} \leftrightarrow A_{headspace}$ $\quad K_{mh}=\frac{C_h}{C_m}$ Equation I.12.

$A_{headspace} \leftrightarrow A_{fiber\ coating}$ $\quad K_{hf}=\frac{C_f}{C_h}$ Equation I.13.

where K_{mh} is the distribution constant of the analyte A between the sample matrix and the headspace, K_{hf} is the distribution constant of the analyte A between the headspace and the fiber coating, C_m is the concentration of the analyte A in the sample matrix, C_h is the concentration of the analyte A in the headspace, and C_f is the concentration of the compound A in the fiber coating. In the equilibrium, the amount of the analyte is constant in each phase, and can be described by the following equation:

$$n=\frac{C_0V_mV_fK_{mh}K_{hf}}{V_fK_{mh}K_{hf}+V_hK_{mh}+V_m}$$ Equation I.14.

where n is the total amount of the analyte A extracted by the fiber coating, C_o is the initial concentration of the analyte A in the sample matrix, V_m is the volume of the matrix, V_h is the volume of the headspace, and V_f is the volume of the fiber coating.

When the partitioning relies on an **adsorption** mechanism given the nature of the fiber coating, much complex equations are involved in DI-SPME and HS-SPME [165], because there is a competition of the different target analytes for the active fiber sites.

Regarding the nature of the support of the SPME coatings, original fused silica has been replaced with metal supports in order to increase the lifetime of the fibers. These improvements are commercially available with special metal alloy in the needle, plunger, and fiber core (support) [166].

SPME is considered a true solventless miniaturized technique (particularly certain when combined with GC), able to isolate (and preconcentrate) the target analytes from the matrix (aqueous matrix in DI-SPME and any type of matrix in HS-SPME) in one step. Together with its impressive greenness characteristics, its great success also relies on:

- The simplicity of the method, allowing the extraction/preconcentration of the target analytes and their injection using one device in only two simple steps: extraction (exposure to the sample) and desorption (expose to the desorption system).

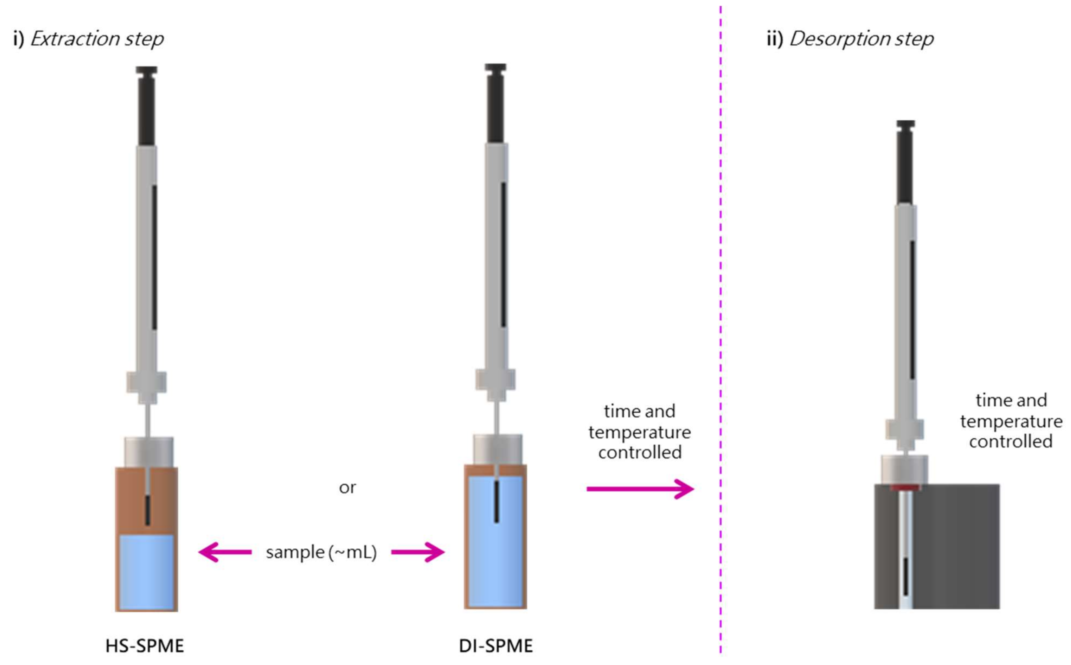

Figure I.20. Different operational modes of the SPME technique. The desorption step is represented in this case with a GC injector. Offline desorption modes have not been plotted.

- The commercial availability of 6 polymer coatings in various thicknesses: carbowax-polyethylene glycol (CW-PEG), carboxen/polydimethylsiloxane (CAR/PDMS), divinylbenzene/carboxen/polydimethylsiloxane (DVB/CAR/PDMS), polydimethylsiloxane/divinylbenzene (PDMS/DVB), polyacrylate (PA), and polydimethylsiloxane (PDMS).
- The fully automation of the complete method, in both GC and LC, when using autosamplers.
- The possibility of *in-situ* measurements [108].

The limitations of this technique are associated mainly to the number of coatings available and the long extraction times required (around roughly 1 h per sample, but this is minimized by the automation aspect) [108]. First, although the availability of commercial coatings is relatively broad for the extraction of polar and non-polar analytes, this is not enough to cover the wide variety of emerging contaminants with different nature present in the environment. Second, there can occur competitive adsorption in porous coating fibers. The amount of analyte that is extracted depends on the distribution coefficient between the coating and the sample matrix, and between the air and the sample matrix (the Henry's law constant). Consequently, one analyte present in high amounts in the sample can prevent the adsorption of other analytes that are present at low concentration levels. Third, the polymeric nature of the coating, a viscous material, requires long periods of time in the extraction step to ensure the distribution equilibrium of the compounds. Consequently, sometimes the equilibrium is not attained. In any case, it is possible to work at extraction times lower than the equilibrium time if the preconcentration achieved is sufficient, as long as the extraction time is kept constant for samples and standards [167]. Finally, carryover effects can be associated to the extraction of non-volatile analytes, which could generate irreproducibility in the method. This aspect is particularly significant when working with LC and CE, because the offline desorption in static mode with organic solvents is less efficient than the thermal desorption in GC.

Several modifications of the coating materials and supports have been proposed to improve the stability and the efficiency of the technique. The incorporation of novel materials is an outstanding research area nowadays, in this and other analytical sample preparation methods [147], and thus will be specifically described in Section I.3.2.3. Among the modifications of the technique, it is important to highlight *in-tube* SPME, TFME, and SBSE, which are normally classified as independent sorbent-based microextraction methods.

In-tube SPME

In-tube SPME was introduced by Eisert and Pawliszyn in 1997 [168], and it implies the use of a coating as extraction phase inside an open tube (covering its internal walls), in order to facilitate the automation in LC instrumentation. The modalities can be classified in two: the dynamic mode, if the analytes are passed through the tube by pumping of the samples or under gravitational flow using needles or tubes, and the static mode, if the analytes are transferred into the sorbent by diffusion. Anyway, the coating is supported on a fused-silica rod or inside of tube or capillary. Figure I.21. shows general considerations and a scheme of the technique.

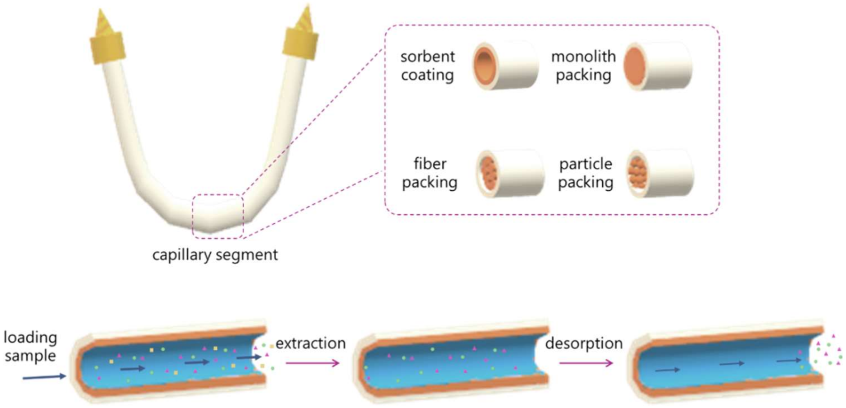

Figure I.21. Different sorbent coating approaches of the *in-tube* SPME technique.

The main advantage of *in-tube* SPME is its easy automation. Additionally, *in-tube* SPME also improved the extraction efficiency and mainly the sensitivity of those methodologies based on the combination SPME with LC (because the offline desorption of conventional fibers with organic solvents is always accompanied by a loss of preconcentration). Furthermore, it can overcome the drawbacks associate to conventional SPME fiber, such as fragility, low sorption capacity, and typically bleeding of the fiber coating [147]. It can be expected that the sensitivity can improve using longer tubes and, at the same time, increase amount of sorbent. Among their limitations, it is necessary to prevent plugging of the capillary column and flow lines during the extractive procedure, normally performing a previous filtration of the samples [108].

SBSE

SBSE is another variant of SPME, which can be even considered a variant of TFME, developed in 1999 [169], that consists in the use of a magnetic cylindrical bar coated with a polymer, typically a thin layer of PDMS. The bar is stirred directly in the aqueous sample during the extraction procedure, in order to facilitate the distribution of the target analytes between the matrix sample to the extractive material (Figure I.22.). Nowadays, the stir bar is commercially known as Twister® (Gerstel commercial brand) [170], and there are two dimensions available (10 or 20 mm length) for two types of coating (PDMS and PDMS/ethylene glycol copolymer) and in two thickness (0.5 or 1.0 mm).

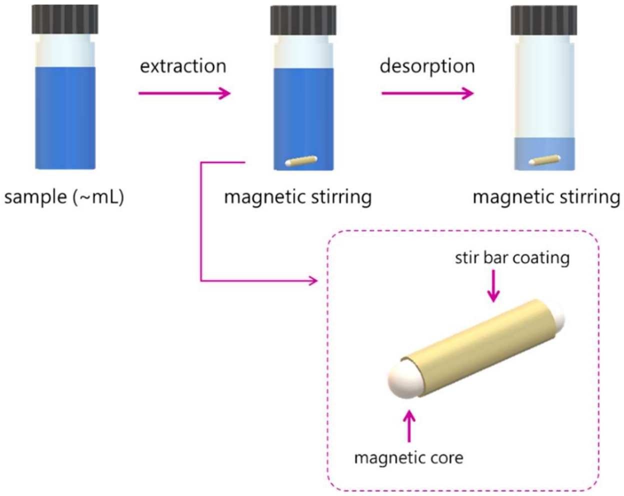

Figure I.22. Scheme of the general procedure of the SBSE technique.

The desorption step can be carried out thermally, by the commercial thermal desorption unit (TDU, also from Gerstel), or performing a back extraction step with a low volume of an organic solvent (liquid desorption). The latter is applied to those methodologies that involve the determination of non-volatile or thermal labile compounds from aqueous samples. Generally, liquid desorption is performed with non-polar solvents if GC analyses is going to be used, or polar solvents if the combination is with LC. After desorption, proper cleaning of the stir bar is needed to minimize carry-over.

Regarding advantages of SBSE with respect to other sorbent-based microextraction techniques, SBSE is more sensitive for low polar compounds due to the higher volume of the coating respect to conventional SPME [171]. The main disadvantage is its limitations for the extraction of polar analytes, because only stir bars with coatings based on PDMS are commercially available.

TFME

Several geometries of the SPME fiber have been proposed with the objective of increasing the amount of extraction phase exposed without increasing the thickness [172]. A simple increase in the thickness of a conventional fiber is normally accompanied by longer extraction times, which is detrimental for GAC. Thus, thin film SPME (TFME), developed in 2003, increases the support area, while keeping thin films of coatings. This simple strategy allows for higher surface exposed while keeping the extraction times to typical ones of conventional SPME. Thus, different supports have been developed for the performance of TFME, like thin film on a blade support (96-blade blade configuration), arrow, and in-tip, have been developed for TFME [173], as it is indicated in Figure I.23.

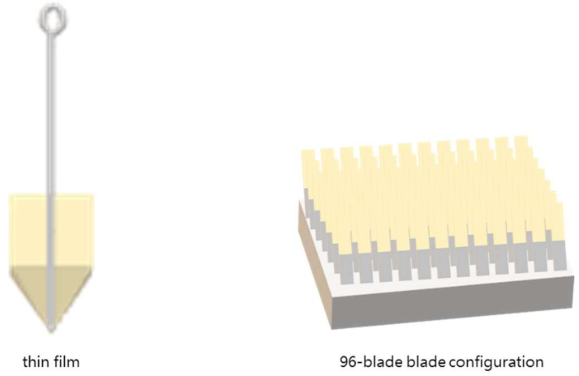

Figure I.23. Typical supports developed for TFME technique.

The advantages of TFME *versus* conventional SPME include fastness, and quite high enrichment factors given the increasing amount of sorbent material. However, the geometry of the TFME devices are still limited in online applications, and the autosamplers to perform both extraction and desorption using TFME have not been developed yet.

3.2.3. Novel materials in sorbent-based microextraction techniques for water samples

Despite the improvements mentioned before, mainly developed in the last decade, regarding sample preparation approaches, together with simultaneous advances in analytical instrumentation, there is still a requirement of improving the extraction efficiency of the analytical methodologies. Particularly in the field of analytical sample preparation, conventional materials present some limitations to address current applications, such as the low selectivity (especially regarding high polar analytes), and even low efficiency when incorporated to many microextraction methods.

Advances in sorbent-based microextraction techniques have taken place in most cases with parallel research on new materials to be used as microextraction sorbent materials [174-176], thus somehow justifying the higher number of applications developed in the last decades compared to that of liquid-phase microextraction approaches (Figure I.14.).

The requirements that a novel material should ideally fulfil to be an adequate sorbent to be incorporated in a sorbent-based microextraction method include: simple preparation, cheap preparation, low toxicity, high surface area, simple chemical tuneability, ability to interact with analytes of quite different nature or selectively with a target compound, ability to ensure a fast physical and chemical equilibrium when interacting with target analytes, and chemical and thermal stability.

Among all the solid sorbent materials reported in analytical microextraction, it is important to highlight the following ones: molecularly-imprinted polymers (MIPs) [177], carbon-based nanomaterials [176], metallic nanoparticles (metallic NPs) [178], anchored ionic liquids (ILs) – thus ensuring their solid nature - and solid derivatives [179], and metal-organic frameworks (MOFs) [162,180].

Molecularly-imprinted polymers (MIPs)

MIPs are tailor-made materials with recognition sites able to guest specific compounds [181]. Wulff and Sarham were the first to develop MIPs with selective sites for glyceric acid enantiomers [175]. MIPs are fabricated by the polymerization of two type of monomers (the functional and the cross-linkers) in the presence of the template molecule, leading to a highly cross-linked polymer. The polymerization is usually induced by thermal or UV radiation. Later, the template molecules are removed by different strategies, and permanent recognition sites are left in the polymeric structure with this removal. These tailored recognition sites, given their shape, size, and functionalities allow to increase the preferential extraction of the target analytes (or compounds with quite similar structures to that of the target compound). Figure I.24. shows a scheme of MIP, including the most representative monomers, cross-linkers, and templates of MIPs used in analytical approaches.

MIPs characterize for their stability and robustness. They are resistant to a wide range of pH values, presence of organic solvents of different nature, and are even thermally stable at relatively high temperatures. All these characteristics justify the interest on MIPs in analytical extraction methods, because they can provide great advances in selectivity, simplicity in the procedures by avoiding other clean-up steps, and reduction of interferences in the final extract thus ensuring the absence of overlapping chromatographic peaks and matrix effects [182].

However, the compatibility of the MIPs with water or polar solvents and the incomplete removal of the templates are the main drawback of the sorbents [174]. The main interaction of MIPs with target analytes is normally accomplished through H-bonds, and thus such interaction is highly influenced when water is involved (in other words, water can reduce the recognition ability of many MIPs). Clearly, a material with poor water compatibility is not adequate in the monitoring of pollutant in water samples. Furthermore, many desorption steps in sorbent-based microextraction methods are accomplished with solvents of certain polarity, and thus the MIP should have better compatibility with them. This limitation can be improved with the introduction of hydrophilic functional groups in their structures, but this is not always complete neither quantitative [183]. On the other hand, the incomplete removal of the templates when preparing the MIP material will further reduce the accuracy and the performance of the entire microextraction method, because there is a reduced number of adsorption sites in the MIP.

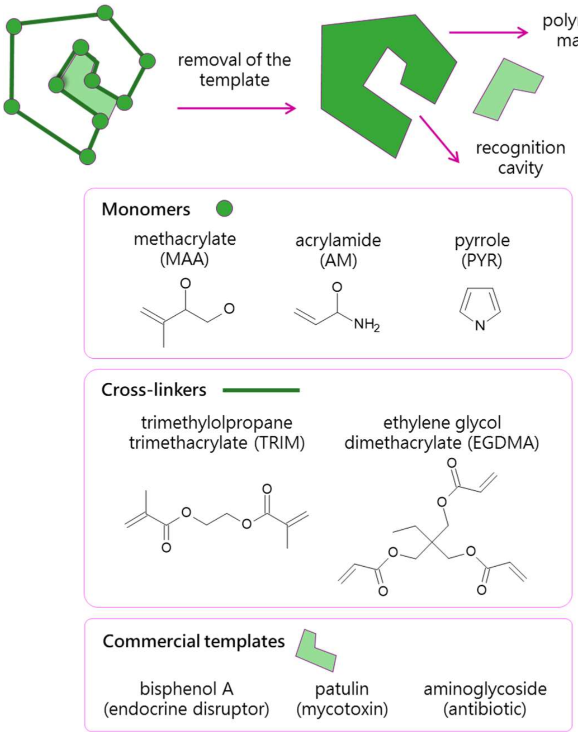

Figure I.24. Scheme of a MIP with several representative structural units.

MIPs have been widely and successfully applied in biological analytical methods and in the treatment of other complex samples, given their excellent selectivity [184,185]. In environmental analytical applications, trends have moved to the development of new devices or supports for these materials. Thus, MIPs have been used in SPE-cartridges [186,187], but these applications require large amounts of organic solvents to ensure proper elution through the compact packing of MIPs in the SPE devices [181]. Other devices for MIPs include filters [188], tips of micro-pipettes [189], SPME fiber coatings [190,191], *in-tube* SPME [192], and SBSE [193], all devices for the analysis of water samples. Several applications also report the use of MIPs in D-µSPE [194]. Magnetic MIPs have been employed in M-D-µSPE when combined with magnetic nanoparticles of magnetite, taking advantage of all features associated to magnetic materials [195-198]. MIP monolith containing magnetic nanoparticles has been also used [199], and the monolith was also successfully employed in D- µSPE [182].

Carbon-based nanomaterials (CNMs)

Main allotropes of carbon used as sorbents in analytical sample microextraction include: fullerenes, carbon nanotubes (CNTs), graphene, and graphene oxide (GO). Figure I.25. shows different allotropic forms of carbon-based nanomaterials. CNMs characterize for certain special properties, regardless of its allotropic form: thermal stability, high specific surface area, adequate thermal conductivity, and tuneable surface properties [174].

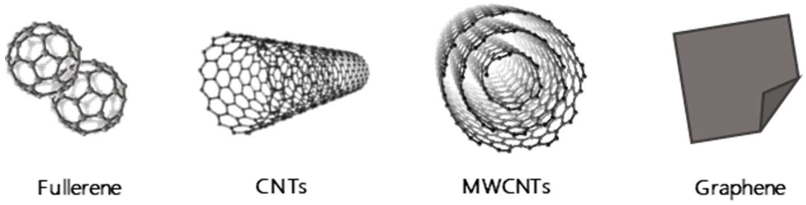

Figure I.25. Main allotropic forms of carbon-based materials used as sorbents in analytical microextraction approaches.

The first CNM material was reported in 1985 by Kroto [200]; but the first application of a CNM material as sorbent in SPE was reported in 1994 by Gallego *et al.* [201]. Since then, the development and the application of these materials as sorbent materials have increased significantly.

Fullerenes are polyhedral nanostructures composed by five and six membered rings of sp^2 carbons forming an icosahedral polygon. Fullerenes are characterized by their low tendency to form aggregates, thus presenting adequate features for SPE procedures (packed material). Despite the satisfactory surface area and the low electron delocalization of the material, its low water solubility is the main limitation justifying the reduced number of applications as sorbent in analytical sample microextraction [202].

CNTs can be referred as graphite sheets rolled up into tiny tubes. They can be classified as single-walled carbon nanotubes (SWCNTs), with tube diameters between 0.2 and 2 nm, and multi-walled carbon nanotubes (MWCNTs), with diameters between 2 and 100 nm. Lengths of the tubes are from 0.5 to 50 µm. Thus they combine nanoscale properties given their diameter, with microscopic properties given its length, in other words, a useful nano-micro combination. MWCNTs include two or more cylindrical shells of graphene, connected together by Van der Walls forces. All CNTs present good electrical properties, large surface area, and high mechanical and thermal stability [202]. However, among their disadvantages, these materials also present low water solubility as fullerenes. Furthermore, their cylindrical form somehow reduces the available surface to interact with target analytes. The chemical modification of CNTs with specific functional groups has been also adopted, intending this way to increase the selectivity and availability of these materials. First applicability of CNTs as sorbent material in an analytical extraction took place in 2003 [203], and nowadays these carbon materials are the most widely used in microextraction among all the CNMs, particularly for the analysis of environmental samples [204], and particularly when using MWCNTs [205], chemically modified [206] or not.

Graphene is a thin honeycomb two-dimensional lattice of carbon atoms. Since it was discovered in 2004 by Geim and Novoselov [207], graphene has been a highly interesting material in many scientific fields, not only in analytical sample preparation, due to its physical and chemical properties, such as mechanical resistance, large delocalized electron system, thermal and electrical stability, and outstanding nano-micro properties [202]. There is also a group of characteristics that make them quite attractive sorbents in microextraction when compared with other CNMs: much higher surface area, low cost, easy synthesis, and feasibility for post-synthetic chemical functionalization. Furthermore, graphene offers a strong affinity for π-π interactions, which it is proper for the selective extraction of pollutants that contains aromatic rings in their structure.

In many aspects, GO, obtained from the oxidative conversion of graphene, is a more versatile material. Like graphene, GO is a monolayer of two-dimensional carbon-based materials, but it also contains multi-functional groups, such as carboxyl, epoxy, ketone and hydroxyl groups. The main advantage of GO is that it is quite simple to have its surface full of activate sites, thus enhancing its selectivity.

The most frequent format of usage of CNMs is in SPE cartridges [208-210], although there are also D-µSPE applications [211,212], including the magnetic version M-D-µSPE [213,214]. CNMs have been also employed in the fabrication of SPME fibers to provide more stable coatings [174]. As examples, hybrid materials based on CNTs [215], neat graphene [216], and modified GO [217,218] have been employed as sorbent coatings in SPME for the monitoring of pollutants in water samples.

Metallic nanoparticles (metallic NPs)

Metallic nanoparticles (metallic NPs) can involve different inorganic and inorganic/organic hybrid nanoparticles, such as metal NPs, metal oxide NPs, and magnetic nanoparticles (MNPs). Metallic NPs are quite interesting materials given their properties derives from the nanosized, together with adequate surface are and mostly simple synthesis [176]. In general, most neat metallic NPs (metal NPs and metal oxide NPs) are poor stable and lack of selectivity through target analytes [219]. MNPs present the same properties, but its strong paramagnetic behaviour together with their easy surface modification (which further permit their stabilization), justify the large number of applications compared to metallic NPs [220,221]. Figure I.26. shows the structure and TEM images of widely used metallic NPs, and MNPs based on magnetite (α-Fe_3O_4).

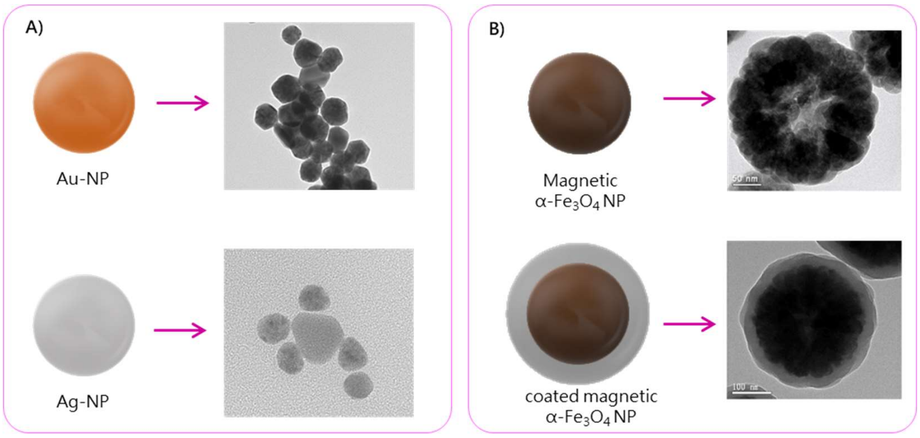

Figure I.26. Representative forms and TEM images of **A)** metallic NPs and **B)** MNPs widely used in sorbent-based microextraction applications. TEM images of magnetic NPs are adapted from [221].

Inorganic metal NPs refer mainly to gold-based NPs (Au-NPs), and silver-based NPs (Ag-NPs). Metallic NPs have been used as coatings for SPME applications [222-225], and also in *in-tube* SPME [226].

Among the metal oxide NPs, it is important to highlight TiO_2, Al_2O_3, ZnO, ZrO_2, MnO and CeO_2. In general, these oxides in their nanosized form present higher thermal, mechanical and chemical stabilities. TiO_2 NPs have been particularly useful for the extraction and preconcentration of metal ions at trace levels from waters [219]. Metal oxide NPs are also employed after proper functionalization or after being coated with polymers, forming hybrid materials as sorbents in microextraction [227,228].

MNPs present poor stability and form easily large aggregates, altering their magnetic properties, while being labile to oxidation. MNPs are commonly used as the core material in M-D-µSPE approaches, normally being coated with silica, polymers, or a variety of sorbent materials, in all the cases with the purpose of increasing the lifetime of the MNPs while keeping their magnetism, while also incorporating additional materials able to interact more selectively with target analytes. MNPs are composed mainly of iron, nickel, cobalt, and their corresponding oxides. The most frequent MNPs used in microextraction are magnetite (α-Fe_3O_4) and maghemite (Fe_2O_3), due to their low cost and toxicity. In general, MNPs coated with silica [229], polymers [230], zeolite [231], surfactants [232], or even ionic liquids [233], have been successfully employed in M-D-µSPE applications intended for pollutants in water samples.

ILs anchored to a surface and polymeric ionic liquids

ILs are salts in liquid state at temperatures below the boiling point of water (100 ºC at atmospheric pressure), and are referred as non-molecular solvents. Those ILs that melt at room temperature are named room-temperature ionic liquid (RTILs). They are formed by an organic cation (asymmetrically substituted in most cases) and an organic (or inorganic) anion. Typical cations are imidazolium, pyridinium, pyrrolidinium or quaternary ammonium; while the anions commonly used are trifluoromethylsulfonate, trifluoroethanoate, Cl^-, Br^-, and PF_6^-. An IL can present only one cation (in most cases), but ILs can also be di-cationics, tri-cationics, and also multi-cationics [234]. Figure I.27. shows the most representative cations and anions that form ILs, and a representative polymeric IL (PIL).

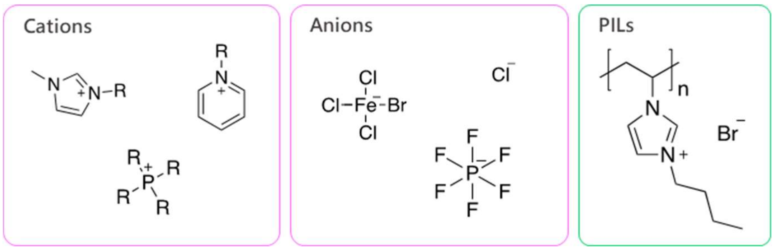

Figure I.27. Representative cations and anions that form the ILs most commonly used in analytical microextraction methods, and one representative PIL.

ILs are characterized by a wide liquid range and a negligible vapor pressure at room temperature. They are also considered as designer solvents, due to the almost unlimited possibility of combining anions, cations, and alkyl substituents in cations to form them. ILs are easy tunable: simple changes in the cation, in the anion, or a simple modification of any of the substituents, can modify significantly the melting points, the density, the polarity, the viscosity, and even their miscibility with organic solvents or with water [235]. Although, the first IL was discovered in 1914 [236], it was not until 1992 that analytical chemistry started to incorporate ILs [237]. Their successful use as extraction solvent is due to their ability to establish interactions with target compounds through hydrophobic/hydrophilic interactions, hydrogen bonding, π-π, ion exchange, or electrostatic interactions, among others.

Clearly, neat ILs cannot be used in sorbent-based microextraction approaches given their liquid nature (and indeed most of their applications are in the LPME field [238,239]). However, ILs-based sorbents have been developed, being confined in porous structures [240] or chemically attached to solid supports [233,241]. Furthermore, polymeric ILs (PILs), formed by polymerization of IL monomers, being solid in nature, have been also used in sorbent-based microextraction [242]. PILs characterize for presenting those properties inherent to ILs (high solvation ability) together with that of polymers [243].

Among the hybrid materials based on ILs, CNs-based supports have been used as support of ILs for the analysis of water samples for online SPE application [244]. ILs have been anchored to silica to perform D-μSPE applications [245]. They have been also used in M-D-μSPE using

MNPs as core [246], or anchored to silica coating Fe_2O_4 [247]. Magnetic NPs coated with PILs have also been successfully employed in M-D-μSPE [248]. Regarding the use of ILs in SPME, PILs have been an outstanding material, also employed in many applications for emerging contaminants in water samples [249-252]. Furthermore, the fabrication of a fiber-*in-tube* device coated by an IL has been also described in combination with LC for an online analysis [253]. Other online approaches incorporating ILs include IL-based monolith by *in-tube* SPME [254]. PILs in μSPE have been also employed, specifically in a tip device where the PIL was *in-situ* prepared [255], or stir-cake device (a mode of SBSE) for the analysis of environmental water [256]. An interesting approach developed by the group of Chisvert used a stir-bar coated with a magnetic IL (MIL) followed by the direct desorption of the analytes in a thermal desorption unit [257,258].

Metal-organic frameworks (MOFs)

MOFs are microporous crystalline polymers with a highly ordered three-dimensional structure, that present unique and excellent characteristics. MOFs were developed in the nineties by different groups: Robson [259], Kitagawa [260], Yaghi [261], and Férey [262], but the "MOF" term was coined by Yagui and Li in 1995 [261]. They are composed by an inorganic secondary building unit (SBU), metal ion/s or metal/s cluster, and an organic linker (or more than one linker) connected by coordination bonds, which provided an exceptional porosity and impressive surface areas. Figure I.28. shows the structures of representative MOFs.

From a theoretical perspective, there is almost an infinite number of possible combinations to form MOFs by varying the SBUs. In fact, more than 20,000 different MOFs have been registered in the Cambridge Structural Database (CSD); and many of them have been prepared for a wide range of applications. The interest on MOFs is associated to their unique structural characteristics, that are accompanied by:

- Tuneability
- Possibility of post-synthetic modifications and functionalization
- High porosity (pore volumes up to 100 Å)
- Thermal resistance (from 200 to 500 ºC in many cases) and mechanical stability
- Low crystal densities (even down to 0.13 $g{\cdot}cm^{-3}$)
- High surface area (from 200 to 10,000 $m^2{\cdot}g^{-1}$)

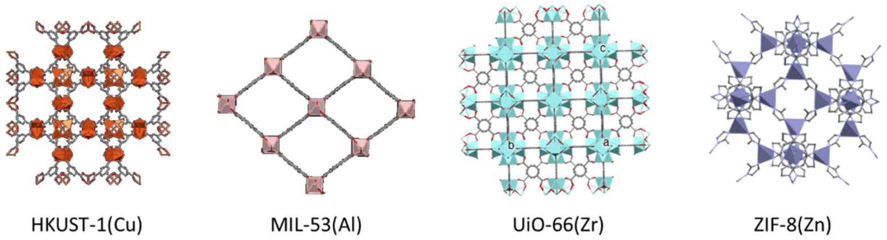

Figure I.28. Representative MOFs: HKUST-1(Cu), MIL-53(Al), UiO-66(Zr), and ZIF-8(Zn).

Many different routes have been described to prepare MOFs, in all cases following crystallization approaches (solvothermal, microwave-assisted, electrochemical, mechanochemical, sonochemical, layer-by-layer…) using aqueous or non-aqueous media [263,264]. The solvothermal (or hydrothermal, depending on the solvent media) approach is the most widely used. This consist in the mixing of the reagents (the metal salt, the ligands, and the solvent), and their introduction inside a proper vessel (usually is used a Teflon lined vessel). Then the vessel is introduced into a stainless steel reactor, and subjected to high temperatures (from 80 to 250 ºC) for a certain period of time. Common synthesis times when using the solvothermal approach range from 3 to 96 h, or even more. Other approaches, which are faster (usually no longer than 60 min), require the utilization of microwaves, ultrasounds, or a mechanic-chemical synthesis [162].

The MOF structure is highly dependent on its preparation; and thus, small variations in the preparation method are exerting an enormous influence in the structure and properties of the MOFs obtained. In this sense, it is possible to control the resulting porosity and other features by modifying parameters during their preparation [265] such as: the amount of MOF precursors (metal/s and/or linker/s), solvent nature and amount, temperature, time, type and amount of modifier/s, or the size of the reactor.

MOFs have been also pointed out as promising materials in energy and environmental fields. At the beginning, main applications of MOFs focused on gas storage [266,267], taking advantage of their exceptional porosity. Progressively, MOFs have been explored widely in biomedical applications [268,269], in catalysis [270,271], and as sensors [272,273]. Some reported MOFs incorporating biomolecules and/or biocompatible metals have shown to be excellent materials in imaging and drug delivery [268,274]. Furthermore, luminescent MOFs have been proposed as potential materials in the electrochemical field [275,276], and in separation applications [277,278]. Specifically, the applications of MOFs in the Analytical Chemistry field have been more recent, and in fact, it has not been until the last decade that MOFs were tested as powerful materials in analytical separations. The emerging studies of MOFs in Analytical Chemistry have been the topic of recent review articles in: i) the field of analytical sample preparation (with MOFs being used as sorbent materials) [162,279,280] and ii) chromatography (with MOFs being used as novel stationary phases) [281,282]. Around 200 publications in journals belonging to the Journal of Citation Report (JCR) focus on the use of MOFs in analytical sample preparation and/or chromatography [283] The interest of MOFs is linked to the necessity of overcoming problems of common sorbents in those procedures.

In recent years, an increasing number of applications include MOF or their hybrid materials in analytical sample preparation [280], being included in the increasing number of improvements in the analytical techniques, with new devices and systems, even with the proposal of new MOFs designed specifically for analytical microextraction [284]. Figure I.29. shows the number of publications using MOFs (or MOF-based sorbents) in the analysis of environmental water samples, and in the different sorbent-based microextraction techniques referred in Sections I.3.2.1. and I.3.2.2.

The emerging contaminants most usually monitorized in waters when using MOFs as sorbents have been drugs, pesticides, and PAHs. Undoubtedly, MOFs have been more widely used for the extraction of pollutants in water using µSPE (~115 studies) than using SPME (~40 studies). Among µSPE modes, D-µSPE and M-D-µSPE have been the most widely used, taking advantage of the simplicity of the procedures and the strong efficiency of the interaction MOF-target analytes. Regarding SPME, the mode *in-tube* SPME based on MOFs as sorbents have not been developed for the analysis of environmental water samples.

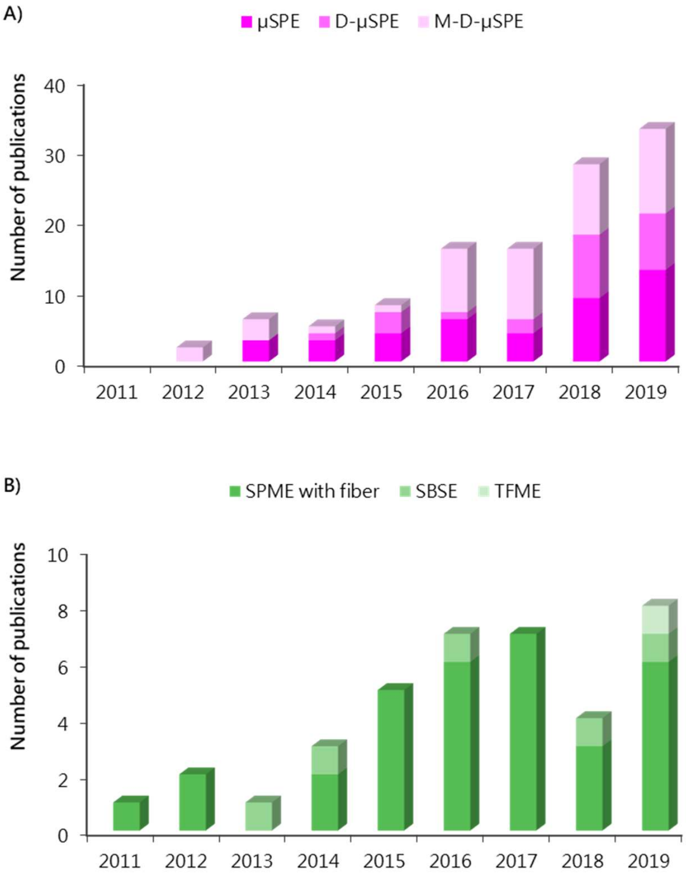

Figure I.29. Number of publications using MOFs (or MOF-based sorbents) in the analysis of environmental water samples using **A)** μSPE or **B)** SPME modalities.

Regardless the type of sample analyzed, the nature of the target analytes determined, or the technique employed, the MOFs most frequently employed as sorbents in sorbent-based microextraction are MIL-101(Cr), MIL-101(Fe), HKUST-1(Cu), MOF-5(Zn), MIL-53(Al), and UiO-66(Zr) [283,285]. Table I.3. lists several examples of MOFs which are now quite known in the analytical chemistry field [286-292]. Specifically, the MOFs most widely used in the analysis of environmental water samples are HKUST-1(Cu), MIL-101(Cr), MIL-100(Fe), MIL-53(Al), UiO-66(Zr), and ZIF-8(Zn). At the same time, new MOFs have been synthetized and proposed for microextraction, such as CIM-80 (Al^{3+} plus mesaconate linker) [284] used in D-µSPE for the determination of different pollutants in waters or the Ti-MOF (Ti^{4+} plus 5-aminoisophtalic acid linker) in M-D-µSPE for the determination of caffeic acid in water samples [293].

Recently, it is also proposed the modification of the MOFs by incorporating certain functional groups in their structures, intending the improvement of the interactions MOF-target analyte. Thus, it has been described the amino functionalization in the ligands of the MOF [294-301], or even the post-functionalization of the MOF [302,303].

The applications of MOFs in static µSPE hardly use neat MOFs. Thus, only MIL-101(Cr) and ZIF-8(Zn) have been used in MOF-based devices for the analysis of water samples. Among then, it can be highlighted the use of MOF in µSPE static with cartridges [304,305], or in polypropylene membranes [306-308].

Regarding D-µSPE, traditional neat MOFs have been used successfully, such as MIL-101(Cr) for the preconcentration of endocrine disruptors [309], ZIF-8(Zn) for pesticides [310], HKUST-1(Cu) for PAHs [311], MIL-100(Fe) for phthalic acid esters [312], and TMU-6(Zn) for plasticizers [313]. Not only neat MOFs have been used in D-µSPE, but also hybrid materials. In this sense, the non-ionic surfactant Triton X-114 has been used in D-µSPE for the improvement of the extraction efficiency of MIL-101(Cr) in an aqueous matrix, by helping in its dispersion [309]. In other study, the adsorption capacity of the neat HKUST-1(Cu) powder was compared with those of fullerene/HKUST-1(Cu) and graphene/HKUST-1(Cu), also using D-µSPE, showing that better results were obtained with the composite graphene/HKUST-1(Cu) [311].

The higher number of applications in M-D-µSPE necessarily utilizes magnetic composites based on MOFs because the MOFs require their incorporation or modification with a magnetic material, being magnetite MNPs the most used. Such magnetic composites can include the MOF in a heterogeneous composite (denoted as composite Type A, and referred as Fe_3O_4/MOF) [314-317], or it can form a core-shell structure coated by the MOF (denoted as composite Type B, and referred as Fe_3O_4@MOF) [290,302,303,318-329]. In other cases, magnetite MNPs nanoparticles are coated with other materials before incorporating the MOF, such as silica [290,303,318,320,321,322,330], N-(n-propyl)ethylenediamine [322], or L-cysteine [324]. The presence of these coatings and functionalization groups not only gives stabilization to the magnetic core but also permits an increase in the number and type of interactions with target analytes because other materials are involved in the extraction.

Several studies have reported the calcination of already synthetized MOFs, and their further use as extractant sorbents in sorbent-based microextraction methods [331,332]. However, this strategy is still subject to controversy, since the physic-chemical properties that make the MOFs excellent sorbents (its crystallinity) is lost with the calcination, leaving to an amorphous material mostly formed by carbonaceous structures and isolated metals in the sorbent.

With regard to the use of MOF in SPME for the analysis of environmental water samples, neat MOFs have been successfully attached by different methods to stainless steel supports, such as MIL-101(Cr) [333,334], MIL-101(Fe) [335], HKUST-1(Cu) [336], MOF-177(Zn) [337], and MOF-74(Ni) [338]. The methods more frequently used for the coating of the MOFs are the *in-situ* hydrothermal growth [335], the sol-gel approach [336], or the electrodeposition [339]. The most easy and simple method implies the previous synthesis of the neat MOF and its further attachment to the metallic steel using glues [333,334,340,341].

SBSE has been the less explored mode for MOFs. As representative applications, a poly(ethylene glycol) modified column of MIL-101(Cr) was fabricated and used as stir-bar for the determination of drugs in water samples [342]. Other SBSE applications described the use of the amino functionalized MIL-53(Al) [296], MIL-101(Cr) [297], and UiO-66(Zr) [298] for the determination of PAHs and pesticides.

To date, there is only one study regarding the use of MOF for the monitoring of pollutants in water using TFME [299].

Table I.3. Relevant characteristics of the MOFs most widely used in analytical chemistry.

MOF	Metal cluster	Organic linker	Surface area[a] ($m^2 \cdot g^{-1}$)	Pore size (Å)	Thermal stability[b] (°C)	Ref.
HKUST-1(Cu)	Cu(II)	benzene-1,3,5-tricarboxylate	692	9 & 18	240	[286]
MIL-101(Cr)	Cr(III)	benzene-1,4-dicarboxylate	4100	30 & 34	275	[287]
MIL-100(Fe)	Fe(II)	benzene-1,3,5-tricarboxylate	2800	25 & 29	300	[288]
MIL-53(Al)	Al(III)	benzene-1,4-dicarboxylate	1140	8.5	500	[289]
MOF-5(Zn)	Zn(II)	benzene-1,4-dicarboxylate	2900	12	300	[290]
UiO-66(Zr)	Zr(IV)	benzene-1,4-dicarboxylate	1187	8 & 10	540	[291]
ZIF-8(Zn)	Zn(II)	2-methylimidazol	1630	3.4 & 11.6	500	[292]

[a] Value obtained using the Brunauer-Emmett-Teller (BET) isotherm, except for MIL-100(Fe), MOF-5(Zn), and UiO-66(Zr), for which the Langmuir isotherm was used

[b] Temperature at which the decomposition of the MOF starts

3.3. Microextraction techniques for the monitoring of PCPs and DBPs in waters

Within the monitoring of emerging contaminants, analytical microextraction techniques have been widely employed for the determination both PCPs and DBPs. Table I.4. and Table I.5. collect an overview on the current analytical applications for the determination of PCPs [113,343-366], and DBPs [127,367-381] in environmental water samples using microextraction procedures in combination with HPLC or GC. The selected articles cover the most relevant reported methodologies in the last years, trying to include representative examples of the different microextraction techniques.

Among the emerging contaminants considered in the Doctoral Thesis, PCPs have been the most widely monitored in water samples. This probably links to the necessity of evaluating their contents in different waters to support future policies on their regulation. The reported microextraction-based method mainly focused on the monitoring of UV-filters, preservatives (mainly parabens), and musk fragrances. Disinfectants and siloxanes have received less attention, and insect repellents are usually determined together with other PCP groups [382,383]. As it is commented in Section I.1.4., one of the challenges for Analytical Chemistry is the multiclass analysis to cover entire groups of emerging contaminants. Thus, few microextraction applications have been developed for groups of PCPs [113,345,384,385], mainly due to the difference in the nature of the chemicals included in the label PCP. In general, semi-volatile UV-filters have been studied together with musk fragrances [113,345,385].

Regarding the chromatographic method, HPLC is used commonly for parabens and disinfectants, while UV-filters, musk fragrances, and siloxanes are monitorized using GC given their volatile nature. Sometimes, derivatization steps are included for the monitoring of parabens in GC [356]. Certainly, the detection technique most used is mass spectrometry (MS) [113,345-349,351,352,356-366], although some authors have used ultraviolet (UV) [344,350,353] or diode-array detection (DAD) [343,344,355] for UV-filters and parabens. In any case, it can be highlighted an evident trend to ensure the fully automation of the overall method [347,353,357,359].

Regarding the type of microextraction method used, both liquid-based and sorbent-based microextraction have been employed for all the PCPs, but recently there is an increasing number of sorbent-based microextraction applications. DLLME is the most commonly used mode of LPME for the monitoring of PCPs [343-347,353,358,362,364]. The technique is usually assisted by ultrasound in order to obtain a better analytical performance in the preconcentration of UV-filters [345], musk fragrances [345,358], and siloxanes [364], whereas air assistance is the less used [343,347]. In order to improve the handling of the techniques, an automated DLLME based on the solidification of the organic phase (SFO-DLLME) was developed for the monitoring of preservatives in tap, sea, and pool water [353]. Regarding automation, an online and dynamic SDME method has been employed for the extraction of musk fragrances from river and seawater samples [357]. Regarding the nature of the solvents used in LPME for the extraction of PCPs, the most remarkable improvement has been the *in*-situ DLLME using the [BMIM]Br and [BeEOHIM]Br ILs for the determination of UV-filters in pool waters and lakes [346]. More recently, novel deep eutectic solvents have been also reported for the monitoring of UV-filters in water, in combination with HPLC [343,344].

There are few applications on the use of static µSPE and this group of contaminants in waters, using cartridges [348,359], or in membrane formats [349], being the dispersive version the most successful one. Thus, parabens have been monitorized in several water samples by D-µSPE [355], and with M-D-µSPE the target analytes included parabens [356], disinfectants [363], and siloxanes [365]. Among the SPME techniques, the most commonly mode used SPME fibers, both in direct immersion mode or in headspace applications for UV-filters [113,351], musk fragrances [113], and siloxanes [366], or only direct immersion for UV-filters [350], and musk fragrances [360,361]. SBSE has been combined with GC-MS through a thermal desorption unit (TDU) for the preconcentration of UV-filters in river, sea, and pool waters [352]. Recently, a new microextraction procedure, named vacuum-assisted sorbent extraction (VASE), has been reported using sorbent pen (SP) technology for the extraction of UV-filters in environmental water samples [386].

Regarding the use of novel solid sorbent materials for the analytical microextraction of PCPs, MOFs and carbon nanomaterials have been the most studied. MIL-101(Cr) has been used in µSPE using cartridges for the determination of UV-filters [348], whereas HKUST-1 has been utilized in D-µSPE for parabens [355]. On the other hand, carbon nanomaterials have been more widely used in the monitoring of PCPs [349,350,356,361,363,365]. Specifically, MWCNTs have been used in membranes [349], and coated in magnetic MPs [356]. Finally, it can be highlighted that the use of PILs in SPME has been successful for the analysis of tap water, pool, and lakes [351].

Table I.4. Current analytical applications of microextraction methods followed by chromatographic tools for the determination of PCPs in environmental water samples, grouped in the table by types of PCPs.

Microextraction method	Extraction solvent or sorbent	Chromatographic technique	Analytes	Sample	Novelty	E_F[a]	LOD[b] ($ng \cdot L^{-1}$)	RSD[c] (%)	Ref.
UV-filters									
air assisted DLLME	DES DL-menthol(HBA):decanoic acid (HBD) in 1:1 (v:v) ratio	HPLC-DAD	4OH-BP, BP, BP1, BP3, BP2, BP6	pool water, river water, and wastewater	DES solvent and air assisted	144-154	50-200	<5.6	[343]
DLLME	DES trioctylmethylammonium chloride (HBA):decanoic acid (HBD) in 1:3 (v:v) ratio	HPLC-UV	BP, BP1, BP3	pool water and river	DES solvent	67-76	150-300	<5.9	[344]
US-DLLME	extractant: 1,1,2-trichloroethane dispersor: 2-propanol	GC-MS	BP, MBC, OD-PABA, EHMC, OCR, DTS	tap water, seawater, river, influent and effluent wastewater			0.1-20	<10	[345]
in-situ DLLME	[BMIM$^+$][Br$^-$] [BeEOHIM$^+$][Br$^-$]	GC-MS	EHS, BS, HMS, BP3, MA, EHMC	pool water and lake	*in-situ* IL solvent		5-10000	<14	[346]
air-assisted DLLME	extractant: trichloroethylene dispersor: acetone derivatization: N,O-bis(trimethylsilyl)trifluoroacetamide	GC-MS	EHS, BP, HMS, IAMC, BP3, MBC, MA, ETO, OD-PABA, EHMC, OCR	seawater and pool water	online	7.9-12.9	23-160	<16.8	[347]

Table I.4. (continuation).

Microextraction method	Extraction solvent or sorbent	Chromatographic technique	Analytes	Sample	Novelty	E_F[a]	LOD[b] ($ng\cdot L^{-1}$)	RSD[c] (%)	Ref.
µSPE static (cartridges)	MIL-101(Cr)	GC-MS	HMS, BP3, MBC, OD-PABA, EHMC, OCR	lake, river, seawater and pool waters	MOF sorbent		1-11.7	<10	[348]
µSPE static (membrane)	MWCNTs	GC-MS	BP3, OD-PABA, EHMC, EHS	tap, river, pool, and wastewater	carbon nanomaterial sorbentl		3-18	<15	[349]
DI-SPME	NiO/TiO_2CNSs	HPLC-UV	EHS, HMS, BP3, IAMC, MBC, MA, ETO, OD-PABA, EHMC, OCR	river, lake, and wastewater	carbon nanomateria sorbent	89.6-221	11-42	<8.2	[350]
HS-SPME	PDMS/DVB	GC-MS/MS	EHS, HS, BP, BP3, MA, ETO, OD-PABA, EHMC, OCR	river			0.025-2.7	<15	[113]
HS-SPME	monomer: $[VBC_{16}IM^+][NTf_2^-]$ crosslinker: $[(VBIM)_2C_{12}^{2+}]\ 2[NTf_2^-]$	GC-MS	EHS, HS, IMC, 4-MBC, BZ3, EHMC, OD-PABA, OCR	tap, pool and lake water	PIL sorbent		2.8-26	<15	[351]
SBSE	$CoFe_2O_4$@oleic acid	GC-MS	EHS, HMS, BP, HS2, BP3, MA, ETO, OD-PABA, EHMC, OCR	river, seawater and pool waters		68-690	43-148	<11.3	[352]

Table I.4. (continuation).

Microextraction method	Extraction solventor sorbent	Chromatographic technique	Analytes	Sample	Novelty	E_F[a]	LOD[b] (ng·L^{-1})	RSD[c] (%)	Ref.
Preservatives									
SFO-DLLME	extractant: 1-dodecanol dispersor: methanol	HPLC-UV	MPB, EPB, PPB, BPB	tap, seawater, and pool water	online	11-22	1-1300	<8.6	[353]
µSPE static (syringe)	chitosan coated activated carbon	HPLC-DAD	MPB, EPB, PPB, BPB	influent and effluent wastewater	biomaterial sorbent		6-15	<5	[354]
D-µSPE	HKUST-1(Cu)	HPLC-DAD	MPB, EPB, PPB, iPPB, BPB, iBPB, BzPB	tap and pool waters	MOF sorbent		100-600	<12	[355]
M-D-µSPE	Fe_3O_4@MWCNTs	GC-MS	MPB, EPB, PPB, iPPB, BPB, iBPB, BzPB, PhPB	river, harbour, pool, tap, and wastewater	Carbon nanomaterial sorbent		30-2000	<8.6	[356]
Musk fragrances									
dynamic SDME	n-hexane	GC-MS	ADBI, AHMI, ATII, HHCB, AHTN	river and seawater	online		3.4-11	<11.1	[357]
US-DLLME	extractant: 1,1,2-trichloroethane dispersor: 2-propanol	GC-MS	DPMI, ADBI, AHMI, ATII, HHCB, AHTN, EXA, EB, MA, MX, MM, MT, MK	tap, seawater, river, influent and effluent wastewater			0.1-10.9	<12	[345]

Table I.4. (continuation).

Microextraction method	Extraction solvent or sorbent	Chromatographic technique	Analytes	Sample	Novelty	E_F[a]	LOD[b] ($ng{\cdot}L^{-1}$)	RSD[c] (%)	Ref.
US-DLLME	extractant: chloroform dispersor: acetonitrile	GC-MS	DPMI, ADBI, AHMI, HHCB, AHTN, EXA, EB, MA, MX, MM, MT, MK	tap, sea, and river, influent and effluent wastewater			1-54	<13.5	[358]
μSPE static (micro columns)	Oasis® HLB	GC-MS	DPMI, ADBI, AHMI, ATII, HHCB, AHTN, MX, MM, MK, exaltone, exaltolide, muscone, ambrettolide, musk MC4, civetone, musk NN	wastewater	online		1-30	<14	[359]
HS-SPME	PDMS/DVB	GC-MS/MS	ADBI, DPMI, AHMI, HHCB, AHTN, MK, ambrettolide	river			0.023-1.1	<15	[113]
DI-SPME	MIL-53(Al)-NH_2	GC-MS	HHCB, AHTN, muscone, MX, MK	tap and river	MOF sorbent	15-8678	0.025-0.83	<9.8	[360]
DI-SPME	graphene-NH_2	GC-MS	HHCB, AHTN, muscone, MX, MK	tap and river	carbon nanomaterial sorbent		0.046-5.96	<12	[361]

Table I.4. (continuation).

Microextraction method	Extraction solvent or sorbent	Chromatographic technique	Analytes	Sample	Novelty	E_F[a]	LOD[b] ($ng \cdot L^{-1}$)	RSD[c] (%)	Ref.
Disinfectant									
DLLME	extractant: $[C_8MIM][PF_6]$ dispersor: $[C_4MIM][BF_4]$	HPLC-ESI-MS-MS	TCS, TCB	lake, water, tap water, snow water and river	IL sorbent		230-350	<6.41	[362]
M-D-µSPE	Fe_3O_4@carbon nanodots	LC-MS/MS	TCS	wastewater	magnetic carbon nanomaterial sorbent		24-81	<4.7	[363]
Siloxanes									
US-DLLME	chlorobenzene	GC-MS	L2, L4, L5, D3, D4, D5, D6	wastewater		260-856	2-1400	<29	[364]
M-D-µSPE	Fe_3O_4@GO	GC-MS	L3, L4, L5, D4, D5, D6	wastewater	magnetic carbon nanomaterial sorbent		3-100	<24	[365]
HS-SPME	PDMS/DVB	GC-MS	L2, L3, L4, L5, D3, D4, D5, D6	wastewater			0.001-0.074	<17	[366]

ATII: traseolide
BS: benzyl salicylate
D3: hexamethylcyclotrisiloxane
DTS: drometrizoletrisiloxane
EHS: 2-ethylhexyl salicylate
ETO: etocrylene
EXA: exaltolide
IAMC: isoamyl methoxycinnamate
L2: hexamethyldisiloxane
MA: methyl anthranilate
MT: musk tibetene
OD-PABA: octyldimethyl-p-aminobenzoic acid
OPB: octylparaben
PhPB: phenylparaben

In last years, DBPs have not been considered as PCPs, and this can be observed in the lower number of publications reported on them in microextraction approaches. This fact can be linked to their already inclusion in past regulations, and the existence of official methods for their determination. Among the DBPs, the four THMs (TCM, BDCM, DBCM, and TBM) are the most studied ones, followed by HAAs, and, more recently, it has emerged a number of studies for the monitoring of halogenated DBPs (HANs and HNMs) and iodinated DBPs (i-THMs and i-HAAs). Given the similarities of their chemical nature, very often authors considered several groups of DBPs for their extraction in water sample in the same analytical method [370,377]. DBPs are generally determined using GC in combination with electron capture detection (ECD) [367,368,371,373], or more frequently MS [369,370,372,374-381]. Due to their non-volatile nature, HAAs are normally determined by HPLC [127], an also i-DBPs [377].

The LPME techniques more employed for the monitoring of DBPs in environmental waters are HF-LPME and DLLME. HF-LPME has been more used for the microextraction of THMs [367,368], while DLLME has been successfully used for THMs [369], HAAs [127], HANs [374-376], and HNMs [369,374,375]. The monitoring of DBPs in water samples using LPME techniques has limited the use of conventional organic solvents (1-octanol, ethyl acetate, isopropylether, methyl tert-butyl ether, or dichloromethane, among others).

Regarding the sorbent-phase microextraction methods, SPME is undoubtedly the most successful technique to determine DBPs in urban and environmental waters, mainly in the HS mode for THMs [371,372], and HAAs [373], and halonitriles [381], and few studies work in DI [370]. With regard to static µSPE, commercial sorbents in cartridges are commonly used [377]. The use of novel extractive material in solid-based microextraction has been more successful than in liquid-phase microextraction. Thus, a MIL-96(Al)-coated fiber has been successfully employed in DI-SPME in combination with GC-MS for the determination of THMs and HNMs in groundwater, pond water, and tap water samples [370]. Furthermore, the MIP EDGMA-MAA was used in µSPE cartridges for the monitoring of other DBPs [379].

Table I.5. Current analytical applications of microextraction methods followed by chromatographic tools for the determination of DBPs in environmental water samples, grouped in the table by types of DBSs.

Microextraction method	Extraction solvent or sorbent	Chromatographic technique	Analytes	Sample	Novelty	E_F[a]	LOD[b] ($ng \cdot L^{-1}$)	RSD[c] (%)	Ref.
THMs									
HF-LPME	1-octanol	GC-ECD	TCM, BDCM, DBCM, TBM	tap water		330-455	17-37	<10.3	[367]
HF-LPME	1-octanol	GC-ECD	TCM, BDCM, DBCM, TBM	surface and groundwater		21-56	3-44	<22	[368]
DLLME	ethyl acetate	PTV-GC-MS	TCM, BDCM, DBCM, TBM	tap water and pool water			18-60	<7.4	[369]
DI-SPME	MIL-96(Al)	GC-MS	TCM, BDCM, DBCM, TBM	groundwater, pond water, and tap water	MOF		30-110	<10.1	[370]
HS-SPME	PDMS	GC-ECD	TCM, BDCM, DBCM, TBM	pool water			11800-4000	<10	[371]
HS-SPME	CAR/PDMS/DVB	GC-MS	TCM, BDCM, DBCM, TBM	recycling plant water			3-20	<23	[372]

Table I.5. (continuation).

Microextraction method	Extraction solvent or sorbent	Chromatographic technique	Analytes	Sample	Novelty	E_F[a]	LOD[b] (ng·L^{-1})	RSD[c] (%)	Ref.
HAAs									
VA-DLLME	isopropyl ether	HPLC-DAD	MCAA, MBAA, DCAA, BCAA, DBAA, TCAA, BDCAA, CDBAA, TBAA	tap water, pool, and desalination plant water		10.3-29.2	1020-60100	<23	[127]
HS-SPME	PDMS	GC-ECD	MCAA, DCAA, TCAA, MBAA, DBAA, TBAA, BCAA	tap water			20-700	<12	[373]
HANs									
DLLME	methyl tert-butyl ether	GC-MS	BAN, CAN, DBAN, DCAN, TCAN, BDCAN, DBCAN, TBAN, BCAN	tap water and pool water			700-1600	<17	[374]
DLLME	extractant: dichloromethane dispersor: methanol	GC-MS	TCAN, DCAN, BCAN, DBAN	tap water			750-1150	<21.3	[375]
DLLME	extractant: dichloromethane dispersor: methanol	PTV-GC-MS	MCAN, MBAN, MIAN, DCAN, DBAN, BCAN, TCAN	surface waters			0.4-13.2	<10.2	[376]

Table I.5. (continuation).

Microextraction method	Extraction solvent or sorbent	Chromatographic technique	Analytes	Sample	Novelty	E_F[a]	LOD[b] ($ng \cdot L^{-1}$)	RSD[c] (%)	Ref.
HNMs									
DLLME	methyl tert-butyl ether	GC-MS	BCNM, BDCNM, CNM, DBCNM, DBNM, DCNM, TBNM, BNM, TCNM	tap water and pool water			400-1700	<19	[374]
DLLME	extractant: dichloromethane dispersor: methanol	GC-MS	CP	tap water			870	<16.4	[375]
DLLME	ethyl acetate	PTV-GC-MS	CNM, DCNM, TCNM, BNM, BCNM, BDCNM, DBNM, DBCNM, TBNM	tap water and pool water			9-400	<8.6	[372]
DI-SPME	MIL-96(Al)	GC-MS	TCNM	groundwater, pond water, and tap water			47	<7	[370]
i-DBPs									
DI-HF-LPME	1-octanol	GC-ECD	i-THMs (6)	surface and groundwater		311-1016	1-3	<12	[368]

Table I.5. (continuation).

Microextraction method	Extraction solvent or sorbent	Chromatographic technique	Analytes	Sample	Novelty	E_F[a]	LOD[b] ($ng \cdot L^{-1}$)	RSD[c] (%)	Ref.
DLLME	extractant: dichloromethane dispersor: methanol	GC-MS	i-THMs (6)	tap water			380-1190	<20.5	[375]
µSPE static (cartridges)	Oasis® MAX cartridges	HPLC-MS/MS	i-HAAs (2)	tap water			0.04-0.15	<8.3	[377]
µSPE static (cartridges)	Oasis® MAX cartridges	HPLC-MS/MS	i-DBPs (4)	tap water			0.02-0.06	<15.6	[377]
HS-SPME	DVB/CAR/PDMS fiber	GC-MS	i-THMs (6)	recycling plant water			1-8	<16	[372]
Others DBPs									
DLLME	methyl *tert*-butyl ether	PTV-GC-MS	haloketones (14)	tap water and pool water			6-120	<8.4	[378]
µSPE static (cartridges)	MIP: EDGMA-MAA	HPLC-MS/MS	nitrosamines (5)	bottled, tap water and river	MIP		0.2-0.7	<9.8	[379]
µSPE static (cartridges)	Lichrolut EN and Ambersorb 572	HPLC-MS/MS	nitrosamines (14)	influent and effluent watewater			0.01–2.7		[380]
HS-SPME	DVB/CAR/PDMS	GC-MS	halonitriles (8)	drinking water			0.5-29	<26	[381]

REFERENCES

[1] Guidelines for Drinking-water Quality, Fourth Edition: Incorporating the First Addendum. World Health Organization (2017).

[2] G. Nichols, I. Lake, and C. Heaviside. Atmosphere 9 (2018) 385.

[3] World Population Prospects: The 2015 Revision, Methodology of the United Nations Population Estimates and Projections. United Nations, Department of Economic and Social Affairs, Population Division (2015).

[4] The United Nations World Water Development Report 2015: Water for a sustainable world. United Nations World Water Assessment Programme (2015).

[5] V.G. Gude. Water Res. 89 (2015) 87–106.

[6] I.Y. López-Pacheco, A. Silva-Núñez, C. Salinas-Salazar, A. Arévalo-Gallegos, L.A. Lizarazo-Holguin, D. Barceló, H.M.N. Iqbal, and R. Parra-Saldívar. Sci. Total Environ. 690 (2019) 1068–1088.

[7] S.Y. Wee and A. Z. Aris. Environ. Int. 106 (2017) 207–233.

[8] D. Barceló and A.G. Kostianoy (Editors). The Handbook of Environmental Chemistry. Volume 46: Emerging Contaminants in River Ecosystems. Occurrence and Effects Under Multiple Stress Conditions, Springer (2016).

[9] S.D. Richardson. Anal. Chem. 75 (2003) 2831–2857.

[10] K. Fischer, E. Fries, W. Körner, C. Schmalz, and C. Zwiener. Appl. Microbiol. Biotechnol. 94 (2012) 11–28.

[11] M. Lei, L. Zhang, J. Lei, L. Zong, J. Li, Z. Wu, and Z. Wang. Biomed Res. Int. (2015).

[12] T. Rasheed, M. Bilal, F. Nabeela, M. Adeel and H.M.N. Iqbalc. Environ. Int. 122 (2019) 52–66.

[13] N.H. Tran, M. Reinhard, and K. Yew-Hoong Gin. Water Res. 133 (2018) 182–207.

[14] J.P.S. Sidhu, W. Ahmed, W. Gernjak, R.Aryal D. McCarthy, A. Palmer, P. Kolotelo, and S. Toze. Sci. Total Environ. 463–464 (2013) 488–496.

[15] F. Hernández, J. Bakker, L. Bijlsma, J. de Boer, A.M. Botero-Coy, Y. Bruinen de Bruin, S. Fischer, J. Hollender, B. Kasprzyk-Hordern, M. Lamoree, F.J. López, T.L. ter Laaki, J.A. van Leerdam, J.V. Sancho, E.L. Schymanski, P. de Voogt, and E.A. Hogendoorn. Chemosphere 222 (2019) 564–583.

[16] S.D. Richardson and T.A. Ternes. Anal. Chem. 90 (2018) 398–428.

[17] M.S. Díaz-Cruz and D. Barceló (Editors). The Handbook of Environmental Chemistry. Volume 36: Personal Care Products in the Aquatic Environment, Springer (2015).

[18] M. Pedrouzo, F. Borrull, R.M. Marcé, and E. Pocurull. Trac-Trends Anal. Chem. 30 (2011) 749–760.

[19] J. Tolls, H. Berger, A. Klenk, M. Meyberg, A.G. Beiersdorf, R. Müller, K. Rettinger, and J. Steber. Environ. Toxicol. Chem. 28 (2009) 22485–2489.

[20] A. Chisvert, J.L. Benedé, and A. Salvador. Anal. Chim. Acta 1034 (2018) 22–38.

[21] L. Meunier, N. Raison-Peyron, and J. Meynadier. Rev. Med. Interne 19 (1998) 247–254.

[22] D.M. Owens and F.M. Watt. Nat. Rev. Cancer 3 (2003) 444–451.

[23] M.S. Díaz-Cruz and D. Barceló. Trac-Trends Anal. Chem. 28 (2009) 708.

[24] C. Plagellat, T. Kupper, R. Furrer, L. Felippe de Alencastro, D. Grandjean, and J. Tarradellas. Chemosphere 62 (2006) 915–925.

[25] Z. Zhang, H. Yang, G. Wu, Z. Li, T. Song, and X.Q. Li. Eur. J. Med. Chem. 46 (2011) 3909–3916.

[26] S. Ramos, V. Homem, A. Alves, and L. Santos. Sci. Total Environ. 526 (2015) 278–311.

[27] M. Krause, A. Klit, M. Blomberg Jensen, T. Søeborg, H. Frederiksen, M. Schlumpf, W. Lichtensteiger, N.E. Skakkebaek, and K.T. Drzewiecki. Int. J. Androl. 35 (2012) 424–436.

[28]. J.M. Brausch and G.M. Rand. Chemosphere 82 (2011) 1518–1532.

[29] D. Kim, G.L. Amy, and T. Karanfil. Water Res. 81 (2015) 343–355.

[30] E.J. Routledge, J. Parker, J. Odum, J. Ashby, and J.P. Sumpter. Toxicol. Appl. Pharmacol. 153 (1998) 12–19.

[31] A. Tartaglia, A. Kabir, S. Ulusoy, E. Sperandio, S. Piccolantonio, H. I. Ulusoy, K.G. Furton, and M. Locatelli. J. Chromatogr. B 1125 (2019) 121707.

[32] F. Vela-Soria, L.M. Iribarne-Durán, V. Mustieles, I. Jiménez-Díaza, M.F. Fernández, and N. Olea. J. Chromatogr. A 1546 (2018) 1–9.

[33] P. Dualde, O. Pardo, F. Corpas-Burgos, J. Kuligowski, M. Gormaz, M. Vento, A. Pastor, and V. Yusà. Chemosphere 240 (2020) 124829.

[34] P.D. Darbre, A. Aljarrah, W.R. Miller, N.G. Coldham, M.J. Sauer, and G.S. Pope. J. Appl. Toxicol. 24 (2003) 5−13.

[35] J.R. Byford, L.E. Shaw, M.G.B. Drew, G.S. Pope, M.J. Sauer, and P.D. Darbre. J. Steroid Biochem. Mol. Biol. 80 (2002) 49−60.

[36] G. Shanmugam, B.R. Ramaswamy, V. Radhakrishnan, and H. Tao. Microchem. J. 96 (2010) 391–396.

[37] L. Vallecillos, F. Borrull, and E. Pocurull. Trac-Trends Anal. Chem. 72 (2015) 80–92.

[38] M. Arbulu, M.C. Sampedro, N. Unceta, A. Gómez-Caballero, M.A. Goicolea, and R.J. Barrio. J. Chromatogr. A 1218 (2011) 3048–3055.

[39] P. Gautam, J.S. Carsella, and C.A. Kinney. Water Res. 48 (2014) 247–256.

[40] A.R.M. Silva and J.M.F. Nogueira. Talanta 74 (2008) 1498–1504.

[41] P. Herrero, F. Borrull, R.M. Marcé, and E. Pocurull. J. Chromatogr. A 1355 (2014) 53–60.

[42] Z.Q. Shi, Y.S. Liu, Q. Xiong, W.W. Cai, and G.G. Ying. Sci. Total Environ. 661 (2019) 407–421.

[43] A. Kanetoshi, H. Ogawa, E. Katsura, and H. Kaneshima. J. Chromatogr. A 389 (1987) 139–153.

[44] J.H. Guo, X.H. Li, X.L. Cao, Y. Li, X.Z. Wang, and X.B. Xu. J. Chromatogr. A 1216 (2009) 3038.

[45] N. Veldhoen, R.C. Skirrow, H. Osachoff, H. Wigmore, D.J. Clapson, M.P. Gunderson, G.V. Aggelen, and C.C. Helbing. Aquat. Toxicol. 80 (2006) 217–227.

[46] J.M. Brausch and G.M. Rand. Chemosphere 82 (2011) 1518–1532.

[47] F.B. Antwi, LM. Shama, and R.K.D. Peterson. Regul. Toxicol. Pharmacol. 51 (2008) 31–36.

[48] A.M. Peck. Anal. Bioanal. Chem. 386 (2006) 907–939.

[49] M. Tavaresa, M.R.M. da Silva, L.B.O. de Siqueira, R.A.S. Rodrigues, L. Bodjolle-d'Almeida, E.P. dos Santos, and E. Ricci-Júnior. Int. J. Pharm. 539 (2018) 190–209.

[50] S.D. Costanzo, A.J. Watkinson, E.J. Murby, D.W. Kolpin, and M.W. Sandstrom. Chemosphere 64 (2007) 1808–1817.

[51] J. Sanchís, E. Martínez, A. Ginebreda, M. Farré, and D. Barceló. Sci. Total Environ. 443 (2013) 530–538.

[52] C. Sparham, R. Van Egmond, C. Hastie, S. O´Connor, D. Gore, and N. Chowdhury. J. Chromatogr. A. 1218 (2011) 817–823.

[53] F. Rocha, V. Homem, J. Castro-Jiménez, and N. Ratola. Sci. Total Environ. 650 (2019) 2364–2373.

[54] J. Bridges and K.R. Solomon. J. Toxicol. Env. Health-Pt b-Crit. Rev. 19 (2016) 345–379.

[55] A. Farasani and P.D. Darbre. J. Appl. Toxicol. 37 (2017) 454–461.

[56] S.Y. Kimura, A.A. Cuthbertson, J.D. Byer, and S.D. Richardson. Water Res. 148 (2019) 324–333.

[57] J.J. Rook. Water Treat. Exam. 23 (1974) 234–243.

[58] L. Yang, X. Chen, Q. Shef, G. Caoa, Y. Liua, V.W.C. Chang, and C.Y. Tangh. Environ. Int. 121 (2018) 1039–1057.

[59] W. Kanchanamayoon. Chromatographia 78 (2015) 1135–1142.

[60] E.J. Daiber, D.M. DeMarini, S.A. Ravuri, H.K. Liberatore, A.A. Cuthbertson, A. Thompson-Klemish, J.D. Byer, J.E. Schmid, M.Z. Afifi, E.R. Blatchley, and S.D. Richardson. Environ. Sci. Technol. 50 (2016) 6652–6662.

[61] D. Kim, G.L. Amy, and T. Karanfil. Water Res. 81 (2015) 343–355.

[62] MWH (MontgomeryWatson Harza), 2005. Water Treatment: Principles and Design. John Wiley & Sons, NJ, USA.

[63] L. Alexandrou, B.J. Meehan, and O.A.H. J. Sci. Total Environ. 637–638 (2018) 1607–1616.

[64] S.D. Richardson, F. Fasano, J.J. Ellington, F.G. Crumley, K.M. Buettner, J.J. Evans, B.C. Blount, L.K. Silva, T.J. Waite, G.W. Luther, A.B. McKague, R.J. Miltner, E.D. Wagner, and M.J. Plewa. Environ. Sci. Technol. 42 (2008) 8330–8338.

[65] S.D. Richardson, M.J. Plewa, E.D. Wagner, R. Schoeny, and D.M. DeMarini. Mutat. Res. 636 (2007) 178–242.

[66] S. Chowdhury, K. Alhooshani, and T. Karanfil. Water Res. 53 (2014) 68–109.

[67] A. Ng, D. Weerakoon, E. Lim, and L.P. Padhye. Water Environ. Res. 91 (2019) 1294–1325.

[68] S.D. Richardson. Trac-Trends in Anal. Chem. 22 (2003) 666–684.

[69] H. A. Hasan, M.H. Muhammad, and N.I. Ismail. J. Water Process Eng. 33 (2020) 101035

[70] E.D. Wagner and M.J. Plewa. J. Environ. Sci. 58 (2017) 64–76.

[71] H. Baribeau, Foundation, A.R, 2006. AWWA Research Foundation.

[72] A. Kozari, A. Paloglou, and D. Voutsa. Science of the Total Environment 700 (2020) 134449.

[73] Directive 2000/60/EC of the European Parliament and of the Council of 23rd October 2000 establishing a community framework for the action in the field of water policy.

[74] Directive 2008/105/EC of the European Parliament and of the Council of 16th December 2008 on environmental quality standards in the field of water policy.

[75] Directive 2013/39/UE of the European Parliament and of the Council of 12th August 2013 on the modification of the Directives 2000/60/EC and 2008/105/EC regarding the priority substances in the field of water policy.

[76] Council Directive 98/83/EC of 3rd November 1998 on the quality of water intended for human consumption.

[77] European Council. Council of the European Union. Safe and clean drinking water: EU updates quality standards, https://www.consilium.europa.eu/en/press/press-releases/2019/03/05/safe-and-clean-drinking-water-eu-updates-quality-standards (last accessed: 27th January 2020).

[78] Procedure 2017/0332/COD on the Proposal for a Directive of the European Parliament and of the Council on the quality of water intended for human consumption (recast).

[79] United States Environmental Protection Agency: Water Topics, https://www.epa.gov/environmental-topics/water-topics (last accessed: 27th January 2020).

[80] United States Code of Federal Regulations, Title 40: Protection of Environment, Chapter I: Environmental Protection Agency, Subchapter D: Water Programs, Part 131: Water Quality Standards.

[81] United States Environmental Protection Agency: Drinking Water Requirements for States and Public Water Systems, https://www.epa.gov/dwreginfo/drinking-water-regulations (last accessed: 27th January 2020).

[82] United States Environmental Protection Agency. Quick reference guide: Stage 1 and 2 Disinfectants and Disinfection Byproducts Rules, https://www.epa.gov/ground-water-and-drinking-water/national-primary-drinking-water-regulations#Byproducts (last accessed: 27th January 2020).

[83] United States Environmental Protection Agency: Contaminant Candidate List (CCL) and Regulatory Determination, https://www.epa.gov/ccl/basic-information-ccl-and-regulatory-determination (last accessed: 27th January 2020).

[84] World Health Organization: Drinking-water, https://www.who.int/en/news-room/fact-sheets/detail/drinking-water (last accessed: 27th January 2020).

[85] Directive 1223/2009/CE of the European Parliament and of the Council of 30th November 2009 on cosmetics products.

[86] U.S. Food & Drug Administration: Cosmetics Guidance & Regulation, https://www.fda.gov/cosmetics/cosmetics-guidance-regulation (last accessed: 27th January 2020).

[87] California Office of Environmental Health Hazard Assessment: The Proposition 65 List, https://oehha.ca.gov/proposition-65/proposition-65-list (last accessed: 27th January 2020).

[88] J. Wilkinson, P.S. Hooda, J. Barker, S. Barton, and J. Swinden. Environ. Pollut. 231 (2017) 954–970.

[89] M. Marchal and J. Beltran. Int. J. Environ. Anal. Chem. 96 (2016) 1213–1246.

[90] Y. Yu and D.A. Reckhow. Environ. Sci. Technol. 51 (2017) 1488–1497.

[91] C. Haman, X. Dauchy, C. Rosin, and J.-F. Munoz. Water Res. 68 (2015) 1–11.

[92] I. Montesinos, M.J. Cardador, and M. Gallego. J. Chromatogr. A 1218 (2011) 2497–2504.

[93] A. Aisharaa, M. Sajid, C. Basheer, K, Alhooshani, and H.K. Lee. J. Sep. Sci. 39 (2016) 3610–3615.

[94] W. Li, Y. Liu, J. Duan, and D. Mulcahy. Anal. Methods 5 (2013) 2258–2266.

[95] A. Speltini, F. Maraschi, M. Sturini, M. Contini, and A. Profumo. Anal. Bioanal. Chem. 409 (2017) 6709–6718.

[96] C. Li, J. Chen, Y. Chen, J, Wang, H. Ping, and A. Lu. Molecules 23 (2018) 318.

[97] M.P. de Souza, T.M. Rizzetti, J.Z. Francesquett, O.D. Prestes, and R. Zanella. Anal. Methods 10 (2018) 697–705.

[98] R.A. Pérez, B. Albero, M. Férriz, and J.L. Tadeo. J. Pharm. Biomed. Anal. 146 (2017) 79–85.

[99] M.K. Fontes, B.G. de Campos, F.S. Cortez, F.H. Pusceddu, B.B. Moreno, L.A. Maranho, D.T. Lebre, L.L. Guimarães, and C.D.S. Pereira. Mar. Pollut. Bull. 149 (2019) 110545.

[100] H. Joerss, C. Apel, and R. Ebinghaus. Sci. Total Environ. 686 (2019) 360–369.

[101] F. Riva, E. Zuccato, E. Davoli, E. Fattore, and S. Castiglioni. J. Hazard. Mater. 361 (2019) 103–110.

[102] H. Zhang, D. West, H, Shi, Y. Ma, C. Adams, and T. Eichholz. Water Air Soil Pollut. 230 (2019) 28.

[103] Z. Niu, Z. Zhang, J. Li, J. He, and Y. Zhang. Environ. Sci. Pollut. Res. 26 (2019) 10854–10866.

[104] L. Gusmaroli, S. Insa, and M. Petrovic. Anal. Bional. Chem. 410 (2018) 4165–4176.

[105] V. Salvatierra-stamp, R. Muñiz-Valencia, J.M. Jurado, and S.G. Ceballos-Magaña. Microchem. J. 140 (2018) 87–95.

[106] W. Li, L. Huang, D. Guo, Y. Zhao, and Y. Zhu. J. Chromatogr. A 1571 (2018) 76–83.

[107] M. Čelić, M. Farré, M.L. de Alda, S. Pérez, D. Barceló, and M. Petrović. In: S. Fanali, P.R. Haddad, C.F. Poole, and M.-L. Riekkola (Editors), Liquid Chromatography, Elsevier (2017) 451–477.

[108] M. de la Guardia and S. Garrigues (Editors) Green Analytical Chemistry, Volume 57: Theory and Practice, Elsevier (2010).

[109] E. Carasek, L. Morés, and J. Merib. Trends Environ. Anal. Chem. 19 (2018) e00060.

[110] S. Armenta, S. Garrigues, F.A. Esteve-Turrillas, and M. de la Guardia. Trac-Trends Anal. Chem. 116 (2019) 248–253.

[111] B.L. Milman and I.K. Zhurkovich. Trac-Trends Anal. Chem. 97 (2017) 179–187.

[112] S. Ramos, V. Homem, and L. Santos. J. Chromatogr. A 1590 (2019) 47–57.

[113] M. Celeiro, J.P. Lamas, M. Vila, C. Garcia-Jares, V. Homem, N. Ratola, T. Dagnac, and M. Llompart. J. Chromatogr. A 1607 (2019) 460398.

[114] A. Godayol, E. Besalú, E. Anticó, and J.M. Sanchez. Chemosphere 119 (2015) 363–370.

[115] E.Y. Companioni-Damas, F.J. Santos, and M.T. Galceran. Talanta 89 (2012) 63–69.

[116] L.C. dos Reis, L. Vidal, and A. Canals. J. Sep. Sci. 41 (2019) 4177–4184.

[117] J. On, H. Pyo, and S.-W. Myung. Sci. Total Environ. 639 (2018) 208–216.

[118] L. Correa, J.A. Fiscal, S. Ceballos, A. de la Ossa, G. Taborda, C. Nerin, and M. Rosero-Moreano. J. Sep. Sci. 38 (2015) 3945–3953.

[119] B. Woo, J.-H. Park, S. Kim, J. Lee, J.-H. Choi, and H. Pyo. Sci. Total Environ. 640–641 (2018) 581–590.

[120] B. Zhang, G. Xu, L. Li, X. Wang, N. Li, R.-S. Zhao, and J. Lin. Chem. Eng. J. 350 (2018) 240–247.

[121] T. Bond, M.R. Templeton, N.H.M. Kamal, N. Graham, and R. Kanda. Water Res. 85 (2015) 85–94.

[122] M. Pedrouzo, F. Borrull, R.M. Marcé, and E. Pocurull. Anal. Bioanal. Chem. 397 (2010) 2833–2839.

[123] M. Mei and X. Huang. J. Chromatogr. A 1525 (2017) 1–9.

[124] T.A. Kung, S.H. Lee, T.C. Yang, and W.H. Wang. Sci. Total Environ. 635 (2018) 1302–1307.

[125] M.S. Noorashikin, S. Mohamad, and M.R. Abas. Desalin. Water Treat. 57 (2016) 22353–22361.

[126] P. Li, X. Liu, and X. Wang. Acta Chromatogr. 27 (2015) 255–266.

[127] P. Rocío-Bautista, V. Pino, B. Delgado, A.M. Afonso, and J.H. Ayala. Anal. Methods 6 (2014) 4115–4123.

[128] C. Planas, O. Palacios, F. Ventura, M.R. Boleda, J. Martín, and J. Caixach. Anal. Bioanal. Chem. 411 (2019) 3905–3917.

[129] D.J. Munch and D.P. Hautman. Method 551.1: Determination of chlorination disinfection byproducts, chlorinated solvents, and halogenated pesticides/herbicides in drinking

water by liquid-liquid extraction and gas chromatography with electron-capture detection, United States Environmental Protection Agency (1995).

[130] L. Vallecillos, F. Borrull, J.M. Sanchez, and E. Pocurull. Talanta 132 (2015) 548–556.

[131] M. Pedrouzo, F. Borrull, R.M. Marcé, and E. Pocurull. J. Chromatogr. A 1216 (2009) 6994–7000.

[132] P.T. Anastas and J.C. Warner (Editors) Green Chemistry: Theory and Practice, Oxford University Press (1998).

[133] A. Gałuszka, Z. Migaszewski, and J. Namieśnik. Trac. Trends Anal. Chem. 50 (2013) 78–84.

[134] National Environmental Methods Index (NEMI). https://www.nemi.gov/home/ (last accessed: 27th January 2020).

[135] D. Raynie and J.L. Driver. In: 13th Green Chemistry and Engineering Conference, Washington DC (2009).

[136] M. de la Guardia and S. Garrigues (Editors) Challenges in Green Analytical Chemistry, Royal Society of Chemistry (2011).

[137] A. Gałuszka, P. Konieczka, Z.M. Migaszewski, and J. Namieśnik, Trac-Trends Anal. Chem. 37 (2012) 61–72.

[138] S. Armenta, M. de la Guardia, and J. Namieśnik. In: M. Valcárcel, S. Cárdenas, and R. Lucena (Editors) Analytical Microextraction Techniques, Bentham Science Publishers (2016) 3–27.

[139] J. Płotka-Wasylka. Talanta 181 (2018) 204–209.

[140] S. Ziegler, R.C. Woodward, H. Ho-Ching Iu, and L.J. Borle. IEEE Sens. J. 9 (2009) 354–376.

[141] M. Tobiszewski, A. Mechlińska, B. Zygmunt, and J. Namieśnik, Trac-Trends Anal. Chem. 28 (2009) 943–951.

[142] AENOR ASTM D8143-17. Standard Test Method for the Determination of the EU-8 List of PAH Compounds in Carbon Black.

[143] B. Alberto, J.L. Tadeo, and R.A. Pérez. Trac-Trends Anal. Chem. 118 (2019) 739–750.

[144] M. Yousefi, M. Rahimi-Nasrabadi, S.M. Pourmortazavi, M. Wysokowski, T. Jesionowski, H. Ehrlich, and S. Mirsadeghi. Trac-Trends Anal. Chem. 118 (2019) 182–193.

[145] V. Andreu and Y. Picó. Trac-Trends Anal. Chem. 118 (2019) 709–721.

[146] M. Sajid and J. Płotka-Wasylka. Trac-Trends Anal. Chem. 103 (2018) 74–86.

[147] J. Płotka-Wasylka, N. Szczepańska, M. de la Guardia, and J. Namieśnik. Trac-Trends Anal. Chem. 73 (2015) 19–38.

[148] J.S. da Silva Burato, D.A. Vargas Medina, A.L. de Toffoli, E.V. Soares Maciel, and F.M. Lanças. J. Sep. Sci. 43 (2020) 202–225.

[149] S. Liu and P.K. Dasgupta. Anal. Chem. 67 (1995) 2042–2049.

[150] H. Liu and P.K. Dasgupta. Anal. Chem. 68 (1996) 1817–1821.

[151] M.A. Jeannot and F.F. Cantwell. Anal. Chem. 68 (1996) 2236–2240.

[152] M.A. Jeannot and F.F. Cantwell. Anal. Chem. 69 (1997) 235–239.

[153] J.M. Kokosa, A. Przyjazny, and M.A. Jeannot (Editors) Solvent Microextraction: Theory and Practice, John Wiley & Sons, Inc. (2009).

[154] A. Spietelun, Ł. Marcinkowski, M. de la Guardia, and J. Namieśnik. Talanta 119 (2014) 34–45.

[155] Y. Yamini, M. Rezazadeh, and S. Seidi. Trac-Trends Anal. Chem. 112 (2019) 264–272.

[156] M.A. Farajzadeh, S.E. Seyedi, M.S. Shalamzari, and M. Bamorowat, J. Sep. Sci. 32 (2009) 3191–3200.

[157] A. Saleh, Y. Yamini, M. Faraji, M. Rezaee, and M. Ghambarian. J. Chromatogr. A 1216 (2009) 6673–6679.

[158] L. Guo and H.K. Lee. J. Chromatogr. A 1218 (2011) 5040–5046.

[159] S. Pedersen–Bjergaard and K.E. Rasmussen. Anal. Chem. 71 (1999) 2650–2656.

[160] M. Rezaee, Y. Assadi, M.R. Millani, E. Aghaee, F. Ahmadi, and S. Berijani. J. Chromatogr. A 1116 (2006) 1–9.

[161] C. Basheer, A.A. Alnedhary, B.S.M. Rao, S. Valliyaveettil, and H.K. Lee. Anal. Chem. 78 (2006) 2853–2858.

[162] P. Rocío-Bautista, P. González-Hernández, V. Pino, J. Pasán, and A.M. Afonso. Trac-Trends Anal. Chem. 90 (2017) 114–134.

[163] C.L. Arthur and J. Pawliszyn. Anal. Chem. 62 (1990) 2145–2148.

[164] A. Kloskowski and M. Pilarczyk. Anal. Chem. 81 (2009) 7363–7367.

[165] T. Górecki, X. Yu, and J. Pawliszyn. Analyst 124 (1999) 643–649.

[166] SUPELCO® SPME Metal Fiber Assemblies Product Information. https://www.sigmaaldrich.com/content/dam/sigma-aldrich/docs/Supelco/Product_Information_Sheet/t405058.pdf. (last accessed: 27th January 2020)

[167] V. Jalili, A. Barkhordari, and A. Ghiasvand. Microchem. J. 152 (2020) 104319.

[168] R. Eisert and J. Pawliszyn. Anal. Chem. 69 (1997) 3140–3147.

[169] E. Baltussen, P. Sandra, F. David, and C. Cramers. J. Microcolumn. Sep. 11 (1999) 737–747.

[170] GERSTEL Twister® Product Information. http://www.gerstel.com/en/twister-stir-bar-sorptive-extraction.htm. (last accessed: 27th January 2020).

[171] J.M.F. Nogueira. Anal. Chim. Acta 757 (2012) 1–10.

[172] A. Gutiérrez-Serpa, D. Schorn-García, F. Jiménez-Moreno, A.I. Jiménez-Abizanda, and V. Pino. Microchim. Acta 186 (2019) 311.

[173] H. Piri-Moghadam, Md.N. Alam, and J. Pawliszyn. Anal. Chim. Acta 984 (2017) 42–65.

[174] Y. Chen, L. Xia, R. Liang, Z. Lu, L. Li, B. Huo, G. Li, and Y. Hu. Trac-Trends Anal. Chem. 120 (2019) 115652.

[175] B.H. Fumes, M. Ribeiro Silva, F. Nascimento Andrade, C.E. Domingues Nazario, and F.M. Lanças. Trac-Trends Anal. Chem. 71 (2015) 9–25.

[176] Y. Wen, L. Chen, J. Li, D. Liu, and L. Chen. Trac-Trends Anal. Chem. 59 (2014) 26–41.

[177] I. Pacheco-Fernández, A. Gutiérrez-Serpa, P. Rocío-Bautista, and V. Pino. In: W. Verreau and G. Baril (Editors), Molecularly imprinted polymers as promising sorbents in SPME applications, Nova Science Publishers (2017) 147–168.

[178] R. Lucena, B.M. Somonet, S. Cárdenas, and M. Valcárcel. J. Chromatogr. A 1218 (2011) 620–637.

[179] T.D. Ho, C. Zhang, L.W. Hantao, and J.L. Anderson. Anal. Chem. 86 (2014) 262–285.

[180] A. Gutiérrez-Serpa, I. Pacheco-Fernández, J. Pasán, and V. Pino. Separations 6 (2019) 47.

[181] E. Turiel and A. Martín-Esteban. Trac-Trends. Anal. Chem. 118 (2019) 574–586.

[182] A. Azizi and C.S. Bottaro. J. Chromatogr. A 1610 (2020) 460534.

[183] A. Ostovan, M. Ghaedi, M. Arabi, Q. Yang, J. Li, and L. Chen. ACS Appl. Mater. Interfaces 10 (2018) 4140–4150.

[184] R. Mirzajani and F. Kardani. J. Pharmaceut. Biomed. 122 (2016) 98–109.

[185] X. Su, X. Li, J. Li, M. Liu, F. Lei, X. Tan, P. Li, and W. Luo. Food Chem. 171 (2015) 292–297.

[186] R. Guedes-Alonso, S. Santana-Viera, Z. Sosa-Ferrera, and J.J. Santana-Rodríguez. J. Sep. Sci. 38 (2015) 3961–3968.

[187] H. Sun, Y. Li, C. Huang, J. Peng, J. Yang, X. Sun, S. Zang, J. Chen, and X. Zhang. J. Sep. Sci. 38 (2015) 3412–3420.

[188] X. Sun, X.-Y. Jiao, J. Li, and L. Xu. J. Chromatogr. A 1543 (2018) 1–13.

[189] T. Du, J. Cheng, M. Wu, X. Wang, H. Zhou, and M. Cheng. J. Chromatogr. B 951-952 (2014) 194–109.

[190] C. Cai, P. Zhang, J. Deng, H. Zhou, and J. Cheng. J. Sep. Sci. 41 (2018) 1104–1111.

[191] M. Zhang and J. Huang. RSC Adv. 6 (2016) 94098–94104.

[192] M. Zarejousheghani, M. Moder, and H. Borsdorf. Anal. Chim. Acta 798 (2013) 48–55.

[193] X.U. Zhi-gang, D.U. Zhuo, L. Hai-xian, H.U. Yu-ling, and L.I. Gong-ke. Chem. Res. Chin. U 28 (2012) 594–599.

[194] X. Chen and N. Ye. RSC Adv. 7 (2017) 34077.

[195] F. Chen, J. Zhang, M. Wang, and J. Kong. J. Sep. Sci. 38 (2015) 2670–2676.

[196] X. Wang, P. Huang, X. Ma, H. Wang, X. Lu, and X. Du. Talanta 166 (2017) 300–305.

[197] X. Yuan, X. Li, P. Guo, Z. Xiong, L. Zhao. Anal. Methods 10 (2018) 4404–4413.

[198] L. Guo, X. Ma, X. Xie, R. Huang, M. Zhang, J. Li, G. Zeng, and Y. Fan. Chem. Eng. J. 361 (2019) 245–255.

[199] M. Díaz-Álvarez, E. Turiel, and A. Martín-Esteban. J. Chromatogr. A 1469 (2016) 1–7.

[200] H.W. Kroto, J.R. Heath, S.C.O. Brien, R.F. Curl, and R.E. Smalley. Nature 318 (1985) 162–163.

[201] M. Gallego, Y.P. e Pena, and M. Valcárcel. Anal. Chem. 66 (1994) 4074–4078.

[202] E.V. Soares Maciel, A.L. de Toffoli, E. Sobieski Neto, C.E. Domingues Nazario, and F.M. Lanças. Trac-Trends Anal. Chem. 119 (2019) 115633.

[203] N. Shahabadi, A. Khorshidi, H. Zhaleh, and S. Kashanian. J. Drug Deliv. Sci. Technol. 46 (2018) 55–65.

[204] X.-Y. Song, J. Chen, and Y.-P. Shi. Trac-Trends. Anal. Chem. 86 (2017) 263–275.

[205] B. Socas-Rodríguez, J. González-Sálamo, J. Hernández-Borges, and M.Á. Rodríguez-Delgado. Trac-Trends. Anal. Chem. 96 (2017) 172–200.

[206] C.-S. Jon, L.-Y. Meng, and D. Li. Trac-Trends. Anal. Chem. 120 (2019) 115641.

[207] K.S. Novoselov, A.K. Geim, S.V. Morozov, D. Jiang, Y. Zhang, S.V. Dubonos, I.V. Grigorieva, and A.A. Firsov. Science 306 (2004) 666–669.

[208] I. Reinholds, I. Pugajeva, D. Zacs, E. Lundanes, J. Rusko, I. Perkons, and V. Bartkevics. Environ. Monit. Assess. 189 (2017) 568.

[209] S. Dahane, M.D. Gil García, A. Uclés Moreno, M. Martínez Galera, M. del M. Socías Viciana, and A. Derdour. Microchim. Acta 182 (2015) 95–103.

[210] X. Zhu, Y. Cui, X. Chang, and H. Wang. Talanta 146 (2016) 358–363.

[211] M. Krawczyk and M. Jeszka-Skowron. Microchem. J. 126 (2016) 296–301.

[212] I. López-García, J.J. Marín-Hernández, and M. Hernández-Córdoba. Anal. Methods 11 (2019) 635–641.

[213] Y. Huang, J. Peng and X. Huang. J. Chromatogr. A 1546 (2018) 28–35.

[214] S. Xue, C. Wang, and Y. Wei. RSC Adv. 7 (2017) 11921.

[215] M.N. Yazdi, Y. Yamini, and H. Asiabi. J. Chromatogr. A 1554 (2018) 8–15.

[216] Q. Wu, C. Feng, G. Zhao, C. Wang, and Z. Wang. J. Sep. Sci. 35 (2012) 193–199.

[217] S. Li, F. Zhu, R. Jiang, and G. Ouyang. J. Chromatogr. A 1429 (2016) 1–7.

[218] E. Memarian, S.S. Hosseiny Davarani, S. Nojavan, and S.K. Movahed. Anal. Chim. Acta 935 (2016) 151–160.

[219] S.C. Bernardo, A.C.A. Sousa, M.C. Neves, and M.G. Freire. In: A. Hussain Bhat, I. Khan, M. Jawaid, F.O. Suliman, H. Al-Lawati, and S.M. Al-Kindy (Editors), Use of nanomaterials in the pretreatment of water samples for environmental analysis, Springer (2019) 103–142.

[220] P. Rocío-Bautista and V. Pino. In: J.L. Anderson, A. Berthod, V. Pino, and A.M. Stalcup (Editors), Extraction methods facilitated by the use of magnetic nanoparticles, Wiley (2015) 475–502.

[221] P. Yu, Q. Wang, X. Zhang, X. Zhang, S. Shen, and Y. Wang. Anal. Chim. Acta 678 (2010) 50–55.

[222] A. Gutiérrez-Serpa, P. Rocío-Bautista, V. Pino, F. Jiménez-Moreno, and A.I. Jiménez-Abizanda. J. Sep. Sci. 40 (2017) 2009–2021.

[223] A. Gutiérrez-Serpa, P.I. Napolitano-Tabares, V. Pino, F. Jiménez-Moreno, A.I. Jiménez-Abizanda. Microchim. Acta 185 (2018) 341.

[224] C. Liu, X. Zhang, L. Li, J. Cui, Y.-e. Shi, L. Wang, and J. Zhan. Analyst 140 (2015) 4668–4675.

[225] Y. Yang, Y. Li, H. Lu, X. Wang, and X. Du. J. Chromatogr. A 1372 (2014) 25–33.

[226] N. Jiang, J. Wang, W. Li, J. Xiao, J. Xi, X. Lin, Z. Xie, L. You, and Q. Zhang. J. Chromatogr. A 1585 (2019) 19–26.

[227] A. Mollahosseini, Y. Elyasi, and M. Rastegari. Microchem. J. 151 (2019) 104191.

[228] P. Serra-Mora, R. Herráez-Hernández, and P. Campíns-Falcó. J. Chromatogr. A (2019) 460819.

[229] M. Zhang, J. Yang, X. Geng, Y. Li, Z. Zha, and S. Cui. J. Chromatogr. A 1598 (2019) 20–29.

[230] M. He, S. Su, B. Chen, and B. Hu. Talanta 207 (2020) 120314.

[231] P. Baile, L. Vidal, and A. Canals. J. Chromatogr. A 1603 (2019) 33–43.

[232] M.M. Ariffin, N.M. Sohaimi, B.S. Yih, and N.M. Saleh. Anal. Methods 11 (2019) 4126.

[233] M. Cordero-Vaca, M.J. Trujillo-Rodríguez, C. Zhang, V. Pino, J.L. Anderson, A.M. Afonso. Anal. Bioanal. Chem. 407 (2015) 4615–4627.

[234] O. Nacham, A. Martín-Pérez, D.J. Seteyer, M.J. Trujillo-Rodríguez, J.L. Anderson, V. Pino, and A.M. Afonso. Colloids Surf. A Physicochem. Eng. Asp. 469 (2015) 224–234.

[235] B. Clare, A. Sirwardana, and D.R. MacFarlane. In: B. Kirchner (Editor) Synthesis, purification and characterization of ionic liquids, Springer-Verlag (2010) 1–40.

[236] P. Walden. Bull. Acad. Sci. 1800 (1914) 405–422.

[237] J.S. Wilkes and M.J. Zaworotko. J. Chem. Soc., Chem. Commun. (1992) 965–967.

[238] M J. Trujillo-Rodríguez, P. Rocío-Bautista, V. Pino, and A.M. Afonso. Trends Anal. Chem. 51 (2013) 87–106.

[239] R. Marcinkowska, K. Konieczna, Ł. Marcinkowski, J. Namieśnik, and A. Kloskowski. Trends Anal. Chem. 119 (2019) 115614.

[240] K. Yavir, Ł. Marcinkowski, R. Marcinkowska, J. Namieśnik, and A. Kloskowski. Anal. Chim. Acta 1054 (2019) 1–16.

[241] L. Vidal, M.-L. Riekkola, and A. Canals. Anal. Chim. Acta 715 (2012) 19–41.

[242] M. Mei, X. Huang, and L. Chen. Trac-Trends. Anal. Chem. 112 (2019) 123–134.

[243] M.J. Trujillo-Rodríguez, H. Nan, M. Varona, M.N. Emaus, I. D Souza, and J.L. Anderson. Anal. Chem. 91 (2018) 505–531.

[244] A. Cruz Sotolongo, M.M. Messina, F.J. Ibañez, and R.G. Wuilloud. Talanta 210 (2020) 120614.

[245] M. Llaver, E.A. Coronado, and R.G. Wuilloud. Spectrochim. Acta B 138 (2017) 23–30.

[246] X. Cao, L. Shen, X. Ye, F. Zhang, J. Chen, and W. Mo. Analyst 139 (2014) 1938.

[247] Q. Jiang, Q. Liu, Q. Chen, W. Zhao, G. Xiang, L. He, X. Jiang, and S. Zhang. J. Sep. Sci. 39 (2016) 3221–3229.

[248] F. Aflatouni and M. Soleimani. Chromatographia 81 (2018) 1475–1486.

[249] J. An and J.L. Anderson. Talanta 182 (2018) 74–82.

[250] Y. Zhang and Y. Duan. Anal. Bioanal. Chem. 411 (2019) 2209–2221.

[251] M. Merdivan, V. Pino, and J.L. Anderson. Environ. Technol. 38 (2017) 1897–1904.

[252] T.D. Ho, B.R. Toledo, L.W. Hantao, and J.L. Anderson. Talanta 118 (2014) 172–179.

[253] M. Sun, J. Feng, Y. Bu, and C. Luo. J. Chromatogr. A 1458 (2016) 1–8.

[254] M. Mei and X. Huang. J. Chromatogr. A 1525 (2017) 1–9.

[255] L. Chen, J. Pei, X. Huang, and M. Lu. J. Chromatogr. A 1564 (2018) 34–41.

[256] L. Chen, M. Mei, X. Huang, and D. Yuan. Talanta 152 (2016) 98–104.

[257] J.L. Bendé, J.L. Anderson, and A. Chisvert. Talanta 176 (2018) 253–261.

[258] A. Chisvert, J.L. Benedé, J.L. Anderson, S.A. Pierson, and A. Salvador. Anal. Chim. Acta 983 (2017) 130–140.

[259] B.F. Hoskins and R. Robson. J. Am. Chem. Soc. 112 (1990) 1546–1554.

[260] S. Kitagawa, S. Matsuyama, M. Munakata, and T. Emori. J. Chem. Soc., Dalton Trans. (1991) 2869–2874.

[261] O.M. Yaghi and H. Li. J. Am. Chem. Soc. 117 (1995) 10401–10402.

[262] D. Riou and G. Férey. J. Mater. Chem. 8 (1998) 2733–2735.

[263] P. Kumar, K. Vellingiri, K.H. Kim, R.J.C. Brown, and M.J. Manos. Microporous Mesoporous Mater. 253 (2017) 251–265.

[264] C. Pettinari, F. Marchetti, N. Mosca, G. Tosi, and A. Drozdov. Polym. Int. 66 (2017) 731–744.

[265] H. Furukawa, K.E. Cordova, M. O'Keeffe, and O.M. Yaghi. Science 341 (2013) 1230444.

[266] X. Yang and Q. Xu. Cryst. Growth Des. 17 (2017) 1450–1455.

[267] H. Li, K. Wang, Y. Sun, C.T. Lollar, J. Li, and H.-C. Zhou. Mater. Today 21 (2018) 108–121.

[268] M.-X. Wu and Y.-W. Yang. Adv. Mater. 29 (2017) 1606134.

[269] H. Cai, Y.-L. Huang, and D. Li. Coord. Chem. Rev. 378 (2019) 207–221.

[270] L. Zhu, X.-Q. Liu, H.-L. Jiang, and L.-B. Sun. Chem. Rev. 117 (2017) 8129–8176.

[271] C. Xu, R. Fang, R. Luque, L. Chen, and Y. Li. Coord. Chem. Rev. 388 (2019) 268–292.

[272] W.P. Lustig, S. Mukherjee, N.D. Rudd, A.V. Desai, J. Li, and S.K. Ghosh. Chem. Soc. Rev. 46 (2017) 3242–3285.

[273] A. Amini, S. Kazemi, and V. Safarifard. Polyhedron 177 (2020) 114260.

[274] A.C. McKinlay, R.E. Morris, P. Horcajada, G. Ferey, R. Gref, P. Couvreur, and C. Serre. Angew. Chemie 49 (2010) 6260–6266.

[275] P. Kumar, A. Deep, and K.-H. Kim. Trends Anal. Chem. 73 (2015) 39–53.

[276] Y. Cui, F. Zhu, B. Chen, and G. Qian. Chem. Comm. 51 (2015) 7420–7431.

[277] J. Pei, K. Shao, L. Zhang, H.-M. Wen, B. Li, and G. Qian. Top. Curr. Chem. 377 (2019) 33.

[278] J. Li, H. Wang, X. Yuan, J. Zhang, and J. W. Chew. Coord. Chem. Rev. 404 (2020) 213116

[279] P. Rocío-Bautista, I. Pacheco-Fernández, J. Pasán, and V. Pino. Anal. Chim. Acta 939 (2016) 26–41.

[280] F. Maya, C.P. Cabello, R.M. Frizzarin, J.M. Estela, G.T. Palomino, and V. Cerdà. Trends Anal. Chem. 90 (2017) 142–152.

[281] J. Zhang and Z. Chen. J. Chromatogr. A 1530 (2017) 1–18.

[282] K. Yusuf, A. Aqel, and Z. Alothman. J. Chromatogr. A 1348 (2014) 1–16.

[283] I. Pacheco-Fernández, P. González-Hernández, J. Pasán, J.H. Ayala, and V. Pino. In: M. de la Guardia and F.A. Esteve-Trurrillas (Editors) Handbook of Smart Materials in Analytical Chemistry, Wiley (2018) 463–502.

[284] P. Rocío-Bautista, V. Pino, J.H. Ayala, C. Ruiz-Pérez, O. Vallcorba, A.M. Afonso, and J. Pasán. RSC Adv. 8 (2018) 31304–31310.

[285] P. González-Hernández, A. Gutiérrez-Serpa, P. Rocío-Bautista, J. Pasán, J.H. Ayala, and V. Pino. In: V. Mittal (Editor) Metal Organic Frameworks, Central West Publishing (2019) 99–136.

[286] S.S.-Y. Chui, S.M.-D. Lo, J.P.H. Charmant, A.G. Orpen, and I.D. Williams. Science 283 (1999) 1148–1150.

[287] G. Férey, C. Mellot-Draznieks, C. Serre, F. Millange, J. Dutour, S. Surblé, and I. Margiolaki. Science 309 (2005) 2040–2042.

[288] P. Horcajada, S. Surblé, C. Serre, D. Y. Hong, Y.K. Seo, J.S. Chang, J.-M. Grenèche, I. Margiolaki, and G. Férey. Chem. Commun. 27 (2007) 2820–2822.

[289] T. Loiseau, C. Serre, C. Huguenard, G. Fink, F. Taulelle, M. Henry, T. Bataille, and G. Férey. Chem. Eur. J. 10 (2004) 1373–1382.

[290] H. Li, M. Eddaoudi, M. O'Keeffe, and O.M. Yaghi. Nature 402 (1999) 276–279.

[291] J.H. Cavka, S. Jakobsen, U. Olsbye, N. Guillou, C. Lamberti, S. Bordiga, and K.P. Lillerud. J. Am. Chem. Soc. 130 (2008) 13850–13851.

[292] K.S. Park, Z. Ni, A.P. Côté, J.Y. Choi, R. Huang, F.J. Uribe-Romo, H.K. Chae, M. O'Keeffe, and O.M. Yaghi. Proc. Natl Acad. Sci. USA 103 (2006) 10186–10191.

[293] Z. Moradi, E.A. Dil, and A. Asfaram. Analyst 144 (2019) 4351–4361.

[294] Y. Jia, Y. Zhao, M. Zhao, Z. Wang, X. Chen, and M. Wang. J. Chromatogr. A 1551 (2018) 21–28.

[295] Y. Dou, L. Guo, G. Li, X. Lv, L. Xia, and J. You. Microchem. J. 146 (2019) 366–373.

[296] C. Hu, M. He, B. Chen, C. Zhong, and B. Hu. J. Chromatogr. A 1356 (2014) 45–53.

[297] Z. Xiao, M. He, B. Chen, and B. Hu. Talanta 156 (2016) 126–133.

[298] J.-H. Yang, C.-X. Cui. L.-B. Qu, J. Chen, X.-M. Zhou, and Y.-P. Zhang. Microchem. J. 141 (2018) 369–376.

[299] H. Bahrami, B. Rezaei, and M.T. Jafari. Anal. Methods 11 (2019) 1073–1079.

[300] I. Taima-Mancera, P. Rocío-Bautista, J. Pasán, J.H. Ayala, C. Ruiz-Pérez, A.M. Alfonso, A.B. Lago, and V. Pino. Molecules 23 (2018) 2869.

[301] G. González-Rodríguez, I. Taima-Mancera, A.B. Lago, J.H. Ayala, J. Pasán, and V. Pino. Molecules 24 (2019) 3656.

[302] S.E. Moradi, A.M.H. Shabani, S. Dadfarnia, and S. Emami. Anal. Methods 8 (2016) 6337–6346.

[303] H. Su, Y. Lin, Z. Wang, Y.-L. E. Wong, X. Chen, and T.-W.D. Chan. J. Chromatogr. A 1466 (2016) 21–28.

[304] L. Hao, X. Liu, J. Wang, C. Wang, Q. Wu, and Z. Wang. Talanta 142 (2015) 104–109.

[305] P. Nurerk, M. Llompart, P. Donkhampa, O. Bunkoed, and T. Dagnac. J. Chromatogr. A 1610 (2020) 460564.

[306] D. Ge and H.K. Lee. J. Chromatogr. A 1218 (2011) 8490–8495.

[307] Z. Huang and H.K. Lee. J. Chromatogr. A 1401 (2015) 9–16.

[308] S.C. Tan and H.K. Lee. Microchim. Acta 186 (2019) 165.

[309] Z. Huang and H.K. Lee. Talanta 143 (2015) 355–373.

[310] A. Amiri, R. Tayebee, A. Abdar, and F.N. Sani. J. Chromatogr. A 1597 (2019) 39–45.

[311] A. Amiri, F. Ghaemi, and B. Maleki. Microchim. Acta 186 (2019) 131.

[312] J. González-Sálamo, M.Á. González-Curbelo, J. Hernández-Borges, and M.Á. Rodríguez-Delgado. Talanta 195 (2019) 236–244.

[313] E. Tahmasebi, M. Y. Masoomi, Y. Yamini, and A. Morsali. RCS Adv. 6 (2016) 40211.

[314] P. Rocío-Bautista, V. Pino, J.H. Ayala, J. Pasán, C. Ruiz-Pérez, and A.M. Afonso. J. Chromatogr. A 1436 (2016) 42–50.

[315] X. Cao, G. Liu, Y. She, Z. Jiang, F. Jin, M. Jin, P. Du, F. Zhao, Y. Zhang, and J. Wang. RCS Adv. 6 (2016) 113144.

[316] T. Wang, S. Liu, G. Gao, P. Zhao, N. Lu, X. Lun, and X. Hou. Microchim. Acta 184 (2017) 2981–2990.

[317] J. Ma, G. Wu, S. Li, W. Tan, X. Wang, J. Li, and L. Chen. J. Chromatogr. A 1553 (2018) 57–66.

[318] S.-H. Huo and X.-P. Yan. Analyst 137 (2012) 3445–3451.

[319] X. Chen, N. Ding, H. Zang, H. Yeung, R.-S. Zhao, C. Cheng, J. Liu, and T.-W. D. Chan. J. Chromatogr. A 1304 (2013) 241–245.

[320] G.-H. Wang, Y.-Q. Lei, and H.-C. Song. Anal. Methods 6 (2014) 7842.

[321] J. Ma, Z. Yao, L. Hou, W. Lu, Q. Yang, J. Li, and L. Chen. Talanta 161 (2016) 686–692.

[322] M. Xu, K. Chen, C. Luo, G. Song, Y. Hu, and H. Cheng. Chromatographia 80 (2017) 463–471.

[323] H. Liu, L. Chen, and J. Ding. Microchim. Acta 184 (2017) 4091–4098.

[324] L. Lian, X. Zhang, J. Hao, J. Lv, X. Wang, B. Zhu, and D. Lou. J. Chromatogr. A 1579 (2018) 1–8.

[325] H. Kalantari and M. Manoochehri. Microchim. Acta 185 (2018) 196.

[326] Y. Li, X. Zhou, L. Dong, Y. Lai, S. Li, R. Liu, and J. Liu. Environ. Pollut. 252 (2019) 1574–1581.

[327] N. Jalilian, H. Ebrahimzadeh, and A. A. Asgharinezhad. Microchim. Acta 186 (2019) 597.

[328] S. Liu, S. Li, W. Yang, F. Gu, H. Xu, T. Wang, D. Sun, and X. Hou. Talanta 194 (2019) 514–521.

[329] E.M. Peña-Méndez, R.M. Mawale, J.E. Conde-González, B. Socas-Rodríguez, J. Havel, and C. Ruiz-Pérez. Talanta 207 (2020) 120275.

[330] S. Rezabeyk and M. Manoochehri. Microchim. Acta 185 (2018) 365.

[331] S.-H. Huo, H.-Y. An, J. Yu, X.-F. Mao, Z. Zhang, L. Bai, Y.-F. Huang, and P.-X. Zhou. J. Chromatogr. A 1517 (2017) 18–25.

[332] L. Hao, X. Meng, C. Wang, Q. Wu, and Z. Wang. J. Chromatogr. A 1605 (2019) 460364.

[333] L. Xie, S. Liu, Z. Han, R. Jiang, H. Liu, F. Zhu, F. Zeng, C. Su, and G. Ouyang. Anal. Chim. Acta 853 (2015) 303–310.

[334] Z. Zang, G. Zhang, Q. Chang, Z. Zhang, C. Wang, and Z. Wang. Anal. Methods 7 (2015) 918–923.

[335] Y.-Y. Wu, C.-X. Yang, and X.-P. Yan. J. Chromatogr. A 1334 (2014) 1–8.

[336] G. Zhang, X. Zang, Z. Li, C. Wang, and Z. Wang. Talanta 129 (2014) 600–605.

[337] G. Wang, Y. Lei, and H. Song. Talanta 144 (2015) 369–374.

[338] F. Wei, Y. He, X. Qu, Z. Xu, S. Zheng, D. Zhu, and H. Fu. Anal. Chim. Acta 1078 (2019) 70–77.

[339] H. Bagheri H. Javanmardi, A. Abbasi, and S. Banihashemi. J. Chromatogr. A 1431 (2016) 27–35.

[340] X. Hu, C. Wang, J. Li, R. Luo, C. Liu, X. Sun, J. Shen, W. Han, and L. Wang. ACS Appl. Mater. Interfaces 10 (2018) 15051–15057.

[341] S. Wei, X. Kou, Y. Liu, F. Zhu, J. Xu, and G. Ouyang. Talanta 211 (2020) 120706.

[342] Y. Wang, M. Jia, X. Wu, T. Wang, J. Wang, and X. Hou. Microchem. J. 146 (2019) 214–219.

[343] D. Ge, Y. Zhang, Y. Dai, and S. Yang. J. Sep. Sci. 41 (2018) 1635–1643.

[344] H. Wang, L. Hu, X. Liu, S. Yin, R. Lu, S. Zhang, W. Zhou, and H. Gao. J. Chromatogr. A 1516 (2017) 1–8.

[345] S. Ramos, V. Homem, and L. Santos. J. Chromatogr. A 1590 (2019) 47–57.

[346] S.A. Pierson, M.J. Trujillo-Rodríguez, and J.L. Anderson. J. Sep. Sci. 41 (2018) 3081–3088.

[347] S. Clavijo, J. Avivar, R. Suárez, and V. Cerdà. J. Chromatogr. A 1443 (2016) 36–34.

[348] P. Nurerk, M. Llompart, P. Donkhampa, O. Bunkoed, and T. Dagnac. J. Chromatogr. A 1610 (2020) 460564.

[349] M. Vosough, Z. Hassanbeigi, and A. Salemi. J. Sep. Sci. 41 (2018) 2401–2410.

[350] H. Wang, J. Du, Q. Zhen, R. Zhang, X. Wang, and X. Du. Talanta 191 (2019) 193–201.

[351] M.J. Trujillo-Rodríguez, H. Nan, and J.L. Anderson. J. Chromatogr. A 1540 (2018) 11–20.

[352] J.L. Benedé, A. Chisvert, D.L. Giokas, and A. Salvador. Talanta 147 (2016) 246–252.

[353] D.A.V. Medina, Á.J. Santos-Neto, V. Cerdà, and F. Maya. Talanta 189 (2018) 241–248.

[354] G.P. Mashile, A. Mpupa, and P.N. Nomngongo. Molecules 23 (2018) 1450.

[355] P. Rocío-Bautista, C. Martínez-Benito, V. Pino, J. Pasán, J.H. Ayala, C. Ruiz-Pérez, and A.M. Afonso. Talanta 139 (2015) 13–20.

[356] M. Pastor-Belda, L. Marín-Soler, N. Campillo, P. Viñas, and M. Hernández-Córdoba. J. Chromatogr. A 1564 (2018) 102–109.

[357] X. Wang, K. Yuan, H. Liu, L. Lin, and T. Luan. J. Sep. Sci. 37 (2014) 1842–1849.

[358] V. Homem, A. Alves, A. Alves, and L. Santos. Talanta 148 (2016) 84–93.

[359] L. Vallecillos, F. Borrull, and E. Pocurull. J. Chromatogr. A 1364 (2014) 1–11.

[360] L. Xie, S. Liu, Z. Han, R. Jiang, F. Zhu, W. Xu, C. Su, and G. Ouyang. Anal. Bioanal. Chem. 409 (2017) 5239–5247.

[361] S. Li, F. Zhu, R. Jiang, and G. Ouyang. J. Chromatogr. A 1429 (2016) 1–7.

[362] R.-S. Zhao, X. Wang, J. Sun, C. Hu, and X.-K. Wang. Microchim. Acta 174 (2011) 145–151.

[363] V.A. Muckoya, P.B. Njobeh, P.N. Nomngongo, and J.C. Ngila. Chromatographia (2020) IN PRESS.

[364] C. Cortada, L.C. dos Reis, L. Vidal, J. Llorca, and A. Canals. Talanta 120 (2014) 191–197.

[365] L.C. dos Reis, L. Vidal, and A. Canals. J. Sep. Sci. 41 (2019) 4177–4184.

[366] E.Y. Companioni-Damas, F.J. Santos, and M.T. Galceran. Talanta 89 (2012) 63–69.

[367] L. Correa, J.A. Fiscal, S. Ceballos, A. de la Ossa, G. Taborda, C. Nerin, and M. Rosero-Moreano. J. Sep. Sci. 38 (2015) 3945–3953.

[368] A. Domínguez-Tello, A. Arias-Borrego, T. García-Barrera, and J.L. Gómez-Ariza. J. Chromatogr. A 1402 (2015) 8–16.

[369] I. Montesinos and M. Gallego. J. Chromatogr. A 1248 (2012) 1–8.

[370] B. Zhang, G. Xu, L. Li, X. Wang, N. Li, R.-S. Zhao, and J. Lin. Chem. Eng. J. 350 (2018) 240–247.

[371] R. Maia, M. Correia, I.S.B. Pereira, and V.M. Beleza. Microchem. J. 112 (2014) 164–171.

[372] S. Allard, J.W.A. Charrois, C.A. Joll, and A. Heitz. J. Chromatogr. A 1238 (2012) 15–21.

[373] B. Hammami and M.R. Driss. J. Anal. Chem. 68 (2013) 671–679.

[374] R.A.A. Carter, D.S. Liew, N. West, A. Heitz, and C.A. Joll. Chemosphere 220 (2019) 314–323.

[375] J. On, H. Pyo, and S.-W. Myung. Sci. Total Environ. 639 (2018) 208–216.

[376] H. Ma, Y. Li, H. Zhang, S.M. Shah, and J. Chen. J. Chromatogr. A 1358 (2014) 14–19.

[377] S. Hu, T. Gong, J. Ma, Y. Tao, and Q. Xian. Chemosphere 198 (2018) 147–153.

[378] M. Serrano, M. Silva, and M. Gallego. J. Chromatogr. A 1358 (2014) 232–239.

[379] Z. Li, J. Wang, X. Chen, S. Hu, T. Gong, and Q. Xian. Food Chem. 292 (2019) 267–274.

[380] Y. Qian, M. Wu, W. Wang, B. Chen, H. Zheng, S.W. Krasner, S.E. Hrudey, and X.-F. Li. Anal. Chem. 87 (2015) 1330–1336.

[381] I. Kristiana, C. Joll, and A. Heitz. J. Chromatogr. A 1225 (2012) 45–54.

[382] A.K. Huba, M.F. Mirabelli, and R. Zenobi. Anal. Chim. Acta 1030 (2018) 125–132.

[383] J. Quintana, A. de la Cal, and M.R. Boleda. Sci. Total. Environ. 692 (2019) 952–965.

[384] M. Mokhtari, H. Hamaizi, M.D. Gil García, and M. Martínez Galera. Microchem. J. 153 (2020) 104515.

[385] C.A. Chávez-Moreno, L. Hinojosa-Reyes, E.J. Ruiz-Ruiz, A. Hernández-Ramírez, and J.L. Guzmán-Mar. J. Sep. Sci. 41 (2018) 4488–4497.

[386] M.J. Trujillo-Rodríguez, J.L. Anderson, S.J.B. Dunham, V.L. Noad, and D.B. Cardin. Talanta 208 (2020) 120390.

CHAPTER II

Hypothesis and objectives

Harmful chemical substances are introduced in the environment mainly due to anthropogenic activities, producing the contamination of the ecosystems by direct discharge or through their migration in the environment. Due to the water cycle, drinking waters can experience contamination in lower or higher extent, thus involving a direct or indirect potential risk for all living organisms. The growing of the global population, not only implying an increase in the consumption of certain chemical substances but also by the demand of higher amounts of quality water, and the ineffectiveness of the treatments in WWTPs to remove a variety of contaminants, justify the increased presence of pollutants in the environment.

The term emerging contaminants refer to those chemical substances recently categorized as hazardous or labelled as potentially risky for the human health and the environment, but their presence in the environment is not necessarily new. The emerging contaminants can be harmful or can form harmful metabolites, thus being under study due to their environmental fate, their bioactivity, and their high persistence in some cases.

Giving the current regulations and/or concerns of the potential effects of the emerging contaminants, scientific efforts focus on the study of their occurrence, fate, and monitoring. In this sense, the Analytical Chemistry field plays an important role in the development of adequate analytical methods to ensure proper monitoring. Green Chemistry principles concur in parallel to this context, and indeed monitoring strategies must follow environmental-friendly requirements according to GAC.

The classic analytical procedures for environmental monitoring involve several steps, high consumption of toxic organic solvents, and long analysis times. In addition to this, emerging pollutants are present in environmental waters at trace levels, thus requiring in most cases prior extraction steps to increase the sensitivity. Clearly, analytical methods require high improvements to fulfill green aspects.

In this sense, trends in analytical sample preparation focus on the development of new methodologies able to provide adequate analytical performance (in terms of accuracy, precision and sensitivity) and, at the same time, able to comply with regulations and GAC requirements. Among reported strategies, those linked to miniaturization are of particular interest.

Microextraction techniques can be categorized according to the nature of the material used as extractant: liquid (liquid-based microextraction) or solid (sorbent-based microextraction).

The research on new materials able to be incorporated in these microextraction approaches, maintaining or even improving the analytical performance despite miniaturization issues, while permitting improved environmental-friendly aspects, is a hot topic nowadays. Among the variety of materials proposed and used successfully in analytical sample preparation and in microextraction methods, MOFs can be highlighted due to their unique and exceptional physical-chemical properties: in particular, their impressive surface area, their chemical and thermal stability in many cases, and their outstanding synthetic tuneability.

The main goal of this Doctoral Thesis is the development of analytical methods based on the use of microextraction techniques to monitor two important groups of emerging contaminants: PCPs and DBPs, in environmental water samples, intending to compile most requirements of GAC while ensuring adequate analytical performance. To achieve this goal, the following partial objectives are established:

- *Selection of the proper method for the target analytes considered*

The nature of the target analytes (PCPs or DBPs) is going to dictate the use of LC or GC, the nature of the detection system combined with the selected chromatographic technique, as well as the most suitable microextraction method to be utilized. In all cases, novel methods, properly evaluated *versus* conventional approaches, will be proposed to detect and quantify PCPs and DBPs in environmental waters of different nature.

- *Synthesis and characterization of novel MOFs to be incorporated in sorbent-based microextraction techniques*

Despite the fact that a number of MOFs have been already successfully used as extraction sorbents in DµSPE and SPME, issues associated to low efficiency in the desorption step have been described, and few applications take advantage of their synthetic tuneability. In this sense, it is intended the design and synthesis of novel MOFs with different functionalization groups in their structures (to improve interactions with target analytes), while ensuring a crystal structure able to facilitate the diffusion of extracted compounds within the pores of the material (thus improving their further desorption). All designed MOFs should also present proper characteristics as sorbents in microextraction. Thus, the complete characterization of the MOFs is essential, and a number of techniques will be used for this purpose, such as, powder X-ray diffraction (PXRD) and single crystal X-ray, thermal gravimetric analysis (TGA), infrared spectroscopy (IR), N_2 adsorption isotherms, and scanning electron microscopy (SEM), among others.

Taking into account that the interactions of analytes and MOFs used as sorbents in microextraction will determine the extraction efficiency of the entire method, it results mandatory to have a better understanding of these interactions. In this sense, studies on the adsorption capacity, release performance, and the kinetic behavior of the MOFs considered in this Doctoral Thesis are quite important.

Last, but not least, proper description of the structures, together with computational analysis, will be useful to understand the presence of preferential sites for adsorption of target analytes in these materials.

- *Evaluation and optimization of the variables that affect the analytical methods selected for the target analytes*

The conditions of the entire analytical method, including both the chromatographic and the microextraction conditions, clearly affect the performance and obviously the sensitivity of the overall method.

Regarding the chromatographic separation of the target analytes, the instrumental conditions (GC or LC, combined with the most proper detectors) are evaluated to obtain the maximum response and, at the same time, with the minimum time required.

On the other hand, it is also important to select proper conditions of each microextraction procedure, ensuring the maximum extraction efficiencies, optimum preconcentration, high reproducibility, as well as meeting GAC requirements (low consumption of sample, reagents, sorbents or solvents, low energy requirements, automation if possible, and low times). To achieve this goal, the main variables influencing the microextraction procedure will be studied and subjected to optimization. The optimization will be carried out using experimental design tools in all cases, except in the LPME application due to the simplicity of the extraction procedure.

- *Validation of the optimum methods in terms of quality analytical parameters*

Once the optimum conditions are selected, the overall analytical method requires validation. Quality analytical parameters of the calibration together with the evaluation of the overall method in terms of extraction efficiency, sensitivity, accuracy, and precision will be pursued.

- *Application of the developed methods to the analysis of water*

The validated method will be employed in the analysis of environmental water samples from different sources. Thus, the optimum method will be used for the analysis of samples that can be subject of possible contamination with the emerging contaminants considered (PCPs or DBPs, depending of the sample). Furthermore, the matrix effects will be evaluated in order to determine if the results are affected by the composition of the sample.

According to the background and objectives set, this Doctoral Thesis is indexed in the following chapters:

- **Chapter I - Introduction**. In this chapter, the background about the presence of emerging contaminants in the environment is presented, giving special attention to PCPs and DBPs, as well as stating the need of development of proper analytical extraction method to expand the results on the research about their fate and environmental levels. Trends in Analytical Chemistry referred to analytical sample preparation are also described, together with the GAC principles and the current microextraction methods proposed for this goal. Due to their wide used in this Thesis Doctoral, the use of MOFs in sorbent-based analytical sample preparation methods is also described. Finally, an overview on the current analytical methods described for the monitoring of PCPs and DBPs is presented.

- **Chapter II - Hypothesis and objectives**. Main hypothesis and objectives are described in this chapter, to show the different approaches pursued in this Doctoral Thesis.

- **Chapter III - Experimental**. In this experimental chapter, the analyte standards, the solvents, the reagents, the materials, and the instrumentation required for the development of the pursued objectives, are described. The procedures are also described, both for the optimum analytical methods and for the synthesis and characterization of MOFs. Furthermore, the type of samples and their collection are detailed.

- **Chapter IV - Results and discussion**. This chapter gather up two Sections according with the development of method to monitor emerging contaminants using: a) liquid-based microextraction techniques (Section IV.1.), or b) using sorbent-based microextraction techniques (Section IV.2.). This last Section also divides in the µSPE (Section IV.2.1.) and SPME applications (Section IV.2.2.). In each Section, the results obtained for the different applications developed using the microextraction techniques are exposed and discussed. Giving the important use of MOFs as sorbents in this Doctoral Thesis, particularly in µSPE, Section IV.2.1. includes the complete characterization of the MOFs synthesized, including a computational study, and the results obtained in the kinetic and adsorption/release studies.

- **Chapter V - Conclusions**. The relevant conclusions achieved in this Doctoral Thesis are summarized in this chapter, giving an overview of the most relevant results and their significance.

CHAPTER III

Experimental

III.1. Analytes

All the analytes studied in this Doctoral Thesis belong to two different groups of emerging contaminants. Table III.1. summarizes the main physicochemical characteristics of the 30 PCPs and the 16 DBPs considered. The studied subgroups of PCPs included preservatives (7), UV-filters (8), musk fragrances (7), disinfectants (1), insect repellents (1), and siloxanes (6); while the subgroups of DBPs included THMs (4), HANs (6), and HNMs (6).

All the standards were supplied at a purity higher than 97%. Methylparaben (MPB), ethylparaben (EPB), propylparaben (PPB), isobutylparaben (iBPB), triclosan (TCS), and bromochloroacetonitrile (BCAN), were purchased from Dr Ehrenstorfer GmbH (Augsburg, Germany); butylparaben (BPB), benzylparaben (BzPB), benzophenone (BP), benzophenone-3 (BP3), 3-(4-methylbenzylidene) camphor (MBC), octocrylene (OCR), 2-ethylhexyl salicylate (EHS), benzyl salicylate (BS), menthyl anthranilate (MA), 2-ethylhexyl 4-(dimethylamino)benzoate (OD-PABA), N,N-diethyl-m-toluamide (DEET), octamethyltrisiloxane (L3), octamethylcyclotetrasiloxane (D4), decamethyltetrasiloxane (L4), decamethylcyclopentasiloxane (D5), dodecamethylpentasiloxane (L5), dodecamethylcyclohexasiloxane (D6), tribromomethane (TBM), bromodichloromethane (BDCM), dibromochloromethane (DBCM), dichloroacetonitrile (DCAN), trichloroacetonitrile (TCAN), bromoacetonitrile (BAN), and bromonitromethane (BNM), were supplied by Sigma-Aldrich (Steinheim, Germany); isopropylparaben (iPPB) was supplied by Alfa Aesar (Karlsruhe, Germany); cashmeran (DPMI), celestolide (ADBI), phantolide (AHMI), traseolide (M-MK), galaxolide (HHCB), tonalide (AHTN), and musk ketone (MK), were supplied by LGC Standards (Barcelona, Spain); bromodichloroacetonitrile (BDCAN), chloronitromethane (CNM), dichloronitromethane (DCNM), dibromonitromethane (DBNM), bromochloronitromethane (BCNM), and bromodichloronitromethane (BDCNM) were acquired from CANSYN (Toronto, Canada), and finally trichloromethane (TCM) and dibromoacetonitrile (DBAN) were purchased from Supelco (Bellefonte, PA, USA).

Table III.1. Main physicochemical characteristics of target analytes studied (SciFinder® 2019).

Analyte (abbreviation)	CAS number	Molecular weight	Boiling point (ºC)	log K_{OW}	pK_a	Vapor pressure (Pa)
PCPs						
Preservatives						
Methylparaben (MPB) 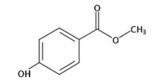	99-76-3	152.15	265.0	1.882	8.31	739.94
Ethylparaben (EPB) 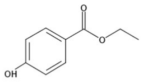	120-47-8	166.17	297.5	2.391	8.31	101.19
Isopropylparaben (iPPB) 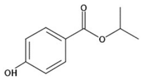	4191-73-5	180.2	286.9	2.745	8.40	197.32
Propylparaben (PPB) 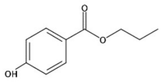	94-13-3	180.20	102.0	2.901	8.23	123.99
Isobutylparaben (iBPB) 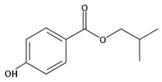	4247-02-3	194.23	302.0	3.250	8.17	74.13
Butylparaben (BPB) 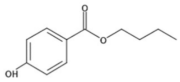	94-26-8	194.23	309.0	3.410	8.22	47.46
Benzylparaben (BzPB) 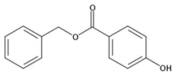	94-18-8	228.24	389.8	3.568	8.18	0.17
Disinfectants						
Triclosan (TCS) 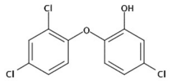	3380-34-5	289.54	50	5.343	7.80	4.35
Insect repellents						
N,N-Diethyl-m-toluamide (DEET) 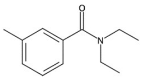	134-62-3	191.27	160	2.419	-1.37	179.98

Table III.1. (continuation).

Analyte (abbreviation)	CAS number	Molecular weight	Boiling point (ºC)	$\log K_{OW}$	pK_a	Vapor pressure (Pa)
UV-filters						
Benzophenone (BP) 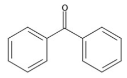	119-61-9	182.22	305.4	3.214	-	109.72
Benzophenone-3 (BP3) 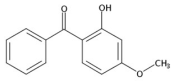	131-57-7	228.24	155	3.995	7.56	0.70
3-(4-Methylbenzylidene) camphor (MBC) 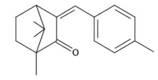	36861-47-9	254.37	198	3.385	-	1.33
Octocrylene (OCR) 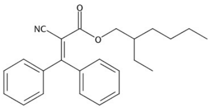	6197-30-4	361.48	218	6.893	-	$3.33\cdot10^{-4}$
2-Ethylhexyl salicylate (EHS) 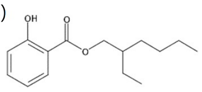	118-60-5	250.33	189	5.934	8.13	10.76
Benzyl salicylate (BS) 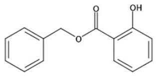	118-58-1	228.24	168	4.209	8.11	23.33
Menthyl anthranilate (MA) 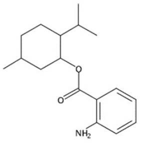	134-09-8	275.39	177	6.085	2.17	0.58
2-Ethylhexyl 4-(dimethylamino)benzoate (OD-PABA) 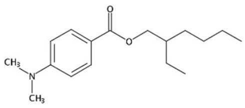	21245-02-3	277.4	325	5.412	2.39	0.61

Table III.1. (continuation).

Analyte (abbreviation)	CAS number	Molecular weight	Boiling point (ºC)	log K_{OW}	Vapor pressure (Pa)
Musk fragrances					
Cashmeran (DPMI) 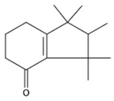	33704-61-9	206.32	286.1	3.437	358.64
Celestolide (ADBI) 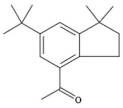	13171-00-1	244.37	309.0	3.761	86.93
Phantolide (AHMI) 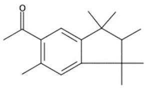	15323-35-0	244.37	336.6	4.536	14.80
Traseolide (M-MK) 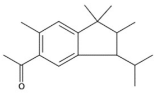	68140-48-7	258.40	350.0	5.018	6.04
Galaxolide (HHCB) 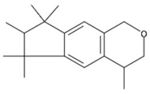	1222-05-5	258.40	129.0	5.043	55.20
Tonalide (AHTN) 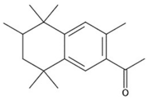	21145-77-7	258.40	124.0	5.063	3.81
Musk ketone (MK) 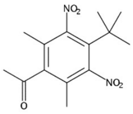	81-14-1	294.30	369.0	2.510	1.63

Table III.1. (continuation).

Analyte (abbreviation)	CAS number	Molecular weight	Boiling point (ºC)	log K_{OW}	Vapor pressure × 10^5 (Pa)
Siloxanes					
Linear siloxanes					
Octamethyltrisiloxane (L3) 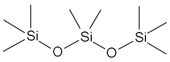	107-51-7	236.53	153	3.646	5.81
Decamethyltetrasiloxane (L4) 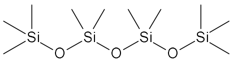	141-62-8	310.69	194	4.824	0.84
Dodecamethylpentasiloxane (L5) 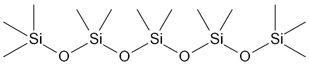	141-63-9	384.84	232	6.002	0.01
Cyclic siloxanes					
Octamethylcyclotetrasiloxane (D4) 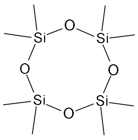	556-67-2	296.62	175	6.980	2.09
Decamethylcyclopentasiloxane (D5) 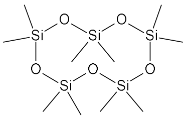	541-02-6	370.77	210	8.13	0.37
Dodecamethylcyclohexasiloxane (D6) 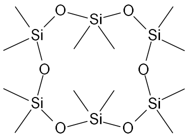	540-97-6	444.92	245	8.87	0.07

Table III.1. (continuation).

Analyte (abbreviation)	CAS number	Molecular weight	Boiling point (ºC)	log K_{OW}	Vapor pressure × 10^5 (Pa)
DBPs					
THMs					
Trichloromethane (TCM) 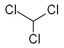	67-66-3	119.38	61.2	1.935	266.64
Bromodichloromethane (BDCM) 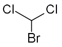	75-25-4	163.83	90.0	2.040	87.06
Dibromochloromethane (DBCM) 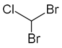	124-48-1	208.28	120.0	2.206	28.00
Tribromomethane (TBM) 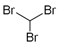	75-25-2	252.73	149.1	2.435	6.89
HANs					
Dichloroacetonitrile (DCAN) 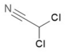	3018-12-0	109.94	112.5	0.938	28.93
Trichloroacetonitrile (TCAN) 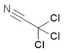	545-06-2	144.39	85.7	2.146	91.46
Bromoacetonitrile (BAN) 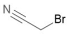	590-17-0	119.95	60.0	0.506	4.24
Dibromoacetonitrile (DBAN) 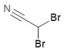	3252-43-5	198.84	67.0	1.565	2.80
Bromochloroacetonitrile (BCAN) 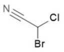	83463-62-1	154.39	125.0	1.220	19.73
Bromodichloroacetonitrile (BDCAN) 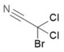	60523-73-1	188.84	55.0	2.387	34.13

Table III.1. (continuation).

Analyte (abbreviation)	CAS number	Molecular weight	Boiling point (ºC)	log K_{OW}	Vapor pressure × 10^5 (Pa)
HNMs					
Chloronitromethane (CNM) 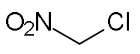	1794-84-9	95.49	122.5	0.373	18.53
Dichloronitromethane (DCNM) 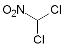	7119-89-3	129.93	106	1.067	36.80
Bromonitromethane (BNM) 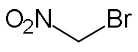	563-70-2	139.94	149	0.875	5.89
Dibromonitromethane (DBNM) 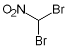	598-91-4	218.83	116	2.051	4.61
Bromochloronitromethane (BCNM) 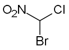	135531-25-8	174.38	132.7	1.528	11.69
Bromodichloronitromethane (BDCNM) 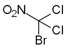	918-01-4	208.83	52	2.634	25.33

III.2. Solvents, reagents and solutions

Ultrapure water was obtained through the Milli-Q gradient system A10 of Millipore (Watford, UK). Acetonitrile (ACN) of LC-MS grade was purchased from VWR International (Barcelona, Spain), while methanol of LC-MS grade and cyclohexane (CHN) of LC-MS grade was purchased from Honeywell (Seelze, Germany). Methanol, acetone, and trichloromethane, all of HPLC grade, were acquired from Sigma-Aldrich. The solvents octanol, decanol, trichloromethane, and tetrachloroethylene, which were used as extractant solvents in different methods of this Doctoral Thesis, were supplied by Sigma-Aldrich; while dichloromethane was acquired from Scharlau (Barcelona, Spain). Ethyl acetate was purchased from Panreac (Barcelona, Spain). Sodium chloride (purity ≥ 99.5%) was acquired from Sigma-Aldrich.

The surfactants used in the evaluation of the extraction of PCPs by vortex assisted emulsification microextraction (VAEME) (Section IV.1.2.1.) included three conventional surfactants and two ionic liquids (ILs)-based surfactants: the cationic cetyltrimethyl ammonium bromide (CTAB), the nonionic polyoxyethylene-10-lauryl ether ($C_{12}E_{10}$), the anionic sodium dodecyl sulfate (SDS), the cationic hexadecylpyridinium chloride monohydrate (C_{16}PyCl), and the cationic 1-hexadecyl-3-methylimidazolium bromide (C_{16}MImBr). CTAB, $C_{12}E_{10}$ and C_{16}PyCl were purchased from Sigma-Aldrich, SDS was acquired from Merck (Darmstadt, Germant), and C_{16}MImBr was synthesized and fully characterized according to a previous study [1].

An acetic/acetate buffer solution was prepared using glacial acetic acid acquired from Merck, and anhydrous sodium acetate (>99%) from Sigma-Aldrich, for the pH adjustment of the samples containing PCPs (Section IV.2.1.2. y Section IV.2.1.3.).

Other studies (Section IV.2.2.1.) required the preparation of buffer solutions for a variety of samples containing DBPs. The following chemicals were used in their preparation: anhydrous potassium hydrogen phosphate (Panreac), potassium dihydrogen phosphate and anhydrous disodium tetraborate (>98%) (Merck), and 0.1 mol·L^{-1} hydrogen chloride solution (Panreac).

Several samples required a pretreatment step to ensure the elimination of the residual chlorine present in them. For this purpose, the quenching agents used were: ammonium chloride (Merck), L(+)-ascorbic acid (VWR International), and pentahydrate sodium thiosulphate (Panreac). The dechlorinating agent solutions (ammonium chloride, ascorbic acid and sodium thiosulphate) were prepared at a concentration level of 0.21 mol·L^{-1}.

2.1. Reagents for the synthesis of MOFs

Up to 8 MOFs were synthesized in this Doctoral Thesis: HKUST-1(Cu), MIL-53(Al), UiO-66(Zr), CIM-81(Zn), CIM-82(Zn), CIM-83(Zn), CIM-91(Zn), and CIM-92(Zn).

The synthesis of MOFs required a number of salts and organic ligands: copper(II) nitrate hemipentahydrate (98%), aluminum(III) nitrate nonahydrate (98%), zirconium chloride (98%), zinc(II) nitrate hexahydrate (98%), mesaconic acid (99%), benzene-1,3,5-tricarboxylic acid (95%), benzene-1,4-dicarboxilic acid (98%), 2-amino-benzene-1,4-dicarboxylic acid (99%), 1,2,4-triazol (98%), and 3-amino-1,2,4-triazol (95%), all purchased from Sigma-Aldrich.

Absolute ethanol and methanol were supplied by Panreac, whereas hydrogen chloride (37%) was acquired from Honeywell. Urea (99%), N,N-dimethylformamide (DMF), N,N-dimethylacetamide (DMA), and ethylene glycol, were acquired from Sigma-Aldrich.

2.2. Standards solutions

Individuals stock solutions of each target analyte were prepared in an adequate solvent (ACN, methanol or CHN, depending on the analyte and on the further analytical technique) at concentration levels between 1000 and 4000 μg·mL^{-1}. Once prepared, they were stored in amber glass bottles at 4 ºC, except the more volatile analytes (methylsiloxanes, musk fragrances, THMs, HANs, and HNMs), which were stored at –20 ºC. An intermediate standard solution containing all the analytes belonging to the same family were prepared weekly by proper dilution of the stock solutions using the same solvent. Working aqueous standard solutions were prepared daily, also performing proper dilution of the intermediate standard solution.

III.3. Materials and apparatus

Durapore Filters of Millipore of 0.22 μm were used for the filtration of ultra-high performance liquid chromatography (UHPLC) mobile phases. The working standard solutions employed for the calibration curves were also filtered before UHPLC injection using Chromafil®Xtra PET 20/25 filters (0.20 mm), acquired from Macherey Nagel (Düran, Germany).

Hamilton® 700 series syringes supplied by Sigma-Aldrich, were used for the injection of extracts and standards in the UHPLC.

The salinity measurement of the samples analyzed in Section IV.2.2.2. was carried out with a Crison model EC-Meter GLP31 (Hach Lange, Spain) conductimeter.

For the VAEME (Section IV.1.2.1.) and D-µSPE procedures (Sections IV.2.1.3. and IV.2.1.4.), Pyrex® centrifuge tubes of 15 mL capacity (Staffordshire, UK) were used. Additionally, a glass syringe Fortuna Optima® of 2 mL capacity (Sigma-Aldrich), and 0.2 µm PVDF (polyvinylidene fluoride) Whatman™ syringe filters (GE, Healthcare, Buckinghamshire, UK) were used in the D-µSPE procedures using MOFs (Sections IV.2.1.3. and IV.2.1.4.). After the extraction of target analytes, round bottom flask of 10 mL of capacity and amber vials of 2 mL capacity were also used for the final extracts.

A Reax Top vortex from Heidolph (Schwabach, Germany), a centrifuge Eppendorf® model 5720 (Hamburg, Germany), and a rotavap IKA RV10 with a vacuum controller CVR 3000 supplied by VWR International, were used in the dispersive extraction procedures (Sections IV.1.2.1., IV.2.1.2 and IV.2.1.3.).

All SPME procedures (Section IV.2.2.) were carried out using 20 mL amber glass vials, fitted with magnetic metal caps, and polytetrafluoroethylene (PTFE)/silicone septa, all supplied by Agilent Technologies (Santa Clara, CA, USA). Stir bars of PTFE (12 × 4.5 mm) were supplied by Sigma-Aldrich. The commercial SPME fibers were supplied by Supelco (Bellefonte, PA, USA), specifically: DVB/CAR/PDMS (50/30 µm), CAR/PDMS (75 µm), PDMS/DVB (65 µm), PDMS (100 µm), and PA (85 µm).

For the synthesis of MOFs (Sections IV.2.1.), the oven used was the Universal UF30 model supplied by Memmert (Schwabach, Germany), and the 45 mL teflon solvothermal reactors and the stainless steel autoclaves were supplied by Parr Instrument Company (Moline, IL, USA).

III.4. Cleaning protocols

All the glassware was cleaned with detergent, tap water and ultrapure water, in that order. Then, the non-graduated glassware was heated in an oven at 550 ºC for three hours to ensure removal of any organic matter still present. The graduated glassware used for applications based on metal-organic framework was washed with nitric acid solution at 5% (v/v). In general, remaining volumetric flasks (not intended for MOFs applications) were cleaned with a solution of Nochromix® (prepared using 100 g and 3.785 L of pure sulfuric acid (97.0%), both supplied by Sigma-Aldrich), and finally rinsed with ultrapure water.

III.5. Instrumentation and software

5.1. Chromatographic equipment

The determination of PCPs by liquid chromatography (Sections IV.1.2.1., IV.2.1.2., and IV.2.1.3.,) was carried out using a UHPLC 1260 Infinity Series (Agilent Technologies) with a quaternary pump, and a Rheodyne 7725i injection valve with a loop of 5 µL. The detector was a Vis-UV ProStar 325 LC Detector Series supplied by Varian (Palo Alto, CA, USA). Two chromatographic columns were used: a ZORBAX Eclipse Plus C18 (2.1 mm × 50 mm × 1.8 µm) (Section IV.1.2.1.), and an InfinityLab Poroshell 120 EC-C18 column (4.6 mm × 50 mm × 2.7 µm) (Section IV.2.1.2. and IV.2.1.3.), both purchased from Agilent Technologies. The pumps were controlled with the OpenLAB CDS ChemStation Edition software version C.01.04 (Agilent Technologies), and the data acquisition was controlled by the LC WorkStation software version 6.41 from Varian.

The determination of DBPs by gas chromatography and flame ionization detection (Section IV.2.2.1.) was carried out using a Varian 450 model CP-3800 GC equipped with a flame ionization detector (FID) and a Factor Four VF-5ms fused silica capillary column (30 m × 0.25 mm × 0.25 µm film thickness). The GC-FID included a CombiPAL autosampler from CTC Analytics (Zwingen, Switzerland). The GC-FID and data acquisition were controlled with the MS Workstation software version 6.9.3 (Varian), whereas the autosampler was controlled with the Cycle Composer software version 1.5.3 (CTC Analytics).

The determination of PCPs by gas chromatography and mass spectrometry (Section IV.2.1.4. and IV.2.2.2.) was carried out using a 7820A gas chromatograph from Agilent Technologies, equipped with a HP-5ms ultra inert capillary column (30 m × 0.25 mm × 0.25 µm), and coupled to an Agilent 5977B mass spectrometer equipped electronic impact ionizer and a simple quadrupole as mass analyzer. The equipment was controlled with the MassHunter GC/MS Acquisition software version B.07.04 (Agilent Technologies).

PCPs were also determined by gas chromatography in a screening study (Section IV.2.2.2.) using GC with flame ionization detection, specifically the GC-FID 2010 Plus from Shimadzu (Kioto, Japan), equipped with a DB-5ms ultra inert column (30 m × 0.250 mm × 0.25 µm), supplied by Agilent Technologies. Data acquisition was controlled with the GC Analysis software version 2.42.00 (Shimadzu).

5.2. Instrumentation for the characterization of MOFs

Phase identification of MOF crystals HKUST-1(Cu), MIL-53(Al), UiO-66(Zr), CIM-81(Zn), CIM-82(Zn), CIM-83(Zn), CIM-91(Zn), and CIM-92(Zn) was carried out by powder X-ray diffraction. An Empyrean Diffractometer supplied by PANalytical (Eindhoven, Netherlands) operating with Bragg-Brentano geometry was used. Data collection was carried out using Cu-Kα radiation (λ = 1.5418 Å) over the angular range from 5.01° to 80.00° (0.02° steps) with a total exposure time of 30 min. Graphical representation of the powder patterns was carried out with FullProf software [2].

The single crystal X-ray measurements for DMA@CIM-81, acetone@CIM-81, and acetone@CIM-91 were carried out in an an Agilent Supernova diffractometer with Mo radiation (λ = 0.71073 Å) at 150.0 K (except CIM-81@acetona that was measured at 293 K) equipped with an EosS2 detector. DMF@CIM-91 and CIM-92 were measured on an Agilent Supernova diffractometer with Cu radiation (λ = 1.5418 Å) at 293 K equipped with an ATLAS detector. Data were indexed, integrated and scaled with CrysAlisPRO program [3]. The crystal structures were solved by direct methods and refined with the full-matrix least-squares technique on F^2 by using the SHELXS-2013 and SHELXL-2013 programs included in the Olex2 software package [4]. C- and N-bound H atoms were placed in their expected positions and refined as riding with Uiso(H) = 1.5Ueq(C) for methyl H atoms and 1.2Ueq(N,C) otherwise. All the non-hydrogen atoms were refined anisotropically. The electron density corresponding to more disordered solvent molecules in were masked out (solvent mask in the Olex2 software). The electron counts in DMA@CIM-81 and acetone@CIM-81 inside each one of the two remaining pores in the unit cell is 48 and, 35 electrons, respectively. They roughly correspond to a molecule of DMA (48 electrons) and a molecule of acetone (32 electrons). The graphical manipulations were performed with the DIAMOND [5] and mercury [6] software.

High resolution powder diffraction patterns at different temperatures were measured at the BL04-MSPD beamline [7] of ALBA synchrotron (Barcelona, Spain), at 17.5 keV (λ = 0.70815 Å), equipped with the Mythen-II detector (Dectris) in the 0.37-43.2° angular range.

IR spectra (450 – 4000 cm^{-1}) were recorded for the powdered crystals by an IRAffinity–1 spectrophotometer from Shimadzu (Kyoto, Japan) equipped with a Pike technologies GladiATR.

The nitrogen adsorption isotherms were obtained with a surface area analyzer Gemini V 2365 Model, supplied by Micromeritics (Georgia, USA), at 77 K in the range $0.02 \leq P/P_0 \leq 1.00$. The Brunauer, Emmet and Teller (BET) method was used to calculate the surface area.

Thermogravimetric analysis on freshly crushed crystals was carried out in a thermal analyzer Perkin-Elmer Pyris Diamond TG/DTA (Massachusetts, USA), typically requiring few milligrams placed on an alumina crucible under a nitrogen atmosphere at a flow rate of 0.02 L·min^{-1}. The temperature was ramped from 25 to 250 ºC at a heating rate of 5 ºC min^{-1}.

The intermolecular interactions between CIM-81 and solvent molecules of acetone or molecules of PPB were computationally studied using semiempirical PM6 and Density Functional Theory (DFT) methods as implemented in Gaussian09 [8]. The 6-31g(d,p) basis set was used for all atoms except the metal atoms, for which the SDD basis set was used.

5.3. Statistical analysis

The Statgraphics Centurion XV software, version 15.1.02, was used for the statistical analyses of the experimental design (Statgraphics Technologies, The Plains, VA, USA). Excel software from Microsoft Office® (Redmond, WA, USA) was also used for statistical calculations.

III.6. Procedures

6.1. Synthesis of MOFs

Up to 8 MOFs were synthesized, characterized and evaluated in this Doctoral Thesis: HKUST-1(Cu), MIL-53(Al), UiO-66(Zr), CIM-81(Zn), CIM-82(Zn), CIM-83(Zn), CIM-91(Zn), and CIM-92(Zn). Table III.2. summarizes the structure and the composition of these MOFs. Three of them are well-known MOFs that have been used in analytical extraction procedures: HKUST-1(Cu), MIL-53(Al), and UiO-66(Zr), and thus named conventional MOFs from this point of view from now on. The other MOFs have been named in our research group using the abbreviation CIM (Canary Islands Materials) to refer to novel MOFs used in microextraction procedures for the first time and named in this project as: CIM-80(Al); CIM-81(Zn), and its functionalized CIM-82(Zn) and CIM-83(Zn); and CIM-91(Zn), and its functionalized CIM-92(Zn). All the MOFs were synthesized by the solvothermal method.

$[Cu_3(btc)_2(H_2O)_3]$ (HKUST-1(Cu))

HKUST-1(Cu) was synthesized following a previous study [9]. An aqueous solution of $Cu(NO_3)_2{\cdot}5H_2O$ (1.255 g, 5.4 mmol) was added dropwise to 15 mL of an ethanol solution of H_3btc (0.630 g, 3 mmol), followed by stirring for 20 min. The mixture was transferred to a solvothermal reactor (45 mL), and then heated at 120 ºC for 24 hours. The obtained blue crystals were filtered by gravity, washed with ethanol, and dried at room temperature. HKUST-1(Cu) was heated at 150 ºC for 24 hours in order to remove guest molecules from the pores of the crystalline structure. The yield was 90%.

[AlOH(bdc)] (MIL-53(Al))

MIL-53(Al) was synthesized following a previous study [10]. $Al(NO_3)_3{\cdot}9H_2O$ (1300 mg, 3.5 mmol) and benzene-1,4-dicarboxylic acid (288 mg, 1.7 mmol) were dissolved in 15 mL of ultrapure water. The mixture was transferred to a solvothermal reactor (45 mL), and heated at 220 ºC during 72 hours. The obtained crystals were filtered by gravity, washed with ultrapure water, and dried at 50 ºC for 24 hours. MIL-53(Al) was heated at 150 ºC for 24 hours in order to remove guest molecules from the pores of the crystalline structure. The yield was 45%.

$[Zr_6O_4(OH)_4(bdc)_6]$ (UiO-66(Zr))

UiO-66(Zr) was synthesized following a previous study [11]. $ZrCl_4$ (233 mg, 1 mmol) and benzene-1,4-dicarboxylic acid (246 mg, 1.5 mmol) were dissolved in 15 mL of DMF and 1 mL of concentrated HCl. The mixture was transferred to a solvothermal reactor (45 mL), and heated at 150 ºC during 24 hours. The obtained colorless crystals were filtered by gravity, and washed with DMF and methanol. UiO-66(Zr) was then heated at 150 ºC for 24 hours in order to remove guest molecules from the pores of the crystalline structure. The yield was 95%.

$[Zn_2(tz)_2(bdc)]$ (CIM-81(Zn))

The synthesis of the CIM-81(Zn) MOF involved a mixture of $Zn(NO_3)_2{\cdot}6H_2O$ (592 mg, 2 mmol), 1,2,4-triazole (140 mg, 2 mmol), and benzene-1,4-dicarboxylic acid (170 mg, 1 mmol), all dissolved in 15 mL of DMA. The final mixture was placed in a Parr Teflon-lined stainless steel vessel (45 mL) under autogenous pressure, and heated at 120 ºC for 72 hours. The obtained colorless crystals were filtered by gravity, washed with DMA and acetone, and dried at 50 ºC. Afterwards, the MOF was immersed in acetone for 24 hours to remove the guest molecules (repeating this step two times), followed by drying at 100 ºC. The yield was 83%.

$[Zn_2(tz\text{-}NH_2)_2(bdc)]$ (CIM-82(Zn))

The synthesis of the CIM-82(Zn) MOF required a mixture of $Zn(NO_3)_2{\cdot}6H_2O$ (592 mg, 2 mmol), 3-amino-1,2,4-triazole (168 mg, 2 mmol), and benzene-1,4-dicarboxylic acid (170 mg, 1 mmol), all dissolved in 15 mL of a mixture 1:1 (v/v) of water:ethylene glycol. The final mixture was placed in a Parr Teflon-lined stainless steel vessel (45 mL) under autogenous pressure, and heated at 130 ºC for 16 hours. The obtained colorless crystals were filtered by gravity, washed with water and ethylene-glycol, and dried at 50 ºC. Afterwards, the MOF was activated by immersion in acetone for 24 hours to remove the guest molecules (repeating this step two times), followed by drying at 100 ºC. The yield was 60%.

[$Zn_2(tz)_2(bdc\text{-}NH_2)$] (CIM-83(Zn))

The synthesis of the CIM-83(Zn) MOF involved a mixture of $Zn(NO_3)_2{\cdot}6H_2O$ (592 mg, 2 mmol), 1,2,4-triazole (140 mg, 2 mmol), and 2-amino-benzene-1,4-dicarboxylic acid (181 mg, 1 mmol), all dissolved in 15 mL of DMF. The final mixture was placed in a Parr Teflon-lined stainless steel vessel (45 mL) under autogenous pressure, and heated at 120 ºC for 72 hours. The obtained colorless crystals were filtered by gravity, washed with DMF and acetone, and dried at 50 ºC. Afterwards, the MOF was activated by immersion in acetone for 24 hours to remove the guest molecules (repeating this step two times), followed by drying at 100 ºC. The yield was 71%.

[$Zn_2(tz)_2(bdc)$] (CIM-91(Zn))

The synthesis of the CIM-91(Zn) MOF required a mixture of $Zn(NO_3)_2{\cdot}6H_2O$ (592 mg, 2 mmol), 1,2,4-triazole (140 mg, 2 mmol), and benzene-1,4-dicarboxylic acid (170 mg, 1 mmol), all dissolved in 15 mL of DMF. The final mixture was placed in a Parr Teflon-lined stainless steel vessel (45 mL) under autogenous pressure, and heated at 120 ºC for 72 hours. The obtained colorless crystals were filtered by gravity, washed with DMF and acetone, and dried at 50 ºC. Afterwards, the MOF was activated by immersion in acetone for 24 hours to remove the guest molecules (repeating this step two times), followed by drying at 100 ºC. The yield was 83%.

[$Zn_2(tz\text{-}NH_2)_2(bdc)$] (CIM-92(Zn))

The synthesis of the CIM-92(Zn) MOF required a mixture of $Zn(NO_3)_2{\cdot}6H_2O$ (592 mg, 2 mmol), 3-amino-1,2,4-triazole (168 mg, 2 mmol), and benzene-1,4-dicarboxylic acid (170 mg, 1 mmol), dissolved in 15 mL of DMF. The final mixture was placed in a Parr Teflon-lined stainless steel vessel (45 mL) under autogenous pressure, and heated at 130 ºC for 16 hours. The obtained colorless crystals were filtered by gravity, washed with DMF and acetone, and dried at 50 ºC. Afterwards, the MOF was activated by immersion in acetone for 24 hours to remove the guest molecules (repeating this step two times), followed by drying at 100 ºC. The yield was 60%.

Table III.2. Group of physicochemical characteristics of MOFs utilized in this Doctoral Thesis.

MOF name / formula	Structure	Building units
HKUST-1(Cu) $[Cu_3(btc)_2(H_2O)_3]$	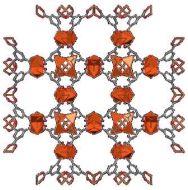	*Metal* Cu(II) *Ligand* benzene-1,3,5-tricarboxylic acid (H_3btc) 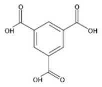
MIL-53(Al) [AlOH(bdc)]	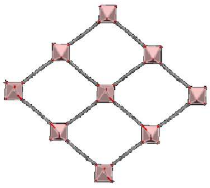	*Metal* Al(III) *Ligand* benzene-1,4-dicarboxylic acid (H_2bdc) 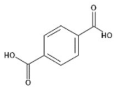
UiO-66(Zr) $[Zr_6O_4(OH)_4(bdc)_6]$	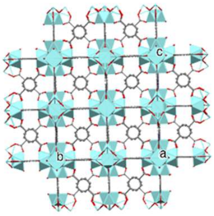	*Metal* Zr(IV) *Ligand* benzene-1,4-dicarboxylic acid (H_2bdc) 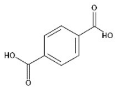
CIM-80(Al) [Al(bd-Me)]	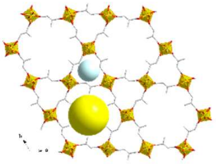	*Metal* Al(III) *Ligand* (2E)-2-methyl-2-butenedioic acid (H_2bd-Me) 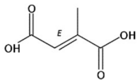

Table III.2. (continuation).

MOF name / formula	Structure	Building units
CIM-81(Zn) $[Zn_2(tz)_2(bdc)]$ *Tetrahedral*	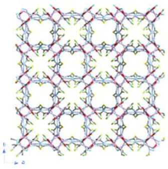	*Metal* Zn(II) *Ligand* 1,2,4-triazol (Htz) 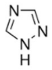 benzene-1,4-dicarboxylic acid (H_2bdc) 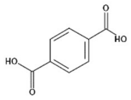
CIM-82(Zn) $[Zn_2(tz\text{-}NH_2)_2(bdc)]$ *Tetrahedral*	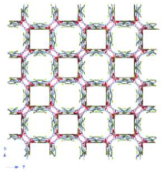	*Metal* Zn(II) *Ligand* 3-amino-1,2,4-triazol (Htz-NH_2) 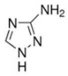 benzene-1,4-dicarboxylic acid (H_2bdc) 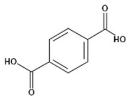
CIM-83(Zn) $[Zn_2(tz)_2(bdc\text{-}NH_2)]$ *Tetrahedral*	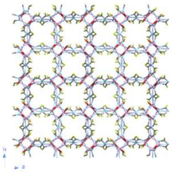	*Metal* Zn(II) *Ligand* 1,2,4-triazol (Htz) 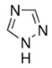 2-amino-benzene-1,4-dicarboxylic acid (H_2bdc-NH_2) 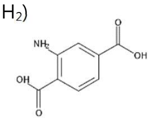

Table III.2. (continuation).

MOF name / formula	Structure	Building units
CIM-91(Zn) $[Zn_2(tz)_2(bdc)]$ *Orthorhombic*	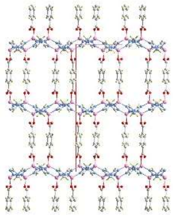	*Metal* Zn(II) *Ligand* 1,2,4-triazol (Htz) 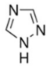 benzene-1,4-dicarboxylic acid (H_2bdc) 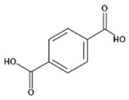
CIM-92(Zn) $[Zn_2(tz\text{-}NH_2)_2(bdc)]$ *Orthorhombic*	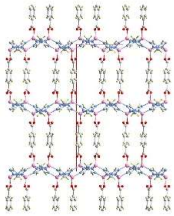	*Metal* Zn(II) *Ligand* 3-amino-1,2,4-triazol ($Htz\text{-}NH_2$) 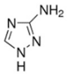 benzene-1,4-dicarboxylic acid (H_2bdc) 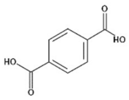

SPME fibers based on CIM MOFs

The stationary phase based on the CIM-80(Al) MOF, assembled to generate a SPME fiber, followed the procedure described in patent P201900092 [12], belonging to the research group members.

6.2. Analytical microextraction procedures

VAEME in combination with UHPLC-UV

All the variables exerting an influence on the VAEME performance for the monitoring of PCPs were optimized (Section IV.1.2.1.). The optimum microextraction method required 8 mL of a water sample containing 15% (w/v) of NaCl, and the addition of 200 µL of trichloromethane. The emulsification was subjected to vortex stirring for 3 minutes, followed by centrifugation during 5 minutes at 1917 x g. The obtained microdroplet (containing extracted analytes) was sampled and placed in a vial of 2 mL of capacity with the aid of a microsyringe. Afterwards, the solvent was evaporated to dryness under vacuum evaporation. Finally, the extract were reconstituted with 100 µL of the initial chromatographic mobile phase, which is a mixture of 35:65 (v/v) of acetonitrile:water (ACN:H_2O). The reconstituted extract was then injected in the UHPLC.

The optimum separation required a binary mobile phase composed of acetonitrile and water with a 0.1% (v/v) of acetic acid in the aqueous phase, at constant flow rate of 0.5 $mL{\cdot}min^{-1}$, and at constant temperature of 25 ºC. Thus, 35% (v/v) of acetonitrile was kept isocratic during the initial 5.5 minutes, followed by a linearly elution gradient from 35 to 70% (v/v) of acetonitrile in 5.5 minutes, and then kept again under isocratic conditions for 4 additional minutes. The wavelength of the detector was fixed at 254 nm from 0 to 7 minutes, and then at 289 nm during the rest of the chromatogram.

D-µSPE in combination with UHPLC-UV

All the variables exerting an influence on the D-µSPE performance for the monitoring of PCPs were optimized (Section IV.2.1.3.). The optimum microextraction method required the addition of 10 mg of the CIM-81(Zn) MOF to 10 mL of water sample, having the pH adjusted to 5 with an acetic/acetate buffer. The aqueous sample is then subjected to vortex agitation for 1 minute, and then centrifuged during 3 minutes at 2504 × g. The MOF (containing extracted analytes) is then separated and the desorption step was carried out using 1.2 mL of methanol, and vortex agitation for 4 minutes. The desorption solvent (containing the extracted and preconcentrated analytes) is then filtered (0.2 µm), and subjected to dryness under vacuum evaporation. Finally, the target analytes are reconstituted in 100 µL of the initial chromatographic mobile phase, a mixture of 50:50 (v/v) of ACN:H_2O. The final reconstituted extract was then injected in the UHPLC.

The optimum separation required a binary mobile phase composed of acetonitrile and water with a 0.1% (v/v) of acetic acid in the aqueous phase, at constant flow rate of 0.5 $mL{\cdot}min^{-1}$, and at constant temperature of 25 ºC. The optimum separation was obtained by the follow gradient: initially 50% (v/v) of acetonitrile, that was maintained isocratic during 1 minute, followed by a linear elution gradient from 50% to 90% (v/v) of acetonitrile up to 8 minutes, and finally the acetonitrile was maintained at 90% (v/v) for 4 additional minutes. The wavelength of the detector was fixed initially at 254 nm, and at 5.7 minutes it was changed to 289 nm, being then kept constant until the end of the chromatographic run.

D-µSPE in combination with GC-MS

The variables exerting an influence in the D-µSPE performance in combination with GC-MS for the monitoring of PCPs were optimized (Section IV.2.1.4.). The optimum microextraction method required the addition of 10 mg of the CIM-81(Zn) MOF to 10 mL of the aqueous sample, having the pH adjusted to 5 with an acetic/acetate buffer. The aqueous sample is then subjected to vortex agitation for 1 minute, and then centrifuged for 3 minutes at 2504 × g. The MOF (containing extracted analytes) is then separated and the desorption step was carried out using 1.2 mL of methanol, and vortex agitation for 4 minutes. The desorption solvent (containing the extracted and preconcentrated analytes) is filtered (0.2 µm), and evaporated under vacuum. Finally, the target analytes are reconstituted in 100 µL of a mixture 9:1 (v/v) of cyclohexane:ethyl acetate (CHN:EA). The final reconstituted extract was then injected in the GC.

The optimum oven program for the GC separation of the PCPs started at 70 ºC and increased at a rate of 15 $ºC{\cdot}min^{-1}$ up to 300 ºC, being then held for 5 minutes. Helium was used as carrier gas at 1 mL·min^{-1}. The temperature of the transfer line was set at 290 ºC, 230 ºC for the ionization source, and 150 ºC for the quadrupole. The ionization by electronic impact (EI) was carried out at 70 eV. The volume of the extract (or standard) injected in the GC-MS was 2 µL in splitless mode at 280 ºC, and with a solvent delay of 7.5 minutes.

SPME (commercial fibers) in combination with GC-FID

All the variables exerting an influence on the SPME performance for the monitoring of DBPs were optimized (Section IV.2.2.1.). The optimum microextraction method required 10 mL of blending desalinated water sample, containing a methanol content fixed to 1% (v/v) and a 30% (w/v) of sodium chloride to adjust the ionic strength. The pH of the aqueous samples was adjusted at 7 using a buffer solution of 0.12 M H_2HPO_4 / 0.08 M KH_2PO_4, and the contain of NH_4Cl was adjusted at 0.22 mg as quenching agent to ensure inhibition of the residual chlorine. The HS-SPME method was completely automated with the CombiPAL autosampler. The optimum conditions required the exposure of the commercial CAR/PDMS fiber, in headspace mode, for 60 minutes at 30 ºC under constant stirring rate of 250 min^{-1}. Afterwards, the SPME fiber was retracted and exposed to the GC injection port at 250 ºC for 2 minutes, to ensure complete desorption of the target analytes.

For the chromatographic separation, nitrogen was used as the carrier gas at flow rate of 1 mL·min^{-1}. Sample injection was performed in splitless mode. The injector temperature was set at 250 ºC. The FID detector was kept at 280 ºC, using an air flow of 300 mL·min^{-1}, a make-up flow of nitrogen of 30 mL·min^{-1}, and a hydrogen flow of 30 mL·min^{-1}. The chromatographic oven temperature program was: initially 40 ºC for 3 minutes, followed by an increase at 12 ºC·min^{-1} up to 100 ºC, then increased at 30 ºC·min^{-1} up to 250 ºC, and finally held at 250 ºC for 5 min.

SPME (MOF-based fibers) in combination with GC-FID and GC-MS

All the variables exerting an influence on the SPME performance for the monitoring of PCPs were optimized (Section IV.2.2.2.). The optimum microextraction method required 10 mL of aqueous sample, containing a methanol content fixed to 1% (v/v) and a 20% (w/v) of sodium chloride to adjust the ionic strength. The optimum conditions required the exposure of a labmade SPME fiber based on the CIM-80(Al) MOF, in headspace mode, for 40 minutes at 50 ºC under constant stirring rate of 700 min^{-1}. Afterwards, the fiber was retracted, and exposed to the GC injection port at 270 ºC for 10 minutes to ensure the complete desorption of the target analytes. Additionally, the fiber was held 5 minutes in the injection port to ensure the elimination of carry over effects.

GC-FID was also used in the screening and optimization studies. Helium was employed as the carrier gas at flow rate of 1.2 mL·min^{-1}. In this GC, the splitless mode was used during the sample injection at 250 ºC. The FID detector was kept at 280 ºC, using an air flow of 400 mL·min^{-1}, a make-up flow of helium of 30 mL·min^{-1}, and a hydrogen flow of 40 mL·min^{-1}. The chromatographic oven temperature program was: initially 40 ºC for 5 min, followed by an increase at 5 ºC min^{-1} up to 180 ºC and then held for 10 minutes, followed by an increase at 10 ºC·min^{-1} up to 300 ºC and then held for 5 min

The final validation study was accomplished using GC-MS, using helium as carrier gas at 1 mL·min^{-1}. The injection was performed in splitless mode, opening the split at 0.75 mL·min^{-1} after 10 minutes. The oven program for the gas chromatographic separation of the PCPs started at 40 ºC, held for 5 minutes, followed by an increase at a rate of 7 ºC·min^{-1} up to 180 ºC, then held for 10 minutes, and finally increased at 20 ºC·min^{-1} up to 300 ºC, and held this last temperature for 4 min. The temperature of the transfer line, the ionization source and the quadrupole were set at 280 ºC, 250 ºC, and 150 ºC, respectively. The ionization by electronic impact (EI) was carried out at 70 eV. The solvent delay was set at 5 minutes.

6.3. Adsorption isotherm studies

All the experiments were carried out in duplicate using amber vials (20 mL) under continuous shaking. The analytical determination of the target analyte PPB in the UHPLC-UV was carried out under isocratic conditions, using a binary mobile phase composed of 50:50 (v/v) of ACN and H_2O, with a 0.1% (v/v) of acetic acid in the aqueous phase, at constant flow rate of 0.5 mL·min^{-1} and at a temperature of 25 ºC.

For the kinetic studies, 5 mg of MOF were added to 10 mL of PPB aqueous solution (10 mg·L^{-1}) and, at several pre-fixed times (being the maximum 24 h), small aliquots of the aqueous solution were taken, filtered, diluted (1:25, v/v), and injected in the chromatograph to determine the PPB still remaining in the aqueous phase.

For the study of adsorption capacity, 5 mg of MOF were added to 10 mL of an aqueous solution of PPB at different concentration levels (0.1, 0.5, 1, 3, 5, 10, 30 and 50 mg·L^{-1}) and, after 24 hours, the aqueous solutions were filtered, diluted using different ratios (depending on the initial concentration of PPB), and injected in the chromatograph.

For the release studies, 5 mg of MOF were added to 10 mL of an aqueous solution of PPB (100 mg·L^{-1}) and, after 24 hours, the water was removed. Then, 5 mL of methanol were added to perform desorption, and small aliquots of the methanol containing desorbed PPB were taken at pre-fixed times (5, 10, 30, 45, 60, 90, 120, and 1440 minutes), filtered, diluted (1:25, v/v), and injected in the chromatograph.

III.7. Sample collection

Once the samples were collected, they were stored at 4 ºC and protected from light until their analysis. As a general criterion, samples were not kept for more than one week since their collection before being analyzed in the case of PCPs, and for no more than 24 hours for DBPs. All the samples were analyzed in triplicate.

Samples analyzed in Section IV.1.2.1.

All the water samples were collected in Tenerife (Canary Islands, Spain). The swimming pool waters were sampled in two public pools. The seawaters were sampled in two different beaches, located in the north and south of the island, respectively. Tap water taken at the laboratory was also analyzed. Two more samples were taken from a WWTP, and collected in different days. Wastewaters were sampled directly in the plant. In all the cases, the sampling was carried out avoiding the formation of bubbles, and using clean amber glass bottles of 100 mL in volume. They were also kept in a portable fridge until they reached the laboratory.

Samples analyzed in Section IV.2.1.3.

Three wastewater samples were analyzed in this study. Wastewaters were provided by an environmental analysis laboratory from Tenerife (Canary Islands), after sampling the effluents of different WWTPs. The sampling was carried out in bottles of 200 mL in volume, ensuring the absence of air bubbles. The samples were kept in a portable fridge until they reached the laboratory.

Samples analyzed in Section IV.2.1.4.

Two bottled waters (acquired in local shops) and tap water (collected in the laboratory, and analyzed the same day of the sampling) were used in the analyses.

Samples analyzed in Section IV.2.2.1.

Four different blending desalinated water samples were collected in the South of Tenerife Island (Spain) using amber bottles of 125 mL containing 1.3381 g of anhydrous K_2HPO_4 and 0.6634 g of KH_2PO_4 (to ensure a pH value of 7); and 2.75 mg of NH_4Cl as quenching agent for the residual chlorine. The bottles were completely filled to avoid the presence of any headspace (preventing in this way DBPs evaporation).

Samples analyzed in Section IV.2.2.2.

Three wastewater and three seawater samples were analyzed in this study. Wastewaters were provided by an environmental analysis laboratory from Tenerife (Canary Islands), after sampling the effluents of different wastewater treatment plants. The sampling was carried out in bottles of 200 mL in volume, ensuring the absence of air bubbles. Samples were kept in a portable fridge until they reached the laboratory.

REFERENCES

[1] Q.Q. Baltazar, J. Chandawalla, K. Sawyer, and J.L. Anderson. Colloid Surf. A-Physicochem. Eng. Asp. 302 (2007) 150–156.

[2] J. Rodríguez-Carvajal. Physica B 192 (1993) 55–69.

[3] Rigaku Oxford Diffraction, CrysAlisPro Software System, version 1.171.36.32, Rigaku Corporation, Oxford, UK, 2013.

[4] O.V. Dolomanov, L.J. Bourhis, R.J. Gildea, J.A.K. Howard, and H. Puschmann. J. Appl. Cryst. 42 (2009) 339–341.

[5] DIAMOND 4.0, Crystal Impact GbR, CRYSTAL IMPACT, K. Brandenburg & H. Putz GbR, Bonn, Germany, 2016.

[6] C.F. Macrae, I. Sovago, S.J. Cottrell, P.T.A. Galek, P. McCabe, E. Pidcock, M. Platings, G.P. Shields, J.S. Stevens, M. Towler, and P.A. Wood. J. Appl. Crystallogr. 53 (2020).

[7] F. Fauth, I. Peral, C. Popescu, and M. Knapp. Powder Diffr. 28 (2013) S360–S370.

[8] Gaussian 09, Revision D.01, M.J. Frisch, G.W. Trucks, H.B. Schlegel, G.E. Scuseria, M.A. Robb, J.R. Cheeseman, G. Scalmani, V. Barone, B. Mennucci, G.A. Petersson, H. Nakatsuji, M. Caricato, X. Li, H.P. Hratchian, A.F. Izmaylov, J. Bloino, G. Zheng, J.L. Sonnenberg, M. Hada, M. Ehara, K. Toyota, R. Fukuda, J. Hasegawa, M. Ishida, T. Nakajima, Y. Honda, O. Kitao, H. Nakai, T. Vreven, J.A. Montgomery, Jr., J.E. Peralta, F. Ogliaro, M. Bearpark, J.J. Heyd, E. Brothers, K.N. Kudin, V.N. Staroverov, T. Keith, R. Kobayashi, J. Normand, K. Raghavachari, A. Rendell, J.C. Burant, S.S. Iyengar, J. Tomasi, M. Cossi, N. Rega, J.M. Millam, M. Klene, J. E. Knox, J.B. Cross, V. Bakken, C. Adamo, J. Jaramillo, R. Gomperts, R.E. Stratmann, O. Yazyev, A.J. Austin, R. Cammi, C. Pomelli, J.W. Ochterski, R.L. Martin, K. Morokuma, V.G. Zakrzewski, G.A. Voth, P. Salvador, J.J. Dannenberg, S. Dapprich, A.D. Daniels, O. Farkas, J.B. Foresman, J.V. Ortiz, J. Cioslowski, and D.J. Fox, Gaussian, Inc., Wallingford CT, 2013.

[9] S.S.-Y. Chui, S.M.-D. Lo, J.P.H. Charmant, A.G. Orpen, and I.D. Williams. Science 283 (1999) 1148–1150.

[10] T. Loiseau, C. Serre, C. Huguenard, G. Fink, F. Taulelle, M. Henry, T. Bataille, and G. Férey. Chem. Eur. J. 10 (2004) 1373–1382.

[11] J.H. Cavka, S. Jakobsen, U. Olsbye, N. Guillou, C. Lamberti, S. Bordiga, and K.P. Lillerud. J. Am. Chem. Soc. 130 (2008) 13850–13851.

[12] I. Pacheco-Fernández, J. Pasán-García, V. Pino-Estévez, P. Rocío-Bautista, A.M. Afonso-Perera, J.H. Ayala-Díaz, and C. Ruiz-Pérez. Fase estacionaria para dispositivo de microextracción en fase sólida, Spain Patent P201900092, ACCEPTED.

CHAPTER IV

Results and discussion

Section IV.1.

Liquid-phase microextraction applications

IV.1.1. A step forward with liquid-phase microextraction

Among all the LPME modes, DLLME is the most widely utilized for obvious advantages such as simplicity, fastness, low requirements of organic solvents consumption during the operation, and high sensitivity given the preconcentration achieved, as it is described in Section I.3.1.3. The success of DLLME bases on the impressive and fast emulsification formed when using a mixture of a water–immiscible extractant solvent and a water–miscible polar dispersive solvent, being the extractant solvent soluble in the dispersive solvent. In addition to this, the ratio aqueous sample to the mixture of solvents is high enough to ensure adequate preconcentration. The *in situ* formed emulsification assists the quick and efficient distribution of the analytes from the aqueous sample to the extractant solvent.

As a disadvantage, the dispersive solvent can solubilize certain amount of the extractant solvent in the process, causing consequently a decrease of the overall extraction efficiency. In this sense, several modifications have been proposed for DLLME intending to overcome this issue. Thus, it has been reported the use of different approaches such as DLLME assisted by ultrasounds, vortex, microwaves, or air current, to ensure the dispersion of the extractant solvent into the aqueous solution and a proper emulsification.

The aim of the study in this chapter is the development of a VAEME method to monitor a group of emerging contaminants in environmental water samples, specifically ten PCPs in different seven water samples. The use of VAEME ensures the replacement of a dispersive solvent by vortex agitation, intending higher efficiency due to absence of the losses of extractant solvent. Furthermore, it implies reduction in the entire consumption of organic solvents, because the dispersive solvent is avoided. The proposed VAEME should also demonstrate the maintenance adequate analytical features for the target analytes when compared to conventional DLLME.

IV.1.1.1. A simplified vortex-assisted emulsification microextraction method for determining personal care products in environmental water samples by ultra-high-performance liquid chromatography

Analytical Methods 7 (2015) 1825–1833

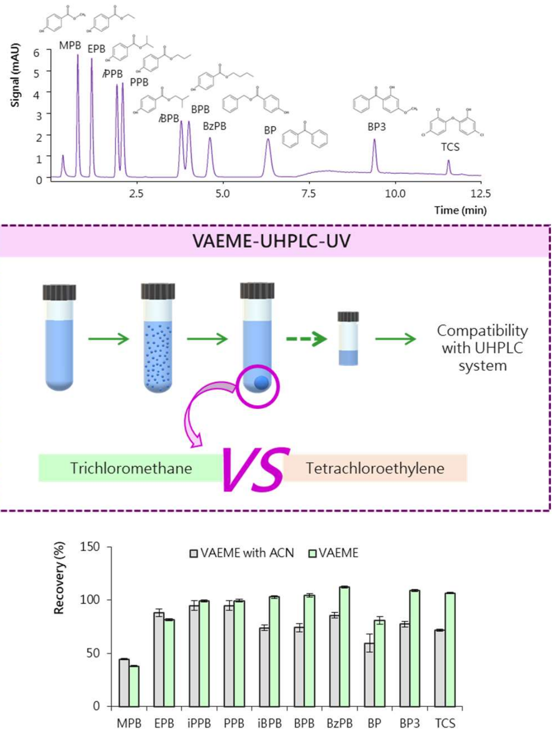

1. Chromatographic performance of PCPs by UHPLC-UV

UHPLC with UV detection was selected for the determination of ten PCPs: MPB, EPB, iPPB, PPB, iBPB, BPB, BzPB, BP, BP3, and TCS (Table III.1.). The optimum conditions for the separation were detailed in Section III.6.2. The retention times (t_R, in min) and their precision are summarized in Table IV.1. The precision for the retention times was evaluated by relative standard deviation (RSD, in %) utilizing the calibrations standards (at different concentration levels). The obtained RSD values were lower than 0.6% (n = 30).

The chromatographic calibration curves ranged from 0.01 to 2.00 mg·L^{-1} for all PCPs studied, using 8 calibration levels. Calibrations exhibited excellent linearity with determination coefficient (R^2) higher than 0.997, as it can be observed in Table IV.1. The detection limits (LODs) and the quantification limits (LOQs) were calculated as the concentrations that provided a signal to noise ratio of 3 and 10, respectively; being also experimentally verified by preparation and UHPLC-UV determination of standards at such levels. Values of LODs ranged from 0.005 mg·L^{-1} for PPB to 0.059 mg·L^{-1} for BP, while LOQs ranged between 0.020 and 0.140 mg·L^{-1} for the same analytes.

The precision of the chromatographic method was evaluated in terms of RSD (in %) at three levels of concentration: 0.1, 1.0 and 1.7 mg·L^{-1}, using intra-day studies. At the lowest level, BP, BP3 and TCS were not included in the precision study because the tested concentration was below their respective LOQs. RSD values at the lowest level (0.1 mg·L^{-1}) ranged from 0.43% for EPB to 1.82% for BPB, and at the highest level (1.7 mg·L^{-1}) ranged from 0.38% for EPB and iPPB, to 2.13% for TCS, showing the high repeatability of the chromatographic method. All precision values have also been included in Table IV.1. Figure IV.1. shows a representative chromatogram of an aqueous standard containing the PCPs at a concentration of 1 mg·L^{-1}.

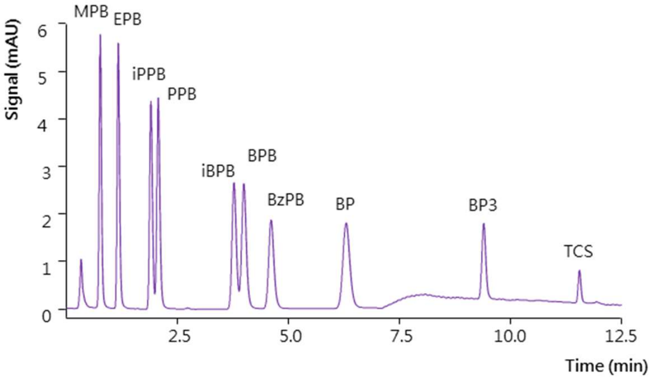

Figure IV.1. Representative chromatogram obtained by UHPLC-UV for a standard mixture of the studied PCPs (1 mg·L^{-1}), using the optimized conditions listed in Section III.6.2.

2. Screening of extractant solvents for VAEME and compatibility with UHPLC

A valid extractant solvent in VAEME should meet several ideal requirements: it must generate quantitative extraction of the studied analytes, its volume should be as lower as possible, and it should be compatible with the further analytical instrument where determination is going to be accomplished.

Initially, octanol, decanol, dichloromethane, trichloromethane and tetrachloroethylene were tested as possible extractant solvents. Their most relevant physicochemical properties are shown in Table IV.2. A reconstitution step was required prior injection to ensure compatibility of these solvents with the further determination by UHPLC. Thus, a volume of 200 µL of these extractant solvents containing a known amount of PCPs (250 µg·L^{-1}), was subjected to evaporation until dryness followed by reconstitution with 100 µL of UHPLC mobile phase (a mixture of 35:65 (v/v) of ACN:H_2O), and UHPLC-UV determination. An initial volume of 200 µL was selected for these experiments, as an estimation of the maximum final volume acceptable for a microdroplet in VAEME, with regards to 8 mL of water as estimated adequate sample volume.

Table IV.1. Several quality analytical parameters of the chromatographic method.

PCPs	t_R / RSD (n = 30)	(Slope ± SD[a]) ×10^{-3}	$S_{y/x}$[b]×10^{-3}	R^2 [c]	LOD[d] (mg·L^{-1})	LOQ[d] (mg·L^{-1})	RSD[e] (%) for the calculated concentration		
							Conc. Level: 0.1 mg·L^{-1}	Conc. level: 1.0 mg·L^{-1}	Conc. level: 1.7 mg·L^{-1}
MPB	0.76 / 0.55	351 ± 3	4.29	0.9997	0.011	0.025	1.10	1.08	0.53
EPB	1.17 / 0.59	361 ± 3	4.78	0.9997	0.013	0.028	0.43	1.06	0.38
iPPB	1.90 / 0.56	324 ± 2	4.05	0.9997	0.010	0.026	1.38	1.07	0.38
PPB	2.07 / 0.56	352 ± 2	3.69	0.9998	0.005	0.020	1.55	1.12	0.40
iBPB	3.77 / 0.43	301 ± 2	3.65	0.9997	0.023	0.061	1.69	1.31	0.48
BPB	3.99 / 0.42	321 ± 5	7.68	0.9990	0.014	0.058	1.82	0.91	0.70
BzPB	4.61 / 0.44	256 ± 3	4.58	0.9994	0.029	0.073	0.91	1.18	0.70
BP	6.30 / 0.36	334 ± 5	8.16	0.9990	0.059	0.140	-	0.61	0.92
BP3	9.40 / 0.18	165 ± 3	5.87	0.9978	0.056	0.126	-	2.31	1.59
TCS	11.56 / 0.12	50 ± 1	2.15	0.9968	0.029	0.110	-	2.82	2.13

[a] Standard deviation associated to the slope

[b] Standard deviation of the residuals

[c] Determination coefficient

[d] Limit of detection and limit of quantification, calculated according to the ratio signal/noise as 3 and 10 times, respectively; and experimentally verified by preparation of standards at such values

[e] Relative standard deviation (intra-day precision, n = 4)

Octanol and decanol were quickly discarded because the stage of evaporation/reconstitution required long times. The times required for evaporation of dichloromethane and trichloromethane were about ~2 minutes, while for tetrachloroethylene was ~7 minutes. The resulting recoveries of this stage (evaporation/reconstitution) can be observed in Figure IV.2. Clearly, dichloromethane is not a valid solvent, probably due to its high volatility, and its use is accompanied by important losses of analytes in this stage. Thus, trichloromethane and tetrachloroethylene were those selected as possible extractant solvents in the VAEME methodology. Tetrachloroethylene presented high recoveries in the stage of evaporation/reconstitution, whereas trichloromethane not only presented acceptable performance in this step, but also because this solvent has similar octanol/water partition coefficient (log K_{OW}) (Table IV.2) to the most polar analyte, MPB (log K_{OW} = 1.88).

Table IV.2. Main physicochemical properties of the solvents initially considered as valid extractant solvents in VAEME (SciFinder® 2019).

Solvent	**Density at 20 ºC ($g{\cdot}mL^{-1}$)**	**Boiling point (ºC)**	**Vapor pressure (Pa)**	**Water solubility at 20 ºC ($g{\cdot}mL^{-1}$)**	**log K_{OW}**
Octanol	0.823	194.7	15.20	3.0×10^{-7}	2.876
Decanol	0.828	227.8	1.97	3.7×10^{-5}	3.895
Dichloromethane	1.252	39.6	59.73×10^{3}	1.3×10^{-2}	1.405
Trichloromethane	1.500	61.2	26.67×10^{3}	8.0×10^{-3}	1.935
Tetrachloroethylene	1.653	119.1	2.57×10^{3}	1.5×10^{-4}	3.070

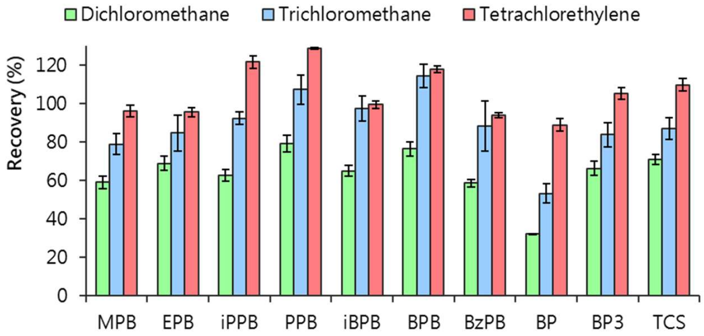

Figure IV.2. Average recoveries (%) only referred to the stage of evaporation/reconstitution for each PCPs studied, as a function of the solvent used in this step. Experiments were performed in triplicate.

3. Optimization of VAEME-UHPLC-UV

The main variables exerting an influence in the VAEME efficiency have been studied, such as: volume of extractant solvent, ionic strength of the aqueous sample, and pH of the aqueous sample. To simplify the optimization of the extraction method, the centrifugation time and velocity were fixed at 5 minutes and 1917 x g, respectively. Higher centrifugation times and velocities are hardly needed to ensure correct separation of the final microdroplet. Previous experiments allowed us to fix the vortex time at 3 minutes, because longer times did not improve the extraction efficiency.

Given the low number of factors needed in the optimization of the VAEME method, a factor by factor optimization was selected. This is also one advantage of the VAEME method: its simplicity. In all experiments, the sample volume was fixed to 8 mL. Optimization was carried out with aqueous standards prepared in ultrapure water, containing the ten PCPs studied at a concentration of 12.5 $\mu g \cdot L^{-1}$.

3.1. Influence of the extractant volume

The volume of the extractant solvent (tetrachloroethylene or trichloromethane) was varied from 50 to 200 µL, in order to obtain a low volume of final microdroplet while ensuring reproducibility as well as easy manipulation. Figure IV.3. shows the average recoveries obtained for each PCP and for each extractant solvent. The pH was not adjusted, and the ionic strength was fixed with NaCl at 20% (w/v), in these initial experiments.

For both solvents, the best volume to work with was 200 µL except for BP, which was 150 µL. Higher volumes were not tried to ensure a microextraction context, and also to avoid further decreases in the enrichment factor. For tetrachloroethylene, recoveries ranged from 3.7 ± 0.3% for MPB to 114 ± 2% for BP3, and for trichloromethane between 38 ± 2% for MPB and 108 ± 2% for BzPB.

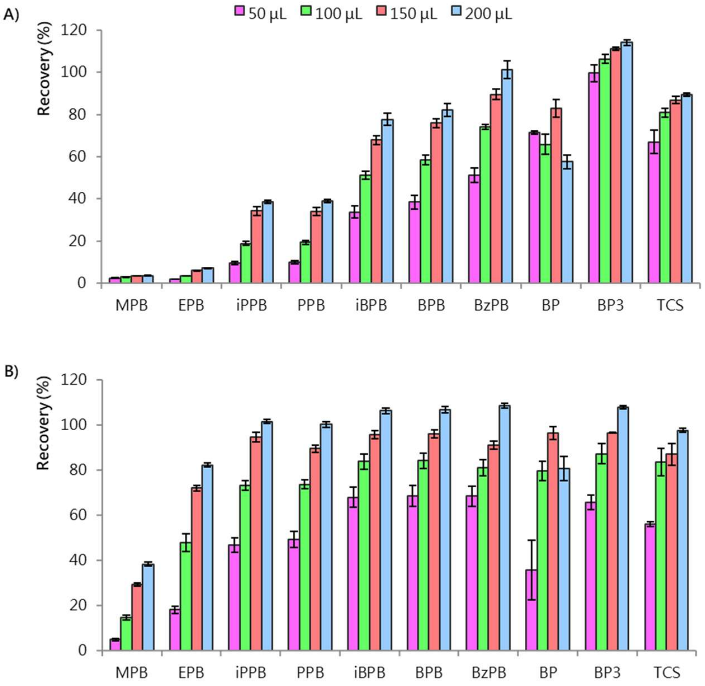

Figure IV.3. Effect of the extractant solvent volume on the overall extraction efficiency by VAEME–UHPLC–UV for the studied PCPs (n = 3), utilizing **A)** tetrachloroethylene, and **B)** trichloromethane. The remaining conditions of the method were described in the text.

3.2. Influence of the ionic strength

In LPME procedures, it is well-known that the addition of salts normally facilitates the handling of the final microdroplet, and also helps in increasing the extraction efficiency in many cases. Thus, the ionic strength was evaluated by the addition of different NaCl amounts, between 0 and 20% (w/v), while keeping other VAEME variables constant: 200 µL for the extractant solvent volume and no adjustment of the pH.

Figure IV.4. shows the average recoveries obtained at different NaCl contents for three PCPs, selected as representative of each family of the PCPs studied. In general, best recoveries were obtained using a NaCl content of 15% (w/v), ranging from 2.90% for MPB (result not included in Figure IV.4.) to 91.2% for TCS when using tetrachloroethylene as extractant solvent, and from 37.8% for MPB (result not included in Figure IV.4.) to 112% for BzPB when employing trichloromethane. In any case, the effect of the NaCl content was not highly significant, particularly if compared with that of the pH.

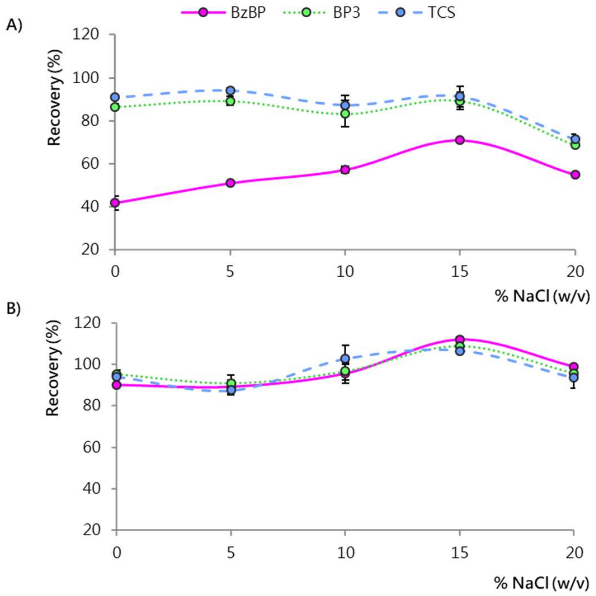

Figure IV.4. Influence of the NaCl content (w/v) in the VAEME efficiency (n = 3) when using as extractant solvents: **A)** tetrachloroethylene, and **B)** trichloromethane. The remaining conditions of the method were described in the text.

3.3. Influence of the pH

The influence of the pH of the aqueous sample is evidently going to affect analytes with basic or acidic groups. It is important to select an appropriate pH, which ensures that PCPs are in their neutral forms prior to extraction. Thus, it is favored their affinity for the organic extractant solvent. The pH was studied at three values: 3, 5 and 7, attending to the nature of the PCPs selected. Other values fixed in the VAEME method were the already optimum values: 200 µL of extractant solvent and 15% (w/v) of NaCl.

Figure IV.5. shows the average recoveries obtained for each PCP studied, using tetrachloroethylene as extractant solvent in the example. Clearly, the best results were obtained using a pH value of 5, which was selected for further studies.

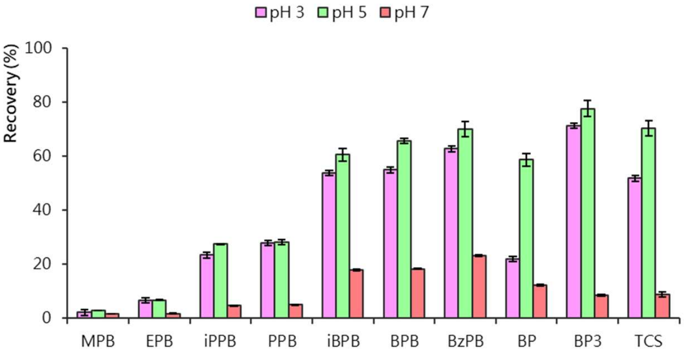

Figure IV.5. Influence of the aqueous sample pH on the VAEME performance, using tetrachlorethylene as extractant solvent in this representative plot. The remaining conditions of the method were described in the text.

4. Quality analytical parameters of the VAEME-UHPLC-UV method

From the optimization study, it is remarkable that best recoveries were obtained using trichloromethane as extractant solvent, particularly for polar analytes. Therefore, this solvent was selected as the optimum extractant solvent for the VAEME-UHPLC-UV method proposed. Figure IV.6 shows a scheme of the microextraction procedure under optimum conditions.

The evaluation of the efficiency of the overall VAEME-UHPLC-UV method required the estimation of several parameters, such as relative recovery (RR), enrichment factor (E_F), and extraction efficiency (E_R). These useful parameters for microextraction methods were calculated using the following equations (and kept throughout the Doctoral Thesis).

The RR was calculated as:

$$RR(\%)=100\cdot\frac{C_{found}}{C_{initial}} \qquad \text{Equation IV.1.}$$

being C_{found} the calculated concentration of the PCPs using the calibration of the overall method (VAEME-UHPLC-UV), and $C_{initial}$ the spiked concentration of PCPs in the water sample. In general, for microextraction methods it is expected to obtain relative recoveries around 100% if the precision of the method is acceptable, as long as the water sample does not present a strong matrix effect.

The E_F of the overall VAEME-UHPLC-UV method is given by:

$$E_F=\frac{C_{droplet}}{C_{initial}} \qquad \text{Equation IV.2.}$$

being $C_{droplet}$ the concentration of PCPs obtained in the final droplet that is injected in the UHPLC, and so it can be calculated with the UHPLC-UV chromatographic calibration. This enrichment factor includes the preconcentration factor of the evaporation/reconstitution stage of the VAEME procedure. The enrichment factor can also be calculated as the ratio of calibrations slopes, being defined as:

$$E_F'=\frac{\text{Slope calibration VAEME-UHPLC-UV method}}{\text{Slope calibration UHPLC-UV method}} \qquad \text{Equation IV.3.}$$

The E_R of the overall method can be calculated by:

$$E_R=100\cdot\frac{E_F}{E_{Fmax}} \qquad \text{Equation IV.4.}$$

being E_{Fmax} the maximum preconcentration that would be achieved if all PCPs (initially present in the water sample) result successfully transferred to the final droplet that is injected in the UHPLC. This value can be estimated from the ratio $V_{initial}/V_{droplet}$, being $V_{initial}$ the initial aqueous sample volume (8 mL).

Figure IV.6. Optimum conditions of the VAEME procedure for the monitoring of 10 PCPs in water samples.

Several quality analytical parameters of the VAEME-UHPLC-UV method were obtained for both solvents: trichloromethane (Table IV.3.) and tetrachloroethylene (Table IV.4.).

For the optimum extractant solvent (trichloromethane), calibrations of the overall method were obtained by preparing aqueous standards with a concentration range between 0.63 and 25 $\mu g \cdot L^{-1}$, using 8 calibration levels, and subjecting them to the optimum VAEME-UHPLC-UV method. The obtained determination coefficients for the overall method were higher than 0.993. LODs and LOQs were experimentally evaluated as the PCP concentration in water that provided a final chromatographic signal to noise ratio of 3 and 10, respectively. LODs oscillated from 0.03 $\mu g \cdot L^{-1}$ for MPB to 1.65 $\mu g \cdot L^{-1}$ for TCS, while LOQs from 0.60 $\mu g \cdot L^{-1}$ for iBPB and 3.61 $\mu g \cdot L^{-1}$ for BP3. These values are quite low, particularly if we take into account that UV detection was used in combination with UHPLC. In the literature, the majority of recent reports utilize UHPLC in combination with MS/MS. Thus, LODs for parabens and UV filters (benzophenones) ranging from 0.4 to 4 $ng \cdot L^{-1}$ have been reported when using SPE and UHPLC-MS/MS and environmental waters [1], and from 2.5 to 5 $ng \cdot L^{-1}$ for BP3 and TCS in environmental waters when using stir-bar sorptive microextraction (SBSE) and UHPLC-MS/MS [2].

Table IV.3. Quality analytical parameters of the calibrations for the overall VAEME-UHPLC-UV method using trichloromethane as extractant solvent.

PCPs	(Slope ± SD[a]) $\times10^{-3}$	$S_{y/x}$ [c] $\times10^{-3}$	R^{2} [d]	LOD[e] ($\mu g\cdot L^{-1}$)	LOQ[e] ($\mu g\cdot L^{-1}$)
MPB	7.6 ± 0.3	7.08	0.9927	0.03	1.78
EPB	18.8 ± 0.6	13.9	0.9944	0.58	0.87
iPPB	22.5 ± 0.5	13.0	0.9966	0.45	0.93
PPB	23.4 ± 0.3	8.17	0.9988	0.52	1.07
iBPB	19.4 ± 0.2	3.96	0.9996	0.26	0.60
BPB	23.1 ± 0.2	4.09	0.9997	0.35	0.69
BzPB	19.0 ± 0.2	5.44	0.9992	0.36	1.13
BP	10.9 ± 0.3	5.04	0.9962	1.33	2.57
BP3	15.4 ± 0.4	9.76	0.9959	1.48	3.61
TCS	3.04 ± 0.05	1.13	0.9986	1.65	3.49

[a] Standard deviation associated to the slope

[b] Standard deviation of the residuals

[c] Determination coefficient

[d] Limit of detection and limit of quantification calculated according to the ratio signal/noise as 3 and 10 times, respectively, and experimentally verified

Table IV.4. Several quality analytical parameters of the calibrations for the overall method (VAEME-UHPLC-UV), using tetrachloroethylene as extractant solvent.

PCPs	Concentration range (μg·L^{-1})	(Slope ± SD[a]) ×10^{-3}	$S_{y/x}$ [c] ×10^{-3}	R^2 [d]	LOD[e] (μg·L^{-1})	LOQ[e] (μg·L^{-1})
MPB	4 – 834	0.23 ± 0.01	4.17	0.9971	0.79	49.8
EPB	2 – 417	1.07 ± 0.02	6.88	0.9985	5.37	8.10
iPPB	0.4 – 88	5.7 ± 0.1	7.00	0.9990	2.36	4.87
PPB	0.4 – 83	5.6 ± 0.1	4.97	0.9993	2.03	4.16
iBPB	0.2 – 44	12.2 ± 0.3	11.0	0.9979	1.13	2.62
BPB	0.2 – 25	12.5 ± 0.1	2.26	0.9997	1.40	2.73
BzPB	0.2 – 35	7.8 ± 0.1	3.02	0.9993	1.12	3.53
BP	6 – 38	19.4 ± 0.5	12.9	0.9980	3.79	7.31
BP3	5 – 35	20.5 ± 0.1	2.78	0.9999	2.71	6.61
TCS	5 – 35	4.68 ± 0.04	0.92	0.9998	3.46	9.99

[a] Standard deviation associated to the slope
[b] Standard deviation of the residuals
[c] Determination coefficient
[d] Limit of detection and limit of quantification calculated according to the ratio signal/noise as 3 and 10 times, respectively, and experimentally verified

The precision of the overall method was evaluated in terms of intra-day and inter-day RSD (in %). This study was carried out at two concentration levels: a low level (3.75 μg·L^{-1}) and an intermediate level (16.2 μg·L^{-1}), with respect to the concentration levels used in the calibrations. Intra-day precision was performed by 3 consecutive determinations at both levels. Their values have been included in Table IV.5., and they ranged between 1.0% for iPPB and 10% for BP at the low spiked level; and between 4.5% for BzPB and 18% for MPB for the intermediate spiked level with the exception of BP which gave a high RSD value of 25%. Inter-day precision was obtained through 3 determinations in 3 non-consecutive days, at the abovementioned spiked levels. An analysis of variance (ANOVA) was performed to determine whether there were significant differences in the results obtained by different days. The ANOVA study indicated that there were not significant differences the results obtained ($\alpha = 0.05$). The RSD values corresponding to the inter-day precision ranged from 4.8% for BP3 to 10% for BP at the low spiked level; and from 4.4%

for iBPB to 7.0% for MPB for the intermediate spiked level, being again the exception BP at this level, with a high RSD value of 27% (Table IV.5.). We observed low reproducibility performance for BP when working at relatively high spiked levels.

The VAEME-UHPLC-UV method was also evaluated in terms of extraction efficiency performance, also at the abovementioned spiked levels. RR (%), E_F, $E_F´$, and E_R (%) values are listed in Table IV.5. The average RR value obtained was 112% at the low spiked level, and 99.2% for the intermediate spiked level, being totally adequate for a microextraction method. The enrichment factors varied between ~20 and ~100 depending on the PCP, and independently on the spiked level. It can be observed the agreement in the enrichment factor values (E_F and $E_F´$), independently on their calculation methods. Clearly, the experimental enrichment factor values obtained are quite close to the maximum enrichment factor, which is 80. Regarding extraction efficiency, the VAEME-UHPLC-UV method was practically quantitative for most PCPs studied, which is not necessary valid for a microextraction methods. Average E_R values were of 82.7% for the low spiked level, and of 76.3% for the intermediate spiked level, for all PCPs studied. It can be also observed that low efficiencies at both spiked levels were obtained for MPB (values of 37.9 and 28.5%, respectively) and for BP (values of 35.1 and 24.7%, respectively). For MPB, reasons can be linked to its low K_{OW} value (and so low affinity for an organic solvent), and for BP to its distinct nature compared to the remaining PCPs (absence of any hydroxyl group in its structure).

Table IV.5. Analytical performance of the overall VAEME-UHPLC-UV method at two different concentration levels, in terms of intra-day precision, inter-day precision, extraction efficiency, relative recovery and enrichment factor.

PCP	Concentration level: 3.75 µg·L^{-1}						Concentration level: 16.2 µg·L^{-1}					
	RSD^{a} intra-day (%)	RSD^{b} inter-day (%)	RR^{c} (%)	E_F^{d}	$E_F^{\prime\, e}$	E_R^{f} (%)	RSD^{a} intra-day (%)	RSD^{b} inter-day (%)	RR^{c} (%)	E_F^{d}	$E_F^{\prime\, e}$	E_R^{f} (%)
MPB	7.4	7.7	114	30.3	21.8	37.9	18	7.0	98.9	22.8	21.8	28.5
EPB	6.8	9.0	118	57.0	52.1	71.2	11	6.8	103	52.7	52.1	65.9
iPPB	1.0	5.9	114	76.0	69.5	95.0	9.5	5.2	103	70.7	69.5	88.4
PPB	2.7	5.6	115	70.7	66.4	88.4	6.8	4.7	104	67.9	66.4	84.9
iBPB	1.4	4.9	115	73.9	64.5	92.4	5.7	4.4	105	67.5	64.5	84.4
BPB	2.1	5.0	116	78.3	72.0	97.9	5.2	4.5	106	75.0	72.0	93.8
BzPB	2.4	5.2	113	85.9	74.1	107	4.5	4.5	107	79.9	74.1	99.9
BP	10	10	87.6	28.1	32.7	35.1	25	26	61.7	19.7	32.7	24.7
BP3	6.4	4.8	114	99.4	93.4	124	6.7	5.6	101	92.4	93.4	115
TCS	5.6	8.0	114	61.8	61.4	77.3	6.7	6.9	104	61.7	61.4	77.1

[a] Relative standard deviation, intra-day precision (n = 3)
[b] Relative standard deviation, inter-day precision (n = 9)
[c] Relative recovery
[d] Enrichment factor calculated as concentrations ratio
[e] Enrichment factor calculated as slopes ratio
[f] Extraction efficiency

5. Assessment of the necessity of surfactants and/or dispersive solvents in VAEME

The main interest of the VAEME method relies on its simplicity: the method does not require a dispersive solvent and/or a co-solvent such as surfactant. However, many studies in literature utilize VAEME in combination with dispersive solvents [3-5] or surfactants [6-12], as an aid in the emulsification procedure. We decided to test if these solvents were really needed in our VAEME application, to help in the improvement of the recoveries for MPB and BP.

At first, we studied if the presence of acetonitrile (a common dispersive solvent) was going to exert an influence in the VAEME performance. Studies were carried out at optimum conditions of neat VAEME with trichloromethane, but also using 500 µL of acetonitrile as dispersive solvent. The aqueous standard concentration of PCPs was 12.5 $\mu g \cdot L^{-1}$. The obtained results implied slight improvements in recoveries for MPB and EPB, but mainly important decreases in recoveries for the rest of PCPs, as it can clearly be observed in Figure IV.7. This is a logical feature, because the dispersive solvent can partially solubilize the extractant solvent. Worse precision was also observed when acetonitrile was utilized. Therefore, acetonitrile was not really required in the proposed VAEME method for the selected group of PCPs.

We also select a wide group of surfactants to carry out the study of the influence of surfactants in the VAEME performance, from a variety of ionic to nonionic surfactants. Among ionic surfactants, the cationic surfactant CTAB, the anionic surfactant SDS, and the IL-based surfactants: hexadecylpyridinium chloride (C_{16}PyCl) and 1-hexadecyl-3-butylimidazolium bromide (C_{16}MImBr) were studied. The nonionic surfactant tested was polyoxyethylene-10-lauryl ether ($C_{12}E_{10}$). In all cases, the tested concentration was close (but slightly lower) than their respective critical micelle concentration values. Figure IV.8. shows the results obtained. Clearly, the use of surfactants was not really successful in the improvement of the overall performance if compared to the neat VAEME method. For the UV filters BP and BP3, it seems that CTAB slightly improves the extraction efficiency *versus* neat VAEME.

Attending to these results, this study did not use any surfactant neither dispersive solvent to aid the microextraction approach, and the simplified VAEME method was adequate to determine the group of PCPs selected.

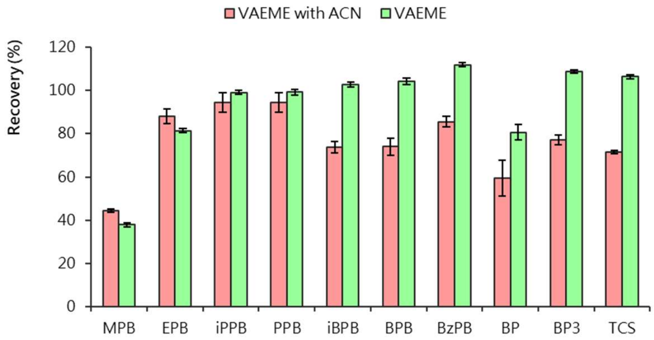

Figure IV.7. Influence of the utilization of acetonitrile in the VAEME performance. Experiments were performed in triplicate.

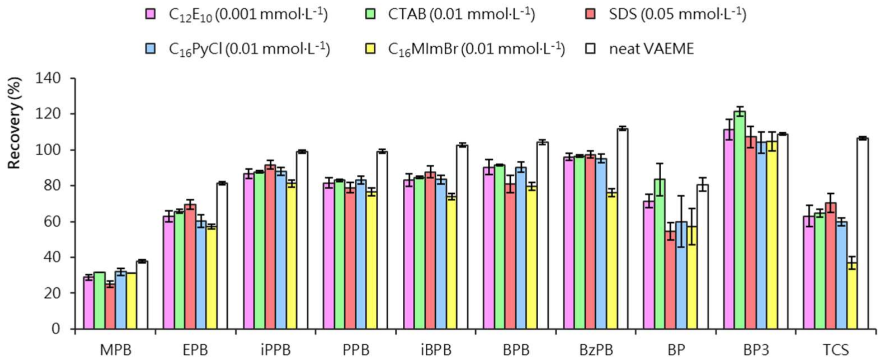

Figure IV.8. Influence of different surfactants in the VAEME performance (n = 3). In all cases, the optimum conditions corresponding to the VAEME method using trichloromethane were employed, with an aqueous standard having a PCP concentration of 12.5 μg·L^{-1}.

6. Analysis of environmental water samples with the optimum VAEME-UHPLC-UV method

Seven environmental water samples were analyzed with the optimized VAEME-UHPLC-UV method for the determination of PCPs. All samples were from the Island of Tenerife: two swimming pool waters (SP1 and SP2), two seawaters (SW1 and SW2), two wastewaters (WW1 and WW2) and one tap water (TW). All waters were analyzed in triplicate with the overall VAEME-UHPLC-UV method (Table IV.6.). MPB was detected in six of the samples analyzed, and was quantified at 1.9 ± 0.1 $\mu g \cdot L^{-1}$ in TW. Other PCPs were also quantified: BPB at 1.1 ± 0.3 $\mu g \cdot L^{-1}$ and TCS at 19.8 ± 0.2 $\mu g \cdot L^{-1}$, in WW1 and WW2, respectively. BPB and iBPB were detected in TW, and BP was detected in SP1 and SP2 while iBPB was only detected in SP1. Obvious caution with these results is advisable, because UV and not MS detection has been utilized in this study. MS is the detector of choice when unequivocal identification is pursued. It must be highlighted that in this VAEME method, the solvent used for injection in the UHPLC is the LC mobile phase, and so the present VAEME-UHPLC-UV method is totally applicable as VAEME-UHPLC-MS method. In any case, these obtained results are totally comparable with those reported in the literature. For example, TCS has been quantified at 0.041 $\mu g \cdot L^{-1}$ in effluents of wastewaters using IL-DLLME-LC-MS/MS [13], and at 0.1 $\mu g \cdot L^{-1}$ in influents of wastewaters using SBSE-UHPLC-MS/MS [14]. Other authors have quantified TCS at 2.08 $\mu g \cdot L^{-1}$ in domestic waters using DLLME-UHPLC-UV [15].

Three representative water samples of different nature were also utilized to evaluate the matrix effect: SP2, SW1 and WW1. These samples were spiked at an intermediate concentration level of PCPs (12.5 $\mu g \cdot L^{-1}$), and then analyzed six times by the overall method (intra-day). Table IV.6. shows the performance of the method with these samples, in terms of relative recovery, intra-day precision, and extraction efficiency.

The average RR values obtained were 93.9 ± 13.1% for SP2, 87.8 ± 15.6% for SW1, and 67.4 ± 14.2% for WW1. Relative recoveries obtained for SP2 and SW1 are similar to those with ultrapure water. However, the matrix effect is clear in the wastewater sample, which can be justified by its high organic matter content.

The average extraction efficiencies were 75.6%, 71.5%, and 54.5% for SP2, SW1 and WW1, respectively. These values are comparable with those obtained with ultrapure water at the intermediate spiked level (82.0%) for swimming pool waters and seawaters, and again the matrix effect is clear for wastewaters.

Table IV.6. Analysis of surface and wastewater samples using the overall optimized procedure.

PCPs	SP1	SP2			SW1			SW2	WW1			WW2	TP
	Level found (µg·L^{-1})	Level found (µg·L^{-1})	Spiked level: 12.5 µg·L^{-1} RR[a] (%)	E_R[b] (%)	Level found (µg·L^{-1})	Spiked level: 12.5 µg·L^{-1} RR[a] (%)	E_R[b] (%)	Level found (µg·L^{-1})	Level found (µg·L^{-1})	Spiked level: 12.5 µg·L^{-1} RR[a] (%)	E_R[b] (%)	Level found (µg·L^{-1})	Level found (µg·L^{-1})
MPB	~1.0<LOQ	~1.3<LOQ	66.6	18.6	~0.5<LOQ	75.2	22.5	~0.8<LOQ	~0.4<LOQ	53.4	16.6	~0.8<LOQ	1.9 ± 0.1[c]
EPB	n.d.	n.d.	89.1	51.5	n.d.	86.5	54.6	n.d.	n.d.	57.0	35.4	n.d.	n.d.
iPPB	n.d.	n.d.	90.2	77.0	n.d.	100	85.9	n.d.	n.d.	65.7	55.8	n.d.	n.d.
PPB	n.d.	n.d.	97.2	78.6	n.d.	103	83.7	n.d.	n.d.	67.3	53.8	n.d.	n.d.
iBPB	~0.4<LOQ	n.d.	95.5	77.0	n.d.	102	82.0	n.d.	n.d.	76.9	62.0	n.d.	~0.3<LOQ
BPB	n.d.	n.d.	106	93.4	n.d.	111	97.7	n.d.	1.1 ± 0.3[c]	91.3	80.2	n.d.	~0.4<LOQ
BzPB	n.d.	n.d.	98.8	92.4	n.d.	99.1	92.6	n.d.	n.d.	74.4	69.8	n.d.	n.d.
BP	~1.7<LOQ	~1.4<LOQ	120	48.8	n.d.	57.0	20.1	n.d.	n.d.	105	29.4	n.d.	n.d.
BP3	n.d.	n.d.	94.8	108	n.d.	95.9	109	n.d.	n.d.	75.8	85.8	n.d.	n.d.
TCS	n.d.	n.d.	65.0	46.7	n.d.	72.4	52.4	n.d.	n.d.	57.6	41.1	19.8 ± 0.2[c]	n.d.

[a] Relative recovery
[b] Extraction efficiency
[c] Standard deviation (n = 3)
n.d.: non-detected

REFERENCES

[1] E. Gracia-Lor, M. Martínez, J.V. Sancho, G. Peñuela, and F. Hernández. Talanta 99 (2012) 1011–1023.

[2] M. Pedrouzo, F. Borrull, R.M. Marcé, and E. Pocurull. Anal. Bioanal. Chem. 397 (2010) 2833–2839.

[3] K. Seebunrueng, Y. Santaladchaiyakit, and S. Srijaranai. Chemosphere 103 (2014) 51–58.

[4] J. López-Darias, M. Germán-Hernández, V. Pino, and A. M. Afonso. Talanta 80 (2010) 1611–1618.

[5] L. Zhang, F. Chen, S. Liu, B. Chen, and C. Pan. J. Sep. Sci. 35 (2012) 2514–2519.

[6] Z.H. Yang, Y.L. Lu, Y. Liu, T. Wu, Z.Q. Zhou, and D.H. Liu. J. Chromatogr. A 1218 (2011) 7071–7077.

[7] R.H. Li, D.H. Liu, Z.H. Yang, Z.Q. Zhou, and P. Wang. Electrophoresis 33 (2012) 2176–2183.

[8] Z.H. Yang, D.H. Liu, W.T. Zhao, T. Wu, Z.Q. Zhou, and P. Wang. J. Sep. Sci. 36 (2013) 916–922.

[9] G. Leng, W. Chen, M. Zhang, F. Huang, and Q. Cao. J. Sep. Sci. 37 (2014) 684–690.

[10] J. Vichapong, R. Burakham, and S. Srijaranai. Talanta 117 (2013) 221–228.

[11] Z.H. Yang, P. Wang, W.T. Zhao, Z.Q. Zhou, and D.H. Liu. J. Chromatogr. A 1300 (2013) 58–63.

[12] Y. Zhang and H.K. Lee. J. Chromatogr. A 1274 (2013) 28–35.

[13] R.S. Zhao, X. Wang, J. Sun, S.S. Wang, J.P. Yuan, and X.K. Wang. Anal. Bioanal. Chem. 397 (2010) 1627–1633.

[14] M. Pedrouzo, F. Borrull, R.M. Marcé, and E. Pocurull. Anal. Bioanal. Chem. 397 (2010) 2833–2839.

[15] J.H. Guo, X.H. Li, X.L. Cao, Y. Li, X.Z. Wang, and X.B. Xu. J. Chromatogr. A 1216 (2009) 3038–3043.

Section IV.2.

Sorbent-based microextraction applications

IV.2.1. A step forward with dispersive miniaturized solid-phase extraction

Among sorbent-based microextraction approaches, the miniaturized solid-phase extraction (μSPE) performed in dispersive mode (D-μSPE) is an approach highly used in analytical laboratories worldwide mainly due to its simplicity, as described in Section I.3.2.1. The simplicity directly links to its performance: a solid sorbent is added to an aqueous sample, followed by stirring, and its further removal to perform desorption and the analytical determination.

D-μSPE, as all sorbent-based miniaturized methods, has enormously benefited from the incorporation of novel materials, thus adding the advantages and advances in microextraction with those of materials science. Among novel materials, this Doctoral Thesis focuses its attention on metal-organic frameworks, given their unique properties, tuneability, and impressive surface areas, as described in Section I.3.2.3.

A step forward in the use of MOFs in D-μSPE lies on the proper design of these materials for microextraction uses. Since MOFs have recently started to be used in this microextraction mode, the construction of simple pillar-layered MOFs seems to be a good choice for several reasons: i) the linkers can be modified with functional groups; and ii) the pillar can be changed to adapt the pore size to that of the analytes. Thus, novels MOFs based on a pillar-layered structure, have been synthesized, characterized, and used for the extraction of several PCPs in water samples in this Doctoral Thesis.

One of the main concerns regarding the use of MOFs in D-μSPE is to determine if the limiting stage is the sorption or the desorption process. In the sorption stage, various features should be considered: i) the surface area of the material; ii) its proper activation; iii) if there could be partial blocking of pores in the MOF by bulky analytes present in the samples; iv) diffusion of the analytes through the pores of the MOF (intending to maximize the adsorption of analytes); and v) hydrophobic/hydrophilic matching between analytes and pores of the MOF. In the desorption stage, the selection of the adequate solvent may be critical to achieve a complete desorption (considering the ability of the solvent to diffuse through the pores of the MOF to efficiently remove the analyte) and the time required for desorption (intending its minimization).

In any case, the better understanding of the interaction of analytes and MOFs is extremely important to improve the design of these materials with microextraction purposes. Therefore, efforts should shift to understand the behavior of the sorbent, its maximum adsorption capacity, its kinetic of adsorption, and the dependence of the extraction efficiency with the sample and extraction conditions.

Regarding their applications, MOFs have been used widely in D-µSPE combined with liquid chromatography, with few applications focusing on the monitoring of volatile or semi-volatile analytes. Moreover, another purpose is to propose a D-µSPE using MOF for the determination of semi-volatile PCPs by GC-MS.

In summary, the main goal of this section focuses on the use of novel MOFs in D-µSPE applications for PCPs, and to correlate their crystal structure, and adsorption capacity with the analytical performance, while setting up LC and GC applications, thus covering non-volatiles and semi-volatiles PCPs. Novels MOFs based on a pillar-layered structure, and named CIM MOFs, were synthesized, characterized, evaluated, and isotherm adsorption studies were carried out to increase the knowledge on their microextraction behavior.

IV.2.1.1. Characterization of MOFs intended for microextraction, including novel and conventional MOFs

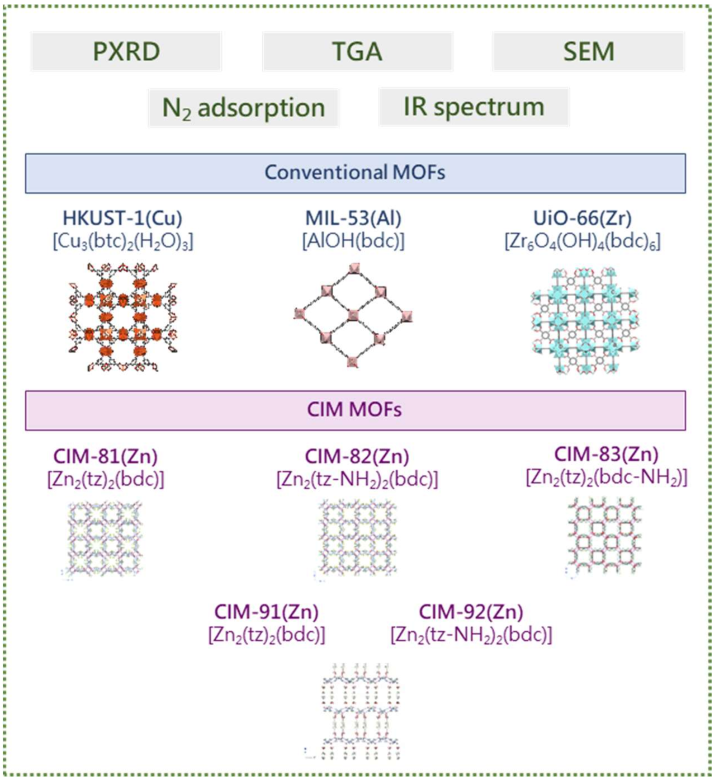

1. Synthesis and characterization of conventional MOFs

Three different conventional MOFs (HKUST-1(Cu), MIL-53(Al), and UiO-66(Zr)), selected given their proved success in microextraction methods [1], were obtained through a solvothermal synthesis through the procedure indicated in Section III.6.1. Table IV.7. summarizes the space group and cell parameters of each structure together with the surface area for each material. The crystalline structure of conventional MOFs was confirmed by powder X-ray diffraction (PXRD), and their porosity and surface area were studied by N_2 adsorption isotherms. Images of the synthesized MOF were obtained by scanning electron microscopy (SEM) to evaluate their morphology.

Table IV.7. Several physicochemical characteristics of MOFs used as microextraction sorbents in this Doctoral Thesis.

MOF abbreviation / formula / structure	Space group	Surface area ($m^2 \cdot g^{-1}$)
HKUST-1(Cu) $[Cu_3(btc)_2(H_2O)_3]$ 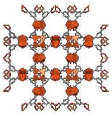	*Fm*-3*m* a = 52.5078(± $1.7 \cdot 10^{-3}$) Å b = 52.5078(± $1.7 \cdot 10^{-3}$) Å c = 52.5078(± $1.7 \cdot 10^{-3}$) Å	1068
MIL-53(Al) $[AlOH(bdc)]$ 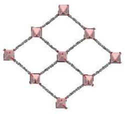	*P*2$_1$/*c* a = 19.50417(± $2.5 \cdot 10^{-4}$) Å b = 15.20143(± $1.3 \cdot 10^{-4}$) Å c = 6.56931(± $9 \cdot 10^{-5}$) Å β = 104.1797(± $1.3 \cdot 10^{-3}$)	978
UiO-66(Zr) $[Zr_6O_4(OH)_4(bdc)_6]$ 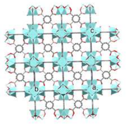	*Fm*-3*m* a = 20.7004(± $2 \cdot 10^{-4}$) Å b = 20.7004(± $2 \cdot 10^{-4}$) Å c = 20.7004(± $2 \cdot 10^{-4}$) Å	1342

The nature of the as-synthesized material was confirmed by comparison of the experimental PXRD pattern with the simulated pattern from the single crystal structure already reported. Figure IV.9. shows such comparison for all conventional MOFs synthesized.

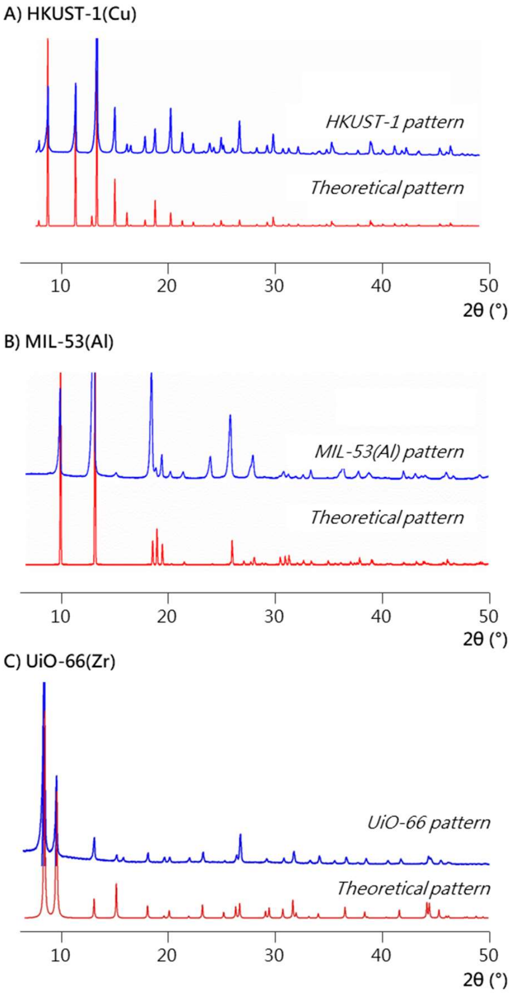

Figure IV.9. PXRD patterns of conventional MOFs synthesized and characterized for microextraction approaches: **A)** HKUST-1(Cu), **B)** MIL-53(Al), and **C)** UiO-66(Zr).

The thermal stability of the conventional MOFs considered have been reported previously. Thus, HKUST-1(Cu) is thermally stable up to 400 °C [2], MIL-53(Al) up to 600 °C [3], and UiO-66(Zr) up to 500 ºC [4].

The study of the porosity and the measurement of surface area was carried out by N_2 adsorption isotherms for each conventional MOF. Figure IV.10. shows the isotherms obtained for the N_2 adsorption at 77 K. In all cases, it can be observed a type I isotherm. The obtained BET surface area values were: 1068 $m^2 \cdot g^{-1}$ for HKUST-1(Cu), 978 $m^2 \cdot g^{-1}$ for MIL-53(Al), and 1342 $m^2 \cdot g^{-1}$ for UiO-66(Zr).

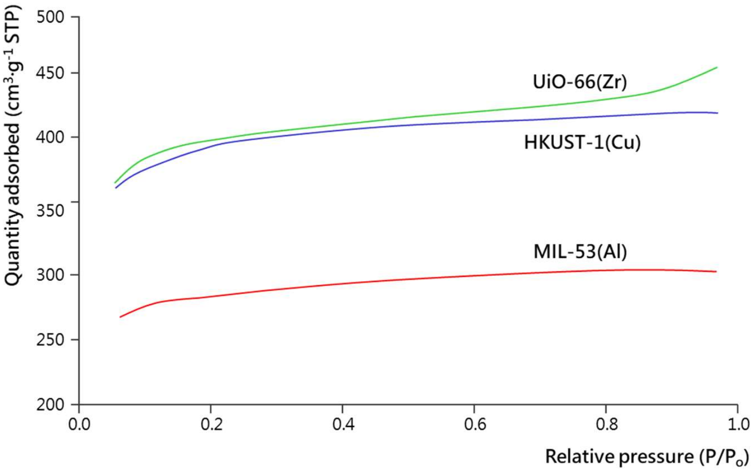

Figure IV.10. N_2 adsorption isotherm of conventional MOFs at 77K for HKUST-1(Cu) (blue line), MIL-53(Al) (red line), and UiO-66(Zr) (green line).

In order to evaluate the microscopic morphologies of the crystals, images were obtained by SEM. Figure IV.11. includes several SEM images of the HKUST-1(Cu), MIL-53(Al) and UiO-66(Zr) MOFs. It can be observed clearly the octahedral crystals of the HKUST-1(Cu). The smallest crystals were UiO-66(Zr) (0.2-0.5 μm), followed by MIL-53(Al) crystals (1-2 μm), and HKUST-1(Cu) (10-25 μm).

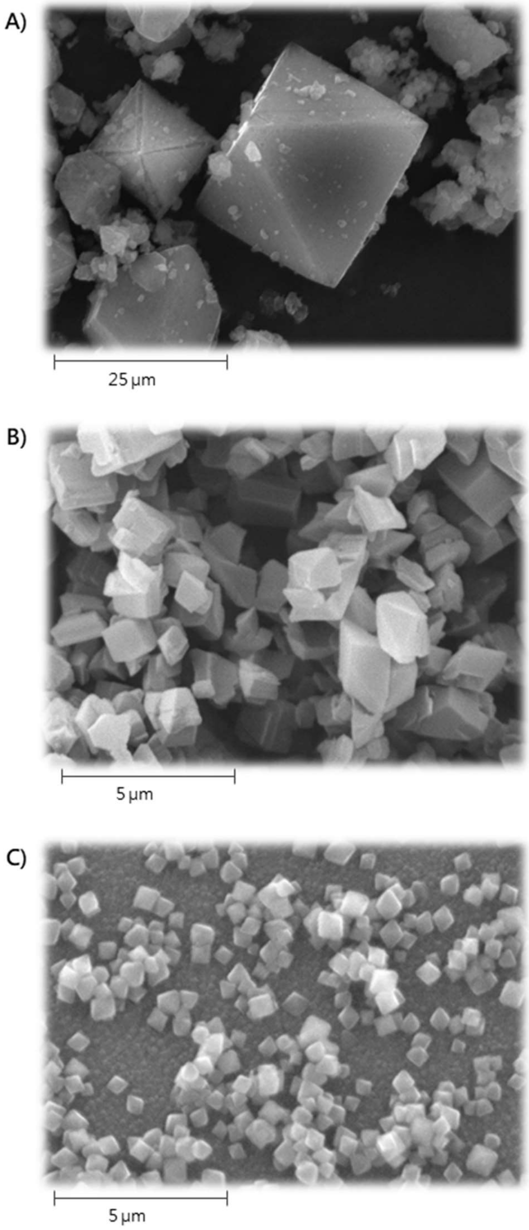

Figure IV.11. SEM images of **A)** HKUST-1(Cu), **B)** MIL-53(Al), and **C)** UiO-66(Zr).

2. Characterization and structural analysis of CIM MOFs

MOFs with a pillared-layer structure have been synthesized. Pillared-layer MOFs have many advantages, for example, they can be functionalized on each one of the two ligands, or the pillar can be easily extended to yield larger pores, and somehow facilitate the diffusion of analytes through the material. Thus, five different CIM MOFs (CIM-81(Zn), CIM-82(Zn), CIM-83(Zn), CIM-91(Zn), and CIM-93(Zn)) were obtained through a solvothermal synthesis through the procedure indicated in Section III.6.1.

CIM-81(Zn), CIM-82(Zn), and CIM-83(Zn), are known MOFs, with their crystal structure previously reported [5,6]. In this Doctoral Thesis, these MOFs were characterized by PXRD, thermogravimetric analysis (TGA), infrared (IR), and N_2 adsorption isotherms, and to gain a better insight of how the analytes and other molecules are anchored in the pores, their single crystal structure was solved for the first time with two host-guest systems: acetone@CIM-81 and DMA@CIM-81. This knowledge will be useful for the computer simulation of the behavior of analytes inside the pores. CIM-91(Zn) was already synthesized and its structure elucidated, but scarcely commented by Yao *et al.* [7]. Nevertheless, we were able to prepare the two host guest systems: acetone@CIM-91 and DMF@CIM-91, which help to understand the adsorption properties of these crystals. CIM-92(Zn) is a new phase obtained and its crystal structure was elucidated by X-ray diffraction. They were also characterized by PXRD, TGA, IR, and N_2 adsorption isotherms. Table IV.8. shows the space group and cell parameters of each structure together with the surface area for each material.

Table IV.8. Several physicochemical characteristics of CIM MOFs used as microextraction sorbents in this Doctoral Thesis.

MOF abbreviation / formula / structure	**Space group**	**Surface area (m^2·g^{-1})**
CIM-81(Zn) $[Zn_2(tz)_2(bdc)]$ 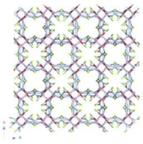	*P4/ncc* a = 13.4523(6) Å b = 13.4523(6) Å c = 27.2990(3) Å	482
CIM-82(Zn) $[Zn_2(tz\text{-}NH_2)_2(bdc)]$ 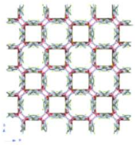	*P4/nnc* a = 12.6724(4) Å b = 12.6724(4) Å c = 25.2868(16) Å	378
CIM-83(Zn) $[Zn_2(tz)_2(bdc\text{-}NH_2)]$ 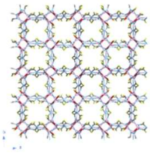	*P4/ncc* a = 13.3567(4) Å b = 13.3567(4) Å c = 27.4176(9) Å	310
CIM-91(Zn) $[Zn_2(tz)_2(bdc)]$ 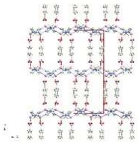	*Pnma* a = 10.1168(3) Å b = 26.4504(10) Å c = 9.6256(3) Å	408
CIM-92(Zn) $[Zn_2(tz\text{-}NH_2)_2(bdc)]$ 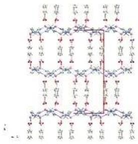	*Pnma* a = 9.7778(3) Å b = 26.9674(7) Å c = 9.2658(3) Å	302

As abovementioned, the nature of the as-synthesized CIM-81(Zn), CIM-82(Zn), and CIM-83(Zn) MOFs was confirmed by comparison of the experimental PXRD pattern with the simulated one from the single crystal structure already reported. In the case of acetone@CIM-81, DMA@CIM-81, CIM-91, and CIM-92, the theoretical pattern is that obtained with single crystal X-ray diffraction. Figure IV.12. shows such comparison for the CIM MOFs synthesized.

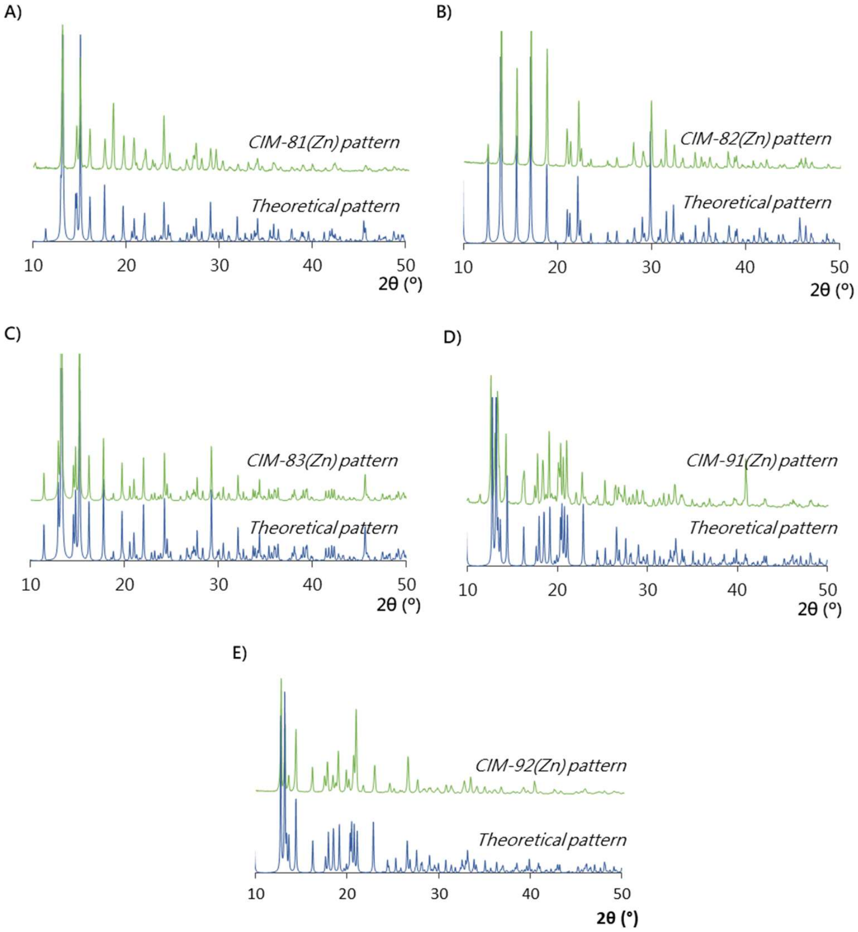

Figure IV.12. PXRD patterns of CIM MOFs synthesized and characterized: **A)** CIM-81(Zn), **B)** CIM-82(Zn), **C)** CIM-83(Zn), **D)** CIM-91(Zn), and **E)** CIM-92(Zn).

The study of the thermal stability was carried out by thermogravimetric analysis. Figure IV.13. shows the thermogravimetric curves obtained.

For CIM-81(Zn), the two weight losses at low temperatures can be attributed to the removal of crystallization solvent molecules. The first one appears at 100-150 ºC with a smooth slope, which can be assigned to water molecules, whereas the next at 200-250 ºC can be assigned to DMA molecules. The abrupt loss at 400 ºC is the first of the ligand degradations, and above this temperature the CIM-81(Zn) is no longer stable.

For CIM-82(Zn), the solvent of its synthesis is a mixture of water:ethylene glycol (1:1 (v/v)), which is lost at around 300 ºC. The ligands degradation is observed in the second weight loss at 450 ºC, and thus this temperature is considered as the maximum thermal stability of the CIM-82(Zn).

For CIM-83(Zn), the first loss is observed at 200-250 ºC due to the removal of the DMF molecules. The next loss is observed around 450 ºC according with the ligand degradations, similar to the CIM-82(Zn) case, and it is considered that the CIM-83(Zn) is no longer stable above this temperature.

For CIM-91(Zn), the loss of the DMF molecules is observed around 200 ºC, and the ligand degradation starts at 380-400 ºC, being this temperature slightly lower to those of the tetragonal CIM MOFs (CIM-81(Zn), CIM-82(Zn), and CIM-83(Zn)). The ligands start a gently degradation and the complete degradation of the CIM-91(Zn) MOF takes place at around 600 ºC.

Finally, for CIM-92(Zn), the removal of crystallization solvent molecules is observed at 150-200 ºC. In this case, the ligand degradation can observe with a great abrupt loss at 400 ºC. This temperature is considered as the maximum thermal stability of the CIM-92(Zn).

In general, CIM MOFs are stable until around 400 ºC, observing their complete decomposition at 600 ºC, with CIM-83(Zn) having slightly higher thermal stability than CIM-81(Zn). Regarding the amino functionalization, it is clear that it did not provide an increasing thermal stability.

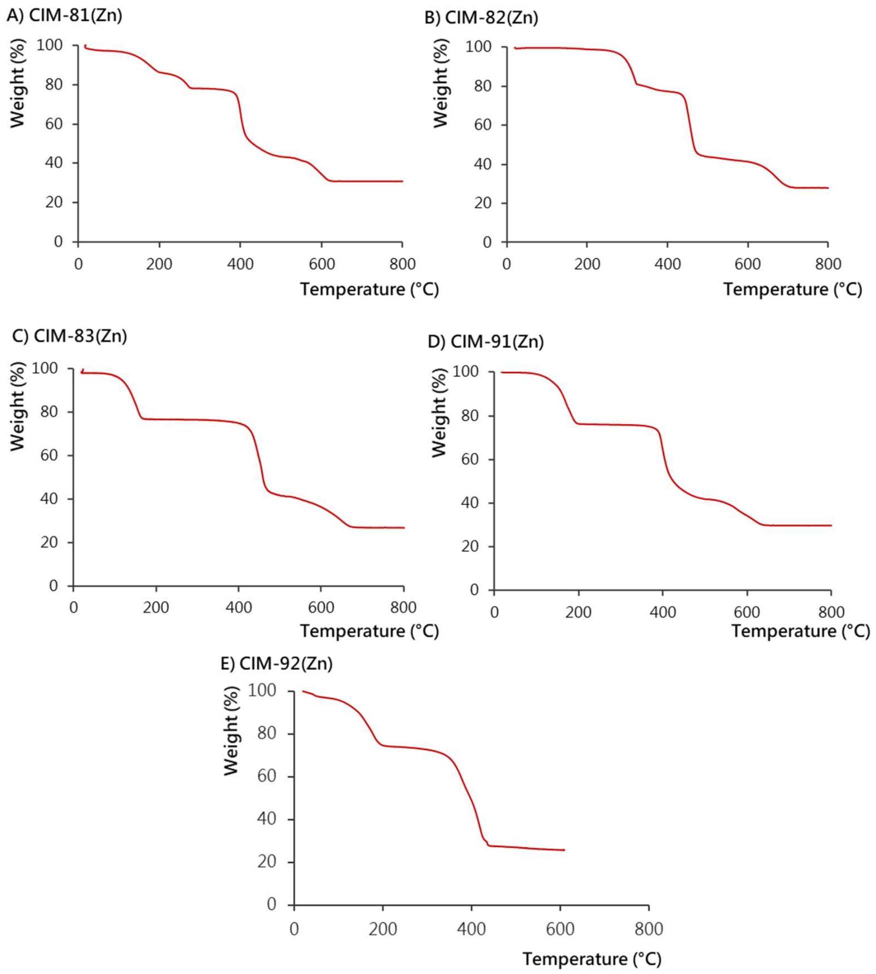

Figure IV.13. Thermogravimetric curves of **A)** CIM-81(Zn), **B)** CIM-82(Zn), **C)** CIM-83(Zn), **D)** CIM-91(Zn), and **E)** CIM-92(Zn).

IR was employed to ensure the elimination of guest solvent molecules during the activation of the MOFs, and to verify the presence of certain functional groups associated to MOF's ligands in the final crystal structure. MOFs intended for microextraction are normally thermally activated to remove guest solvent molecules [8]. Figures IV.14. shows the IR spectrum before and after the solvent-exchange procedure for tetragonal CIM MOFs (CIM-81(Zn), CIM-82(Zn), and CIM-83(Zn)), and Figure IV.15. for orthorhombic CIM MOFs (CIM-91(Zn), and CIM-92(Zn)).

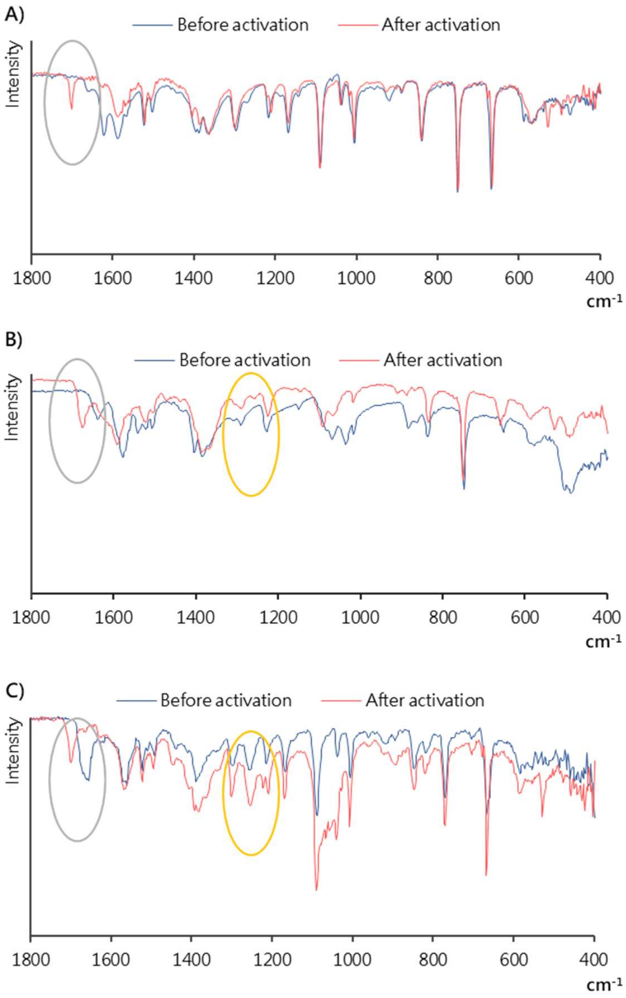

Figure IV.14. FT-IR spectra of **A)** CIM-81(Zn), **B)** CIM-82(Zn), and **C)** CIM-83(Zn) before the solvent-exchange procedure (blue line) and after the activation procedure (red line). Grey circles refer to carboxylic groups and yellow circles refer to amino groups.

Data show the characteristic peaks of the aromatic rings and carboxyl groups, with the peak at 1680-1600 cm^{-1} (indicated in a gray circle in Figures IV.14. and IV.15.) attributed to guest solvent molecules (DMA for CIM-81(Zn), and DMF for CIM-83(Zn), CIM-91(Zn), and CIM-92(Zn)), both before activation. The absence of this band in the activated crystals of CIM MOFs clearly shows the absence of guest solvent molecules in the final framework. After the activation, it can be observed a new band at 1703 cm^{-1} associated to the acetone (solvent used for the activation), supporting the solvent exchange and the activation procedure. The IR bands around 1360-1250 cm^{-1} (indicated in a yellow circle in Figures IV.14. and IV.15.) confirm the presence of amino groups in the functionalized CIM MOFs (CIM-82(Zn), CIM-83(Zn), and CIM-92(Zn)).

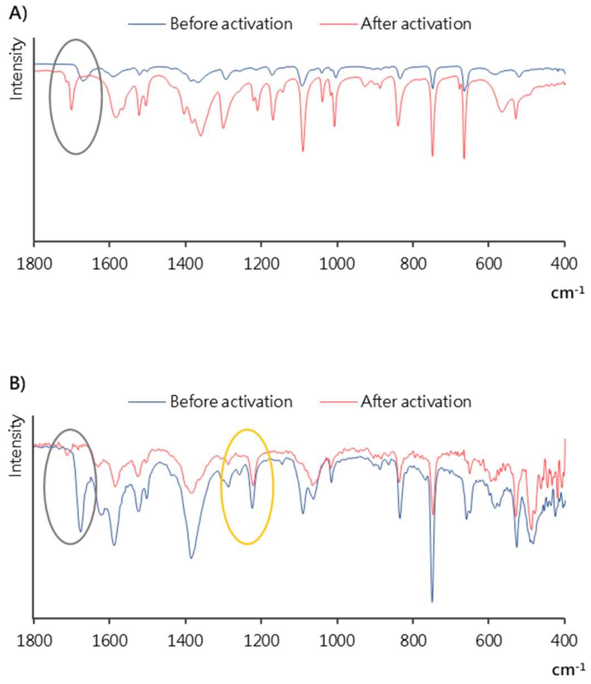

Figure IV.15. FT-IR spectra of **A)** CIM-91(Zn), and **B)** CIM-92(Zn) before the solvent-exchange procedure (blue line) and after the activation procedure (red line). Grey circles refer to carboxylic groups and yellow circles refer to amino groups.

N_2 adsorption isotherms of each CIM MOFs were obtained to study the porosity and the measurement of surface area. For all crystals, the N_2 adsorption (Figure IV.16.) at 77 K yielded a type I isotherm owing to its microporous nature. The BET surface area values obtained were: 482 $m^2{\cdot}g^{-1}$ for CIM-81(Zn), 310 $m^2{\cdot}g^{-1}$ for CIM-83(Zn), 408 $m^2{\cdot}g^{-1}$ for CIM-91(Zn), and 302 $m^2{\cdot}g^{-1}$ for CIM-92(Zn). For the CIM-82(Zn) MOF, the isotherm is not shown in Figure IV.16. given its low adsorption. Its BET surface area was 378 $m^2{\cdot}g^{-1}$, estimated in this case from CO_2 isotherms at 298 K.

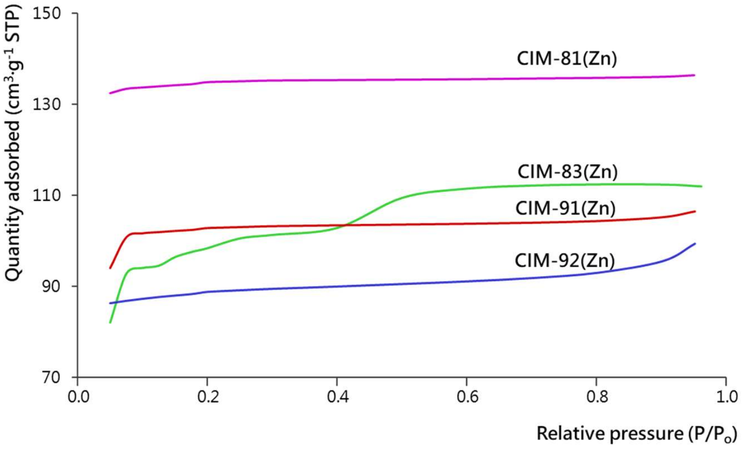

Figure IV.16. N_2 adsorption isotherm of CIM MOFs at 77K for CIM-81 (purple line), CIM-82 (green line), CIM-91 (red line), and CIM-92 (blue line).

In order to evaluate the microscopic morphologies of the crystals, images were obtained by SEM. Figure IV.17. included the SEM image of the novel CIM-81(Zn) MOF as representative example of CIM MOFs (the microscopic structure of all the CIM MOF is the same due to their pillared-layered shape). The CIM-81(Zn) MOF crystals are around 100 μm.

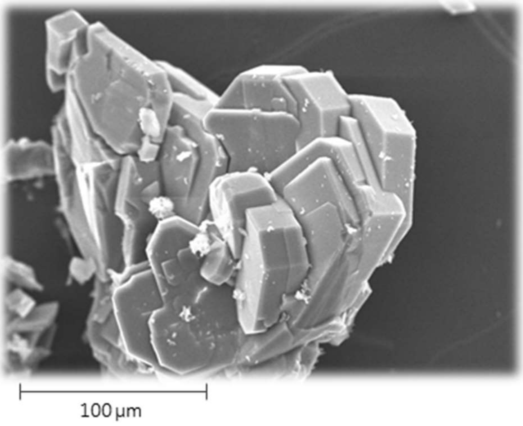

Figure IV.17. SEM images of CIM-81(Zn).

2.1. Description of the structures

The crystal structures of the CIM-81(Zn), CIM-82(Zn), and CIM-83(Zn) MOFs have been previously reported. However, the models proposed for these structures remove the guest solvent molecules and therefore, there is no information on how the guest molecules are anchored to the host framework. This is the reason why it is tried to determine the crystal structure of CIM-81(Zn) with different guest molecules. This was obtained successfully with acetone@CIM-81 and DMA@CIM-81; but it was not possible to obtain good diffraction data from the PPB@CIM-81.

2.1.1. Structural description of CIM-81(Zn), CIM-82(Zn), and CIM-83(Zn)

The CIM-81(Zn) and CIM-83(Zn) MOFs are isomorphous with a general formula of their 3D framework of $[Zn_2(tz)_2(bdc\text{-}X)]$ (X= -H or $-NH_2$), that crystallize in the $P4/ncc$ tetragonal space group. CIM-82(Zn) $[Zn_2(NH_2\text{-}tz)_2(bdc)]$, otherwise, crystallizes also in the tetragonal system but in the $P4/nnc$ space group. In general, the three-dimensional structure is formed by corrugated Zn-triazolate layers of $[Zn_2(tz)_2]_n$ pillared by the terephthalate ligand. Each triazolate ligand links three Zn(II) ions through the typical μ-1,2,4-bridging fashion, to form the layer, whereas the terephthalate ligand acts as a rod-like connector. Each Zn(II) metal center is 4-coordinate with a carboxylate oxygen atom and three nitrogen atoms from three different triazolate ligands forming a tetrahedron. Topologically, considering the $\{Zn_2(tz)_2\}$ units as a 6-connected node and dicarboxylate ligands as the linker, the 3D of CIM-81(Zn) and CIM-83(Zn) structures can be simplified as non-interpenetrated **pcu** topologies [5]. However, CIM-82(Zn) structure can be defined as a 6-connected α-Po topology with the point symbol of $(4^8{\cdot}6^6{\cdot}8)$, showing an intriguing entangled pattern with a self-penetrating framework, where two of the same 6-rings interlocked with each other [9].

The structures of CIM-81(Zn) and CIM-83(Zn) exhibit two different types of pores (A and B), running along the *c* crystallographic direction (Figure I.18.(A)). Both pores are composed of cavities of 6.5 × 6.5 $Å^2$ and approximately 11 Å in length, connected by a narrow window, in such a way that there are eight of these cavities per unit cell (a pair in each of the two A pores and other two in each of the two B pores). The characteristics of these windows formed by four triazolate ligands tilted respect to the pore walls differs from A and B pores. In the A pores, these four triazolate ligands are related by a –4 symmetry axis, leaving two of the hydrogen atoms pointing to one of the cavities and the other two directed to the adjacent one. In the B pores, the triazolate ligands are related by a 4-fold symmetry axis, and thus the four hydrogen atoms point to one of the cavities. However, the separation between H atoms in the B pores is larger (approximately 5 Å) than in the A pores (H···H approximately 4 Å). Although the terephthalate ligands constitute the walls of both pores, the uncoordinated oxygen atoms are closer to the B pores, leading to a more hydrophilic environment in that region. Also, the hydrogen atoms of the aromatic ring of the terephthalate ligand points towards the B pore in CIM-81(Zn) and CIM-83(Zn), as occurs with the amino groups of the 2-aminoterephthalate in CIM-83(Zn).

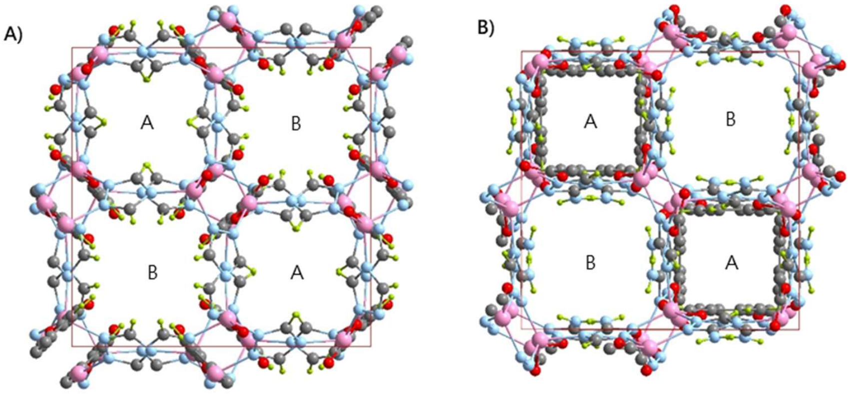

Figure IV.18. View of the crystal structure of **A)** CIM-81(Zn) and CIM-83(Zn), and **B)** CIM-82(Zn) along the *c* axes. A and B pores are indicated.

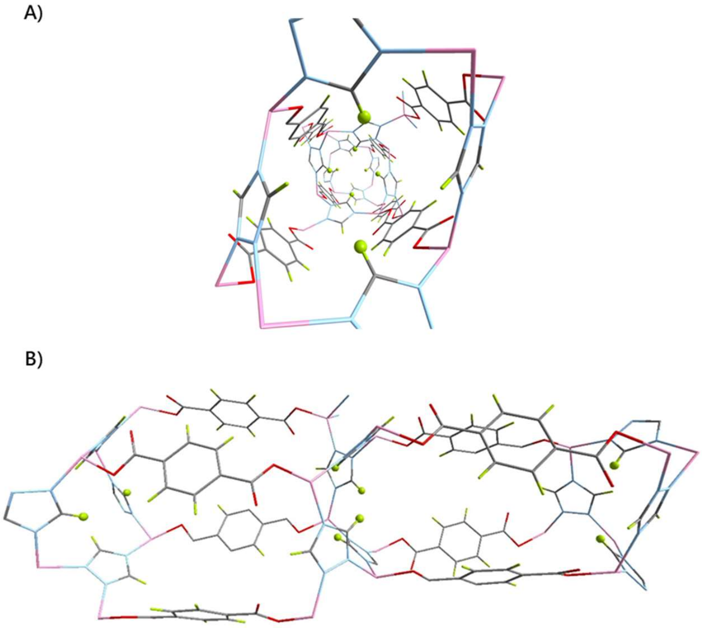

Figure IV.19. Central projections of the A pore of CIM-81(Zn) and CIM-83(Zn) crystal structures **A)** along the crystallographic *c* direction and **B)** a lateral view.

In the case of CIM-82(Zn), there are also two types of pores running along the *c* axis, but in this case there are not narrow windows within the channels, because the triazolate ligands are not tilted respect to the pore walls. The A pores (Figure IV.18.(B)) are slightly narrower than the B pores, where the amino groups of the NH_2-tz are located and also the uncoordinated oxygen atoms of the terephthalate ligand. A PLATON calculation showed an effective solvent accessible voluble of 49.5% for CIM-81(Zn), 22.2% for CIM-82(Zn), and 44.8% for CIM-83(Zn).

The crystal structures of acetone@CIM-81 and DMA@CIM-81 where investigated to get an insight about the possible locations for the adsorbed molecules in these MOFs. In both cases, the guest molecules have a main anchoring point in A pore with the carbonyl oxygen atom establishing two hydrogen bonds with the C–H hydrogen atoms of the triazolate ligands at the channel narrow windows (Figure IV.20.). Two DMA/acetone molecules are located inside each cavity of A pore. In B pore, however, the guest solvents were delocalized and could not be modelled during the refinement. The residual electron density was masked out, and the electron count per B pore in the unit cell (there are two B pores per unit cell) is approximately 48 electrons in the case of the DMA@CIM-81 and 35 electrons for acetone@CIM-81. These values roughly correspond to a single DMA/acetone molecule in the B pore per unit cell for acetone@CIM-81 and DMA@CIM-81, respectively. This implies that A pores host eight DMA/acetone molecules per unit cell, whereas B pores host only two. Given these findings, the preferential adsorption into A pore was also investigated through a computational study.

The wiggling motion of the carboxylate-based ligands may have a key role in the different pores present in these structures: the different degrees of freedom makes that hydrogen atoms pointed differently in channels 1 and 2, and completely block the pores in CIM-82(Zn).

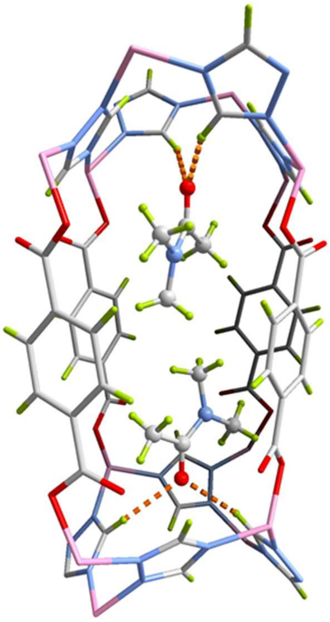

Figure IV.20. Crystal structures of the A pore of DMA@CIM-81.

2.1.2. Structural description of CIM-91 and CIM-92

The CIM-91(Zn) MOF was obtained by simple modification of the synthetic procedure for the tetragonal CIM MOF series, basically, the reaction solvent was changed from DMA to DMF. The crystal structure of CIM-91(Zn) was already reported [7], but the structure was not discussed at all in that reference, and thus it is summarized herein its principal features.

CIM-91(Zn) and CIM-92(Zn) with formula [Zn_2(tz-X)$_2$(bdc)] (X = -H and -NH_2) exhibit a three-dimensional framework and, as occur in the tetragonal CIM MOF series, is formed by Zn-triazolate layers pillared by the terephthalate rod-like ligands. In this case, the compounds crystallize in the orthorhombic *Pnma* space group. Each triazolate ligand connects three Zn(II) ions through a typical μ-1,2,4-bridging mode to form the corrugated layers. Each Zn(II) ions is 4-coordinate with three nitrogen atoms from three triazolate ligands and an oxygen atom from a terephthalate building a tetrahedral polyhedron. The separation between layers is given by the length of the pillar, i.e. the terephthalate ligand, to be approximately 11 Å. As occur in CIM-81(Zn) and CIM-83(Zn), considering the [$Zn_2(tz)_2$] units as six-fold nodes, the topology of the network can be described as a non-interpenetrated **pcu**.

The structure of CIM-91(Zn) exhibits a cross-linked pore system, with channels running along the *a* and *b* directions (Figure IV.21.(A) and 21.(B)). In this case, the pores running along the *b* axis are the equivalent to the A and B pores of the tetragonal CIM MOF series, but here both the hydrogen atoms from the triazolate and those from the terephthalate point towards the channel. Furthermore, the uncoordinated oxygen atoms also locate in these pores. The channels along the *a* axis (Figure IV.21.(C)) are rectangular of dimensions 4.8 ×11 $Å^2$ with the bdc pillars in the long edges and the Zn-triazolate layers in the short ones. In the case of CIM-92(Zn), the pore structure is similar and the amino groups of the NH_2-tz ligand point towards the inner of the pores.

It was possible to solve the crystal structure of acetone@CIM-91 and DMF@CIM-91 with acetone and DMF as guest molecules. Two DMF/acetone molecules per formula unit ([$Zn_2(tz)_2(bdc)$]·2DMF/acetone) are accommodated in the pores. The DMF/acetone molecules are located in the pores close to the hydrogen atom of the C–H of the triazolate ligands establishing C–H···O hydrogen bonds, as it has been observed in the CIM-81(Zn).

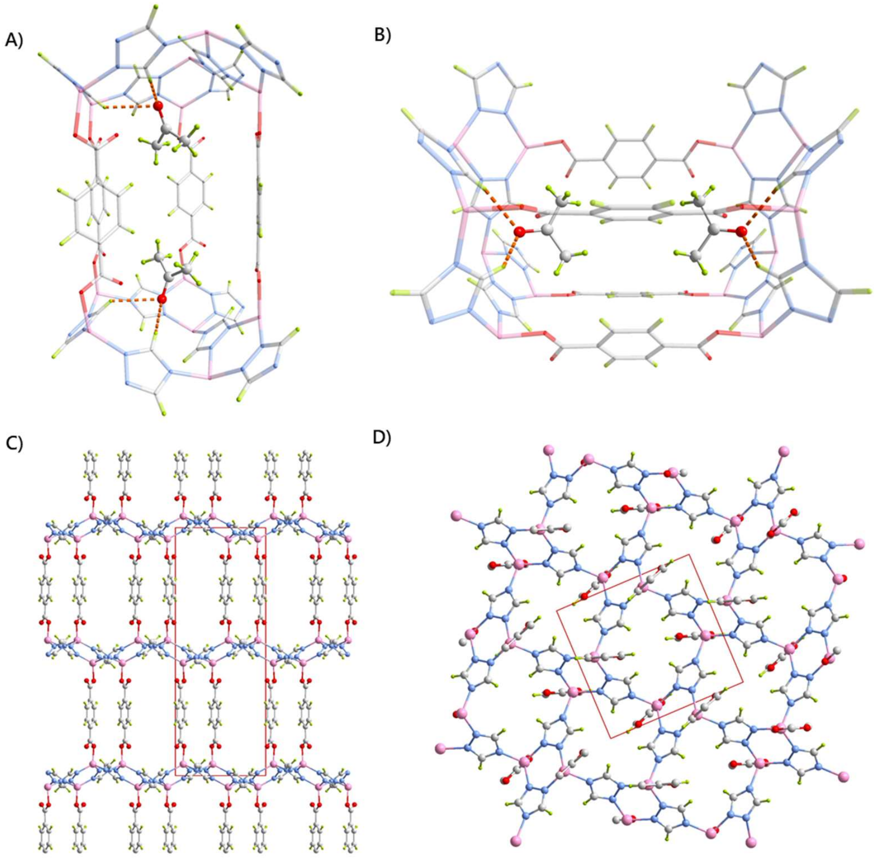

Figure IV.21. Pore cavities of CIM-91 along the **A)** *a* and **B)** *b* directions, and the crystal structure of CIM-91(Zn) along the **C)** *a* direction and **D)** *b* directions.

IV.2.1.2. Adsorption isotherm studies of CIM-81(Zn), CIM-82(Zn), and CIM-83(Zn)

In preparation for submission to ACS Applied Materials and Interfaces

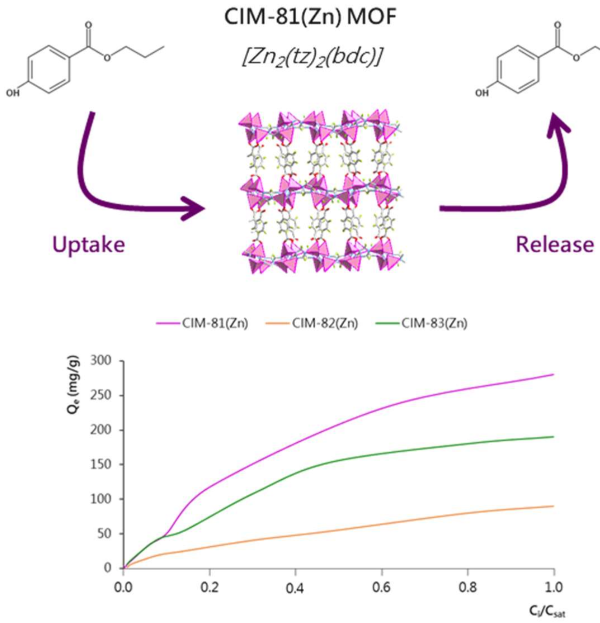

The three tetragonal MOFs: CIM-81(Zn), CIM-82(Zn), and CIM-83(Zn), were selected to carry out the adsorption studies. These MOFs are structurally very similar but the N_2 adsorption shows some differences coming from the amino functionalization (Section IV.2.1.2.). Herein, it has studied the adsorption and release behavior of PPB is an example of the PCP family of parabens, with the ester chain length neither too large to present steric problems during its adsorption, nor too short to be representative of the whole family. Some (but not many) studies have evaluated the adsorption capacity of MOFs for organic compounds present in aqueous samples. Thus, the interaction with several pollutants, such as atrazine [10] and carbamazepine tetracycline hydrochloride [11], have been carried out. In these studies, the authors could obtain the maximum adsorption capacity of the MOFs considered, such as Zr(VI)-based MOF (named NU-1008, NU-901, and NU-1000) [10], and UiO-66(Zr) [11]. The adsorption capacity of MIL-100(Fe) for pharmaceutical pollutants was evaluated in another study, together with a computational study [12]. Other authors have studied the adsorption and the crystallographic interactions between vitamins and drugs and one bimetallic (Ca(II) and Cu(II)) MOFs [13].

The amount of PPB adsorbed was calculated by the difference between the concentration of the initial aqueous solution (C_i) – experimentally confirmed by injection and quantitation using the calibration data – and the concentration at the time of interest (C_t) (quantified with the same calibration) according to the following equation:

$$Q_t = \frac{(C_i - C_t)V}{m} \qquad \text{Equation IV.5.}$$

where Q_t is the amount of PPB adsorbed at the time t, V is the volume of the sample, and m is the mass of MOF used. The experimental procedure required that aliquots were taken to ensure minimum disturbance of the overall volume of the aqueous solutions. The calibration for PPB was obtained using aqueous standard containing a 10% (v/v) of ACN. For 6 concentration levels, the calibration equation was: peak area = $[(142.4 \pm 0.8) \times 10^4] \times$ concentration of PPB (in $mg \cdot L^{-1}$) + $[(-0.3 \pm 0.5)] \times 10^4$, being the $S_{y/x}$ equal to 5403 and $R^2 = 0.999$.

1. Dependency on the sorbent mass

Initially, a study was carried out to preview the dependency of the mass of sorbent used in the adsorption performance of the MOF. Thus, the adsorption experiment was performed with different amounts of CIM-81(Zn) (5, 10, 25 and 50 mg) at two different sample volumes (5 and 10 mL), and employing an aqueous standard of PPB at high content (500 mg·L^{-1}). This concentration corresponds to the solubility of PPB in water at 25 ºC [14], named from now on in this Doctoral Thesis as saturation concentration (C_{sat}). C_{sat} was selected for this series to determine if the upload of PPB in the MOF is saturated in those experiment with less amounts of sorbent. In this study, aliquots were taken after 24 hours (to ensure reaching the equilibrium), diluted conveniently according to the initial concentration of the aqueous solution (C_0), and injected in the UHPLC equipment for the determination of PPB under the conditions described in Section III.6.3.

Figure IV.22. shows the isotherms obtained by the representation of the amount of PPB adsorbed per gram of CIM-81(Zn) MOF (Q_e) *versus* the amount of CIM-81(Zn) MOF (in mg), for the two volumes of aqueous standard of PPB considered. Figure IV.22. includes the plotting of the PPB amount adsorbed considering a 100% efficiency of the sorbent at every mass tested (dashed line), if assuming that the sorbent is able to adsorb the total amount of PPB in the solution (4.64 mg for the 10 mL sample and 2.32 mg for the 5 mL one). The experimental data lay below that curve, indicating that the extraction efficiency of CIM-81(Zn) sorbent is far from the ideal case. The Figure IV.22. also includes the plotting of the simulated PPB amount adsorbed considering the efficiency at the extreme experiments performed (5 mg and 50 mg, dark red and light red in Figure IV.22., respectively). It can be seen that the experimental performance is not constant, varying with the mass of sorbent used. The efficiency in terms of adsorption (mg adsorbed per mg in solution) is higher in the case of 50 mg, being 48%, than at 5 mg (being in this case only 29%). The values for the 5 mL sample are lower, as it is expected, since there are less PPB in the solution (Figure IV.22.). In this case, the adsorption with 50 mg corresponds to an efficiency of 54%, being only 19% with 5 mg.

For the remaining experiments, and for the sake of simplicity, it has been selected 5 mg for the amount of MOF and a sample volume of 10 mL.

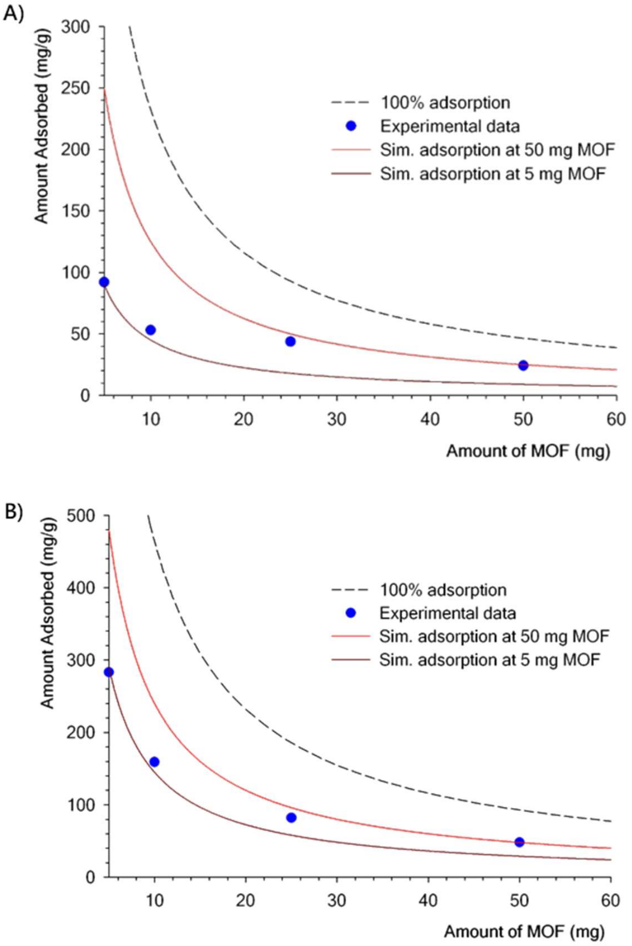

Figure IV.22. Isotherm obtained for the evaluation of amount adsorbed of analyte (PPB) with respect to the sorbent mass (CIM-81(Zn) MOF), for **A)** 5 mL of an aqueous standard of PPB at C_{sat}, and **B)** 10 mL of an aqueous standard of PPB at C_{sat}.

2. Adsorption kinetics

In the kinetic study for the adsorption stage, 5 mg of the tetragonal CIM MOFs were exposed to 10 mL of aqueous solutions at 10 mg·L^{-1} of PPB. Aliquots were taken at different times (1, 5, 30, 60, 90, 120, 360, and 1440 minutes), diluted conveniently (to avoid saturation in the UHPLC-UV signal), and injected in the UHPLC equipment for the determination of PPB under the conditions described in Section III.6.2. Figure IV.23. shows the isotherms obtained by the representation of the amount of PPB absorbed per gram of MOF (Q_e), at each time considered. It has been performed a non-linear regression on these data sets considering the usual equations for the analysis of kinetic data, summarized in Table IV.9. In the case of CIM-81(Zn) and CIM-83(Zn), the pseudo-second order model gives the best fitting (blue solid line in Figure IV.23.), however for the CIM-82(Zn), that adsorbs only ~5% of the PPB present in solution, the best fit is obtained with the pseudo-first order equation. The data from the fittings is presented in Tables IV.10. In the three cases, it can be considered that the equilibrium is achieved at 24 h, being the CIM-83(Zn) kinetics slower than that of CIM-81(Zn). This may be due to the amino functionalization group interacting with PPB, thus slowing its diffusion rate.

The maximum uptake obtained for CIM-81(Zn) was 68%, for CIM-82(Zn) was 5%, and for CIM-83 was 65%. This will be further confirmed with the E_R values in the D-µSPE-UHPLC-UV and D-µSPE-GC-MS analytical method (Sections IV.2.1.3. and IV.2.1.4.).

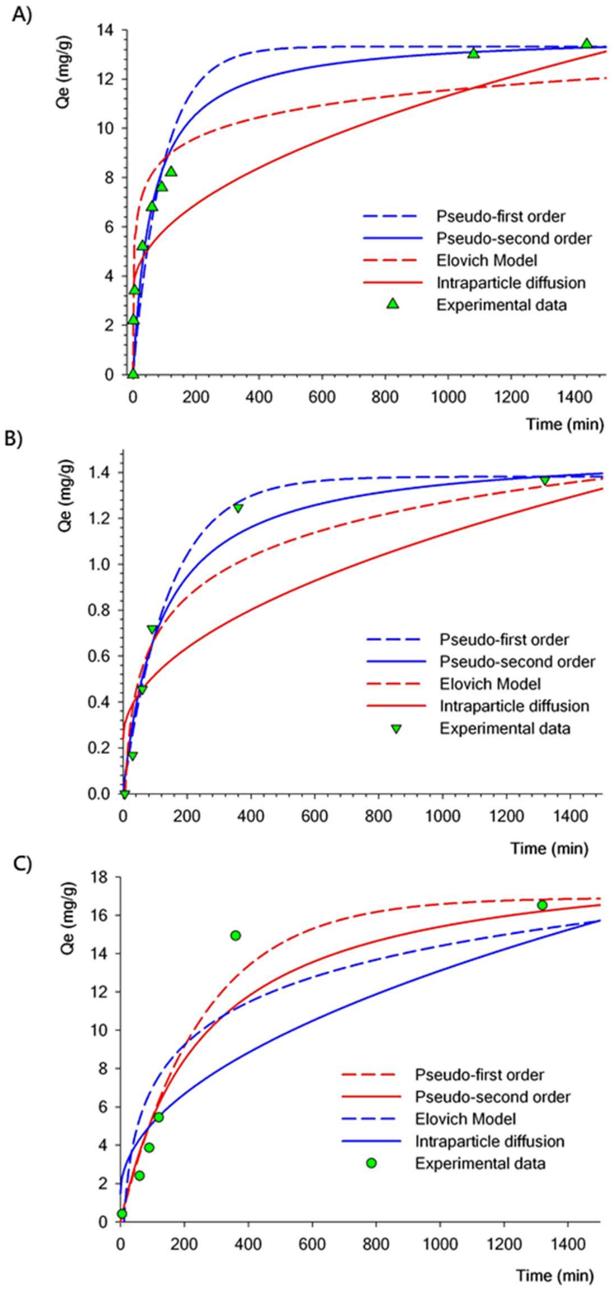

Figure IV.23. Isotherm obtained for the adsorption kinetic study of **A)** CIM-81(Zn), **B)** CIM-82(Zn), and **C)** CIM-83(Zn).

Table IV.9. Kinetic models and the corresponding equations for adsorption isotherms.

Kinetic model	Equation	Description
Pseudo-first order	$Q_t=Q_e(1-e^{-k_1t})$	It is based on the assumption that there is an adsorption site for adsorbate
Pseudo-second order	$Q_t=\frac{k_2 \cdot Q_e^2 t}{1+k_2 \cdot Q_e t}$	It is based on the assumption that the adsorbate is adsorbed onto two active sites
Elovich equation	$Q_t=\frac{1}{\beta}\ln(\alpha\beta)+\frac{1}{\beta}\ln t$	It is based on the assumption that the active sites of the adsorbent are heterogeneous, and therefore they exhibit different activation energies, based on a second order reaction mechanism
Intraparticle diffusion	$Q_t=k_3\sqrt{t}$	It is based on the solute transfer through the internal porous structure and its actual diffusion in the solid, which causes the adsorbent to acquire a homogeneous structure

Q_t, time adsorption capacity ($mg \cdot g^{-1}$)
Q_e, equilibrium adsorption capacity ($mg \cdot g^{-1}$)
t, time (min)
k_1, pseudo-first order constant (min^{-1})
k_2, pseudo-second order constant ($g \cdot mg^{-1} \cdot min^{-1}$)
k_3, diffusion constant ($mg \cdot g^{-1} \cdot min^{-1/2}$)
α, Elovich constant ($mg \cdot g^{-1} \cdot min^{-1}$)
β, Elovich constant ($g \cdot mg^{-1}$)

Table IV.10. Kinetic parameters obtaining by the four models considered (see Table IV.9.) for each tetragonal CIM MOFs.

First order	k_1 (min^{-1})	Q_e (mg·g^{-1})	R^2
CIM-81(Zn)	0.011 (0.001)	13.3 (0.7)	0.931
CIM-82(Zn)	0.0070 (0.0006)	1.38 (0.03)	0.992
CIM-83(Zn)	0.0039 (0.0006)	16.9 (0.7)	0.977
Pseudo-second order	k_2 (g·mg^{-1}·min^{-1})	Q_e (mg·g^{-1})	R^2
CIM-81(Zn)	0.0012 (0.0003)	13.8 (0.6)	0.954
CIM-82(Zn)	0.006 (0.001)	1.51 (0.06)	0.981
CIM-83(Zn)	0.00020 (0.00007)	19 (1)	0.953
Elovich	α (mg·g^{-1}·min^{-1})	β (mg·g^{-1}·min^{-1})	R^2
CIM-81(Zn)	17 (14)	0.8 (0.1)	0.886
CIM-82(Zn)	0.04 (0.01)	3.9 (0.4)	0.944
CIM-83(Zn)	0.3 (0.1)	0.31 (0.05)	0.871
Interparticle	k_3 (mg·g^{-1}·min$^{-1/2}$)		R^2
CIM-81(Zn)	0.25 (0.03)		0.879
CIM-82(Zn)	0.028 (0.006)		0.799
CIM-83(Zn)	0.37 (0.07)		0.833

The kinetics of the desorption of PPB from the MOFs were also studied. Thus, CIM-81(Zn), CIM-82(Zn), and CIM-83(Zn), were exposed to 10 mL of aqueous standard of PPB at a concentration level of 100 mg·L^{-1}. After 24 hours, the remaining PPB (C_f) was determined by taking aliquots, which were conveniently diluted, and injected in the UHPLC equipment for the determination of PPB under the conditions described in Section III.6.3. Immediately after, in order to mimic the D-µSPE procedure that will be further used in Sections IV.2.1.3. and IV.2.1.4. (experimentally described in Section III.6.2.), the aqueous standard solution was removed, and 5 mL of methanol were added to ensure the desorption step. Aliquots of such methanol solution were taken at different times (1, 5, 30, 60, 90, 120, 360, and 1440 minutes), and injected directly (without dilution) in the UHPLC equipment for the determination of PPB under the conditions described in Section III.6.3. Figure IV.24. shows the results obtained over the time, with the release value calculated with the following equation:

$$\text{Release (\%)} = \frac{\text{mg PPB adsorbed - mg PPB released}}{\text{mg PPB adsorbed}} \cdot 100 \qquad \text{Equation IV.6.}$$

For CIM-82(Zn), there is no release, indicating that the low amount adsorbed is difficult to liberate. The release for CIM-81(Zn) is faster than for CIM-83(Zn), CIM-81(Zn) has released 75% of the PPB adsorbed after 60 min, whereas CIM-83(Zn) has only released 50%. Furthermore, the total release is near 85% for CIM-81(Zn) after 24h, and around 70% for CIM-83(Zn). The release kinetic data were fitted through a non-linear regression with a pseudo-first order model giving a well match for the entire time studied, with R^2 values ranging from 0.96 to 0.98. The kinetic parameter is (0.026 ± 0.005) and (0.0065 ± 0.0009) min^{-1} for CIM-81(Zn) and CIM-83(Zn), respectively, supporting the faster release for CIM-81(Zn).

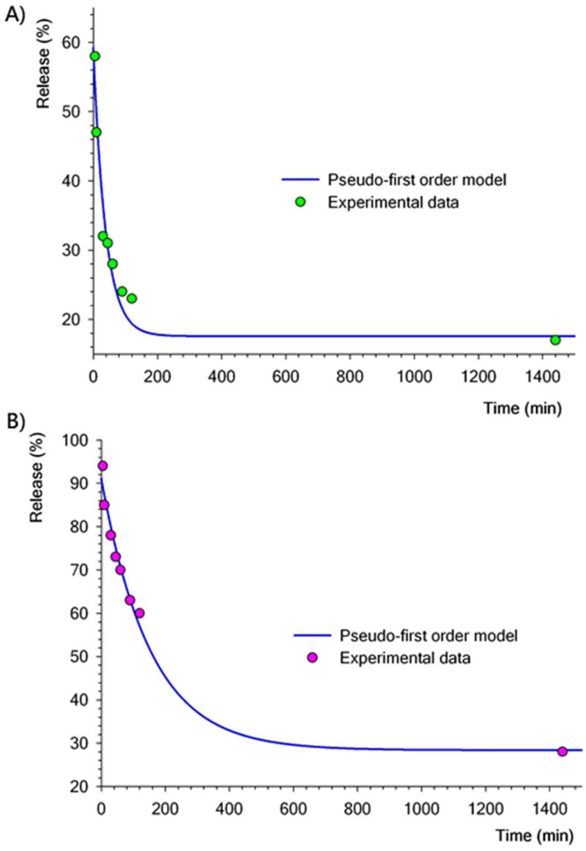

Figure IV.24. Release curves obtained after exposure of the CIM MOFs to an aqueous standard solution of PPB (at a concentration level 100 mg·L^{-1}) after 24 hours, for **A)** CIM-81(Zn) and **B)** CIM-83(Zn).

3. Adsorption isotherm

For the adsorption isotherm, 5 mg of the CIM MOFs were exposed to 10 mL of aqueous solutions at different concentration levels of PPB (1, 5, 10, 50, 100, 200, 300 and 500 mg·L^{-1}). The maximum concentration level was the saturation concentration of PPB (C_{sat}). Aliquots were taken after 24 hours (to ensure that the equilibrium was reached), diluted conveniently according to the initial concentration of the aqueous solution (C_0), and injected in the UHPLC equipment for the determination of PPB under the conditions described in Section III.6.3. Figure IV.25. shows the adsorption isotherms obtained by the representation of the amount of PPB absorbed per gram of MOF (Q_e) with regards to the ratio initial concentration *versus* the saturation concentration of PPB in water (C_i/C_{sat}).

It is obvious that the Q_e value in the equilibrium (after 24 hours) increases with the C_i. Furthermore, this study also supports that the adsorption capacity of the CIM MOFs follows the trend: CIM-81(Zn) > CIM-83(Zn) > CIM-82(Zn).

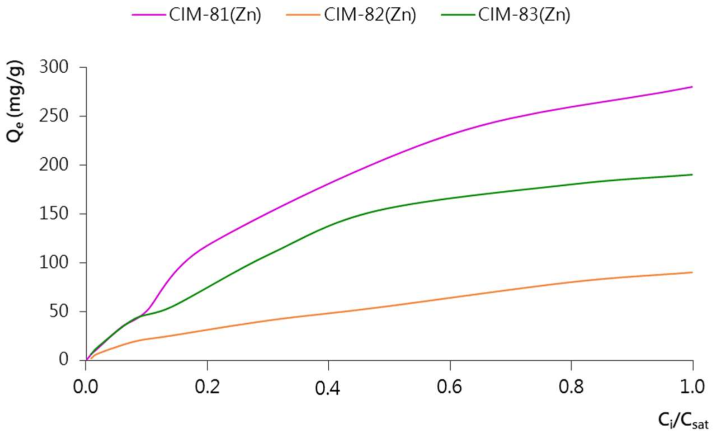

Figure IV.25. Isotherm obtained for the adsorption capacity study of CIM-81(Zn) (lines in purple), CIM-82(Zn) (lines in orange), and CIM-83(Zn) (lines in green). Lines have been plotted simply joining the experimental points, without any mathematical fitting.

In order to carry out a more detailed study about the adsorption performance of the CIM MOFs, the Langmuir and Freundlich isotherm models were applied with the results of the latter experiments abovementioned.

The Langmuir model is described by the following equation:

$$\frac{C_e}{Q_e} = \frac{C_e}{Q^0} + \frac{1}{Q^0 B} \qquad \text{Equation IV.7.}$$

where C_e (mg·L^{-1}) is the concentration of the PPB in the equilibrium, Q^0 (mg·g^{-1}) is the maximum amount of PPB absorbed per gram of MOF, and B (L·mg^{-1}) is a constant related to the affinity of the binding sites.

The linearized Freundlich model is given by the following equation:

$$\log Q_e = \frac{1}{n} \log C_e + \log K \qquad \text{Equation IV.8.}$$

where n is referred to the intensity of the adsorption, and K (mg·g^{-1}) is the adsorption capacity. Thus, the adsorption isotherm for each CIM MOFs using the Langmuir model were plotted presenting Q_e/Q_e *versus* C_e, while for the Freundlich model the plot is $\log Q_e$ *versus* $\log C_e$. The obtained isotherms are shown in Figure IV.26.

Table IV.11. summarizes those parameters obtained from the application of both adsorption models for each CIM MOFs studied. The Langmuir fittings for CIM-81(Zn) and CIM-82(Zn) give better matchings than the Freundlich model, but it is not the case for CIM-83(Zn). The amino group in CIM-83(Zn) seems to provide another binding point for the adsorbates, and the Freundlich model, which considers multiple adsorption sites, yields a better result. The maximum adsorption capacity for CIM-81(Zn) from the Langmuir model (350 mg·g^{-1}) is larger than that observed experimentally (280 mg·g^{-1}) as occur with CIM-82(Zn). Also, the B parameter in the Langmuir model is larger for CIM-83(Zn), indicating that the amino groups are playing an important role in the adsorption. This value for the maximum adsorption capacity exceeds reported values for other adsorbents, activated carbon (167 mg·g^{-1}) [15], or a composite of ionic liquids and mesoporous polymer (20 mg·g^{-1}) [16].

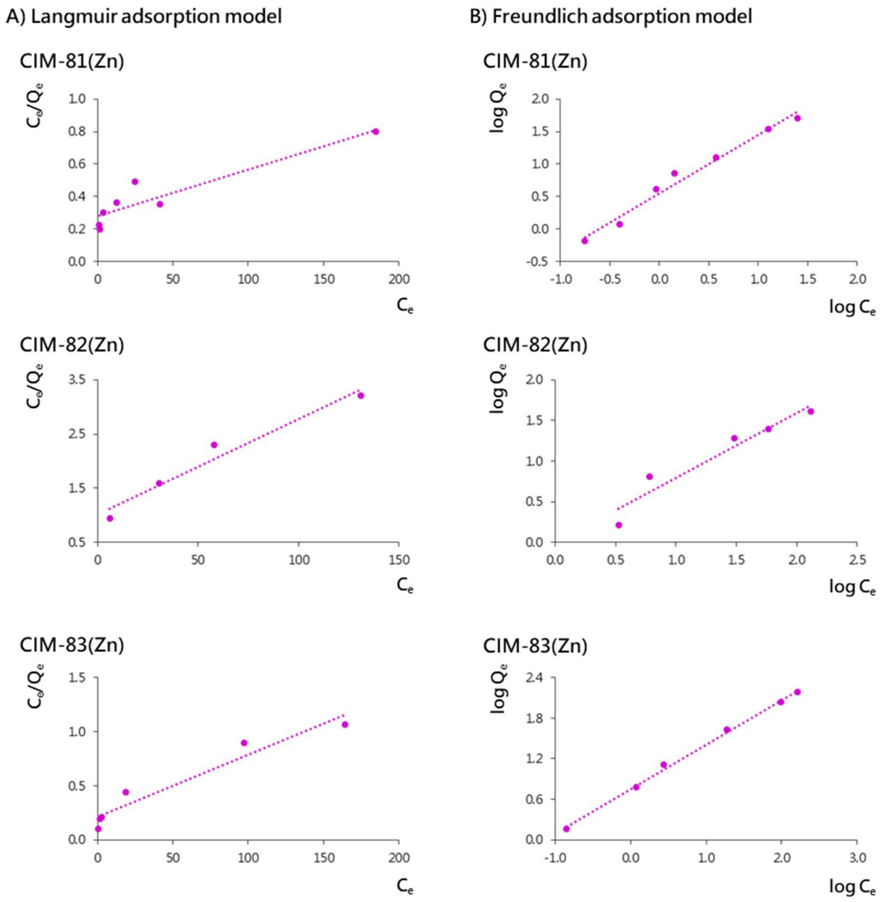

Figure IV.26. Adsorption isotherms obtained by **A)** Langmuir model and **B)** Freundlich model, both for CIM-81(Zn), CIM-82(Zn), and CIM-83(Zn).

Table IV.11. Relevant adsorption parameters obtained from the Langmuir (Equation IV.7.) and Freundlich (Equation IV.8.) adsorption models for CIM-81(Zn), CIM-82(Zn), and CIM-83(Zn).

MOF	**Langmuir**			**Freundlich**		
	Q^{0}[a] ($mg \cdot g^{-1}$)	**B[b] ($L \cdot mg^{-1}$)**	**R^2[c]**	**n[d]**	**K[e] ($mg \cdot g^{-1}$)**	**R^2[c]**
CIM-81(Zn)	347.85	0.0103	0.859	1.12	3.58	0.978
CIM-82(Zn)	56.95	0.0172	0.958	1.24	0.98	0.927
CIM-83(Zn)	173.98	0.0270	0.937	1.52	5.67	0.997

[a] Maximum amount of PPB absorbed per gram of MOF
[b] Constant related to the affinity for the binding sites
[c] Regression coefficient for the adsorption model
[d] Parameter referred to the intensity of the adsorption
[e] Adsorption capacity

4. Computational study

In order to provide a first approach of the possible interactions MOF-PPB, a computational study was carried out. For this study, the following stages were addressed:

1. Prediction of the interacting sites within pores of CIM-81(Zn).
2. Study of the difference in affinity between A pore and B pore towards guest molecules.
3. Evaluation of the binding of PPB into CIM-81(Zn), specifically attending to the two main functional groups: a carbonyl group (-C=O) and a hydroxyl group (-OH) together with a benzene ring, all of them being possible interacting sites.

For the prediction of the interactions between CIM-81(Zn) and the target PPB, the acetone@CIM-81 model was considered. CIM-81(Zn) containing two acetone molecules was taken from the corresponding crystal structure, where the dangling bonds were terminated by methyl groups. A unit model of CIM-81(Zn) is constituted by 452 atoms, and the framework is defined by two different pores. The acetone@CIM-81 model system was used to estimate differences in affinity toward A pore and B pore, as well as differences within the pore between its two different sides (top and bottom, as depicted in Figure IV.27.). Concerning CIM81-PPB, geometry optimizations for different orientations of PPB within the CIM-81(Zn) model were explored.

Geometry optimizations of guest@CIM-81 models were carried out in two different ways, depending on the method employed. In all model systems, it has been assumed that CIM-81(Zn) behaves as a rigid system where atomic positions are not significantly displaced during extraction. Only H atom positions of CIM-81(Zn) were optimized at the corresponding level of theory since atomic positions of lightest atoms are not well described in the crystal structure.

In PM6 optimizations, all H atoms have been optimized together with atoms of solvent or PPB molecules, while keeping frozen the atomic positions of the remaining ones. At the DFT level, in order to make the study affordable, optimizations were carried out in two steps. Firstly, hydrogen atoms of the CIM-81(Zn) model were optimized. Then, molecules of acetone or PPB were incorporated, and finally submitted to further optimization where only the acetone or PPB molecules were optimized together with CIM-81(Zn) hydrogen atoms involved in the binding.

The interaction energies (E_{int}) for the stable complexes found have been computed as the energy difference:

$$E_{int}^{method}=E_{complex}^{method}-\left(E_{CIM\text{-}81(Zn)}^{method}+E_{acetone/PPB}^{method}\right)$$ Equation IV.9.

where $E_{complex}{}^{method}$, $E_{CIM\text{-}81(Zn)}{}^{method}$, and $E_{acetone/PPB}{}^{method}$, were the computed PM6/DFT energies for the complex, the CIM-81(Zn) isolated, and the guest molecule (acetone or PPB) isolated, respectively, at the optimized geometries of the complex. Interaction energies were corrected, $E_{int,corr}{}^{DFT}$, for basis set superposition error (BSSE) by using the counterpoise (CP) method [17]. Therefore, corrected interaction energies were obtained with the following equation:

$$E_{int,corr}^{DFT}=E_{int}^{DFT}-E_{corr,BSSE}^{DFT}$$ Equation IV.10.

DFT optimized geometries were submitted to non-covalent interactions (NCI), analysis with the NCI-PLOT program [18,19]. This analysis permits discerning the location of non-covalent interactions by means of the low reduced density gradient iso-surfaces. These gradient iso-surfaces are coloured based on the sign of the second eigenvalue of the density Hessian (λ_2) times the electron density (ρ(r)), sign(λ_2)ρ(r), where λ_2 can be either positive or negative. Thus, blue regions in Figure IV.27. are negative regions ($\lambda_2 < 0$) that indicate strong attractive non-covalent interactions, while red regions are positive regions ($\lambda_2 > 0$) showing non-bonding, steric clashes. Green regions are regions with λ_2 values close to zero, and reveal van der Waals interactions.

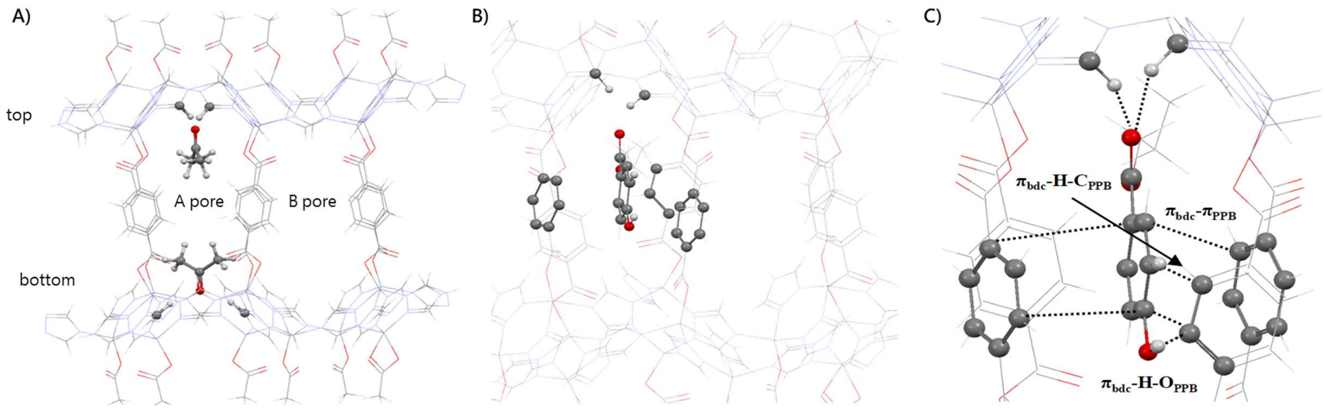

Figure IV.27. Computational modelling of the interactions between CIM-81(Zn) and PPB. **A)** Optimized structure of the reference model systems containing the two different pores in CIM-81(Zn) with two acetone molecules in A pore. **B)** One PPB molecule in A pore with CCOH dihedral angle of 0°.

Figure IV.27.(A) shows the acetone@CIM-81 model system. It can be see that, in A pore, four C-H$_{(tz)}$ groups (two C-H$_{(tz)}$ on the top and two on the bottom side) are available to interact with the C=O group of each acetone. Acetone@CIM-81 PM6 optimized geometry reveals four nearly equivalent short C-H$_{(tz)}$···O=C$_{acetone}$ contacts with H···O distances ranging from 1.98 to 2.02 Å, being shorter than the sum of their Van der Waals radii (2.72 Å), and C-H···O bond angles of 144.1-145.0°. Both bond distances and bond angles obeying the geometrical criteria expected for weak C-H···O hydrogen bonds [20]. In B pore, on the top side, there are four C-H$_{(tz)}$ pointing toward the cavity but they are partially shielded due to close C=O groups of bdc walls (C-H$_{(tz)}$···O=C$_{bdc}$ distances: 2.5 Å), while no C-H$_{(tz)}$ groups are properly available on the bottom side. When two acetone molecules are optimized within B pore, the acetone molecule on the top side is located at a longer distance (C-H$_{(tz)}$···O=C of 2.25-2.30 Å) than within A pore, with more bend C-H$_{(tz)}$···O bond angles of 129º. The acetone molecule on the bottom side approaches the walls by means of less polarized methylenic C-H···O contacts, suggesting weaker H···O interaction.

As expected, a quite large energy difference between both systems is computed. Thus, the interaction energy between acetone molecules and A pore is near four times higher ($E_{int(CIM\text{-}81\text{-}2\times acetone,A\ pore)}$)^{PM6} = -39.57 kcal·mol^{-1}) than that computed between acetone molecules and B pore ($E_{int(CIM\text{-}81\text{-}2\times acetone,B\ pore)}$)^{PM6} = -10.20 kcal·mol^{-1}).

Within A pore, no significant energy difference was found between the complex placing one acetone molecule on the top of the pore ($E_{int(CIM\text{-}81\text{-}acetone,top)}$)^{PM6} = -20.02 kcal·mol^{-1}) and that with one acetone on the bottom ($E_{int(CIM\text{-}81\text{-}acetone,bottom)}$)^{PM6} = -19.93 kcal·mol^{-1}). Accordingly, no significant differences in C-H$_{(tz)}$···O=C$_{acetone}$ distances are observed, all suggesting both sides of A pore are near equivalent for hydrogen bonding.

Bearing the above outcomes in mind, PPB containing a carbonyl group would preclude a similar behaviour. Yet, PPB also features a hydroxyl group and a benzene ring that could play further roles in binding with CIM-81(Zn) pores. Accordingly, it has modelled different PPB@CIM-81 starting geometries where PPB was placed in such a way as to maximize the number of possible intermolecular interactions: C-H$_{(tz)}$···O=C$_{PPB}$, π_{bdc}··· H-O$_{PPB}$, and π_{bdc}···π_{PPB} and submitted them to optimization.

The conformational analysis with PM6 revealed a stable PPB@CIM-81 conformer featuring the three kind of interactions mentioned above. A comparison with a rotamer with

CCOH dihedral angle of 180° (without further optimization) showed that the $\pi_{bdc}\cdots H\text{-}O_{PPB}$ interaction provided a stabilization of 4.35 kcal·mol^{-1}. When this structure was optimized, the resulting geometry revealed shorter $C\text{-}H_{(tz)}\cdots O{=}C_{PPB}$, less stable by 1.64 kcal·mol^{-1}. Therefore, this result would roughly indicate that $\pi_{bdc}\cdots H\text{-}O_{PPB}$ interaction is favoured over $C\text{-}H_{(tz)}\cdots O{=}C_{PPB}$.

Optimization of PPB@CIM-81 with the dispersion-corrected B97D functional [21] provided a similar geometry to that obtained with PM6 (the value shown in parenthesis). Two dissymmetric $C\text{-}H_{(tz)}\cdots O{=}C_{PPB}$ contacts at distances of 2.115 (1.880) Å and 3.136 (3.255) Å and H···O-C bond angles of 156.0° (159.3°) and 146.6° (141.1°), respectively. $\pi_{bdc}\cdots H\text{-}O_{PPB}$ at a distance ranging 2.64-3.73 (2.54-3.45) Å together with stacking $\pi_{bdc}\cdots\pi_{PPB}$ distances ranging 3.75-4.75 (3.57-4.40) Å suggest dispersion-like interactions would play a major role in PPB@CIM-81 systems. For comparison, B97D optimized geometry of acetone@CIM-81 was computed. It displayed two near symmetric $C\text{-}H_{(tz)}\cdots O{=}C_{acetone}$ at 2.196 and 2.239 Å (bond angle of 149.5° average), being slightly longer than those obtained with PM6.

Mulliken charges point to a net charge transfer of 0.13 atomic units (au) upon PPB@CIM-81 binding, where hydrogen atom involved in the shortest $C\text{-}H_{(tz)}\cdots O{=}C_{PPB}$ interaction loses 0.02 au, as expected upon hydrogen bonding [22] The same analysis on acetone@CIM-81 revealed a smaller net charge transfer (0.09 au), but similar electron density loss (0.02 au) of the H atoms involved in the two $C\text{-}H_{(tz)}\cdots O{=}C_{acetone}$ interactions. Weak attractive hydrogen bonding can be visualized in both acetone@CIM-81 and PPB@CIM-81 NCI plots (Figure IV.28.). In the latter, the presence of $\pi_{bdc}\cdots H\text{-}O_{PPB}$, $\pi_{bdc}\cdots H\text{-}C_{PPB}$ and $\pi_{bdc}\cdots\pi_{PPB}$ interactions are confirmed by green NCI surfaces, indicative of weaker attractive dispersion interaction between the two fragments, and thus contributing to the stabilization of the whole system.

Computed interaction energies at B97D level of both acetone@CIM-81 and PPB@CIM-81 model systems indicate stronger interactions in the former ($E_{int,corr(PPB@CIM\text{-}81,top)}^{B97D}$ = -37.13 kcal·mol^{-1}) than in the latter $E_{int,corr(acetone@CIM\text{-}81,top)}^{B97D}$ = -24.46 kcal·mol^{-1}. Nevertheless, it is worth noting that two acetone molecules can be accommodated within A pore with an estimated interaction energy of about (as computed with PM6, see above) twice the interaction energy with one acetone ($2\times E_{int,corr(acetone@CIM\text{-}81(Zn),top)}^{B97D}$) while no stable conformer has been located with two PPB molecules within A pore. Moreover, even if that conformer existed, interaction energy would not be twice that obtained with one PPB molecule, due to nuclear repulsions.

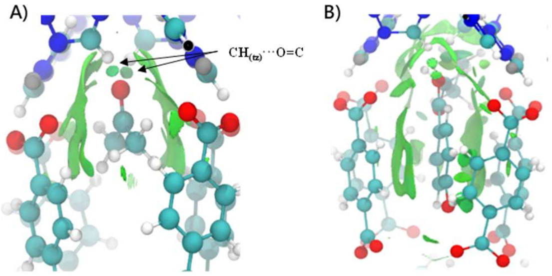

Figure IV.28. Computational modelling of the interactions between CIM-81(Zn) and PPB. **A)** NCI plot of acetone@CIM-81. **B)** NCI plot of PPB@CIM-81. The gradient iso-surface (s = 0.3 au) was plotted with Visual Molecular Dynamics [23] (see text for clarifications with color scale). Main intermolecular distances are also shown.

IV.2.1.3. Application of a pillared-layer Zn-triazolate metal-organic framework in the dispersive miniaturized solid-phase extraction of personal care products from wastewater samples

Molecules 24 (2019) 690:1–7

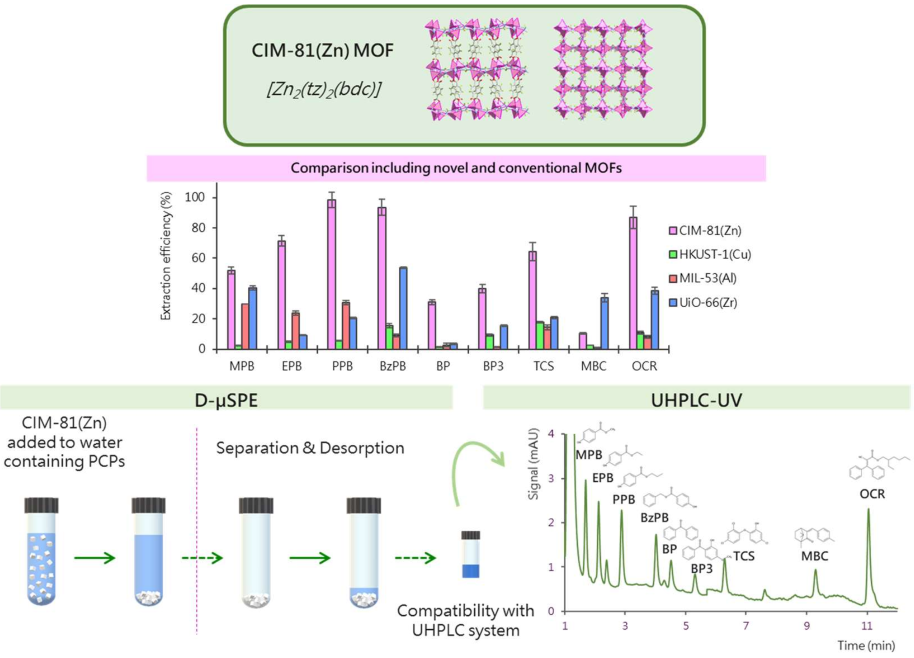

1. Chromatographic performance of PCPs in UHPLC-UV

The optimum chromatographic separation of the 9 PCPs (MPB, EPB, PPB, BzPB, BP, BP3, TCS, MBC, and OCR) was achieved under the conditions described in Section III.6.2., obtaining an adequate resolution of the chromatographic peaks in 11 minutes. The obtained chromatographic retention times for each PCP with the corresponding standard deviation (n = 60) are shown in Table IV.12., together with several quality analytical parameters of the UHPLC-UV method. Calibration curves were obtained by the injection of standard solutions with concentrations from 0.01 to 1.00 μg·mL^{-1} for preservatives, and from 0.10 to 1.00 μg·mL^{-1} for the remaining PCPs. Calibrations exhibited excellent linearity with R^2 higher than 0.993. The LODs and LOQs were estimated as the concentration that provided a chromatographic signal equal to 3 and 10 times the noise, respectively, and were then experimentally confirmed by injection of standards at those levels. LOQs values ranged from 3.3 (for BzPB and BP) to 17 μg·L^{-1} (for BP3 and TCS). Intra- and inter-day precision of the UHPLC-UV method was evaluated in terms of RSD (%), by injecting standard solutions at two levels of concentration: low (0.15 μg·mL^{-1}) and intermediate (0.45 μg·mL^{-1}) in the same day (n = 3), and in three non-consecutive days (n = 9). For the lower concentration level, inter-day RSD values lower than 10% were obtained; being even lower than 6.7% for the higher level of concentration.

2. Preliminary considerations on the use of MOFs in D-μSPE

Different MOFs have been proposed as sorbents in D-μSPE [1], with novel trends aimed at modifying the MOF structure to improve the number and type of interactions with target analytes. Thus, it has been discussed the influence of the functionalization of ligands of MOFs, specifically the incorporation of amino and nitro groups in UiO-66(Zr), with regards to the efficiency of the D-μSPE method for a group of emerging contaminants [24], showing that the UiO-66(Zr)-NO_2 provided better efficiencies than neat UiO-66(Zr). Same authors have also evaluated the microextraction performance of UiO-66(Zr) MOFs functionalized with amine-, nitro-, or mixed groups through the mixed-ligand strategy, to ensure the presence of different functionalization within the same pore environment [25]. The study was carried out for the same

Table IV.12. Several quality analytical parameters of the chromatographic method.

PCP	t_R / RSD[a] (%)	(Slope ± SD[b]) ×10^{-4}	$S_{y/x}$[c] × 10^{-3}	R^2 [d]	LOD[e] (µg·L^{-1})	LOQ[e] (µg·L^{-1})	RSD[f] (%) intra-day / inter-day Conc. level: 0.15 µg·mL^{-1}	RSD[f] (%) intra-day / inter-day Conc. level: 0.45 µg·mL^{-1}
MPB	1.68 / 0.03	390 ± 5	5.2	0.9990	3.0	10	1.6 / 4.8	3.9 / 3.3
EPB	2.10 / 0.03	343 ± 5	5.1	0.9987	4.0	13	1.7 / 7.8	4.9 /3.5
PPB	2.84 / 0.04	306 ± 5	5.0	0.9984	2.0	6.7	1.7 / 2.3	4.3 / 4.2
BzPB	3.98 / 0.05	270 ± 4	3.7	0.9989	1.0	3.3	1.6 / 3.3	4.2 / 4.1
BP	5.27 / 0.04	389 ± 6	5.0	0.9985	1.0	3.3	0.22 / 3.2	3.9 / 3.4
BP3	6.26 / 0.04	258 ± 5	4.4	0.9973	5.0	17	5.9 / 7.1	1.7 / 3.6
TCS	7.65 / 0.06	63 ± 2	1.7	0.9930	5.0	17	3.5 / 8.2	5.6 / 6.7
MBC	9.30 / 0.05	347 ± 7	5.7	0.9942	2.0	6.7	2.8 / 5.9	3.6 / 4.9
OCR	11.07 / 0.05	119 ± 3	2.6	0.9937	3.0	10	7.0 / 10	2.7 / 6.1

[a] Relative standard deviation of the retention times (n = 60)
[b] Standard deviation associated to the slope
[c] Standard deviation of the residuals
[d] Determination coefficient
[e] Limit of detection and limit of quantification calculated according to the ratio signal/noise as 3 and 10 times, respectively
[f] Relative standard deviation for 3 experiments in the same day (intra-day) and for 9 experiments in three non-consecutive days (inter-day)

group of analytes, and the authors reported that different trends are obtained in the extraction efficiency depending of the analyte and the type and degree of functionalization of UiO-66(Zr) MOF. Clearly, the possibility of tuning a MOF to achieve high efficiency in microextraction for a target analysis is quite important.

In any case, all studies of D-µSPE with MOFs show that the limiting step is the desorption using organic solvents, given the strong affinity analytes-MOFs [1,26]. Thus, proper design of MOF should allow adequate affinity analyte-MOF but also adequate ability for further desorption.

In addition, it is well known that the conditions of synthesis of MOFs influence the structure and properties of crystals obtained. There are many variables involved in the solvothermal synthesis, and their modification also drives to tuneability of MOFs. Thus, it is not only possible to tailor the MOF structure, porosity and density by selecting different SBUs combinations, but also controlling the synthetic experimental conditions.

In this sense, the main aim of this study is to tailor a MOF by controlling its synthetic procedure, while ensuring a MOF structure based on pillared layers. Those pillared layers *a priori* can permit easier diffusion of analytes in the MOFs and, in consequence, may facilitate the further desorption step in D-µSPE.

In this study, a MOFs collection have been considered for the evaluation of the D-µSPE microextraction performance of several PCPs belonging to three different groups: preservatives, UV-filters, and disinfectants. A total of 5 pillar-layered MOFs were synthesized and characterized (Section IV.2.1.1.), formed by one central metal, Zn(II), and the combination of two organic linkers based on 1,2,4-triazol and benzene-1,2-dicarboxylic acid, or their amino functionalization of one of them. The use of these MOFs has been previously reported for successful gas storage [5,7,27], but the study included in this Doctoral Thesis reports for first time its analytical utilization.

3. Screening study of pillared MOFs in D-µSPE

The initial screening was the evaluation of five CIM MOFs: CIM-81(Zn), CIM-82(Zn), CIM-83(Zn), CIM–91(Zn), and CIM-92(Zn). The experiments were carried out with the same extraction conditions in all cases, using 10 mL of an aqueous standard containing 0.1 µg·mL^{-1} of PCPs (MPB, EPB, PPB, BzPB, BP, BP3, TCS, MBC, and OCR) at pH 5. The amount de MOF added to the aqueous standard was fixed at 20 mg to ensure the maintaining of an adequate preconcentration. The tube was then subjected to 3 min of vortex agitation during the extraction step, followed by centrifugation for 3 min at 2504 × g. The MOF is then separated of the supernatant and PCPs were desorbed from the MOF using 500 µL of ACN, assisting the desorption by vortex agitation for 3 min. The solvent was taken, evaporated to dryness using a rotavap, and then reconstituted with 100 µL of a mixture ACN:H_2O (ratio 50:50, v/v). The obtained results are shown in Figure IV.29.

For all the PCPs, it can be observed that the amino functionalization of the 1,2,4-triazol ligand for the tetragonal CIM-82(Zn) MOF presented the worst results, even not able to generate any signal after the D-µSPE-UPLHC-UV method for MPB and EPB. On the other hand, the amino functionalization of the 1,2,4-triazol ligand for the orthorhombic CIM-92(Zn) MOF decreases considerably the extraction efficiency for the less polar PCPs (BP3, TCS, MBC, and OCR). For this reason, the CIM-92(Zn) MOF was not considered in the next studies. In all the cases, the amino functionalization of the benzene-1,2-dicarboxylic acid (CIM-83(Zn)) did not improve the obtained results with regards to its analog without any functionalization (CIM-81(Zn)), and therefore this MOF was also rejected.

It can be concluded that, in general, the amino functionalization of these pillar-layered MOFs, does not improve the extraction efficiency in the D-µSPE procedure for this group of analytes.

If comparing the results obtained between CIM-81(Zn) and CIM-91(Zn), the CIM-81(Zn) MOF provided similar or even better results than CIM-91(Zn) for five out of nine PCPs, particularly for the polar PCPs: MPB, EPB, PPB, BzPB, and BP. Furthermore, better precision was observed in the D-µSPE method when using CIM-81(Zn). This can be due to the structural flexibility of the orthorhombic CIM-91(Zn) MOF described in Section IV.2.1.1., which could cause decreases in the reproducibility when applying the D-µSPE method proposed. Considering this screening study, the pillar layered CIM-81(Zn) MOF was selected for the development of a D-µSPE-UHPLC-UV method to monitor 9 PCPs in water samples.

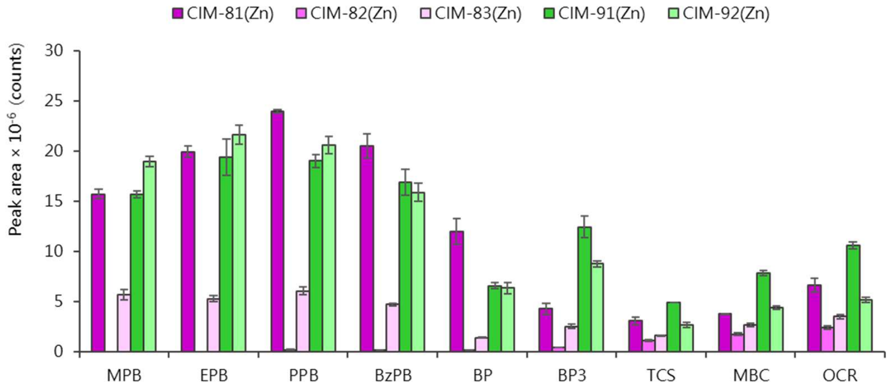

Figure IV.29. Evaluation of the extraction efficiency of PCPs by D-µSPE-UHPLC-UV using the pillar-layered MOF collection, designated as CIM MOFs (CIM-81(Zn) and CIM-91(Zn)) and their functionalized MOFs (CIM-82(Zn), CIM-83(Zn), and CIM-92(Zn)).

Once selected the most efficient pillar layered MOF (CIM-81(Zn)), its analytical performance was compared to that of other well-known "conventional" MOFs: HKUST-1(Cu), MIL-53(Al), and UiO-66(Zr), widely used for their already demonstrated performance in analytical sample microextraction [8,24,28]. The comparison was carried out using the same extraction conditions abovementioned. The obtained results are shown in Figure IV.30. It is remarkable that the CIM–81(Zn) MOF provided the best results, obtaining peak areas higher than the other MOFs for the majority of PCPs studied. The improvement is particularly significant for EPB, PPB, BP, and TCS, thus supporting the interest for this type of MOF structure for analytical microextraction applications.

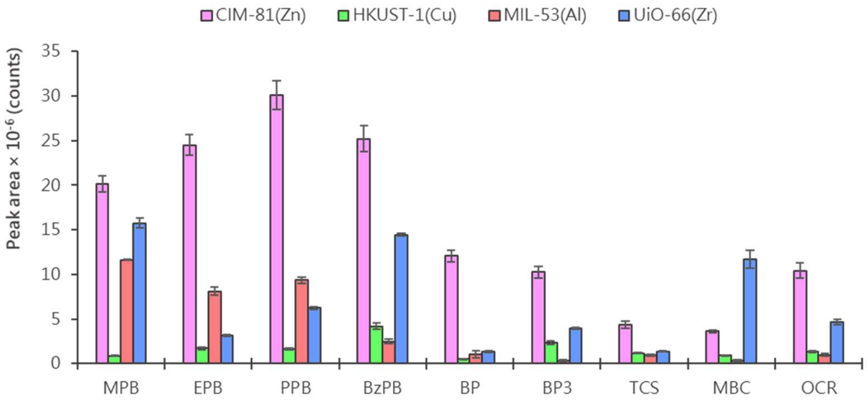

Figure IV.30. Evaluation of the extraction efficiency of PCPs using D-µSPE-UHPLC-UV and different MOFs as sorbents: CIM-81(Zn), HKUST-1(Cu), MIL-53(Al), and UiO-66(Zr).

4. Optimization of the D-µSPE procedure

Once selected the most adequate sorbent (the CIM-81(Zn) MOF), the most relevant variables of the D-µSPE-UHPLC-UV method were considered in the optimization: amount of MOF sorbent, nature and volume of the desorption solvent, vortex time in the extraction step, and vortex time in the desorption step (named extraction time and desorption time, respectively, from here on). Taking into account the importance of the desorption step when using MOFs in µSPE and D-µSPE [29-31], the desorption solvent was studied firstly in the optimization, and once fixed, the remaining variables were evaluated using an experimental design analysis.

4.1. Selection of the desorption solvent

Considering the polarities of the analytes, the organic solvents considered for the desorption step for CIM-81(Zn), already containing trapped PCPs, were: acetonitrile, acetone, trichloromethane, and methanol. Although trichloromethane is a halogenated solvent (not adequate considering GAC), it was considered due to results obtained in Section IV.1.1.1., intending the improvement in the extraction efficiency of MPB. In all cases, the volumes used for the desorption solvent are always low (μL). Figure IV.31. shows the results of this study, performed under the same conditions as those used when comparing MOFs of different nature. It is clear that trichloromethane is not adequate, and it even interferes in the detection of MPB. Acetone and methanol were the solvents able to provide the higher desorption efficiencies. Efficiencies using methanol were adequate for the majority of PCPs, and its handling was simpler with respect to acetone. For this reason, methanol was selected as desorption solvent in the current D-μSPE-UHPLC-UV method.

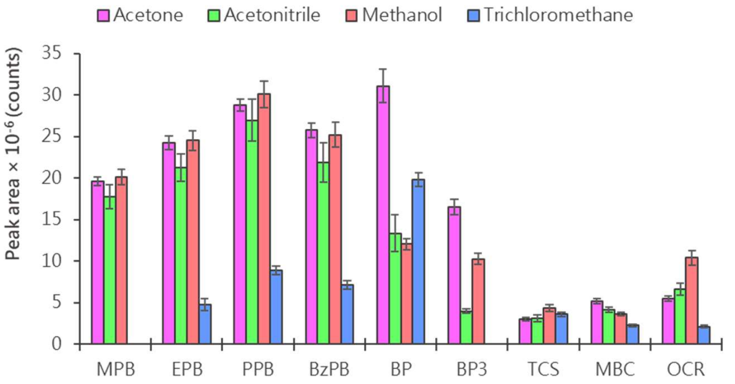

Figure IV.31. Evaluation of several organic solvents as possible desorption solvents for PCPs trapped by the CIM-81(Zn) MOF in D-μSPE-UHPLC-UV. Specific conditions of the experiments described in the text.

4.2. Screening optimization study for the D-μSPE-UHPLC-UV method

Once fixing the MOF nature and desorption solvent nature, remaining parameters in the optimization of the D-μSPE approach: amount of MOF, volume of desorption solvent (volume of methanol), extraction time, and desorption time were subjected to a screening optimization. This screening study included sixteen random experiments (2^n experiments, being n the number of variables). The lowest and the highest values of the variables were the following: 10 and 30 mg of CIM-81(Zn) for the amount of MOF (to ensure greenness by minimizing the amounts required), 200 and 1000 µL of methanol volume (to avoid losses of preconcentration), and 1 and 5 minutes for both extraction and desorption times (to have a fast procedure).

Figure IV.32. shows the obtained results for the effects of the main factors, and the interaction among factors, for representative PCPs (covering examples of the three families: preservatives, UV-filters and disinfectants). The screening study permitted to concluded that, for all PCPs, the extraction time has not influence, while the volume of methanol and the desorption time present a positive influence in the extraction efficiency. On the other hand, the extraction efficiencies are improved significantly when the amount of the sorbent CIM-81(Zn) increased only for MPB, EPB, and PPB. Based on these screening results, the extraction time was fixed to the minimum value (1 minute). Regarding the amount of CIM-81(Zn), given its low influence for the majority of PCPs, it was fixed to 10 mg to ensure greenness and low costs.

4.3. Doehlert design for the D-µSPE-UHPLC-UV method

The most influent variables dictated by the screening analysis (volume of methanol and desorption time), were evaluated with a Doehlert experimental design of two factors. In this design, the experimental points are located in a circle of radius 1, with a spatial distribution located in the vertices of a hexagon [51]. The total number of experiments (*n*) is given by the following equation:

$$n = k^2 + k + 1 \qquad \text{Equation IV.11.}$$

where k is the number of factors. It results also important the adequate assignation of the Doehlert codes according to the relative influence of the variables considered, because codes for factor 1 and factor 2 implied 5 and 3 levels, respectively. Taking into account that the volume of the desorption solvent is related with the amount of CIM-81(Zn), and this value was fixed, the desorption solvent volume requires minor attention than the desorption time. Therefore, the desorption time was selected as factor 1, and the volume of methanol as factor 2. In this case, the ranges studied were between 1 and 7 min for the desorption time, and between 0.2 and 2.0 mL for the volume of methanol. The relationship between coded and real values is given by the following equation:

$$C_i = \frac{(X_i - X_i^0)}{\Delta X_i}\alpha \qquad \text{Equation IV.12.}$$

where C_i is the coded value for the level of factor i, X_i is its real value in an experiment, X^0_i is the real value at the center of the experimental domain, ΔX_i is the step of variation of the real value, and α is the coded value limit for each factor. The code values of a Doehlert design of two factors (implying seven experiments) and the real values of each variable studied are detailed in Table IV.13.

A regression equation was used (equation IV.7.) for the correlation between the response of each experiment and the factors.

$$R = \text{constant} + A[t_{desorption}] + B[mL_{methanol}] + AA[t_{desorption}]^2 + AB[t_{desorptionn}][mL_{methanol}] + BB[mL_{methanol}]^2 \qquad \text{Equation IV.13.}$$

Constants and Doehlert coefficients for each PCP are included in Table IV.13. A response surface methodology (RSM) permitted the selection of the optimum conditions of the variables for each PCP, which are also included in Table IV.14. Figure IV.33. shows the three-dimensional response surfaces obtained (desorption time × volume of methanol × peak areas). For the majority of the target analytes, the optimum value for the desorption time is around 4 min, except for PPB, BzPB, and BP (7 min), and for OCR (1 min). Regarding the volume of the desorption solvent, an adequate desorption of the PCP is reached using 1.2 mL of methanol, except for BP and OCR (2.0 mL). According to these results, 4 min of desorption time and 1.2 mL of methanol were selected as compromise optimum conditions for the group of PCPs studied.

It is also possible to calculate the variation between the response obtained with the particular optimum conditions for each PCP *versus* the compromise conditions selected, using equation IV.13. and the coefficients showed in the Table IV.14. The calculated variation was lower than 30% for all PCPs, except for BP and OCR. These exceptions are linked to the fact that their optimum conditions are quite near to the limits imposed to the variables studied during the optimization. Thus, the optimum conditions obtained in the Doehlert design (4 min of desorption time and 1.2 mL of methanol) are adequate for the target PCPs.

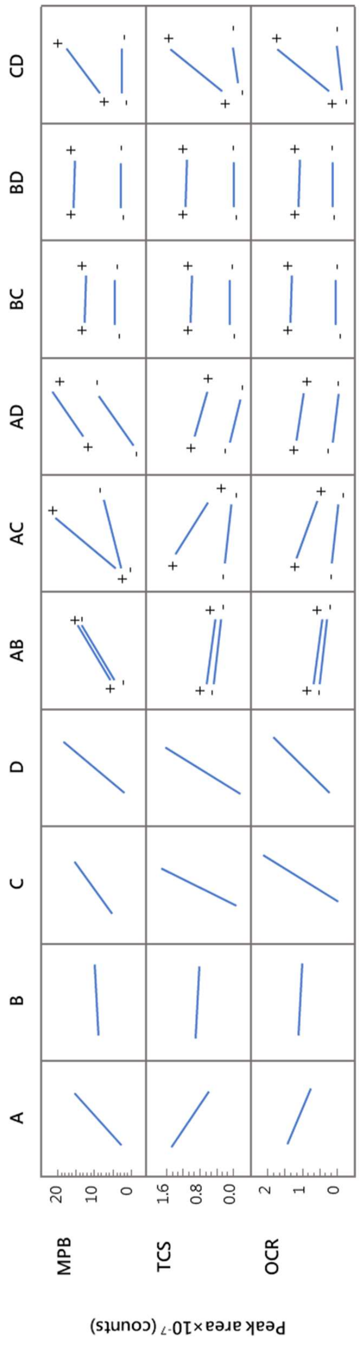

Figure IV.32. Effects of the main factors in the response (as chromatographic peak area) for representative PCPs (MPB, TCS, and OCR), and the interaction among factors obtained in the screening analysis of main variables that influence the D-µSPE-UHPLC-UV; where **A** is the amount of MOF, **B** is the extraction time, **C** is the volume of methanol, and **D** is the desorption time.

Table IV.13. Experiments of the Doehlert design obtained for the coded matrix of two factors with a hexagonal spatial distribution.

Experiment	Factor 1 ($t_{desorption}$)		Factor 2 ($mL_{methanol}$)	
	C_1	X_1 (min)	C_2	X_2 (mL)
1	0	4	0	1.1
2	0.5	5.5	-0.866	0.2
3	-0.5	2.5	0.866	2.0
4	-0.5	2.5	-0.866	0.2
5	0.5	5.5	0.866	2.0
6	-1	1	0	1.1
7	1	7	0	1.1

C_1 and C_2 are the coded values for the 5 and 3 levels, respectively
X_1 and X_2 are the real values of each factor in the experiment

Table IV.14. Results obtained from the analysis of the Doehlert design, where Factor 1 is the desorption time (in minutes) and Factor 2 is the volume of the desorption solvent (methanol, in mL).

PCP	Optimum value of Factor 1	Optimum value of Factor 2	Constant	Coefficients				
				A	B	AA	AB	BB
MPB	3.7	1.257	15298	32786	238	-3989	-2.81	-0.09
EPB	3.6	1.294	37150	18089	196	-1546	-5.35	-0.07
PPB	7.0	0.770	105717	1631	203	2641	-18.33	-0.05
BzPB	7.0	0.882	18644	39917	316	-1166	-24.50	-0.08
BP	7.0	2.000	53538	1282	-2	-836	6.18	-0.01
BP3	4.0	1.322	-8710	27698	208	-3013	-2.67	-0.07
TCS	4.2	1.174	-125176	114136	341	-13583	-0.25	-0.14
MBC	4.4	1.438	-24881	13616	299	-9099	46.76	-0.18
OCR	1.0	2.000	793672	-330717	-509	51200	-57.72	0.39

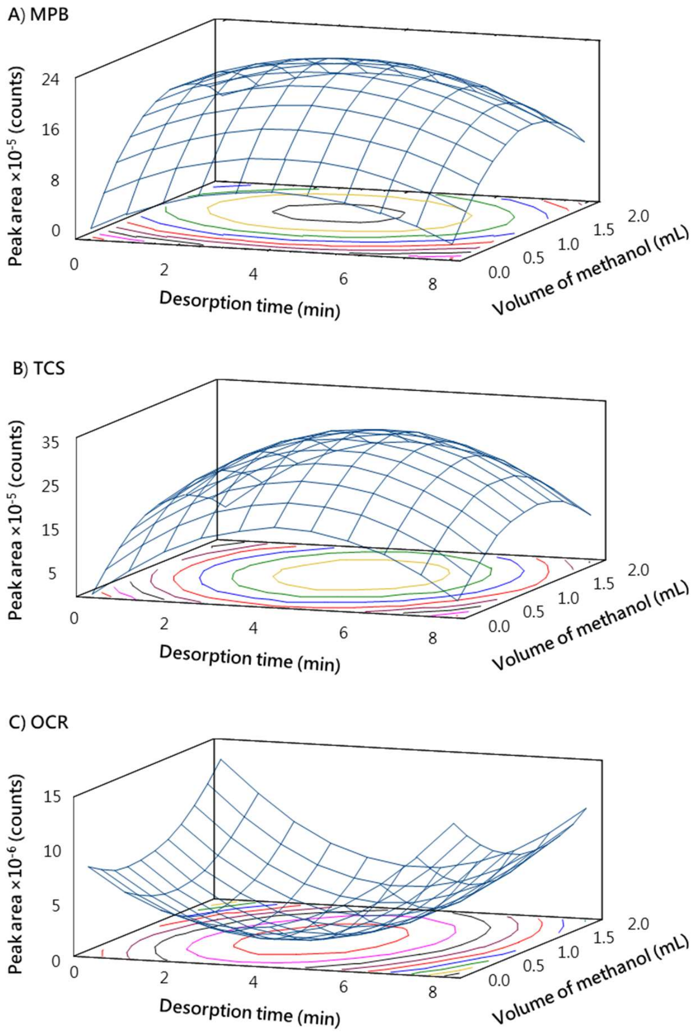

Figure IV.33. Surface responses obtained for representative PCPs: **A**) MPB, **B**) TCS, and **C**) OCR, obtained through the statistical study of the Doehlert experimental design.

5. Analytical performance of the optimized D-μSPE-UHPLC-UV method

The analytical performance of the D-μSPE-UHPLC-UV method was evaluated. The optimum conditions of the microextraction procedure are summarized in Figure IV.34. The extraction efficiency and the intermediate precision was determinate at two concentration levels, low and intermediate values considering the working range of the calibration curve. The obtained results are summarized in Table IV.15.

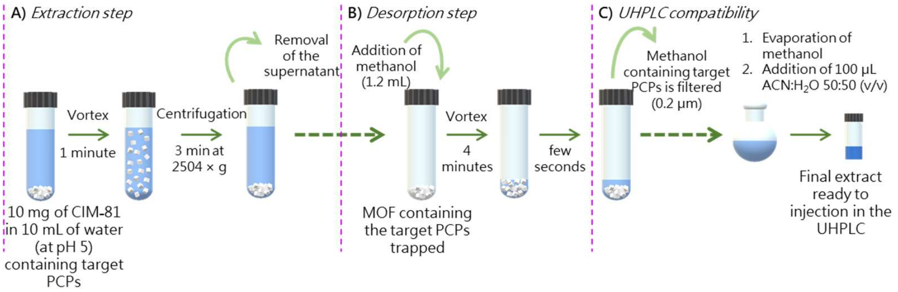

Figure IV.34. Optimum conditions of the miniaturized dispersive solid-phase extraction procedure for the monitoring of PCPs in water samples.

The working range of the calibration curves, performed for the entire method, was from 5 to 100 μg·L^{-1}, with a coefficient of determination (R^2) higher than 0.995 for the 7 calibration levels used. The sensitivity of the method, expressed as the slope of the calibration curve, ranged from (36 ± 1)×10^{-4} for TCS to (350 ± 1)×10^{-4} for OCR. LODs and LOQs were estimated as the concentration that provided a chromatographic signal equal to 3 and 10 time the noise, respectively, and then experimentally confirmed by preparation of aqueous standards at those levels (and subjected to the entire method). LODs ranged between 0.5 μg·L^{-1} for OCR and 1.5 μg·L^{-1} for BP, and LOQs between 1.7 μg·L^{-1} for OCR and 5.0 μg·L^{-1} for BP.

The intermediate precision of the method was evaluated in terms of RSD (in %) for 3 experiments carried out in the same day (intra-day) and for 9 experiments in three different non-consecutive days (inter-day). For the lowest concentration level tested (15 μg·L^{-1}), intra-day RSD value was lower than 8.7% for BP, while inter-day RSD value was lower than 13% for BP3.

The extraction performance was evaluated in terms of RR and E_F, using aqueous standards at the same concentration levels. Average RR values were 115% and 100% for 15 μg·L^{-1} and 45 μg·L^{-1}, respectively. E_F values ranged from 3.6 for MBC to 34 for OCR at 15 μg·L^{-1}, and from 2.6 for BP to 29 for OCR at 45 μg·L^{-1}.

6. Reuse of the CIM-81(Zn) MOF in the D-μSPE-UHPLC-UV method

A study of the reuse of CIM-81(Zn) as sorbent was carried out within a green analytical chemistry perspective. Thus, the MOF used in previous extraction experiments was cleaned thoroughly, and its analytical performance was evaluated in terms of recovery and precision. To accomplish it, the CIM-81(Zn) MOF was washed three times with 1 mL of methanol (desorption solvent), and later subjected to the procedure described in Section III.6.1. to remove the guest molecules. Then, the MOF was used as sorbent in the optimized D-μSPE-UHPLC-UV method. The reuse study, evaluated by the precision and the extraction performance of the entire method, was carried out using two aqueous standards: 15 and 45 μg·L^{-1}. The obtained results for three extraction experiments, reusing the same MOFs, are summarized in Table IV.16.

For both concentration levels, intra-day RSD (n = 3) values ranged between ~4% and ~15%, confirming the good precision of the method, this time reusing the CIM-81(Zn) a second time. Regarding the relative recovery values, RR values ranged from 82.9% for OCR to 129% for TCS at the lower concentration level, and from 74.9% for EPB to 102% for MPB at the intermediate concentration level. An ANOVA was performed to determine whether there were significant differences in the average RR values obtained in the validated method and in the reuse study. The ANOVA study indicated that there were no such significant differences among the results obtained (α = 0.05). Furthermore, the obtained E_F values are practically the same for all PCPs as they were before (see Table IV.15. for a better comparison of the results).

Table IV.15. Several quality analytical parameters of the optimized D-µSPE-UHPLC-UV method.

PCP	(Slope ± SD[a]) × 10^{-4}	$S_{y/x}$[c] × 10^{-3}	R^2 [d]	LOD / LOQ[e] (µg·L^{-1})	E_F' [f]	Concentration level: 15 µg·L^{-1}			Concentration level: 45 µg·L^{-1}		
						RSD[g] (%) intra-day / inter-day	RR[h] (%)	E_F	RSD[g] (%) intra-day / inter-day	RR[h] (%)	E_F
MPB	207 ± 6	5.1	0.9964	0.7 / 2.3	5.3	5.1 / 7.2	122	9.1	2.3 / 7.1	108	6.6
EPB	233 ± 5	5.0	0.9973	1.0 / 3.3	6.8	5.0 / 6.5	125	7.2	2.6 / 5.1	111	7.1
PPB	247 ± 7	6.2	0.9963	0.8 / 2.7	8.1	5.5 / 9.4	108	8.1	5.6 / 8.5	97.7	7.7
BzPB	180 ± 4	3.7	0.9976	0.9 / 3.0	6.7	6.6 / 8.3	121	7.4	3.7 / 7.0	115	7.5
BP	121 ± 4	3.3	0.9957	1.5 / 5.0	3.1	8.7 / 10	112	3.6	4.4 / 9.4	80.9	2.6
BP3	139 ± 4	3.6	0.9961	1.2 / 4.0	5.4	6.2 / 13	118	6.6	6.7 / 9.4	97.8	5.3
TCS	36 ± 1	0.80	0.9971	1.0 / 3.3	5.7	7.2 / 11	94.1	12	4.1 / 8.4	92.8	7.2
MBC	116 ± 3	3.2	0.9956	1.4 / 4.7	3.3	4.6 / 6.6	120	3.6	2.6 / 8.2	99.5	3.2
OCR	350 ± 4	4.0	0.9992	0.5 / 1.7	29	6.6 / 12	112	34	8.0 / 6.0	96.2	29

[a] Standard deviation associated to the slope

[b] Standard deviation of the residuals

[c] Determination coefficient

[d] Limit of detection and limit of quantification calculated according to the ratio signal/noise as 3 and 10 times, respectively

[e] Enrichment factor calculated as ratio of the calibration slope of the chromatographic method and the calibration slope of the overall method

[f] Relative standard deviation: intra-day (n = 3) and inter-day (n = 9 in three different non-consecutive days)

[g] Relative recovery

The structure and crystallinity of the extractant material was assessed after each cycle by means of a PXRD pattern (see Figure IV.35.). After the first extraction cycle, some roughening of the diffraction peaks is observed, but the crystal structure is kept. However, after the second extraction cycle there is a pronounced roughening of the diffraction peaks, but the main ones corresponding to the original structure are still present, indicating some degradation of the framework that possibly compromise the pore structure of the CIM-81(Zn) material. Therefore, the CIM-81(Zn) MOF can be used satisfactorily two times. A third reuse is not possible due to heavy alterations of the CIM-81(Zn) pore structure.

Table IV.16. Precision and recovery studies for the reuse of the CIM-81(Zn) MOF (n = 3) as sorbent in the D-µSPE-UHPLC-UV method proposed.

PCP	Concentration level: 15 µg·L^{-1}			Concentration level: 45 µg·L^{-1}		
	RSD (%)	RR (%)	E_F	RSD (%)	RR (%)	E_F
MPB	8.4	110	8.5	8.2	102	6.3
EPB	12	115	6.5	13	74.9	4.6
PPB	14	115	8.7	11	75.5	5.9
BzPB	14	113	6.8	6.4	86.7	5.5
BP	15	106	3.5	4.3	92.6	2.9
BP3	4.8	91.5	5.1	4.9	75.6	4.1
TCS	6.1	129	14	9.3	86.0	6.9
MBC	11	94.7	2.7	7.6	81.9	2.6
OCR	14	82.9	26	9.2	91.4	27

[a] Relative standard deviation
[b] Relative recovery
[c] Enrichment factor

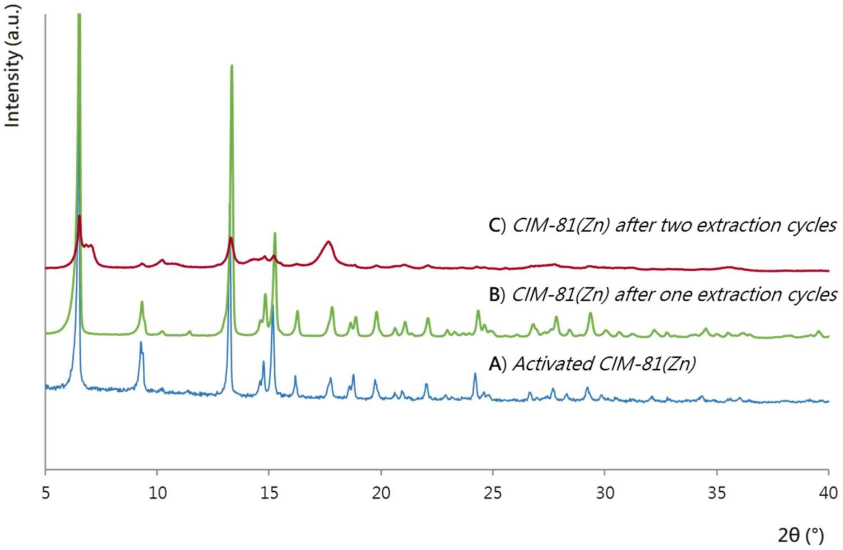

Figure IV.35. XRD patterns of **A**) activated CIM-81(Zn), **B**) CIM-81(Zn) after one extraction cycle, and **C**) CIM-81(Zn) after two extraction cycles.

7. Analysis of samples

A total of three wastewater samples were analyzed, named Sample 1, Sample 2, and Sample 3, using the optimized and validated D-µSPE-UHPLC-UV method. As it is summarized in Table IV.17., four out of the nine PCPs studied (MPB, EPB, TCS, and MBC) were quantified in Sample 1, while 3 of them in Sample 2 (MPB, TCS, and OCR). MPB and TCS were quantified both in Sample 1 and Sample 2 at concentrations of 7.4 ± 0.8 µg·L^{-1} for MPB and 15 ± 1 µg·L^{-1} for TCS, and 7.6 ± 0.9 µg·L^{-1} for MPB and 28 ± 2 µg·L^{-1} for TCS, respectively. Their high and intense use explain the presence of these contaminants in these kind of samples. Other PCPs determined were EPB (13.2 ± 0.3 µg·L^{-1}) and MBC (16 ± 1 µg·L^{-1}) in Sample 1, and OCR (0.6 ± 0.1 µg·L^{-1}) in Sample 2. For the remaining samples, PCPs were not detected.

Possible matrix effects were evaluated in Sample 3 (in which no PCPs were detected), by spiking it at two levels (15 and 45 µg·L^{-1}). Figure IV.36. shows a representative chromatogram, obtained in the analysis of Sample 3 (spiked at 45 μg·L^{-1}). Table IV.17. shows the obtained relative recoveries and enrichment factors. Average relative recoveries were 112 and 107%, with enrichment factors ranging from 2.8 to 29 and from 2.6 to 24, at the lower and higher spiked level, respectively. These values clearly agree with those obtained with aqueous standards, thus showing the absence of matrix effects.

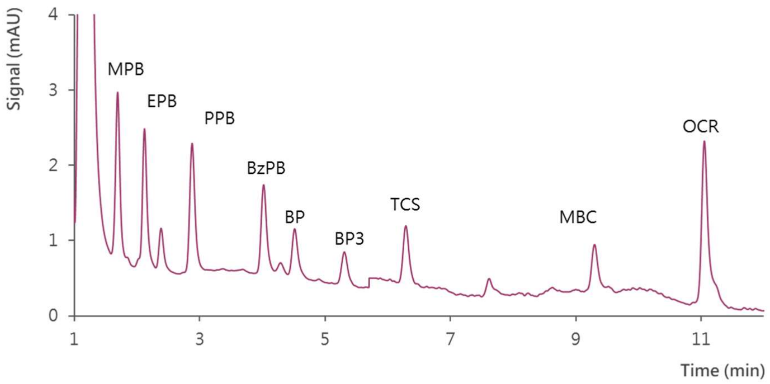

Figure IV.36. Representative chromatogram obtained by subjecting a wastewater sample (spiked at 45 μg·L^{-1}) to the overall optimized D-μSPE-UHPLC-UV method.

Table IV.17. Contents of PCPs ($\mu g\cdot L^{-1}$) found in the analysis of wastewater samples with the entire D-μSPE-UHPLC-UV method proposed for the monitoring of PCPs, and recovery study in these samples at two spiked levels.

PCP	Sample 1	Sample 2	Sample 3*			
			Conc. level: 15 $\mu g\cdot L^{-1}$		Conc. level: 45 $\mu g\cdot L^{-1}$	
			RR^{a} (%)	E_F^{b}	RR^{a} (%)	E_F^{b}
MPB	7.4 ± 0.8	7.6 ± 0.9	101	8.0	113	6.9
EPB	13.2 ± 0.3	n.d.	122	7.0	119	7.6
PPB	n.d.	n.d.	120	9.1	112	8.9
BzPB	n.d.	n.d.	109	6.6	120	7.8
BP	n.d.	n.d.	128	4.2	90.1	2.9
BP3	n.d.	n.d.	112	6.2	122	6.6
TCS	15 ± 1	28 ± 2	127	14	121	8.7
MBC	16 ± 1	n.d.	97.2	2.8	82.9	2.6
OCR	n.d.	0.6 ± 0.1	95.8	29	82.2	24

n.d. non-detected

* PCPs were not detected in Sample 3

[a] Relative recovery

[b] Enrichment factor

IV.2.1.4. Dispersive miniaturized solid-phase extraction using the CIM-81(Zn) metal-organic framework and gas chromatography–mass spectrometry to determine personal care products in waters

LCGC North America 37(4) (2019) 8–15

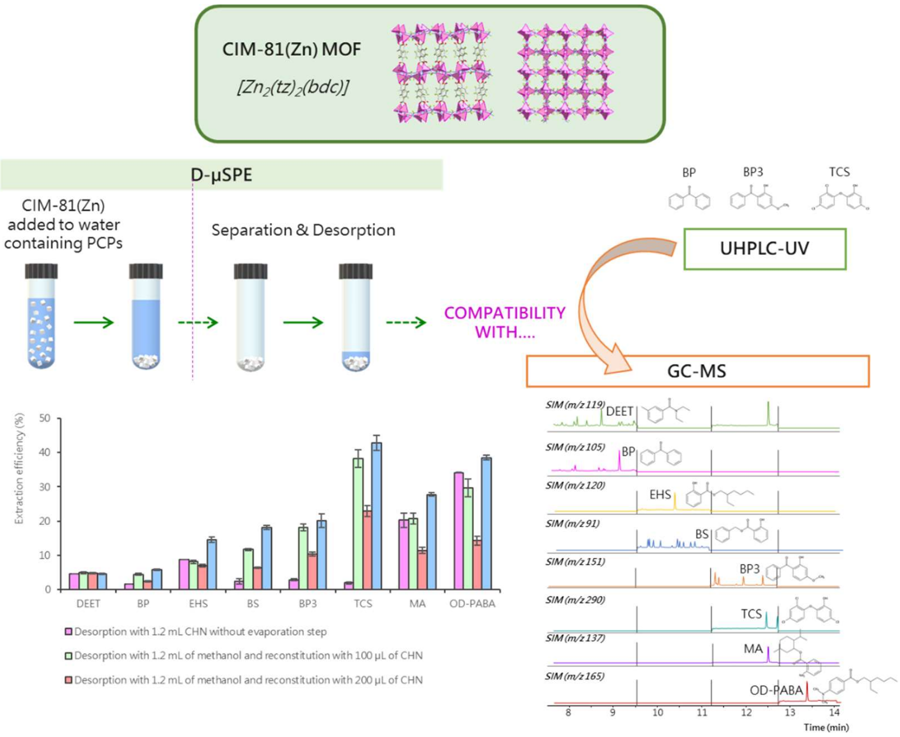

1. Chromatography performance of the PCPs in GC-MS

The optimum chromatographic separation of the selected eight PCPs (DEET, BP, EHS, BS, BP3, TCS, MA, and OD-PABA) took less than 14 minutes; under the conditions described in Section III.6.2. The MS ions used for the monitoring of PCPs and several quality analytical parameters of the GC-MS method are summarized in Table IV.18. The calibration curves were obtained with seven calibration levels, and the calibration ranged from 5 to 100 μg·L^{-1}. For all PCPs, the RSD (in %) for the retention times was lower than 0.07% (n = 40). For all calibrations, the determination coefficients were higher than 0.995.

LODs and LOQs were calculated as the concentration providing 3 and 10 times, respectively, the standard deviation of the signal generated by a low concentration standard. Thus, the obtained LOQs ranged from 0.4 μg·L^{-1} for MA to 4.6 μg·L^{-1} for TCS, as it can be observed in Table IV.18.

The precision of the GC-MS method was evaluated at two levels of concentration: low (15 μg·L^{-1}) and intermediate (45 μg·L^{-1}), and in intra-day (n = 4) and inter-day studies (in three different non-consecutive days, n = 12). For the lower concentration level, intra-day RSD values ranged between 2.6 and 9.7% for BS and BP3 respectively, while inter-day values lower than 15% were obtained in all cases. For the intermediate concentration level, values lower than 4.8 and 9.4% were obtained for the intra-day and the inter-day precision, respectively. Figure IV.37. shows a representative chromatogram obtained by GC-MS of a standard at a concentration of 10 μg·L^{-1}.

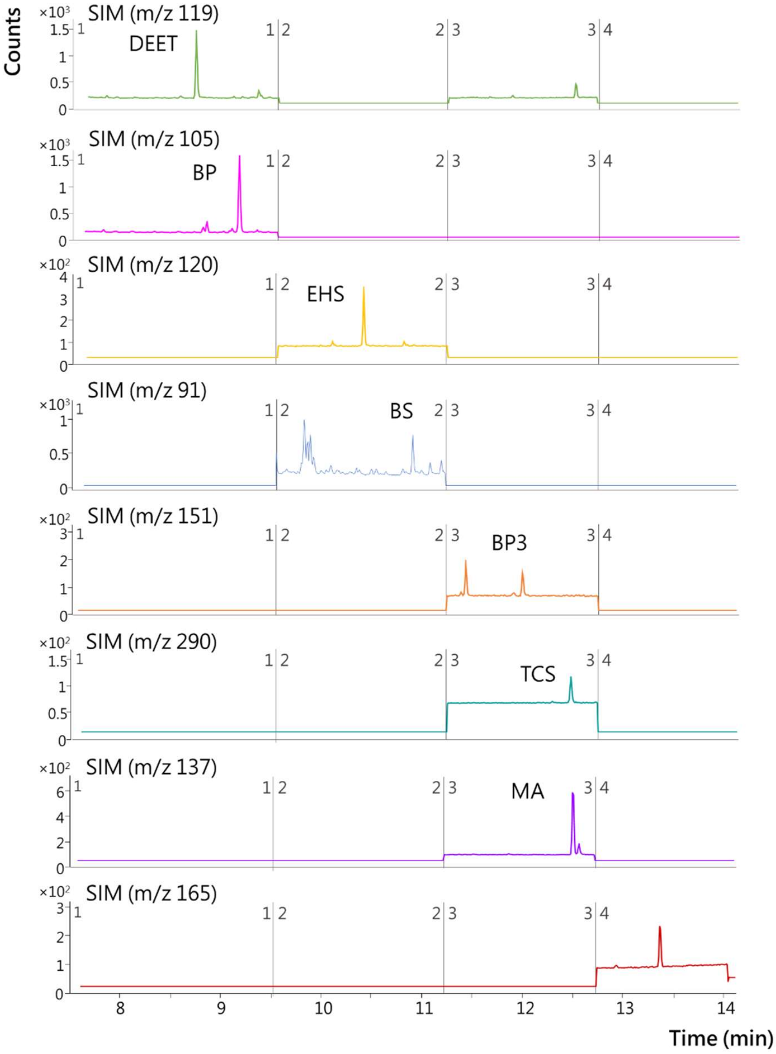

Figure IV.37. Representative chromatogram of a standard solutions of PCPs at a concentration of 10 μg·L^{-1}.

Table IV.18. Several quality analytical parameters of the GC-MS method.

PCP	Monitoring ions[a] (m/z)	t_R / RSD (n = 40)	Slope ± SD[b]	$S_{y/x}$[c]	R^2[d]	LOD[e] (μg·L^{-1})	LOQ[e] (μg·L^{-1})	RSD[f] (%) intra-day / inter-day Conc. level: 15 μg·L^{-1}	RSD[f] (%) intra-day / inter-day Conc. level: 45 μg·L^{-1}
DEET	**119**, 91, 190	8.688 / 0.006	142 ± 3	273	0.998	0.4	0.8	3.3 / 7.3	2.1 / 9.4
BP	**105**, 182, 77	9.130 / 0.002	174 ± 4	1	0.997	0.3	1.4	8.5 / 15	2.0 / 4.8
EHS	**120**, 138, 121	10.381 / 0.001	35 ± 1	57	0.998	0.1	1.1	3.3 / 14	2.7 / 4.6
BS	**91**, 65, 39	10.888 / 0.005	64 ± 2	145	0.997	0.2	1.4	2.6 / 13	4.0 / 7.6
BP3	**151**, 227, 228	11.969 / 0.005	12 ± 1	23	0.998	1.0	3.8	9.7 / 11	4.8 / 8.7
TCS	**290**, 288, 218	12.451 / 0.007	3 ± 1	7	0.997	0.2	4.6	3.6 / 7.3	3.3 / 7.9
MA	**137**, 119, 275	12.498 / 0.002	85 ± 2	232	0.995	0.3	0.4	2.7 / 8.3	4.7 / 5.1
OD-PABA	**165**, 148, 164	13.160 / 0.009	26 ± 1	58	0.997	1.0	2.0	7.7 / 13	4.5 / 9.3

[a] The quantifying ion has been highlighted in bold

[b] Standard deviation associated to the slope

[c] Standard deviation of the residuals

[d] Determination coefficient

[e] Limit of detection and limit of quantification calculated as the concentration providing 3 and 10 times, respectively, the standard deviation of the signal generated by a low concentration standard

[f] Relative standard deviation for 4 experiments in the same day (intra-day) and for 12 experiments in three non-consecutive days (inter-day)

2. Optimization of the D-μSPE procedure in combination with GC-MS

The CIM-81(Zn) MOF has been employed successfully as sorbent in a D-μSPE method for a group of PCPs (with only 3 PCPs in common with the current study), combined with UHPLC-UV (Section IV.2.1.3.) [32]. In fact, the majority of publications for MOFs in D-μSPE are in combination with LC [1,33,34]. Clearly, the adaptation of methods using MOFs in D-μSPE with GC would allow covering the monitoring of semi-volatile PCPs. In this particularly case, CIM-81(Zn) in D-μSPE, the group of PCPs was extended to incorporate DEET, EHS, BS, MA, and OD-PABA, which were not previously studied [32].

With the purpose of simplifying the adaptation of LC methods with MOFs to GC methods, main variables of the microextraction procedure were kept constant. Solvent compatibility is certainly crucial for ensuring proper adaptation of the D-μSPE method to GC-MS. In this sense, the first study evaluated the effects caused by changing the desorption solvent of the D-μSPE method (methanol) by a compatible solvent with the GC column used (i.e. CHN). The experiments required the addition of 10 mg of the CIM-81(Zn) MOF to 10 mL of the aqueous standard containing PCPs at 5 $\mu g \cdot L^{-1}$ (and at pH 5 adjusted with an acetic/acetate buffer solution). After vortex agitation (1 minute) and centrifugation (2504 × g for 3 minutes) of the tube, the aqueous supernatant was removed, and 1.2 mL of desorption solvent (CHN) is added to perform the desorption step of the PCPs. Desorption was facilitated by the application of vortex agitation for 4 minutes. Then, CHN, as desorption solvent, was filtered (0.2 μm), and injected directly in the GC equipment. Experiments were performed in triplicate.

It was observed that the E_R (%) obtained for PCPs were not higher than 7%, except for MA (E_R ~ 20%) and OD-PABA (E_R ~ 33%) (see Figure IV.38.). The selection of CHN as desorption solvent, while adequate for the GC column, was not beneficial in the desorption of PCPs already trapped by the CIM-81(Zn) after D-μSPE. Considering these results, methanol was kept as desorption solvent in D-μSPE with CIM-81(Zn), and therefore a solvent-exchange step was considered. The experiments were carried out using 1.2 mL of methanol as desorption solvent, but followed by an additional step of evaporation and reconstitution. Thus, the methanol was filtered (0.2 μm), and evaporated under vacuum, which required approximately 8 minutes for the evaporation of the solvent until dryness. For a better approach, two volumes of reconstitution solvents were considered: 100 and 200 μL of CHN. The minimum volume required to ensure proper mixing of PCPs in CHN within the round bottom flask of the rotary evaporator is 100 μL; while 200 μL were selected with the objective to test if higher volumes of CHN were required in the reconstitution. This increase in volume would help in ensuring proper solvation of PCPs in the rotary evaporator glass ball, although this is accompanied by losses in the enrichment factor. Giving the results obtained, shown in Figure IV.38., the E_R values obtained for most PCPs improved significantly when methanol is used as desorption solvent, and the reconstitution is carried out with 100 µL of CHN. The E_R values reach up to 40%, supporting the validity of this simple approach. By contrast, it is verified that the increase of the volume of CHN as reconstitution solvent do not benefit the improvement of the E_R values. It must be considered that E_R values close to 100% are hardly obtained in microextraction methods [35], and are acceptable as long as the sensitivity and precision fulfill the requirements pursued.

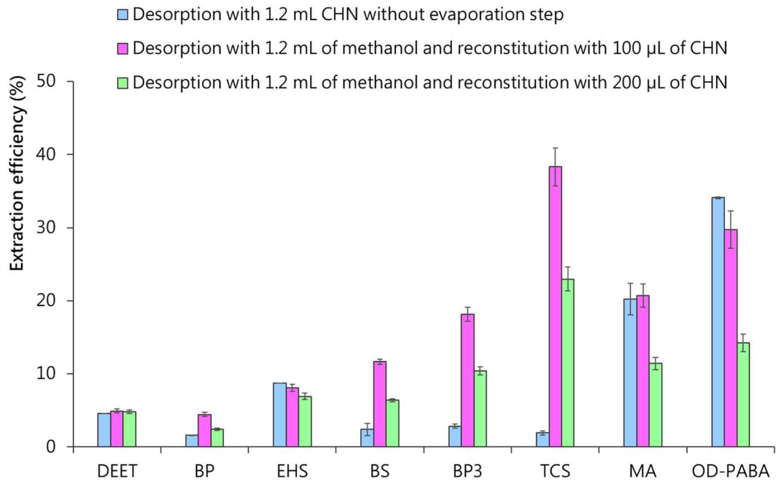

Figure IV.38. Evaluation of the influence of CHN as desorption solvent (blue bars), and different volumes of the CHN as reconstitution solvent after the use of methanol as desorption solvent (100 µL in pink bars and 200 µL in green bars). Experiments were carried out in triplicate.

Ultimately, a slight increase in the polarity of the reconstitution solvent was considered to aid in the solvation of PCPs in CHN. Thus, it was tried a miscible solvent with CHN, compatible with the GC column at the same time, such as ethyl acetate (EA). Specifically, 100 μL of a mixture of CHN:AE (ratio 9:1, v/v), was evaluated as reconstitution solvent. Clearly, the mixture provided better E_R values than those obtained when reconstituting with 100 μL of CHN (see Figure IV.39.), reaching values up to 43%.

In summary, the selected conditions for the D-μSPE-GC-MS method for the group of semi-volatile PCPs were those of the D-μSPE-UHPLC-UV method [36]; but subjecting the methanol desorption solvent (containing trapped PCPs) to: filtration, evaporation, and further reconstitution in 100 μL of a mixture of CHN:AE (ratio 9:1, v/v).

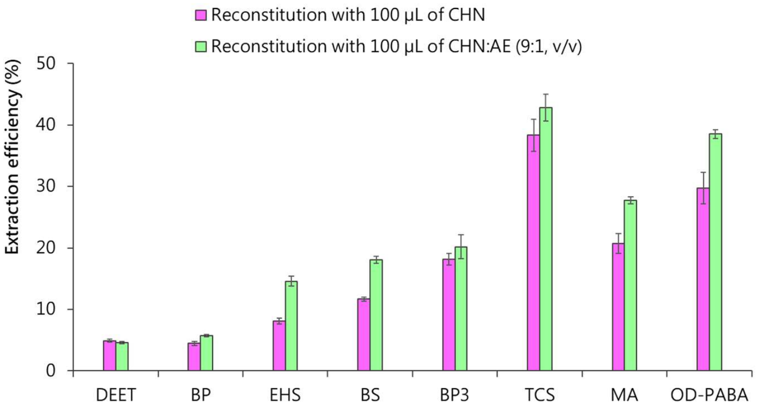

Figure IV.39. Evaluation of the influence of the volume of the reconstitution solvent: 100 μL (pink bars), together with the evaluation of the influence of the solvent polarity in the final reconstitution step (green bars). Experiments were carried out in triplicate.

3. Analytical performance of the optimized D-µSPE-GC-MS method

Under the optimized conditions (Figure IV.40.), the proposed D-µSPE-GC-MS method was validated. Table IV.19. summarizes the quality analytical parameters obtained. The working range of the calibration curve for all PCPs ranged from 0.2 to 15 µg·L^{-1}. Calibration parameters were obtained with six calibration levels, and the precision study was carried out at two calibration levels: low (0.8 µg·L^{-1}) and intermediate (4 µg·L^{-1}), within the calibration range.

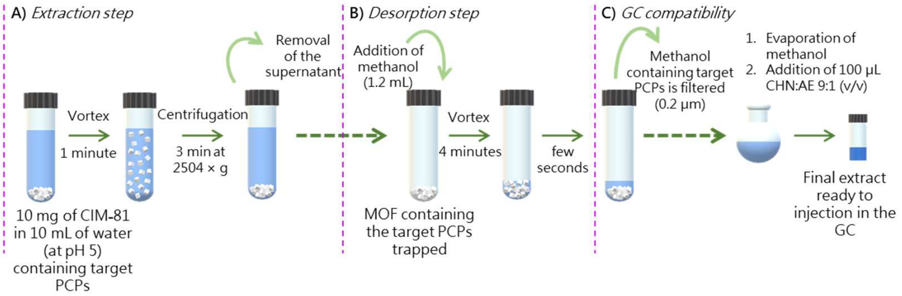

Figure IV.40. Optimum conditions of the miniaturized dispersive solid-phase extraction procedure for the monitoring of 8 PCPs in water samples, using gas chromatography and mass spectrometry detection.

Determination coefficients higher than 0.996 were obtained in all cases. LODs and LOQs were estimated in the same manner as in the gas chromatographic method, as the concentration that provided 3 and 10 times, respectively, the standard deviation of the signal given for the extract of an aqueous standard of low concentration, which was subjected to the entire D-µSPE-GC-MS method. LODs values ranged from 0.01 µg·L^{-1} (MA and OD-PABA) to 0.05 µg·L^{-1} (EHS and TCS), and LOQs values ranged between 0.02 µg·L^{-1} (MA) and 0.50 µg·L^{-1} (EHS and TCS). These values are around 5 and 30 times (depending of the PCP) lower than those obtained with the chromatographic method, and lower than those described in the entire UHPLC-UV method for the PCPs in common (BP, BP3, and TCS) [32].

The E_F of the developed method was calculated using an intermediate aqueous standard subjected to the entire method in triplicate, ranging from 3.1 for DEET to 46 for OD-PABA, as shown in Table IV.19., being the maximum (theoretical) E_F of 100.

The intermediate precision of the method was evaluated in terms of RSD (in %) for experiments carried out in the same day (intra-day, n = 3) and in three different and non-consecutive days (inter-day, n = 9), using two concentration levels. For the low concentration level (0.8 $\mu g \cdot L^{-1}$), intra-day RSD values were lower than 13%, while inter-day RSD values were lower than 11%. The RR were calculated at both concentration levels, ranging between 86.7% for TCS and 116% for EHS at the low concentration level for TCS and OD-PABA.

4. Analysis of samples

The proposed D-µSPE-GC-MS method was applied to the analysis of three samples: one tap water (Sample 1) and two bottled waters (Sample 2 and Sample 3). Table IV.20. summarizes the results obtained. PCPs were not detected in Sample 2 and Sample 3. However, three PCPs were detected in Sample 1. Thus, BP was detected but not quantified, and the quantified PCPs included 5.5 ± 0.9 $\mu g \cdot L^{-1}$ of EHS and 3.3 ± 0.6 $\mu g \cdot L^{-1}$ of TCS.

Furthermore, two of the studied samples were spiked to carry out a recovery study to evaluate possible matrix effects. The results obtained for Sample 2 and Sample 3 using an intermediate concentration level (4 $\mu g \cdot L^{-1}$) are shown in Table IV.20. RR values ranged from 87.1% for DEET to 112% for TCS in Sample 2, and from 80.7% for OD-PABA to 112% in Sample 3, thus pointing out for almost negligible matrix effect. Moreover, the obtained E_F values for the spiked samples are in agreement with those obtained with the aqueous standards (see Table IV.19.), except for OD-PABA. Figure IV.41. shows a representative chromatogram obtained after the analysis of the Sample 2 spiked at 4 $\mu g \cdot L^{-1}$ and subjected to the entire D-µSPE-GC-MS method.

Table IV.19. Several quality analytical parameters of the optimum D-µSPE-GC-MS method.

PCP	Slope ± SD[a]	$S_{y/x}$[b]	R^2[c]	LOD[d] (µg·L^{-1})	LOQ[d] (µg·L^{-1})	E_F[e]	Conc. level: 0.8 µg·L^{-1}		Conc. level: 4 µg·L^{-1}	
							RSD[f] (%) intra-day / inter-day	RR[g] (%)	RSD[f] (%) intra-day / inter-day	RR[g] (%)
DEET	463 ± 8	62.6	0.999	0.03	0.06	3.1	6.6 / 6.1	105	7.7 / 6.9	100
BP	363 ± 2	12.3	0.999	0.03	0.15	5.1	11 / 11	112	7.6 / 7.0	95.8
EHS	62 ± 2	12.3	0.998	0.05	0.50	4.0	13 / 11	116	6.4 / 8.8	96.1
BS	291 ± 8	60.9	0.998	0.04	0.40	8.2	7.7 / 7.4	92.0	5.5 / 7.5	101
BP3	162 ± 1	7.50	0.999	0.04	0.16	26	8.6 / 6.2	94.4	5.6 / 11	96.4
TCS	95 ± 4	27.6	0.996	0.05	0.50	23	5.7 / 7.7	86.7	6.2 / 6.6	102
MA	1992 ± 48	369	0.998	0.01	0.02	21	2.9 / 3.5	96.8	3.7 / 4.2	96.0
OD-PABA	1800 ± 51	351	0.998	0.01	0.03	46	1.7 / 1.7	91.3	6.1 / 4.1	102

[a] Standard deviation associated to the slope

[b] Standard deviation of the residuals

[c] Determination coefficient

[d] Limit of detection and limit of quantification calculated according to 3 and 10 times, respectively, the standard deviation of the signal given for the extract at low concentration level

[e] extraction efficiency

[f] Relative standard deviation for 3 experiments in the same day (intra-day) and for 9 experiments in three non-consecutive days (inter-day)

[g] Relative recovery

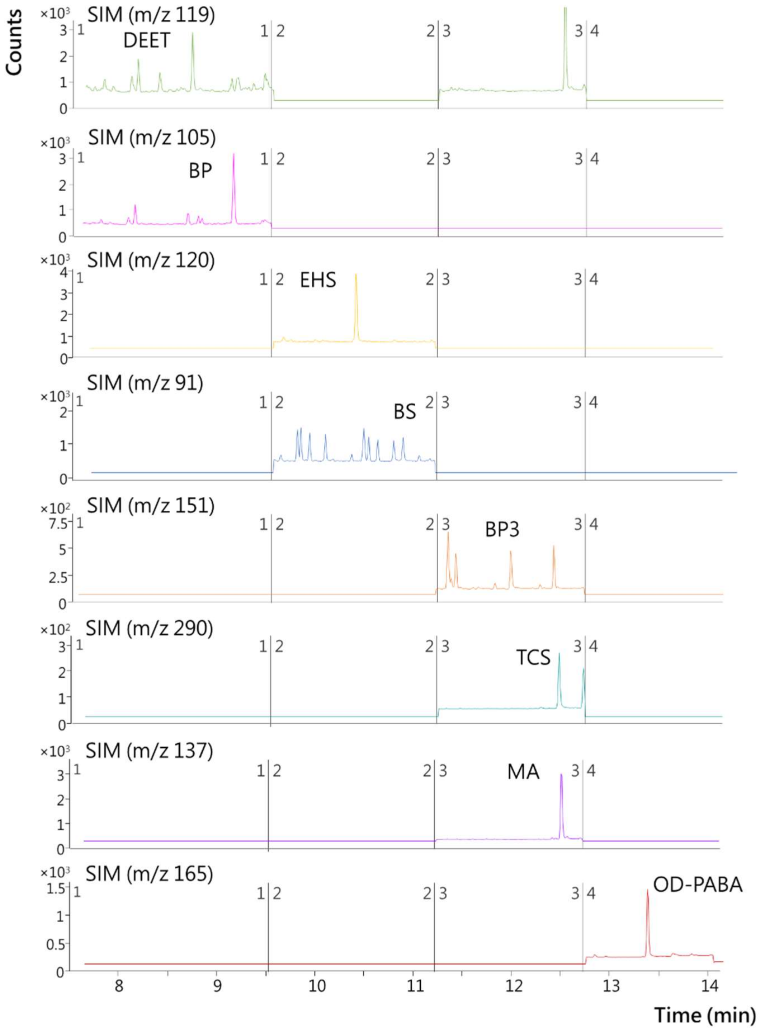

Figure IV.41. Representative chromatogram of the sample 2 spiked with the PCPs at 4 μg·L^{-1} concentration and subjected to the entire D-μSPE-GC-MS method.

Table IV.20. Contents of PCPs (μg·L^{-1}) found after the analysis of samples with the entire D-μSPE-GC-MS method, and their recovery study using an intermediate spiked level (4 μg·L^{-1}).

PCP	**Sample 1**	**Sample 2**			**Sample 3**		
			RR^a (%)	**E_F ^{b}**		**RR^a (%)**	**E_F ^{b}**
DEET	n.d.	n.d.	87.1	3.2	n.d.	89.9	3.2
BP	N.Q.	n.d.	104	4.9	n.d.	103	4.9
EHS	5.5 ± 0.9	n.d.	108	3.7	n.d.	112	3.7
BS	n.d.	n.d.	87.6	8.2	n.d.	109	7.8
BP3	n.d.	n.d.	91.3	26	n.d.	96.4	25
TCS	3.0 ± 0.6	n.d.	112	23	n.d.	109	23
MA	n.d.	n.d.	102	21	n.d.	93.1	21
OD-PABA	n.d.	n.d.	91.8	45	n.d.	80.7	43

n.d. non-detected

N.Q. detected, non-quantified

[a] Relative recovery

[b] Enrichment factor

REFERENCES

[1] P. Rocío-Bautista, P. González-Hernández, V. Pino, J. Pasán, and A.M. Afonso. Trac-Trends Anal. Chem. 90 (2017) 114–134

[2] Q.M. Wang, D. Shen, M. Bülow, M.L. Lau, S. Deng, F.R. Fitch, N.O. Lemcoff, and J. Semanscin. Microporous Mesoporous Mat. 55 (2002) 217–230.

[3] T. Loiseau, C. Serre, C. Huguenard, G. Fink, F. Taulelle, M. Henry, T. Bataille, and G. Férey. Chem. Eur. J. 10 (2004) 1373–1382.

[4] M.J. Katz, Z.J. Brown, Y.J. Colón, P.W. Siu, K.A. Scheidt, R.Q. Snurr, J.T. Hupp, and O.K. Farha. Chem. Commun. 49 (2013) 9449–9451.

[5] Q.-G. Zhai, N. Bai, S. Li, X. Bu, and P. Feng. Inorg. Chem. 54 (2015) 9862–9868.

[6] M.B. Luo, Z.Z. Yuan, W.Y. Xu, F. Luo, J.Q. Li, Y. Zhu, X.F. Feng, and S.J. Liu. Dalton Trans. 42 (2013) 13802–13805.

[7] Z. Yao, Y. Chen, L. Liu, X. Wu, S. Xiong, Z. Zhang, and S. Xiang. ChemPlusChem 81 (2016) 850–856.

[8] P. Rocío-Bautista, C. Martínez-Benito, V. Pino, J. Pasán, J.H. Ayala, C. Ruiz-Pérez, and A.M. Afonso. Talanta 139 (2015) 13–20.

[9] B. Liu, R. Zhao, G. Yang, L. Hou, Y.Y. Wang, and Q.Z. Shi. CrystEngComm 15 (2013) 2057.

[10] I. Akpinar, R.J. Drout, T. Islamoglu, S. Kato, J. Lyu, and O.K. Farha. ACS Appl. Mater. Interfaces 11 (2019) 6097–6103.

[11] C. Chen, D. Chen, S. Xie, H. Quan, X. Luo, and L. Guo. ACS Appl. Mater. Interfaces 9 (2017) 41043–41054.

[12] S. Zhuang, Y. Liu, and J. Wang. Environ. Pollut. 253 (2019) 616–624.

[13] M. Mon, R. Bruno, J. Ferrando-Soria, L. Bartella, L. Di Donna, M. Talia, R. Lappano, M. Maggiolini, D. Armentano, and E. Pardo. Mater. Horizons 5 (2018) 683–690.

[14] PubChem: Solubility of Propylparaben. https://pubchem.ncbi.nlm.nih.gov/compound/7175#section=Solubility (last accessed: 27th January 2020).

[15] M.Á. Bernal, N. Boluda Botella, and D. Prats. Adsorption 25 (2019) 983–999.

[16] M.M. Yusoff, N. Yahaya, N.M. Saleh, and M. Raoov. RSC Adv. 8 (2018) 25617–25635.

[17] S.F. Boys and F. Bernardi. Mol. Phys. 19 (1970) 553–556.

[18] E.R. Johnson, S. Keinan, P. Mori-Sánchez, J. Contreras-García, A.J. Cohen, and W. Yang. J. Am. Chem. Soc. 132 (2010) 6498–6506.

[19] J. Contreras-García, E.R. Johson, S. Keinan, R. Chaudret, J.-P. Piquemal, D.N. Beratan, and W. Yang. J. Chem. Theory Comput. 73 (2011) 625–632.

[20] G.R. Desiraju and T. Steiner (Editors). The Weak Hydrogen Bond in Structural Chemistry and Biology, Oxford University Press (2001).

[21] S. Grimme. J. Comp. Chem. 27 (2006) 1787–1799.

[22] U. Koch and P.L.A. Popelier. J. Phys. Chem. 99 (1995) 9747–9754.

[23] W. Humphrey, A. Dalke, and K. Schulten. J. Molec. Graphics 14 (1996) 33–38.

[24] I. Taima-Mancera, P. Rocío-Bautista, J. Pasán, J.H. Ayala, C. Ruiz-Pérez, A.M. Afonso, A.B. Lago, and V. Pino. Molecules 23 (2018) 2869.

[25] G. González-Rodríguez, I. Taima-Mancera, A.B. Lago, J.H. Ayala, J. Pasán, and V. Pino. Molecules 24 (2019) 3656.

[26] P. Rocío-Bautista, V. Pino, J. Pasán, I. López-Hernández, J.H. Ayala, and C. Ruiz-Pérez. Talanta 179 (2018) 775–783.

[27] X.-L. Hu, Q.-H. Gong, R.-L. Zhong, X.-L. Wang, C. Qin, H. Wang, J. Li, K.-Z. Shao, and Z.-M. Su. Chem. Eur. J. 21 (2015) 7238–7244.

[28] X. Cao, Z. Jiang, S. Wang, S. Hong, H. Li, C. Zhang, Y. Shao, Y. She, F. Jin, M. Jin, and J. Wang. J. Chromatogr. B 1077–1078 (2017) 92–97.

[29] J. González-Sálamo, M.Á. González-Curbelo, J. Hernández-Borges, and M.Á. Rodríguez-Delgado. Talanta 195 (2019) 236–244.

[30] E. Tahmasebi, M.Y. Masoomi, Y. Yamini, and A. Morsali. RSC Adv. 6 (2016) 40211–40218.

[31] M. Safari, Y. Yamini, M.Y. Masoomi, A. Morsali, and A. Mani-Varnosfaderani. Microchim. Acta 184 (2017) 1555–1564.

[32] P. González-Hernández, A.B. Lago, J. Pasán, C. Ruiz-Pérez, J.H. Ayala, A.M. Afonso, and V. Pino. Molecules 24 (2019) 690.

[33] I. Pacheco-Fernández, P. González-Hernández, J. Pasán, J.H. Ayala, and V. Pino. In: M. de la Guardia and F.A. Esteve-Trurrillas (Editors) Handbook of Smart Materials in Analytical Chemistry, Wiley (2018) 463–502.

[34] P. González-Hernández, A. Gutiérrez-Serpa, P. Rocío-Bautista, J. Pasán, J.H. Ayala, and V. Pino. In: V. Mittal (Editor) Metal Organic Frameworks, Central West Publishing (2019) 99–136.

[35] M.J. Trujillo-Rodríguez, P. Rocío-Bautista, V. Pino, and A.M. Afonso. Trac-Trends Anal. Chem. 51 (2013) 87–106.

IV.2.2. A step forward with solid-phase microextraction

The analytical determination of emerging contaminants with a volatile and/or semi-volatile nature requires in general the utilization of GC. Generally, the chromatographic analysis is combined with a previous extraction/preconcentration method to attain an adequate sensitivity. Undoubtedly, the most frequent microextraction technique used with GC is SPME. A variety of its characteristics has been already mentioned in Section I.3.2.2.: fastness, simplicity, low cost, reusability, easily automation, it allows *in-situ* and *in-field* measurements and, mainly, it does not require any organic solvent when combined with GC (being in this sense environmental-friendly).

The majority of SPME-GC applications for emerging contaminants focuses on specific groups of compounds. Therefore, one of the objectives was the development of a SPME-GC method for the analytical determination of three classes of volatiles emerging contaminants belonging to the family of DBPs (THMs, HANs, and HNMs), in environmental waters of different complexity.

The second objective with the use of SPME-GC for emerging contaminants was to set up a method for the analytical determination of methylsiloxanes and musk fragrances (belonging to PCPs), having the last one particular difficulties in their determination (for being widely extended, even in the own components of labware). To sum up, in this case the use of a MOF-based SPME fiber was evaluated, and its performance was compared with that of the most successful commercial SPME fiber.

IV.2.2.1. Monitoring trihalomethanes and nitrogenous disinfection by-products in blending desalinated waters using solid-phase microextraction and gas chromatography

Environmental Technology 38(7) (2017) 911–922

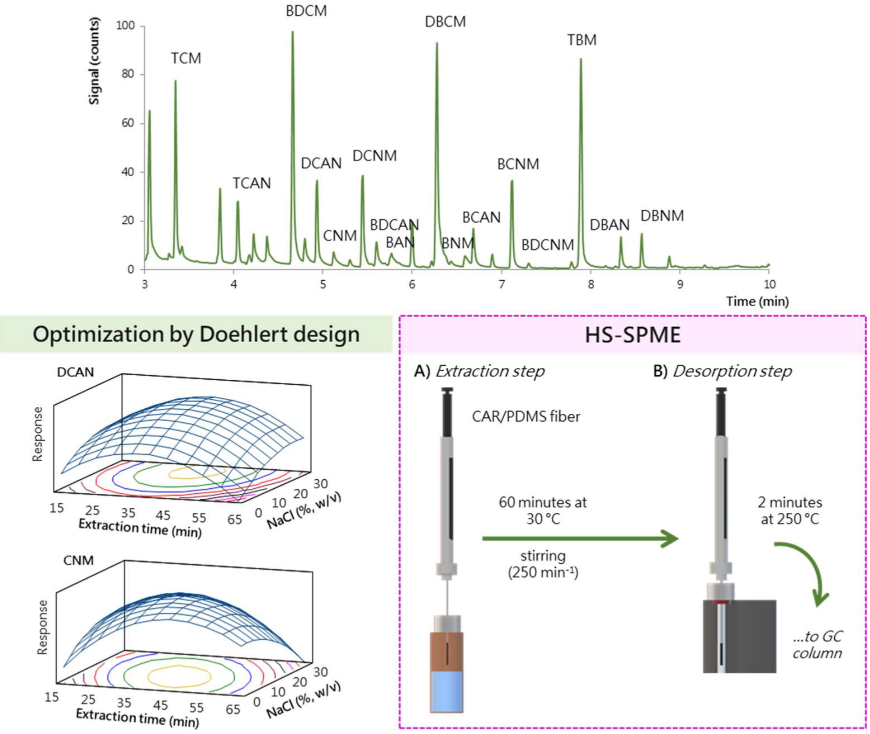

1. Optimization of the HS-SPME-GC-FID method

In this study, 16 DBPs have been selected: 4 THMs (TCM, BDCM, DBCM, and TBM), 6 HANs (DCAN, TCAN, BAN, DBAN, BCAN, and BDCAN), and 6 HNMs (CNM, DCNM, BNM, DBNM, BCNM, and BDCNM). The commercial fiber CAR/PDMS was initially selected to optimize the GC-FID separation. The optimum GC-FID chromatographic conditions are described in Section III.6.2. The complete separation of the analytes was achieved in 9 min. The chromatographic retention times together with their reproducibility values under the optimized chromatographic conditions are shown in Table IV.21. In all cases, for the retention times, RSDs (in %) values lower than 0.22% (n = 32).

Table IV.21. Chromatographic retention times for the group of DBPs studied under the optimum GC-FID conditions.

Analyte	t_R (min)	RSD (%) (n = 32)
TCM	3.34	0.15
TCAN	4.05	0.14
BDCM	4.66	0.10
DCAN	4.92	0.10
CNM	5.12	0.14
DCNM	5.44	0.09
BDCAN	5.60	0.08
BAN	5.77	0.22
DBCM	6.27	0.07
BNM	6.61	0.16
BCAN	6.68	0.07
BCNM	7.11	0.06
BDCNM	7.30	0.05
TBM	7.88	0.05
DBAN	8.34	0.06
DBNM	8.57	0.05

2. Selection of the fiber coating nature

In SPME, the adequate selection of the fiber coating is a key factor to achieve adequate extraction efficiencies and sensitivity. In this study, several fibers were selected according to the polarity of the DBPs: PA, CAR/PDMS, DVB/CAR/PDMS, and PDMS/DVB. Several conditions were initially fixed for the HS-SPME-GC-FID method (and used for the four SPME fibers studied), based on previous screening experiments: 10 mL of ultrapure water containing 1.00 $mg·L^{-1}$ of each DBP under stirring with a stir bar (speed: 250 min^{-1}), 30 min for the extraction time, 30 ºC for the extraction temperature; and 5 min for the desorption time in the GC injector, using a desorption temperature of 250 ºC. In all the experiments, the maximum methanol content in the extraction vials was fixed to 1% (v/v). All SPME fibers were subjected to the maximum temperature than could be used with all of them but also avoiding any possible thermal degradation of DBPs [1,2]. Figure IV.42. shows a comparison of the performance of all SPME fibers selected under these conditions, by plotting the peak areas for each analyte studied. It can be observed that the best results were obtained with the semi-polar fibers CAR/PDMS and DVB/CAR/PDMS for the majority of the DBPs. For THMs, the differences observed between semi-polar and polar fibers were even more pronounced. Given these results, the CAR/PDMS fiber was selected as the optimum for the 16 DBPs considered in this study.

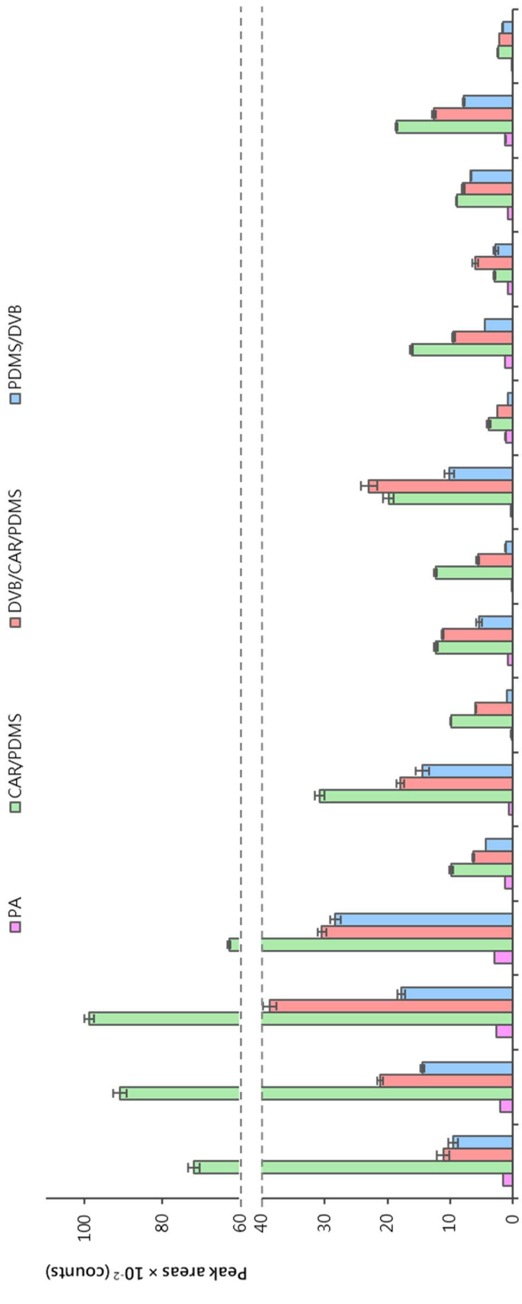

Figure IV.42. Comparison of the analytical performance of the four commercial SPME fibers tested for the DBPs studied. Experiments were performed in triplicate.

3. Optimization of the HS-SPME conditions

Once the nature of the fiber was selected, an optimization of the HS-SPME method (to be combined with GC-FID) was carried out. The main factors considered include: extraction time ($t_{extraction}$), extraction temperature ($T_{extraction}$), desorption time ($t_{desorption}$), and desorption temperature ($T_{desorption}$). An experimental design was selected to minimize the number of experiments and to avoid the existence of data inter-correlated. Firstly, a screening analysis was accomplished to select the most influential variables of the method. Afterwards, those variables were studied in a Doehlert experimental design to choose the optimum conditions.

3.1. Screening analysis for the HS-SPME method

A two-level full factorial design (2^4) was selected in the screening study of the four SPME variables: extraction time, extraction temperature, desorption time and desorption temperature. Factorial designs at two-levels involve relatively few experiments for each variable, and unlike univariate options, they allow the detection and assessment of interactions among variables, particularly when the effects of the variables show non-additivity. The range values given to each factor were: from 15 to 50 min for extraction time, from 30 to 60 ºC for extraction temperature, 2 and 6 min for desorption time, and 150 and 250 ºC for desorption temperature. The experiences were carried out with 10 mL of aqueous standard containing 1.0 $mg \cdot L^{-1}$ of each DBP, using the CAR/PDMS fiber, under stirring with a stir bar (speed: 250 min^{-1}). The ionic strength was not adjusted at this point.

Table IV.22. shows the design matrix of the 16 experiments (which were randomly performed) involving the four variables studied in this screening. Figure IV.43. shows representative results of the effects of the main factors in the response, and the interaction among factors obtained. In general, both the extraction time and desorption temperature had a positive effect in the response, while the extraction temperature had a negative effect. Regarding the interaction among factors, there was a significant interaction between the extraction time and the extraction temperature for most DBPs. Therefore, for further experiments, the desorption time was discarded as significant variable, and thus kept to the minimum value (2 min), whereas the desorption temperature was fixed to the maximum value allowed for the fiber (250 ºC) while avoiding DBPs degradation.

Table IV.22. Design matrix for the screening analysis using a factorial design 2^4.

Experiment	Factor A $t_{extraction}$ (min)	Factor B $T_{extraction}$ (˚C)	Factor C $t_{desorption}$ (min)	Factor D $T_{desorption}$ (˚C)
1	15	30	2	150
2	50	30	2	150
3	15	60	2	150
4	50	60	2	150
5	15	30	6	150
6	50	30	6	150
7	15	60	6	150
8	50	60	6	150
9	15	30	2	250
10	50	30	2	250
11	15	60	2	250
12	50	60	2	250
13	15	30	6	250
14	50	30	6	250
15	15	60	6	250
16	50	60	6	250

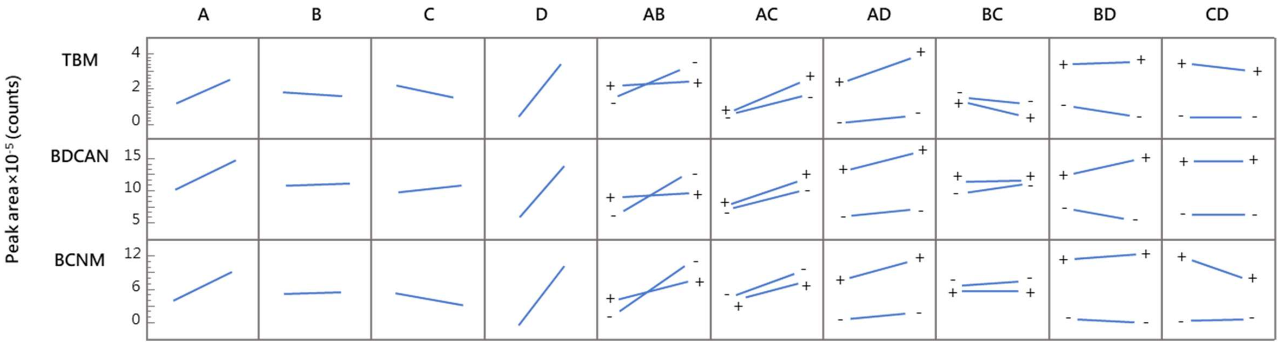

Figure IV.43. Effects of the main factors in the response (as chromatographic peak area for each DBP) and the interaction among factors obtained for the initial screening analysis (**A**: $t_{extraction}$ (min), **B**: $T_{extraction}$ (ºC), **C**: $t_{desorption}$ (min), and **D**: $T_{desorption}$ (ºC); design matrix shown in Table IV.22.). A representative DBP of each group has been selected to show main trends: TBM for THMs, BDCAN for HANs, and BCNM for HNMs.

3.2. Doehlert experimental design for the HS-SPME method

Taking into account the results obtained, and in order to optimize those variables with significant influence, a Doehlert experimental design was carried out. The variables considered in this design were: the extraction time (studied from 30 to 60 min), the extraction temperature (studied from 30 to 50 ºC), and the ionic strength (studied from 0 to 30% (w/v) of NaCl content). Ionic strength was at this point considered because it is well-known that an increase of the ionic strength of the solution generally results in a variation of the gas/liquid equilibrium, which increases the relative volatility of the analytes in the headspace [3].

The Doehlert design for these three variables involved 15 experiments, given by the expression $N = k^2 + k + C_0$, where k is the number of variables and C_0 is the number of center points. Their spatial distribution was located at the 12 vertices of a cuboctahedron, with a center point (performed in triplicate to obtain a better estimation of the pure error) [4]. Table IV.23. shows the coded values and operating levels of the Doehlert design. It is interesting to mention that the Doehlert design has unequal number of experimental levels by factor, and the levels dictated by the design are assigned according to the magnitude of the effect of the variable [5]. In this study, 5, 7 and 3 experimental levels correspond to extraction time (factor 1), ionic strength (factor 2) and extraction temperature (factor 3), respectively.

Based on this experimental design, the following second-order polynomial equation was used to correlate the response and the independent variables:

$$R = \text{constant} + A[t_{\text{extraction}}] + B[\text{NaCl}] + C[T_{\text{extraction}}] + AA[t_{\text{extraction}}]^2 + AB[t_{\text{extraction}}][\text{NaCl}] + AC[t_{\text{extraction}}][T_{\text{extraction}}] + BB[\text{NaCl}]^2 + BC[\text{NaCl}][T_{\text{extraction}}] + CC[T_{\text{extraction}}]^2 \qquad \text{Equation IV.14.}$$

The obtained constants and Doehlert coefficients for each DBP are shown in Table IV.24.

Table IV.23. Matrix of the experiments including the coded values and the operating levels of the Doehlert design utilized for the optimization.

	Factor 1 **$t_{extraction}$ (min)**		**Factor 2** **NaCl (%, w/v)**		**Factor 3** **$T_{extraction}$ (°C)**	
Experiment	***C_1***	**X_1**	***C_2***	**X_2**	***C_3***	**X_3**
1	*0*	37.50	*0*	15	*0*	40
2	*1*	60.00	*0*	15	*0*	40
3	*0.5*	48.75	*0.866*	30	*0*	40
4	*0.5*	48.75	*0.289*	20	*0.817*	50
5	*-1*	15.00	*0*	15	*0*	40
6	*-0.5*	26.50	*-0.866*	0	*0*	40
7	*-0.5*	26.50	*-0.289*	10	*-0.817*	30
8	*0*	37.30	*0*	15	*0*	40
9	*0.5*	48.75	*-0.866*	0	*0*	40
10	*0.5*	48.75	*-0.289*	10	*-0.817*	30
11	*-0.5*	26.25	*0.866*	30	*0*	40
12	*0*	37.50	*0.577*	25	*-0.817*	30
13	*-0.5*	26.25	*0.289*	20	*0.817*	50
14	*0*	37.50	*-0.577*	5	*0.817*	50
15	*0*	37.30	*0*	15	*0*	40

C_1, C_2 and C_3 are the coded value for the levels of the factor 1, 2 and 3, respectively.

The relationship between coded and real values is given by: $C_i = \left[\frac{X_i - X_i^o}{\Delta X_i}\right]\alpha$, where C_i is the coded value for the level of factor i, X_i is its real value in an experiment, X^o_i is the real value at the center of the experimental domain, ΔX_i is the step of variation of the real value, and α is the coded value limit for each factor.

Table IV.24. Constants and Doehlert coefficients values for each DBP, corresponding to Equation IV.14.

Analyte	Constant	A	B	C	AA	AB	AC	BB	BC	CC
TCM	820535	-21716	7455	-11206	170	293	176	-83	-411	72
BDCM	720937	-20482	2967	-4427	212	401	67	-16	-426	44
DBCM	798465	-24140	6679	-4294	263	373	123	-68	-471	52
TBM	-27230	-6419	-6882	20048	133	522	-111	87	-318	-133
DCAN	-39864	2074	1039	3970	-48	7	37	-46	24	-73
TCAN	629541	-14641	-9444	-10813	76	92	214	-13	121	-1
BAN	-109918	4919	7829	2909	-22	-130	-37	-71	-10	-24
DBAN	42045	293	-110	-1673	-24	-36	72	-13	63	-7
BCAN	-66972	-287	-3496	6208	-28	65	57	-54	85	-103
BDCAN	101311	-6976	-1531	2287	107	102	-6	78	-142	5
CNM	-160836	4534	-3759	7162	-76	-65	60	-81	207	-151
DCNM	-114126	4906	-6919	9152	-133	-187	210	-138	415	-299
BNM	61583	1559	-3966	-2212	-28	-73	47	-12	167	-22
DBNM	-48568	4089	-3988	1854	-53	-143	59	-12	232	-95
BCNM	217985	4813	-12537	-6300	-105	-287	201	-23	564	-127
BDCNM	6911	-291	-1556	559	6	28	-10	17	3	-4

A RSM was then employed with the results obtained in the Doehlert, to determine the optimum operating conditions. The three-dimensional surfaces (extraction time × ionic strength as NaCl content) are shown in Figure IV.44. for representative DBPs. The optimum values obtained for the extraction time, the ionic strength, and the extraction temperature for each DBP are shown in Table IV.25. It can be observed than an extraction time of 60 minutes gave adequate extraction efficiencies for all DBPs, except for BAN. As a compromise solution for most DBPs, this time was selected. The remaining variables presented different results depending on the group of DBPs. 30% (w/v) of NaCl was optimum as ionic strength for most DBPs, except for HNMs. For them, extraction efficiencies were higher without salt addition. Regarding the extraction temperature, 30 ºC was optimum for most DBPs, except for HANs. For them, the extraction efficiencies were higher at 50 ºC. Given these results, a compromising situation was taken to select the optimum values of each variable: 60 minutes for the extraction time, 30% (w/v) of NaCl content for the ionic strength, and 30 ºC for the extraction temperature (Table IV.25).

The validity of the compromising conditions selected was evaluated using different approaches. Thus, a study of the relationships attained between the experimental values and the responses obtained for both optimum and compromising conditions was accomplished. Correlation coefficients (R) of 0.960 were obtained between the experimental values under the compromising conditions and the theoretical values (Equation IV.14.) with the optimum conditions; and 0.952 were obtained between the experimental values under the compromising conditions and the theoretical values (Equation IV.14.) with compromising conditions, for all DBPs. Furthermore, the obtained slopes of such correlations had values near the unity in both cases: 1.03 and 1.32, respectively. Likewise, the relationships obtained between the theoretical responses attained using the optimum conditions or when using the compromising conditions were evaluated. A correlation coefficient of 0.946 and a slope of 1.23 were obtained. These values support the acceptability of the optimum conditions selected.

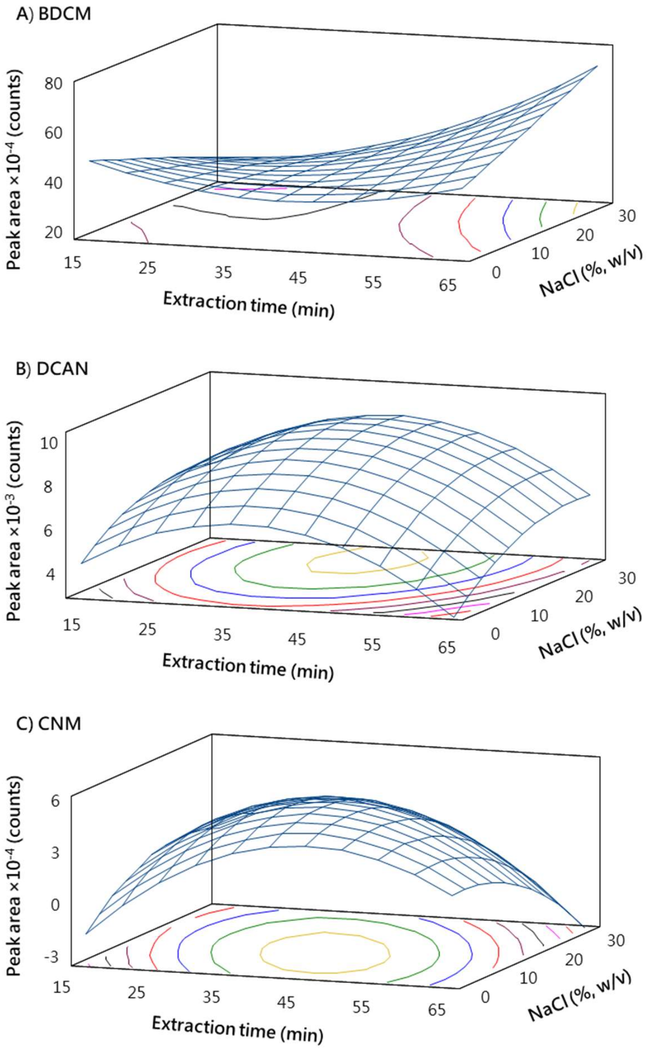

Figure IV.44. Representative results obtained with the statistical study used in the optimization with the Doehlert design for representative analytes, at 30 ºC of extraction temperature: **A)** BDCM for THMs, **B)** DCAN for HANs, and **C)** CNM for HNMs.

Table IV.25. Optimum conditions obtained through the Doehlert design, theoretical response for each DBP when using the optimum conditions in Equation IV.14., and experimental responses obtained when using the compromising conditions for each DBP.

Analyte	$t_{extraction}$ (min)	NaCl (%, w/v)	$T_{extraction}$ (˚C)	Response obtained with Equation IV.14. using optimum conditions	Experimental signal with compromising conditions
TCM	60.0	30.0	34.1	447512	457203
BDCM	60.0	30.0	30.0	696526	629907
DBCM	60.0	30.0	33.6	796270	831554
TBM	60.0	30.0	39.9	816373	548584
DCAN	38.8	24.7	40.9	94425	132420
TCAN	60.0	30.0	50.0	177008	166931
BAN	15.0	30.0	43.1	115210	131398
DBAN	58.5	30.0	50.0	104117	73157
BCAN	60.0	30.0	49.5	129454	87569
BDCAN	60.0	30.0	32.7	202936	229359
CNM	40.7	11.0	39.5	52206	39890
DCNM	42.3	0.0	30.1	127571	52416
BNM	57.6	0.0	30.0	55081	27034
DBNM	54.7	0.0	30.0	83349	23029
BCNM	51.2	0.0	30.0	194501	53678
BDCNM	60.0	30.0	30.3	29021	11999

4. Stability of DBPs in waters: effects of pH and time

Extensive studies have been conducted to investigate the effect of the pH on the formation (or degradation) of DBPs in water. However, the effect of the pH combined with the stability of DBPs with the time has not been studied so much. Thus, it was firstly analyzed 10 mL of an aqueous standard containing 100 µg·L^{-1} of each DBP with the above optimized HS-SPME-GC-FID method. The pH values studied were: 3.5 (adjusted with sulfuric acid 0.1 mol·L^{-1}); 4.5 (corresponding to 30% (w/v) of NaCl already present in the vial); 7.0 (using a buffer solution of 0.2 mol·L^{-1} K_2HPO_4 / 0.08 mol·L^{-1} KH_2PO_4); and 8.0 (using a buffer solution of 0.01 mol·L^{-1} $Na_2B_4O_7$ / 0.02 mol·L^{-1}HCl). The most common pH values in drinking waters are 7.0 and 8.0.

Figure IV.45. shows the variation of the chromatographic peak areas with regard to the pH values studied. The results were grouped according to the family of DBPs. With the exception of DBCM, the influence of the pH was very low for THMs throughout the range studied. The HANs studied presented a similar behavior to THMs, with the exception of TCAN and BDCAN. These two HANs presented opposite behaviors, being the chromatographic peak areas maximum for BDCAN at pH 4.5 and minimum for TCAN at this same pH value. HNMs were undoubtedly the most influenced DBPs with regard to the pH value. All HNMs presented a similar behavior, with higher chromatographic peak areas at pH 4.5. According to these results, it was necessary to find again a compromise solution for all DBPs. Therefore, a pH value of 7 was selected as optimum value.

Once evaluated the stability of DBPs at pH 7, a second studied focused on the stability over time. Thus, 10 mL of an aqueous standard containing 100 µg·L^{-1} of each DBP and adjusted to pH 7 (using 0.12 mol·L^{-1}K_2HPO_4 / 0.08 mol·L^{-1}KH_2PO_4) was analyzed in triplicate using the optimum HS-SPME-GC-FID method, from 0 to 11 hours (results not shown). For a high number of DBPs, the chromatographic peak areas decreased with the time, especially after 6 hours. All THMs had the same behavior, although the decrease of the signal with the time for TCM was lower. With respect to HANs, TCAN and BDCAN presented similar results to THMs, while the signal of the rest studied HANs remained constant over time. Regarding to HNMs, with the exception of DCNM and BCNM whose signals decreased over time, for other HNMs the signal remained substantially constant. According to these results, it is recommended to perform the analysis of the water samples in the shortest possible time, in order to minimize the degradation of most DBPs.

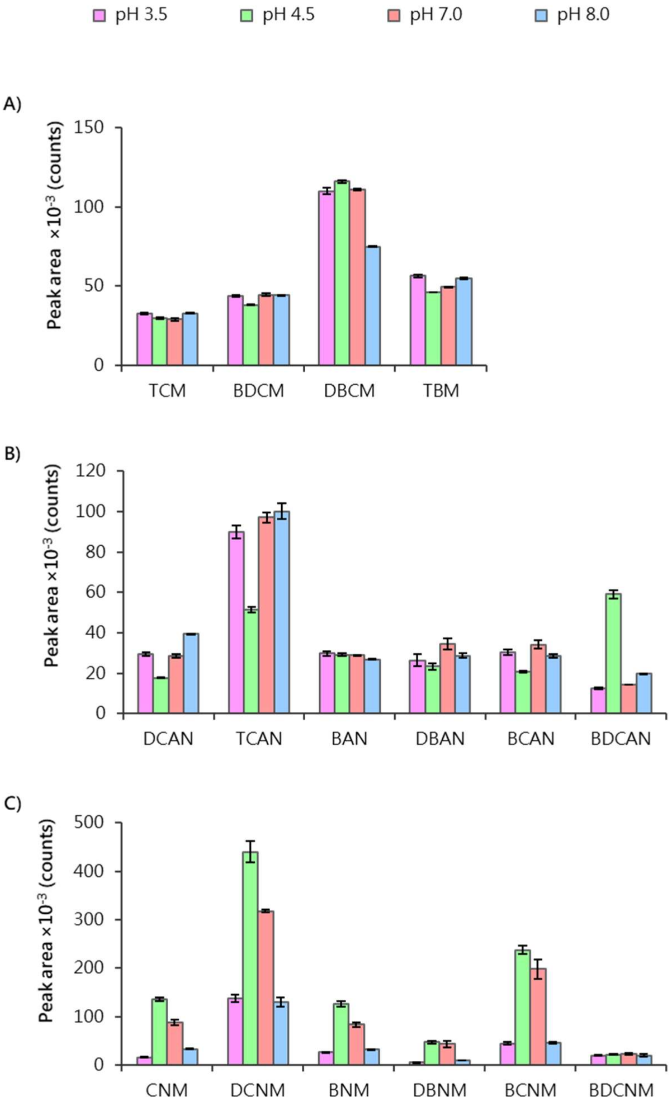

Figure IV.45. Response as a function of the pH, using the optimized HS-SPME-GC-FID method for **A)** THMs, **B)** HANs, and **C)** HNMs.

5. Study of the influence of quenching agents

The residual chlorine present in treated waters is necessary to ensure the quality across the whole distribution network. However, an accurate quantification of DBPs in water samples requires the elimination of this residual chlorine to prevent the formation of DBPs during the holding time between water sampling and analysis. Such elimination of the residual chlorine is normally carried out using a quenching agent [1,6,7]. A proper quenching agent must meet the following requirements: it must experience a rapid and complete reaction with the residual disinfectant; it should be chemically inert with DBPs; and it should not interfere with the further analytical method [8].

The most widely used residual chlorine inhibiting agents include: ascorbic acid [9,10], sodium sulfite [3], sodium thiosulfate [11,12], ammonium sulphate [1], ammonium chloride [6,13] and sodium borohydride [7]. These agents react with residual chlorine by oxidation/reduction reactions, except ammonium chloride [14]. As it has been reported the decomposition of DBPs in presence of quenching agents [8], it is important to select carefully a proper quenching agent able to eliminate the residual chlorine without provoking any kind of DBP decomposition.

Consequently, an initial study was carried out to select the proper quenching agent concentration, using sodium thiosulfate as reference quenching agent. According to the WHO, the reference value of residual chlorine available to prevent the microbiological activity in waters is 5 mg·L^{-1} [15]. The US-EPA establishes the maximum value at 4 mg·L^{-1} [16], and the Spanish legislation at 1 mg·L^{-1} [17]. Therefore, it was considered an intermediate value of 3 mg L^{-1} of residual chlorine in the water sample in this initial study.

In all experiments, 10 mL of an aqueous standard containing 100 µg·L^{-1} of each DBP, at pH 7 (0.12 mol·L^{-1}K_2HPO_4 / 0.08 mol·L^{-1}KH_2PO_4), and the remaining optimized conditions, together with an aliquot of sodium thiosulfate (added at different stoichiometric ratios, but in all cases ensuring its effect respect to the legislated residual chlorine value in waters of 3 mg·L^{-1}), were analyzed in triplicate by the HS-SPME-GC-FID method already developed. The analysis was performed immediately after the addition of the quenching agent. The tested ratios (residual chlorine:sodium thiosulfate) were: 1:10; 1:38 and 1:100. Results are shown in Figure IV.46. In general, it was observed that chromatographic peak areas obtained with the ratios 1:10 and 1:38 were all comparable, except for TCM, BDCM, DCAN and DBAN, which presented a slight improvement with the ratio 1:38. In all cases, the use of the higher ratio 1:100 was accompanied by important decreases of peak areas. Thus, the minimum content of quenching agent (ratio 1:10) was chosen as optimum.

After the selection of the optimum ratio 1:10 (residual chlorine:quenching agent), different quenching agents were tested. Figure IV.47. presents the results obtained for each family of DBPs, as a function of the quenching agent employed, and includes a study without any quenching agent. THMs are clearly the less affected family of DBPs by the nature of the quenching agent. Nevertheless, the signals obtained for HANs and primarily for HNMs were significantly different in the quenched and non-quenched samples, depending on the analyte and the quenching agent considered in each case.

For most HANs and HNMs, sodium thiosulphate as quenching agent showed the most adverse effect. Ascorbic acid and ammonium chloride presented similar performance, but ascorbic acid was worse for most HANs and HNMs. According to these results, ammonium chloride was chosen as the optimum quenching agent of residual chlorine, in a ratio 1:10, for the groups of DBPs studied.

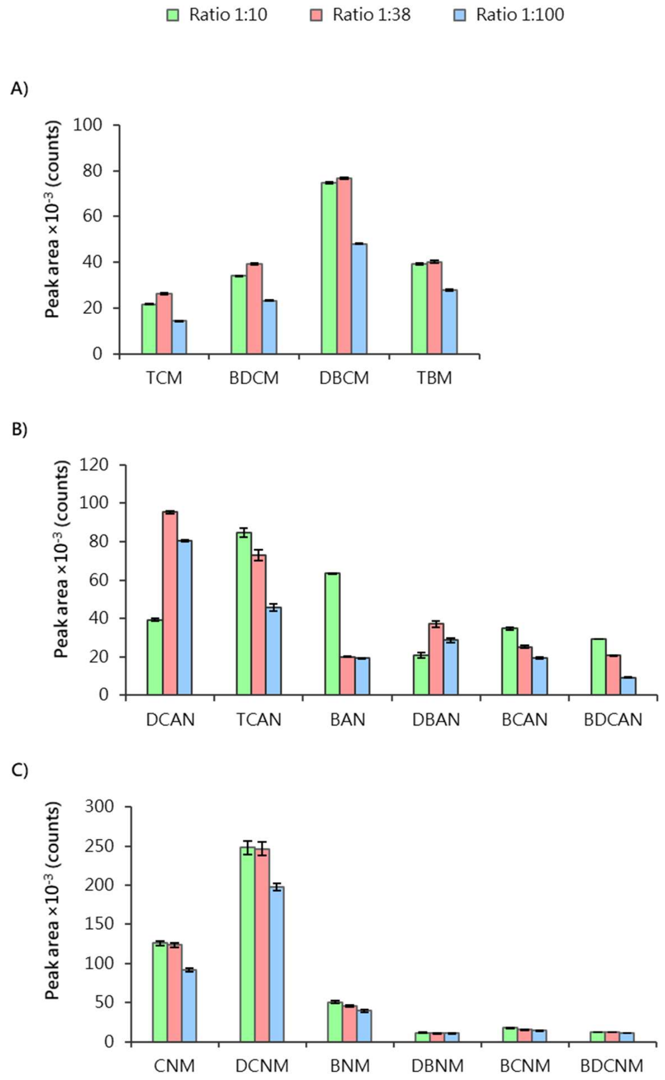

Figure IV.46. Evaluation of the response of DBPs after the application of the optimum HS-SPME-GC-FID method, under different contents of sodium thiosulfate added (stoichiometric ratios, in all cases *versus* the legislated residual chlorine content of 3 mg·L^{-1}) for **A)** THMs, **B)** HANs, and **C)** HNMs.

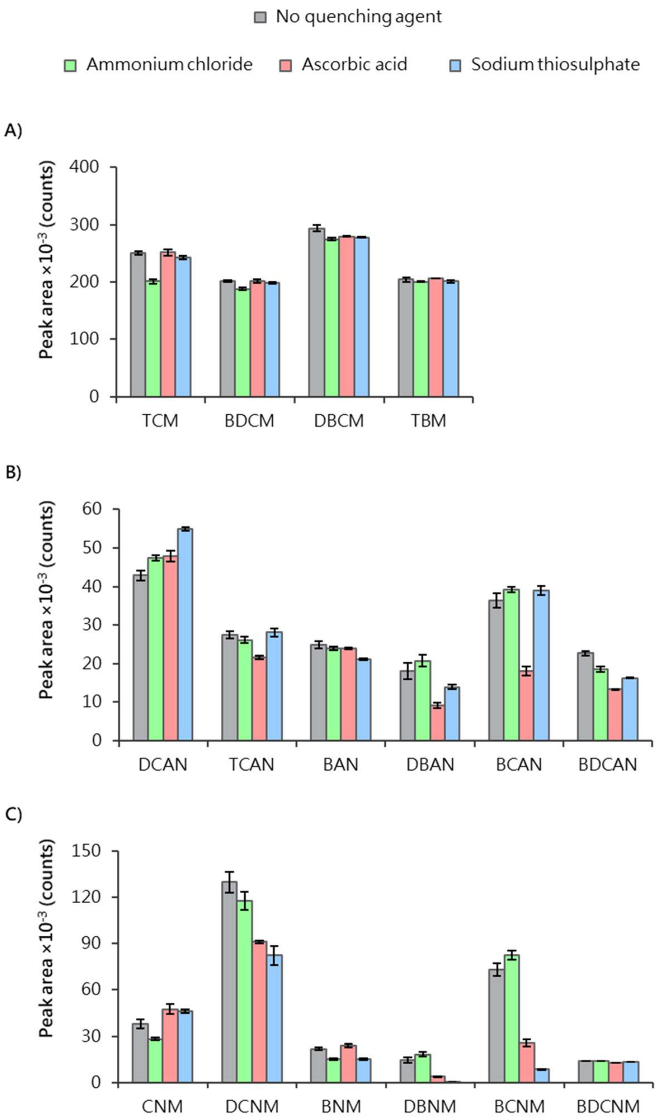

Figure IV.47. Study of the effect of different quenching agents (ascorbic acid, sodium thiosulphate, and ammonium chloride) at the ratio 1:10 (residual chlorine:quenching agent), *versus* the response of DBPs in absence of any quenching agent using the optimum HS-SPME-GC-FID method, for **A)** THMs, **B)** HANs and **C)** HNMs.

A final study was performed to evaluate the stability of DBPs over time, using the variables selected and that affect at the stability of DBPs (sample at pH 7, containing ammonium chloride in a ratio 1:10 with respect to the residual chlorine). The purpose was to establish the maximum time that samples already containing the quenching agent selected (the quenching agent should be added to the water samples right after sampling) can be kept in the laboratory before being analyzed. Figure IV.48. shows the variation of the chromatographic peak areas over time for representative examples of each DBP family, analyzed by the optimum conditions and using ammonium chloride as quenching agent. The experiments were carried out using 10 mL of an aqueous standard containing 100 μg·L^{-1} of DBPs and the remaining optimum conditions. These solutions were stored at 4 ºC once prepared, including the addition of the ammonium chloride. They were analyzed by the optimum HS-SPME-GC-FID method after 0, 6, 24, 48 and 72 hours since their preparation. It was observed that, in general, the peak areas of THMs initially decreased, stabilizing between 24 and 48 hours. The exception was DBCM, which presented increases in the chromatographic peak area with the time. Regarding HANs, the chromatographic peak areas remained substantially constant over time, except for BCAN and TCAN that experienced rapid decreases. With regard to HNMs, they exhibited a similar behavior to THMs. For the majority of HNMs, the peak area sharply fell in the early hours and then remained constant. From these studies, it can be concluded that ammonium chloride is a suitable inhibitor of residual chlorine for all DBPs studied and for the time period considered. However, it is recommended to perform the analysis of blending desalinated waters to determine DBPs within 48 hours after sampling.

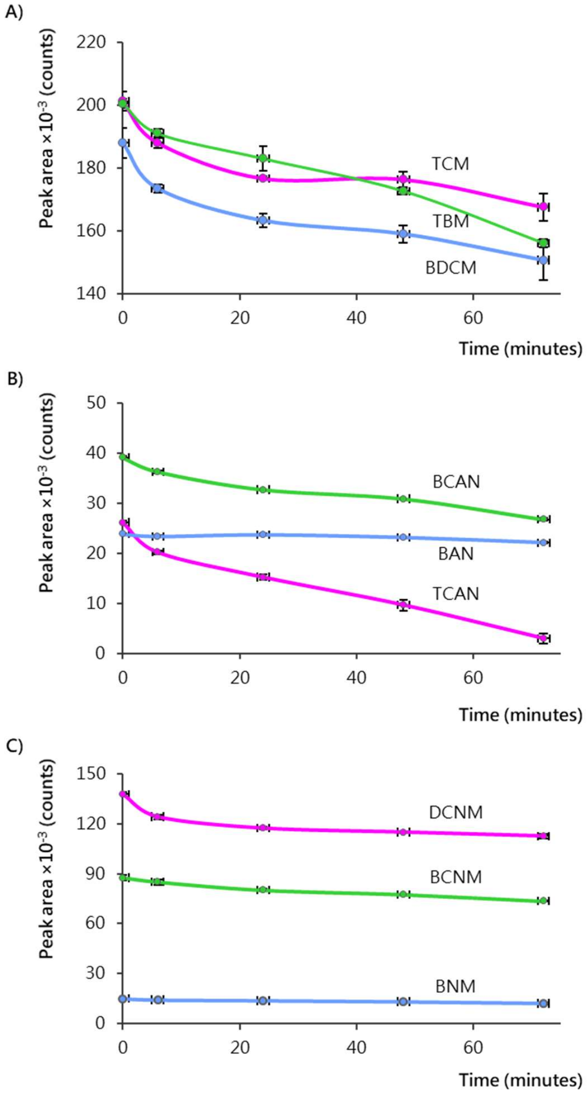

Figure IV.48. Evaluation of the stability of DBPs in presence of the quenching agent ammonium chloride over time for representative DBPs, using the experimental conditions described in the text and the optimized HS-SPME-GC-FID method. **A)** Representative THMs, **B)** representative HANs and **C)** representative HNMs.

6. Quality analytical parameters of the HS-SPME-GC-FID method

Under the optimized conditions of the HS-SPME-GC-FID method (see Figure IV.49.), the quality analytical parameters were obtained for the entire method. Calibrations were constructed using 10 mL of aqueous standards at pH 7, in presence of 30% (w/v) of NaCl, and using a ratio 1:10 (residual chlorine:quenching agent) being ammonium chloride the quenching agent. The calibration range for all DBPs was 10 – 100 μg·L^{-1}. Table IV.26. includes the quality analytical parameters obtained. Figure IV.50. shows a representative chromatogram obtained of the analysis of an aqueous standard containing DBPs at a concentration level of 100 μg·L^{-1} and subjected at the optimum HS-SPME-GC-FID method.

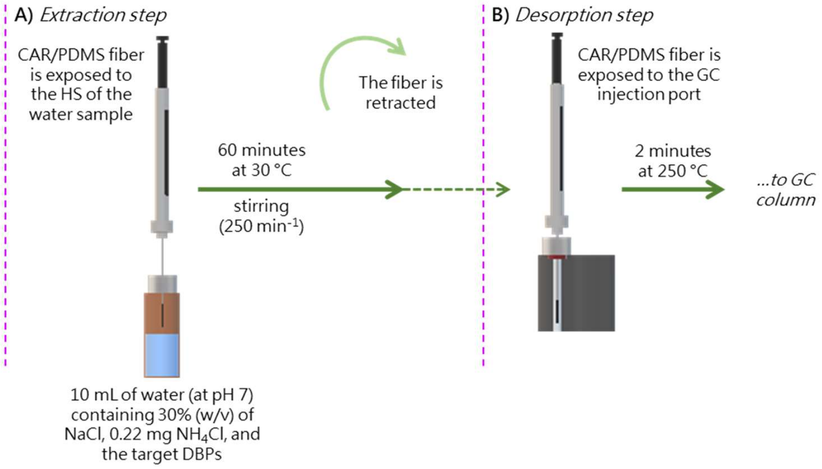

Figure IV.49. Optimum conditions of the proposed HS-SPME method for the monitoring of 16 DBPs in water samples in combination with GC-FID.

Table IV.26. Several quality analytical parameters of the entire HS-SPME-GC-FID method.

DBP	(Slope ± SD[a]) ×10^{-2}	$S_{y/x}$[b] ×10^{-2}	R^2 [c]	LOD[d] (μg·L^{-1})	LOQ[d] (μg·L^{-1})	Conc. level: 25 μg·L^{-1} RSD[e] (%) intra-day / inter-day	RR[f] (%)	Conc. level: 45 μg·L^{-1} RSD[e] (%) intra-day / inter-day	RR[f] (%)
TCM	10.2 ± 0.4	31	0.996	11.6	16.9	6.0 / 8.4	111	5.9 / 8.5	108
BDCM	17.5 ± 0.6	52	0.996	9.10	11.8	7.3 / 7.2	111	7.8 / 9.5	107
DBCM	18.6 ± 0.6	20	0.997	1.00	3.32	7.5 / 6.6	94.2	6.8 / 11	104
TBM	15.2 ± 0.5	42	0.996	2.28	3.03	9.0 / 7.5	103	5.9 / 7.6	107
DCAN	3.8 ± 0.1	8.5	0.998	2.36	7.86	6.8 / 7.9	93.2	2.5 / 5.0	94.4
TCAN	0.71 ± 0.02	1.4	0.998	4.16	11.8	7.7 / 10	112	5.9 / 11	113
BAN	1.7 ± 0.1	5.9	0.995	0.72	20.3	6.8 / 11	103	5.3 / 6.5	81.7
DBAN	1.8 ± 0.1	7.3	0.991	13.7	31.1	7.3 / 16	101	6.5 / 5.8	108
BCAN	3.9 ± 0.1	5.9	0.999	18.0	19.5	6.8 / 12	111	6.2 / 6.1	109
BDCAN	0.56 ± 0.03	1.9	0.994	21.4	34.1	11 / 19	119	14 / 21	115
CNM	2.0 ± 0.1	9.2	0.991	2.34	7.81	12 / 12	44.6	5.9 / 18	85.3
DCNM	8.2 ± 0.4	29	0.995	0.29	5.46	4.2 / 11	92.9	1.6 / 5.6	117
BNM	1.2 ± 0.1	4.1	0.994	2.44	8.12	9.7 / 8.0	83.1	4.8 / 10	82.1
DBNM	1.8 ± 0.1	6.1	0.996	12.3	19.2	7.9 / 10	109	4.6 / 11	111
BCNM	6.7 ± 0.2	20	0.997	7.34	10.2	6.2 / 7.8	93.3	3.2 / 5.6	121
BDCNM	0.17 ± 0.01	0.6	0.996	13.7	40.8	9.6 / 10	114	7.85 / 17	110

[a] Standard deviation associated to the slope

[b] Standard deviation of the residuals

[c] Determination coefficient

[d] Limit of detection and limit of quantification calculated according to the ratio signal/noise as 3 and 10 times, respectively, and experimentally verified

[e] Relative standard deviation: intra-day (n = 4) and inter-day (n = 12, in three different non-consecutive days)

[f] Relative recovery (n = 4)

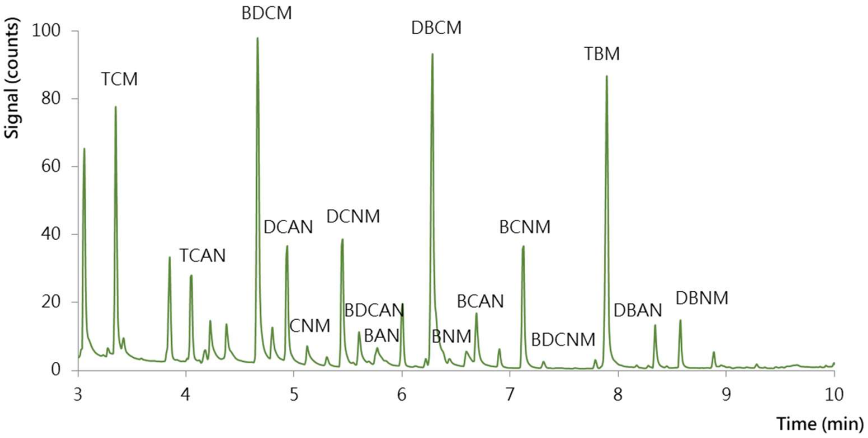

Figure IV.50. Representative chromatogram obtained of the analysis of an aqueous standard (spiked at 100 µg·L^{-1}) and subjected at the optimum HS-SPME-GC-FID method.

Determination coefficients higher than 0.996 were obtained for THMs, and higher than 0.991 for HANs and HNMs. LODs and LOQs were calculated as the concentration of DBP that provided a signal 3 and 10 times higher than noise, respectively, and were validated by decreasing the analyte concentration of a standard (which was subjected to the entire HS-SPME-GC-FID method) until this ratio was achieved. LOQ values commonly ranged from 3.03 µg·L^{-1} for TBM to 20.3 µg·L^{-1} for BAN, with the following exceptions: 31.1 µg·L^{-1} for DBAN, 34.1 µg·L^{-1} for BDCAN, and 40.8 µg·L^{-1} for BDCNM. Although, the obtained LOQ values were higher than others described in the literature using ECD [11,18] or MS [1,19] detection, they can be considered satisfactory attending to the FID detection system employed. Nevertheless, the obtained values were lower than the regulated limits of the US-EPA and also those established by the WHO as guideline values.

The precision of the method was evaluated using two different standards: a low level (25 µg·L^{-1}) and a medium level (45 µg·L^{-1}) concentration, for four replicates within the same day (intra-day precision), and for twelve replicates in three non-consecutive days (inter-day precision). At the low concentration level, intra-day RSD values ranged between 4.2% for DCNM and 12% for CNM, whereas the inter-day RSD values ranged between 6.6% for DBCM and 19%

for BDCAN. With regard to the recovery study, evaluated by RR (%) values, the obtained values were adequate at both concentration levels. At the lowest spiked level, RR values ranged between 83.1% and 114% (with the exception of CNM) and between 81.7% and 121%, for low and medium level concentration, respectively.

7. Analysis of water samples with the optimum HS-SPME-GC-FID method

The validated method was applied to the analysis of four different blending desalinated waters intended for human consumption. TBM was quantified in all samples studied, with contents ranging from 7.3 to 50 $\mu g \cdot L^{-1}$. The same situation occurred for TCAN, with contents between 25.6 and 27 $\mu g \cdot L^{-1}$. DBCM was only quantified in one of the samples at 3.5 $\mu g \cdot L^{-1}$. Other DBPs were detected but non-quantified: BDCM, BDCAN and BDCNM. The rest of DBPs were not detected in the water samples analyzed, as it can be observed in Table IV.27. In general, it is clear that brominated derivatives are the most abundant DBPs in the waters studied. Indeed, it has been stated that the high bromide and iodide concentrations in seawater cause a difference in the formation and speciation in DBP as compared to disinfected fresh waters [20]. The results obtained in this study are in accordance with those considered by WHO, whose studies show that DBPs are dominated by brominated THMs, particularly TBM and, to a lesser extent, DBCM [21].

Finally, the blending desalinated water sample containing the lowest level of DBPs (water sample 2) was selected to evaluate the matrix effect and to calculate the RR (%). The results are summarized in Table IV.27. The sample was spiked with an intermediate level content of each DBP (45 $\mu g \cdot L^{-1}$) and then analyzed in triplicate by the entire method. The relative recoveries (subtracting the amount of DBPs already present in the water samples) were similar to those obtained with ultrapure water (see Table IV.26.). They ranged between 87% for BNM and 115% for BDCAN, except for CNM (59%). Attending to these results, the matrix effect was not significant in the type of samples considered.

Table IV.27. Concentration levels found of DBPs in blending desalinated waters analyzed in triplicate by the optimum HS-SPME-GC-MS method.

Analyte	Level found ± SD (μg·L^{-1})				Recovery study (Water sample 2)
	Water sample 1	Water sample 2	Water sample 3	Water sample 4	RR (%) ± SD
TCM	n.d.	n.d.	n.d.	n.d.	107 ± 3
BDCM	n.d.	N.Q.	n.d.	N.Q.	105 ± 4
DBCM	n.d.	n.d.	n.d.	3.5 ± 0.2	98 ± 2
TBM	22 ± 3	7.3 ± 0.4	12 ± 1	50 ± 2	101 ± 2
DCAN	n.d.	n.d.	n.d.	n.d.	93 ± 2
TCAN	26.9 ± 0.8	27 ± 2	26.9 ± 0.3	25.6 ± 0.5	103 ± 4
BAN	n.d.	n.d.	n.d.	n.d.	94 ± 3
DBAN	n.d.	n.d.	n.d.	n.d.	99 ± 5
BCAN	n.d.	n.d.	n.d.	n.d.	106 ± 2
BDCAN	76 ± 2	n.d.	N.Q.	n.d.	115 ± 6
CNM	n.d.	n.d.	n.d.	n.d.	59 ± 2
DCNM	n.d.	n.d.	n.d.	n.d.	97 ± 3
BNM	n.d.	n.d.	n.d.	n.d.	87 ± 2
DBNM	n.d.	n.d.	n.d.	n.d.	110 ± 2
BCNM	n.d.	n.d.	n.d.	n.d.	99 ± 1
BDCNM	N.Q.	n.d.	n.d.	n.d.	99 ± 5

n.d. = non-detected
N.Q. = non-quantified

IV.2.2.2. Solid-phase microextraction based on the metal-organic framework CIM-80(Al) to determine volatile methylsiloxanes and musk fragrances in aqueous samples using gas chromatography

In preparation for submission to Talanta

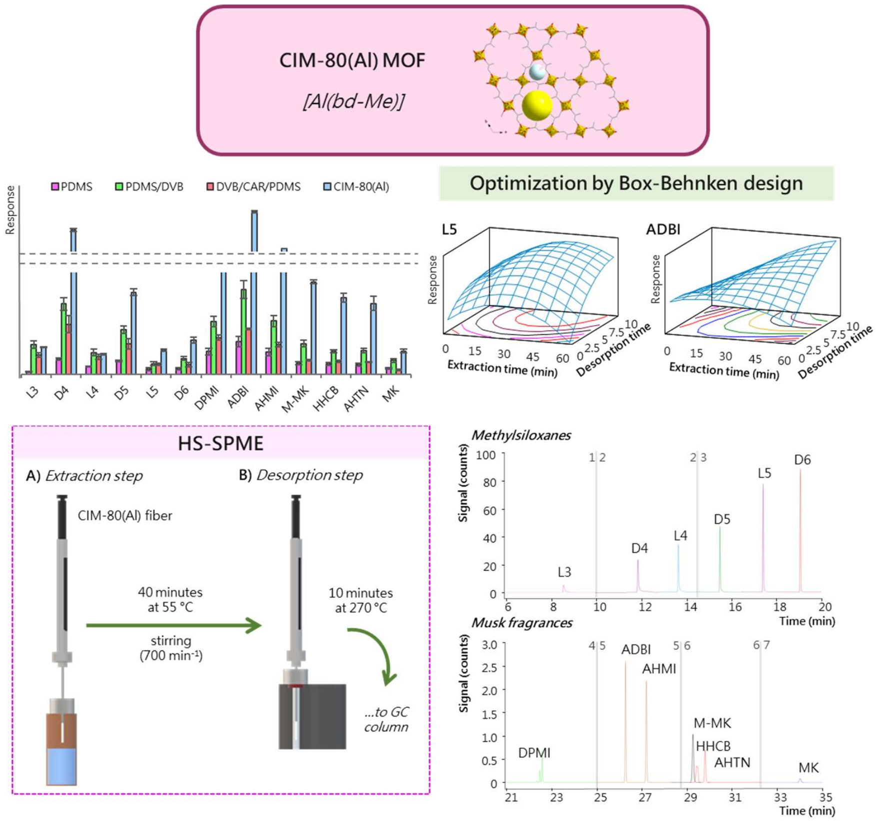

1. Optimization of the GC separation using HS-SPME

A total of 13 PCPs were considered in this study: 6 methylsiloxanes (L3, D4, L4, D5, L5, and D6), and 7 musk fragrances (DPMI, ADBI, AHMI, M-MK, HHCB, AHTN, MK). They were initially studied using GC-FID. The optimum GC-FID chromatographic conditions were described in Section III.6.2., achieving the complete separation of the analytes in 45 min. The chromatographic retention times together with their reproducibility values under the optimized chromatographic conditions are shown in Table IV.28. In all cases, RSD (%) values lower than 0.23% (n = 30) for the retention times were obtained.

Table IV.28. Chromatographic retention times for the group of PCPs studied under the optimum GC-FID conditions.

Analyte	t_R (min)	RSD (%) (n = 30)
L3	9.56	0.23
D4	13.70	0.14
L4	16.20	0.08
D5	18.83	0.05
L5	21.55	0.04
D6	23.76	0.02
DPMI	29.02	0.01
ADBI	34.03	0.11
AHMI	35.11	0.04
M-MK	37.99	0.04
HHCB	38.12	0.04
AHTN	38.46	0.04
MK	43.60	0.01

2. Selection of the best fiber for the HS-SPME-GC-FID method

The analytical performance of different SPME fibers was evaluated under the same experimental conditions, selecting common variables from the scientific literature for HS-SPME methods [22]: 10 mL of an aqueous standard containing 50 µg·L^{-1} of each PCPs and without adjustment of the ionic strength, headspace mode; an extraction temperature of 25 ºC for 40 minutes under stirring with a stir bar (speed: 700 min^{-1}), while performing the desorption of the fiber in the injection port of the GC-FID in splitless mode at 250 ºC for 5 minutes. In all the experiments, the aqueous standard was subjected to 5 minutes of equilibration time, and the maximum acetone content in the extraction vial was fixed to 1% (v/v). Furthermore, the fiber was kept in mode split in the injector port for 5 additional minutes to ensure absence of carry over effects. Attending to the nature of target analytes, for this initial study the selected fibers included a polar commercial fiber (100 µm PDMS), two semi-polar commercial fibers (65 µm PDMS/DVB and 50/30 µm DVB/CAR/PDMS), and one MOF-based fiber (30 µm CIM-80(Al)).

Figure IV.51. shows the performance of these SPME fibers, by plotting the response (expressed as peak area) for each PCP. For a better comparison, the response was normalized by the volume of the fiber coating. Considering the volume of the fiber coating as hollow cylinder, the equation for calculations is the following:

$$V_{\text{coating fiber}} = \pi\cdot(R^2-r^2)\cdot h \qquad \text{Equation IV.15.}$$

being R the sum of the radius of the fiber core and the thickness of the fiber coating, r the radius of the core, and h the length of the fiber coating (1 cm). Thus, the volumes are 0.660 µm^3 for the PDMS fiber, 0.375 µm^3 for PDMS/DVB fiber, 0.478 µm^3 for DVB/CAR/PDMS fiber, and 0.074 µm^3 for CIM-80(Al) fiber.

It is clear that the best results are obtained for the CIM-80(Al)-based fiber, except for analytes L3 and L4, which are also properly extracted by the semi-polar PDMS/DVB fiber. CIM-80(Al) and PDMS/DVB are fibers containing porous coatings. It has been reported that this type of coatings provides better extraction efficiency for semi-volatiles compounds [23].

Given the structures of the methylsiloxanes, it is important to ensure that they do not experience any kind of degradation at temperatures higher than 250 ºC, because it has been reported that the siloxanes can experience thermal degradation [24].

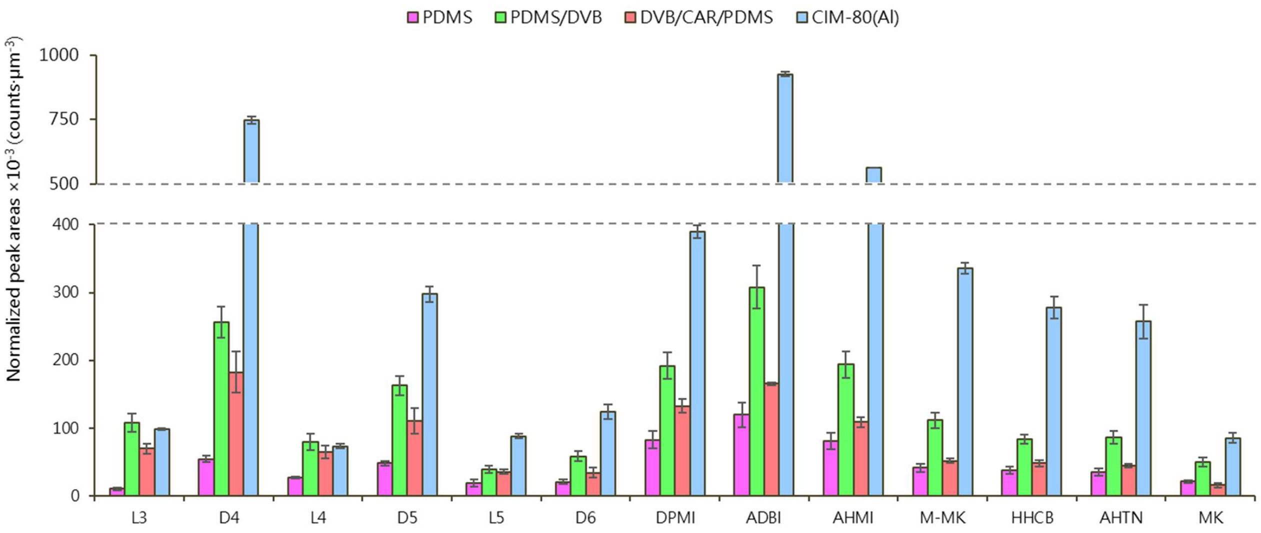

Figure IV.51. Comparison of the analytical performance of the three commercial SPME fibers and the MOF-based fiber tested for two groups of PCPs: methylsiloxanes (3 linear methylsiloxanes and 3 cyclic methylsiloxanes) and musk fragrances (1 nitro musk and 6 polycyclic musk).

The maximum recommended operating temperature for both PDMS/DVB and CIM-80(Al) is 270 ºC. Therefore, experiments were carried out for the CIM-80(Al), the best fiber with attending to the results plotted in Figure IV.51., using as desorption temperatures 250 and 270 ºC. The experiments were carried out using the same conditions as those employed when selecting the best fiber. Results indicated an increase in the peak area when using 270 ºC as the desorption of the PCPs from the CIM-80(Al) fiber. Therefore, this desorption temperature was selected for the remaining experiments.

3. Box-Behnken experimental design for the optimization of the HS-SPME conditions

The optimization of the HS-SPME-GC-FID method was carried out using an experimental design, specifically a Box-Behnken design (BBD). BBD can be considered a combination of a screening analysis and a Central Composite Design (CCD), and it results slightly more efficient than the CCD [25]. For example, if four factors are those required in the optimization, in BBD the matrix can be constructed as three blocks of eight experiments, consisting of a full two factor factorial design with the level of the third set at zero. In this sense, the information that can be obtained from the BBD is the same than that obtained in a screening analysis but adding a third level for each factor. In this study, BBD was selected for the optimization of four variables: ionic strength (studied from 0 to 20% (w/v) of NaCl content), $t_{extraction}$ (studied from 10 to 60 minutes), $t_{desorption}$ (studied from 2 to 10 minutes), and $T_{extraction}$ (studied from 20 to 80 ºC). The $T_{desorption}$ was fixed at 270 ºC according to the previous results.

The BBD is a class of rotatable second-order design based on a three-level incomplete design. The number of experiments for four factors involved 27 experiments, given by the equation $N = 2k(k-1) + C_0$, where k is the number of factors and C_0 the number of center points [25]. Each factor is studied at three levels. The center point is performed in triplicate to obtain a better estimation of the pure error.

Table IV.29. shows the coded values (C_n) of a BBD for four factors, and the real values (x_n) of the resulting experiments. All experiments implied the HS-SPME-GC-FID analysis of 10 mL aqueous standard containing 50 $\mu g \cdot L^{-1}$ of each PCPs. Figure IV.52. shows the three-dimensional response surfaces (extraction time × desorption time × response) obtained by RSM for representative PCPs, fixing the content of NaCl at 20% (w/v), and the extraction temperature at

55 ºC. It can be seen that the range considered for the extraction and desorption times is not enough for musk fragrances. However, the use of extraction times higher than 60 minutes, or desorption times higher than 10 minutes, is not reasonable for a microextraction method and thus they were discarded modifications in the studied ranges for this group of musk.

It is evident that due to the high number of responses (13 analytes) and the clear different physical-chemical characteristics of methylsiloxanes and musk, the conventional graphical optimization by the RSM cannot considered. Thus, a desirability function [26,27] was used. This function is based on the assumption that the proper response (that has many features) is unacceptable if one is outside of a "desirable" limit. This can be expressed with the following equation:

$$d_i^{max} = \begin{cases} 0 & \text{if } f(x) < A \\ \left(\frac{f(x)-A}{B-A}\right)^w & \text{if } A \leq f(x) \leq B \\ 1 & \text{if } f(x) > B \end{cases} \qquad \text{Equation IV.16.}$$

where d_i is the individual desirability values, f(x) the response value, A the minimum response value, B the maximum response values, and w the weight used to determine the importance. The purpose of this function is to find the experimental conditional that ensure compliance with the criteria of all the involved responses and, at the same time, allows to find the best compromise value in the desirable response, converting the multiple response (peak areas of each PCP in this case) into a single one [28]. This last is achieved combining the individual responses into the following composite function:

$$D = \left(d_1^{r1} \times d_2^{r2} \times \ldots \times d_n^{rn}\right)^{1/n} \qquad \text{Equation IV.17.}$$

where D is the overall desirability (ranging from 0 to 1), r_i the parameter that expresses the relative importance of each variable in relation to the others, and n the number of responses. In this study all responses were the same weight (r = 1 for all the cases). D values for each experiment are showed in the Table IV.29.

The Statgraphics software was used for this statistical analysis. The best combination of the experimental factors considered in the BBD indicated the following optimum conditions: 20% (w/v) of NaCl content, 40 minutes of extraction time, 10 minutes of desorption time, and 55 ºC of extraction temperature.

Table IV.29. Matrix of the experiments of the BBD utilized for the optimization of the HS-SPME-GC method, and the overall desirability (D) corresponding of each experiment.

Experiment	Factor 1 NaCl (%, in w/v)		Factor 2 $t_{extraction}$ (min)		Factor 3 $t_{desorption}$ (min)		Factor 4 $T_{extraction}$ (ºC)		D*
	C_1	x_1	C_2	x_2	C_3	x_3	C_4	x_4	
1	*+1*	20	*+1*	60	*0*	6	*0*	50	0.1230
2	*+1*	20	*-1*	10	*0*	6	*0*	50	0.2356
3	*-1*	0	*+1*	60	*0*	6	*0*	50	0.1503
4	*-1*	0	*-1*	10	*0*	6	*0*	50	0.0000
5	*0*	10	*0*	35	*+1*	10	*+1*	80	0.0000
6	*0*	10	*0*	35	*+1*	10	*-1*	20	0.4153
7	*0*	10	*0*	35	*-1*	2	*+1*	80	0.1903
8	*0*	10	*0*	35	*-1*	2	*-1*	20	0.3413
9	*0*	10	*0*	35	*0*	6	*0*	50	0.2652
10	*+1*	20	*0*	35	*0*	6	*+1*	80	0.2090
11	*-1*	0	*0*	35	*0*	6	*+1*	80	0.2590
12	*+1*	20	*0*	35	*0*	6	*-1*	20	0.3790
13	*-1*	0	*0*	35	*0*	6	*-1*	20	0.4433
14	*0*	10	*+1*	60	*+1*	10	*0*	50	0.0000
15	*0*	10	*+1*	60	*-1*	2	*0*	50	0.0000
16	*0*	10	*-1*	10	*+1*	10	*0*	50	0.0000
17	*0*	10	*-1*	10	*-1*	2	*0*	50	0.2152
18	*0*	10	*0*	35	*0*	6	*0*	50	0.4550
19	*+1*	20	*0*	35	*+1*	10	*0*	50	0.0000
20	*-1*	0	*0*	35	*-1*	2	*0*	50	0.2655
21	*+1*	20	*0*	35	*+1*	10	*0*	50	0.2209
22	*-1*	0	*0*	35	*-1*	2	*0*	50	0.2125
23	*0*	10	*+1*	60	*0*	6	*+1*	80	0.1248
24	*0*	10	*+1*	60	*0*	6	*+1*	80	0.3092
25	*0*	10	*-1*	10	*0*	6	*-1*	20	0.0000
26	*0*	10	*-1*	10	*0*	6	*-1*	20	0.0000
27	*0*	10	*0*	35	*0*	6	*0*	50	0.1866

C_1, C_2, C_3 and C_4 are the coded value for the levels of the factor 1, 2, 3 and 4, respectively.

The relationship between coded and real values is given by: $C_i = [(x_i - x^o_i)/\Delta x_i]\cdot\alpha$ where C_i is the coded value for the level of factor i, x_i is its real value in an experiment, x^o_i is the real value at the center of the experimental domain, Δx_i is the step of variation of the real value, and α is the coded value limit for each factor.

* Overall desirability value obtained with the Equation IV.16. and Equation IV.17.

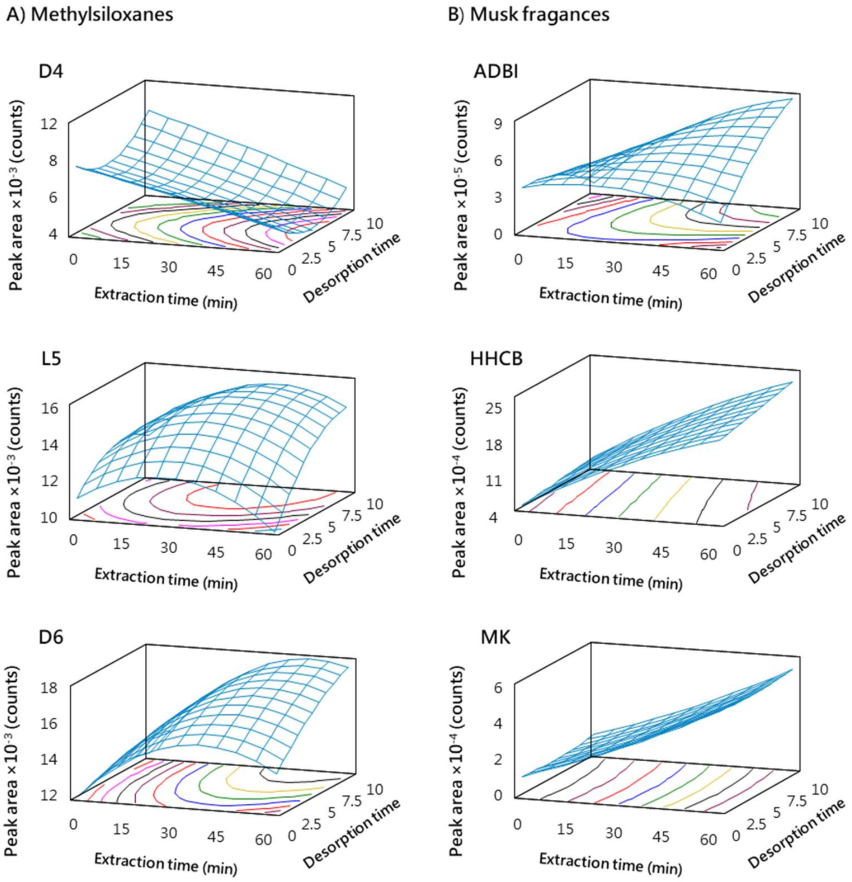

Figure IV.52. Representative results obtained with the statistical study used in the optimization with the BBD for representative analytes: **A)** D4, L5 and D6 for methylsiloxanes, and **B)** ADBI, HHCB, and MK for musk fragrances. Conditions fixed: 20% (w/v) content of NaCl, and 55 ºC of extraction temperature.

4. Combination of the optimized HS-SPME method with GC-MS

To ensure proper identification of target PCPs in real samples, the optimum conditions of the HS-SPME method (see Figure IV.53.) were then used in combination with GC-MS method. The optimum separation with the GC-MS method are described in Section III.6.2. Table IV.30. summarizes the retention times and their RSD values under the adequate chromatographic separation, together with the monitoring ions (indicating the quantifying and qualifying ions) selected for the determination of the target PCPs.

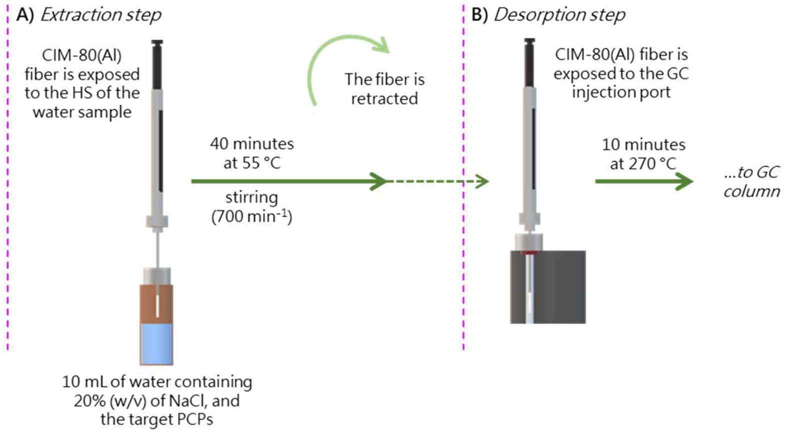

Figure IV.53. Optimum conditions of the HS-SPME procedure for the monitoring of the selected group of PCPs using the CIM-80(Al) MOF-based fiber in combination with GC.

At this point of the study, and before going ahead with the validation of the method, it results very important to evaluate the possible contamination of the PCPs considered, coming from several sources (handling of material, instrumentation, laboratory environment, the own analyses…). PCPs are widespread environments, even forming part of labware. In this sense, possible cross-contamination was evaluated by the analysis of blanks. Thus, 10 mL of ultrapure water containing 20% (w/v) of NaCl and 1% of acetone were analyzed under the optimum HS-SPME-GC-MS conditions, using the CIM-80(Al) fiber and also the commercial PDMS/DVB fiber.

Table IV.30. Monitoring ions and retention times for the PCPs using the GC-MS method.

PCP	SIM segment (time in min)	t_R / RSD (n = 30)	Quantifying ion (m/z)	Qualifying ions (m/z)
L3	1 (5.0)	8.55 / 0.04	221	133,205
D4	2 (10.0)	11.89 / 0.06	281	193,265
L4		13.66 / 0.04	207	295,191
D5	3 (14.5)	15.64 / 0.04	267	355,269
L5		17.56 / 0.02	281	147,265
D6		19.20 / 0.02	341	325,429
DPMI	4 (21.0)	22.51 / 0.02	191	135,206
ADBI	5 (25.0)	26.24 /0.01	229	173,244
AHMI		27.10 /0.02	229	187,145
M-MK	6 (28.5)	29.33 /0.08	215	173,142
HHCB		29.37 / 0.05	243	213,128
AHTN		29.74 / 0.01	243	159,187
MK	7 (32.0)	34.05 / 0.03	279	115,146

The obtained results confirm that the contamination of methylsiloxanes (particularly the cyclic methylsiloxanes) using the PDMS/DVB was 10 times higher respect to the CIM-80(Al) fiber, probably due to the decomposition of the fiber over time (PDMS is formed by siloxanes). Lineal methylsiloxanes were not found after the analysis of blanks with the CIM-80(Al) fiber. For this reason, CIM-80(Al) fiber was selected as the most adequate material for the monitoring of methylsiloxanes using HS-SPME-GC-MS.

Figure IV.54. shows, in green line, a representative chromatogram of the analysis of an aqueous standard containing a concentration level of 10 $\mu g{\cdot}L^{-1}$ with all PCPs subjected to the optimum HS-SPME-GC-MS method, using the CIM-80(Al) fiber. In the same Figure, it is shown the blank analyses obtained with the commercial PDMS/DVB fiber (in blue line) and with the CIM-80(Al) fiber (in red line).

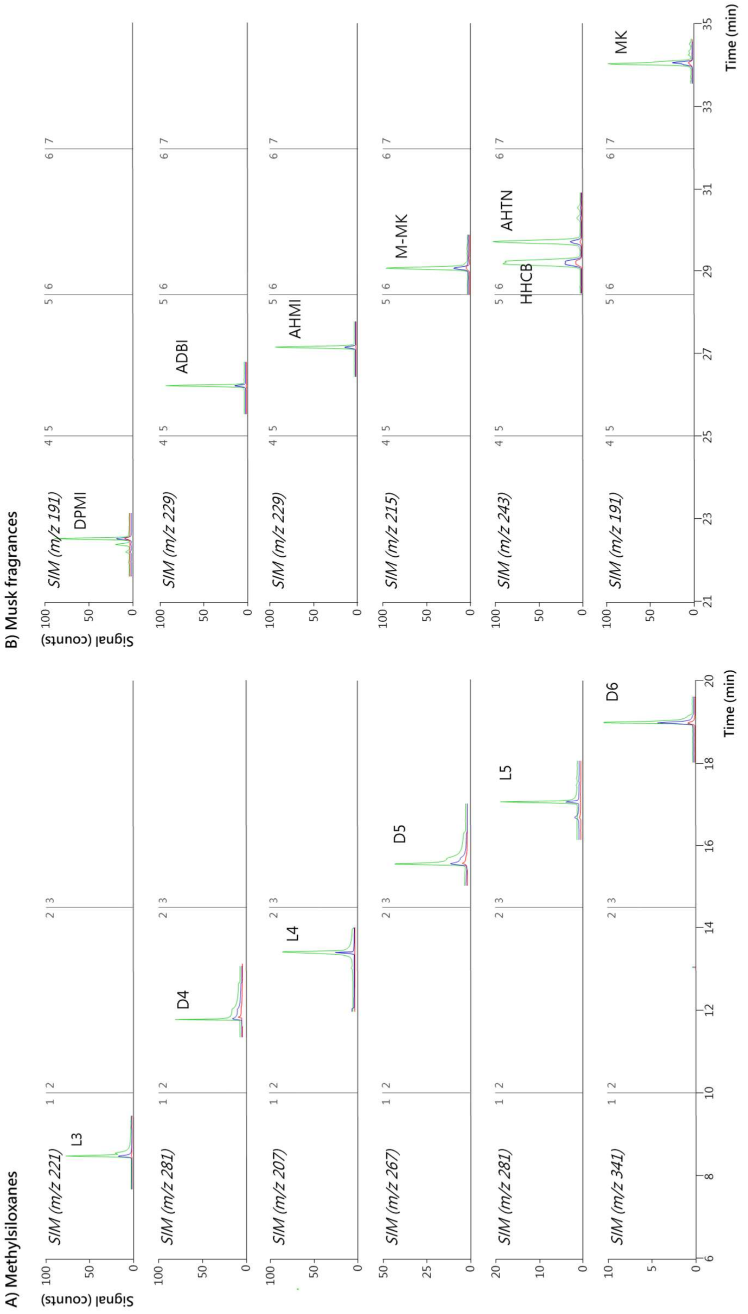

Figure IV.54. Representative SIM chromatogram (with the segments marked by a gray vertical line) of an aqueous standard at 10 μg·L^{-1}(all PCPs) subjected to the optimum HS-SPME-GC-MS method with the CIM-80(Al) fiber: **A)** methylsiloxanes and **B)** musk fragrances.

5. Quality analytical parameters of the HS-SPME-GC-MS method

The validation of the entire method was carried out subjecting aqueous standards with concentration values ranging from 0.02 to 200 µg·L^{-1} (depending on the analyte), using 8 calibration levels, to the optimum HS-SPME-GC-MS. Table IV.31. shows several quality analytical parameters of the HS-SPME-GC-MS method using the CIM-80(Al) fiber. It can be observed that the calibration ranges were from 0.02 to 20 µg·L^{-1} for methylsiloxanes (except L3 and D4, starting at 0.2 µg·L^{-1}), and from 1 to 200 µg·L^{-1} for musk fragrances. Better linearity was obtained for methylsiloxanes (R^2 values higher than 0.9984) *versus* musk fragrances (R^2values higher from 0.9916). LODs and LOQs in all cases were calculated as 3 and 10 times, respectively, the standard deviation value obtained when analyzing an aqueous standard prepared at a low concentration level. Calculated LODs and LOQs were then experimentally verified by preparation of aqueous standards at those calculated LOD and LOQ levels. Thus, LOQs ranged from 0.1 µg·L^{-1} for L3 and L4, to 3.5 µg·L^{-1} for HHCB.

For comparative purposes, several quality analytical parameters of the HS-SPME-GC-MS method were also obtained for the commercial PDMS/DVB fiber, and are included in Table IV.32. It can be observed how calibration ranges were much narrower with this fiber: from 0.02 to 2 µg·L^{-1}for lineal methylsiloxanes; from 0.1 to 10 µg·L^{-1} for cyclic methylsiloxanes, and from 0.5 to 20 µg·L^{-1} for all musk fragrances. It should be noted the high extraction capability of the CIM-80(Al)-based fiber *versus* the commercial PDMS/DVB, particularly if attending to the calibration ranges with regards to the volume of the coating fiber (0.074 µm^3 for the CIM-80(Al) fiber, and 0.375 µm^3 for PDMS/DVB). In contrast with the CIM-80(Al) fiber, the R^2 values were slightly better for musk fragrances (>0.999) than methylsiloxanes (>0.996) when using the commercial fiber, with a similar trend for the LOQs values for musk fragrances: from 0.1 µg·L^{-1} for AHMI to 0.4 µg·L^{-1} for M-MK and AHTN. On the other hand, similar LOQs values were obtained with the commercial fiber when compared with CIM-80(Al) for methylsiloxanes, with values ranging from 0.05 µg·L^{-1} for L3 and L4, to 0.6 µg·L^{-1} for D5 and D6.

Table IV.31. Several quality analytical parameters of the entire HS-SPME-GC-MS method for the CIM-80(Al) fiber.

PCP	Calibration range ($\mu g{\cdot}L^{-1}$)	(Slope ± SD[a]) $\times 10^{-3}$	$S_{y/x}$[b] $\times 10^{-3}$	R^2[c]	LOD[d] ($\mu g{\cdot}L^{-1}$)	LOQ[d] ($\mu g{\cdot}L^{-1}$)
L3	0.2 – 20	101 ± 2	29	0.9987	0.03	0.1
D4	0.2 – 20	206 ± 3	67	0.9984	0.2	0.7
L4	0.02 – 20	240 ± 3	56	0.9986	0.03	0.1
D5	0.02 – 20	326 ± 4	78	0.9990	0.1	0.2
L5	0.02 – 20	1268 ± 8	59	0.9998	0.1	0.4
D6	0.02 – 20	1524 ± 8	62	0.9998	0.2	0.5
DPMI	1 – 200	1.4 ± 0.1	4.5	0.9983	0.5	1.7
ADBI	1 – 200	16.1 ± 0.4	76	0.9962	0.4	1.2
AHMI	1 – 200	17.3 ± 0.2	53	0.9984	0.7	2.2
M-MK	1 – 200	11.5 ± 0.4	76	0.9926	0.4	1.4
HHCB	1 – 200	6.0 ± 0.1	25	0.9971	1.1	3.5
AHTN	1 – 200	9.7 ± 0.3	68	0.9916	0.6	2.0
MK	1 – 200	0.3 ± 0.1	1.4	0.9962	0.7	2.4

[a] Standard deviation associated to the slope

[b] Standard deviation of the residuals

[c] Determination coefficient

[d] Limit of detection and limit of quantification calculated as described in the text

Table IV.32. Several quality analytical parameters of the entire HS-SPME-GC-MS method for the commercial PDMS/DVB fiber.

PCP	Calibration range (μg·L^{-1})	(Slope ± SD^{a}) ×10^{-3}	$S_{y/x}$^{b} ×10^{-3}	R$^{2\ c}$	LOD^{d} (μg·L^{-1})	LOQ^{d} (μg·L^{-1})
L3	0.02 – 2	188 ± 5	9	0.9972	0.02	0.05
D4	0.1 – 10	804 ± 9	74	0.9995	0.2	0.5
L4	0.02 – 2	883 ± 7	13	0.9997	0.02	0.05
D5	0.1 – 10	199 ± 6	50	0.9963	0.2	0.6
L5	0.02 – 2	1457 ± 19	34	0.9993	0.02	0.06
D6	0.1 – 10	212 ± 5	41	0.9978	0.2	0.6
DPMI	0.5 – 20	582 ± 5	94	0.9996	0.09	0.3
ADBI	0.5 – 20	1222 ± 4	81	0.9999	0.06	0.2
AHMI	0.5 – 20	1190 ± 14	264	0.9992	0.03	0.1
M-MK	0.5 – 20	500 ± 7	142	0.9987	0.1	0.4
HHCB	0.5 – 20	607 ± 7	125	0.9993	0.06	0.2
AHTN	0.5 – 20	457 ± 6	111	0.9990	0.1	0.4
MK	0.5 – 20	20 ± 1	4	0.9995	0.6	0.2

[a] Standard deviation associated to the slope
[b] Standard deviation of the residuals
[c] Determination coefficient
[d] Limit of detection and limit of quantification calculated as described in the text

For both fibers, the precision of the method was evaluated at two different concentration levels. The obtained results are included in Table IV.33. and Table IV.34. Regarding the CIM-80(Al) fiber, the intra- e inter-day RSD values at the low concentration level tested were lower than 19% for M-MK and 19% for ADBI, respectively; while for the same concentration level and the commercial PDMS/DVB fiber the intra-day RSD values were lower than 16% for L3 and the inter-day RSD values were lower than 26% for D6. It can be highlighted the worst precision obtained for the commercial PDMS/DVB fiber. The average inter-day RSD value for the CIM-80(Al) fiber was 14% at the low concentration level and 8% at the intermediate concentration level. For the

PDMS/DVB fiber the average RSD values was 18 and 15% for the low and the intermediate concentration level, respectively.

Regarding RR values for the CIM-80(Al) fiber, the average RR value obtained at the low concentration level was 97.3%, being 103% for the intermediate concentration level. For the PDMS/DVB fiber, the averages RR values were slightly lower: 94.5 and 92.1% for the low and intermediate concentration level. Thus, once again and in terms of relative recoveries, it is demonstrated the good analytical performance of the CIM-80(Al) fiber for the group of PCPs selected.

Table IV.33. Precision study of the HS-SPME-GC-MS method for the CIM-80(Al) fiber.

PCP	Low concentration level			Intermediate concentration level		
	Conc. level ($\mu g \cdot L^{-1}$)	RSD[a] (%) intra-day / inter-day	RR[b] (%)	Conc. level ($\mu g \cdot L^{-1}$)	RSD[a] (%) intra-day / inter-day	RR[b] (%)
L3	1	6.0 / 4.1	106	5	3.0 / 6.8	82.0
D4	1	15 / 17	93.9	5	6.1 / 9.2	110
L4	1	18 / 13	88.1	5	4.2 / 7.6	108
D5	1	13 / 9.5	108	5	2.7 / 7.5	96.5
L5	1	4.9 / 7.6	90.7	5	7.2 / 4.1	101
D6	1	8.3 / 12	94.3	5	6.3 / 3.5	97.7
DPMI	10	6.0 / 17	89.7	50	5.1 / 8.3	101
ADBI	10	11 / 19	99.0	50	4.3 / 8.4	100
AHMI	10	15 / 19	81.6	50	14 / 9.4	96.1
M-MK	10	19 / 19	101	50	3.0 / 4.9	109
HHCB	10	12 / 17	104	50	20 / 15	118
AHTN	10	10 / 14	97.1	50	6.7 / 12	113
MK	10	9.1 / 12	112	50	3.3 / 12	103

[a] Relative standard deviation: intra-day (n = 4) and inter-day (n = 12, in three different non-consecutive days)

[b] Relative recovery (n = 4)

Table IV.34. Precision study of the HS-SPME-GC-MS method for the commercial PDMS/DVB fiber.

PCP	Low concentration level			Intermediate concentration level		
	Conc. level ($\mu g \cdot L^{-1}$)	RSD[a] (%) intra-day / inter-day	RR[b] (%)	Conc. level ($\mu g \cdot L^{-1}$)	RSD[a] (%) intra-day / inter-day	RR[b] (%)
L3	0.2	16 / 15	95.8	1	15 / 15	120
D4	1	9.2 / 12	137	5	15 / 16	98.0
L4	0.2	12 / 20	89.9	1	13 / 6.0	84.6
D5	1	10 / 16	110	5	14 / 22	92.2
L5	0.2	8.1 / 15	103	1	18 / 13	110
D6	1	6.0 / 26	145	5	10 / 20	151
DPMI	2	8.5 / 19	85.2	10	1.3 / 7.8	78.0
ADBI	2	9.3 / 22	93.0	10	1.7 / 13	77.2
AHMI	2	4.6 / 21	87.9	10	1.3 / 11	75.4
M-MK	2	5.7 / 19	78.9	10	1.3 / 18	73.4
HHCB	2	6.6 / 17	68.9	10	2.6 / 14	71.8
AHTN	2	7.1 / 20	71.9	10	2.2 / 17	74.6
MK	2	6.5 / 10	61.4	10	4.3 / 18	89.6

[a] Relative standard deviation: intra-day (n = 4) and inter-day (n = 12, in three different non-consecutive days)
[b] Relative recovery (n = 4)

6. Analysis of water samples with the optimum HS-SPME-GC-MS method

The validated method was applied to the analysis of wastewater and seawater samples. In both classes of samples, the ionic strength was adjusted accordingly, after previous measurement of the salinity with a conductimeter. Table IV.35. summarizes the obtained results after the analysis in triplicate of these samples by the HS-SPME-GC-MS method proposed.

PCPs were not detected in any of the seawater samples analyzed (coded as seawater 1, seawater 2, and seawater 3). To date, the presence of methyl-siloxanes in seawater has not been reported. Musk were not detected in seawaters, although it has been reported the presence of several musk (ADBI, HHCB, AHTN, and MK) in seawaters, at quite low levels: between 30 and 100 pg·L^{-1}, using a SPE-GC-MS(QqQ) method [29].

Several PCPs were detected but not quantified in the wastewater samples analyzed (coded as wastewater 1, wastewater 2, and wastewater 3), specifically L5 in wastewater 1, MK in wastewater 2, and L4 in wastewater 3). Methylsiloxanes were not detected in wastewater 3, but D4 was quantified in wastewater 1 and wastewater 2 at 0.8 ± 0.2 and 1.5 ± 0.9 µg·L^{-1}, respectively. It was also possible to quantify other PCPs in wastewater 1: DPMI (37± 5 µg·L^{-1}), HHCB (152.3 ± 0.5 µg·L^{-1}), AHTN (14.6 ± 0.5 µg·L^{-1}), and MK (25 ± 3 µg·L^{-1}); and in wastewater 2: DPMI (3.6 ± 0.4 µg·L^{-1}) and HHCB (28 ± 3 µg·L^{-1}). Figure IV.55. shows a representative chromatogram of the analysis of wastewater 2 subjected to the optimum HS-SPME-GC-MS method, using the CIM-80(Al) fiber.

Table IV.35. Concentration levels found for PCPs in wastewater and seawater samples analyzed in triplicate with the optimized HS-SPME-GC-MS method and the CIM-80(Al) fiber.

PCP	**Level found ± SD (µg·L^{-1}) in wastewater**			**Level found ± SD (µg·L^{-1}) in seawater**		
	Wastewater 1	**Wastewater 2**	**Wastewater 3**	**Seawater 1**	**Seawater 2**	**Seawater 3**
L3	n.d.	n.d.	n.d.	n.d.	n.d.	n.d.
D4	0.8 ± 0.2	1.5 ± 0.9	n.d.	n.d.	n.d.	n.d.
L4	n.d.	n.d.	N.Q.	n.d.	n.d.	n.d.
D5	n.d.	n.d.	n.d.	n.d.	n.d.	n.d.
L5	N.Q.	n.d.	n.d.	n.d.	n.d.	n.d.
D6	n.d.	n.d.	n.d.	n.d.	n.d.	n.d.
DPMI	37 ± 5	n.d.	3.6 ± 0.4	n.d.	n.d.	n.d.
ADBI	n.d.	n.d.	n.d.	n.d.	n.d.	n.d.
AHMI	n.d.	n.d.	n.d.	n.d.	n.d.	n.d.
M-MK	n.d.	n.d.	n.d.	n.d.	n.d.	n.d.
HHCB	152.3 ± 0.5	n.d.	28 ± 3	n.d.	n.d.	n.d.
AHTN	14.6 ± 0.5	n.d.	n.d.	n.d.	n.d.	n.d.
MK	25 ± 3	N.Q.	n.d.	n.d.	n.d.	n.d.

n.d. = non-detected
N.Q. = non-quantified

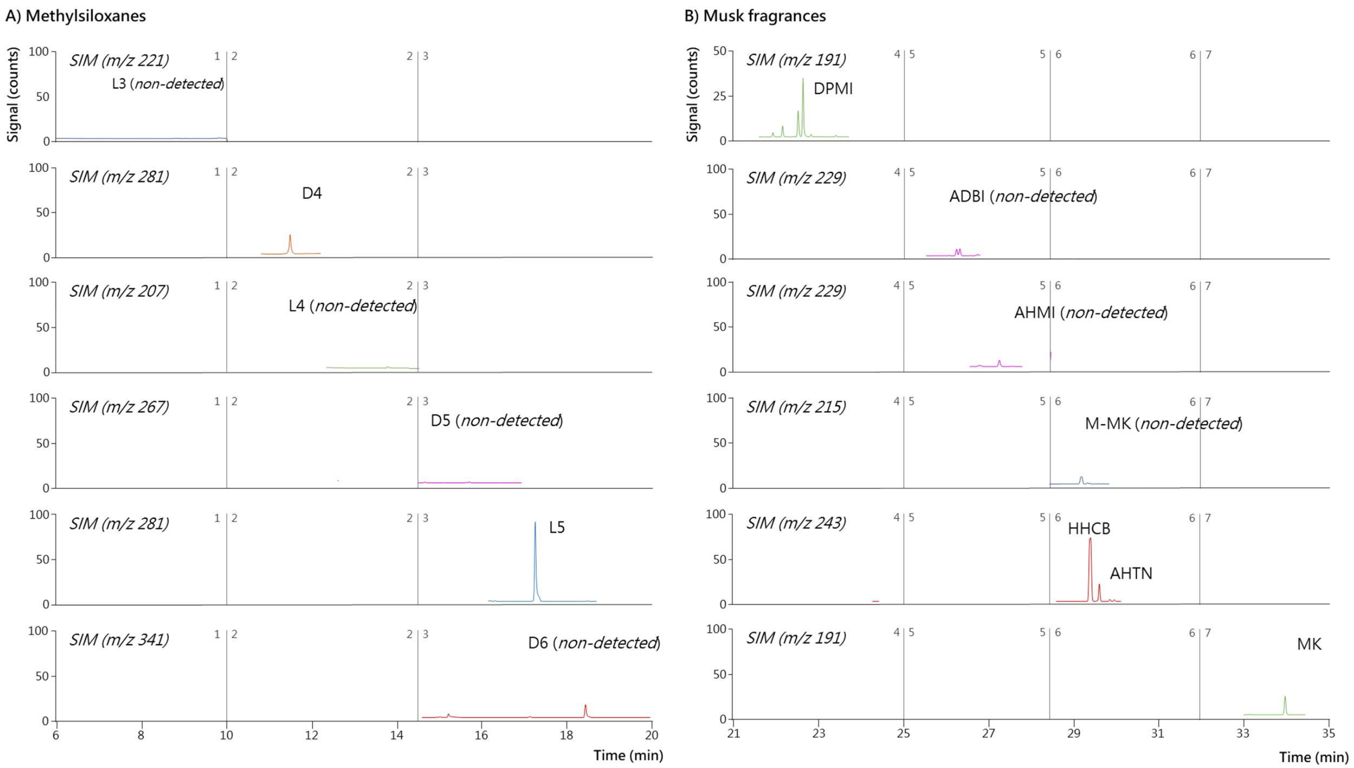

Figure IV.55. Representative SIM chromatogram (with the segments marked by a gray vertical line) of the analysis of the sample Wastewater 2 subjected to the optimum HS-SPME-GC-MS method with the CIM-80(Al) fiber.

7. Matrix effect evaluation

In order to evaluate the matrix effects, two types of the analyzed samples were chosen, each one representing one type of sample (wastewater 2 as wastewater and seawater 3 as seawater), and matrix-matched calibrations were carried out. In the case of wastewater 2, the peak areas of the analytes detected (D4 and MK) were subtracted.

Initially, the matrix-matched calibration was carried out using the same calibration range as that utilized with aqueous standards (see Table IV.31.). However, the linearity was compromised using that range for the group of musk fragrances. Thus, the quality analytical parameters were obtained using 6 calibration levels in all cases and the following calibration ranges for wastewater 2 and seawater 3: from 0.5 to 20 $\mu g \cdot L^{-1}$ for methylsiloxanes; and from 5 to 100 $\mu g \cdot L^{-1}$ for musk fragrances; except for methylsiloxanes, which ranged from 0.5 to 15 $\mu g \cdot L^{-1}$ in the seawater 3. Table IV.36. summarizes several quality analytical parameters of these calibrations. Adequate linearity was obtained being the R^2 values higher than 0.992. The intra-day precision and recovery studies in the spiked samples, as RSD (%, for n = 4) and RR (%, for n = 4) values, respectively, were evaluated using an intermediate spiked level: 5 $\mu g \cdot L^{-1}$ for methylsiloxanes and 50 $\mu g \cdot L^{-1}$ for musk fragrances (as shown in Table IV.36.). Regarding the precision study, RSD values were lower than 19% for HHCB in wastewater 2, and lower than 9.2% for L4 in seawater 3. RR values ranged between 80% for L4 and 120% for D4 for the wastewater sample, and from 76.6% for M-MK to 126% for L4 for the seawater sample.

Table IV.36. Calibrations in wastewater and seawater samples (as matrix solvents) by the optimized HS-SPME-GC-MS method using the CIM-80(Al) fiber, together with a recovery study with an intermediate concentration level.

PCP	Wastewater 2				Seawater 3			
	(Slope ± SD^a)×10^{-3}	$R^{2\,b}$	RSD^c (%)	RR^d (%)	(Slope ± SD^a)×10^{-3}	$R^{2\,b}$	RSD^c (%)	RR^d (%)
L3	0.82 ± 0.04	0.992	7.3	83.1	1.7 ± 0.1	0.994	1.3	102
D4	7.7 ± 0.1	0.999	6.2	120	19.7 ± 0.7	0.996	4.6	98.7
L4	2.3 ± 0.1	0.997	8.0	80.0	3.1 ± 0.1	0.994	9.2	126
D5	5.5 ± 0.2	0.992	7.7	88.8	8.6 ± 0.3	0.994	4.7	99.2
L5	2.6 ± 0.1	0.998	7.4	105	6.7 ± 0.3	0.992	7.2	114
D6	4.8 ± 0.1	0.999	6.7	92.2	12.2 ± 0.5	0.992	2.3	94.4
DPMI	3.7 ± 0.1	0.999	14	86.6	5.2 ± 0.1	0.999	8.0	78.8
ADBI	33.5 ± 0.9	0.998	17	83.8	107 ± 4	0.996	1.5	95.8
AHMI	35 ± 1	0.995	12	96.5	118 ± 4	0.996	1.5	95.3
M-MK	24 ± 1	0.995	16	108	68 ± 2	0.997	6.0	76.6
HHCB	18.4 ± 0.8	0.994	19	99.3	53 ± 1	0.999	7.4	97.4
AHTN	18.2 ± 0.9	0.992	15	99.5	53 ± 1	0.999	4.6	90.1
MK	3.9 ± 0.1	0.998	17	110	8.9 ± 0.3	0.996	2.2	97.8

[a] Standard deviation associate to the slope

[b] Determination coefficient

[c] Intra-day relative standard deviation (n = 4) at a concentration level of 5 μg·L^{-1} for methylsiloxanes and 50 μg·L^{-1} for musk fragrances

[b] Relative recovery (n = 4) at a concentration level of 5 μg·L^{-1} for methylsiloxanes and 50 μg·L^{-1} for musk fragrances

Table IV.37. includes the statistical study regarding matrix-effects, by comparison of the slopes of HS-SPME-GC-MS method using the CIM-80(Al) fiber and performed in ultrapure water. For methylsiloxanes and in both samples studied (seawater and wastewater), the *F*-test showed that the variances of aqueous calibrations *versus* calibrations in the samples were statistically different. Therefore, it is not possible to apply the Student's *t*-test and the calibrations slopes cannot be compared by statistical terms [30]. Thus, it can be concluded that there is a quite obvious matrix effect, but it cannot be statistically proved using this method.

Regarding musk fragrances and both type of samples, the *F*-test shows that the variances of aqueous calibrations *versus* calibrations in the samples are not statistically different. Attending to data included in Table IV.37., covering all results from the Student's *t*-test, it is possible to conclude statistically that there is not any matrix effect in any of the samples considered (in all cases, $t_{exp}<t_{critical}$) for musk fragrances.

In summary, the matrix-matched calibration was not a proper approach for the determination of siloxanes in water samples by the proposed HS-SPME-GC-MS method using the CIM-80(Al) fiber. Therefore, it is recommended the use of the standard addition calibration method for both group of PCPs considered.

Table IV.37. Statistical comparison of the slopes of HS-SPME-GC-MS method using the CIM-80(Al) fiber performed in ultrapure water and in samples (wastewater and seawater as matrix solvents in the calibrations) to evaluate the matrix effect, according to Andrade *et al.* [30].

PCP	Wastewater sample					Seawater sample				
	F-test[a]		Student′s *t*-test[d]			*F*-test[a]		Student′s *t*-test[d]		
	F_{exp}[b]	Result[c]	S^2_{pool}[e]	t_{cal}[f]	Result[g]	F_{exp}[b]	Result[c]	S^2_{pool}[e]	t_{cal}[f]	Result[g]
L3	197.8	$F_{exp} > F_{crit}$	-	-	-	0.5	$F_{exp} > F_{crit}$	-	-	-
D4	777.7	$F_{exp} > F_{crit}$	-	-	-	32.8	$F_{exp} > F_{crit}$	-	-	-
L4	124.7	$F_{exp} > F_{crit}$	-	-	-	1.0	$F_{exp} > F_{crit}$	-	-	-
D5	149.4	$F_{exp} > F_{crit}$	-	-	-	15.3	$F_{exp} > F_{crit}$	-	-	-
L5	1029.8	$F_{exp} > F_{crit}$	-	-	-	7.2	$F_{exp} > F_{crit}$	-	-	-
D6	613.8	$F_{exp} > F_{crit}$	-	-	-	10.3	$F_{exp} > F_{crit}$	-	-	-
DPMI	0.5	$F_{exp} < F_{crit}$	0.3	0.43	$t_{cal} < t_{crit}$	0.3	$F_{exp} < F_{crit}$	0.3	0.65	$t_{cal} < t_{crit}$
ADBI	1.0	$F_{exp} < F_{crit}$	56.5	0.23	$t_{cal} < t_{crit}$	1106.3	$F_{exp} < F_{crit}$	1106.3	0.27	$t_{cal} < t_{crit}$
AHMI	0.2	$F_{exp} < F_{crit}$	69.8	0.21	$t_{cal} < t_{crit}$	1308.4	$F_{exp} < F_{crit}$	1308.4	0.28	$t_{cal} < t_{crit}$
M-MK	0.8	$F_{exp} < F_{crit}$	63.4	0.16	$t_{cal} < t_{crit}$	314.9	$F_{exp} < F_{crit}$	314.9	0.32	$t_{cal} < t_{crit}$
HHCB	0.1	$F_{exp} < F_{crit}$	23.4	0.26	$t_{cal} < t_{crit}$	87.1	$F_{exp} < F_{crit}$	87.1	0.51	$t_{cal} < t_{crit}$
AHTN	0.8	$F_{exp} < F_{crit}$	51.7	0.12	$t_{cal} < t_{crit}$	59.6	$F_{exp} < F_{crit}$	59.6	0.56	$t_{cal} < t_{crit}$
MK	0.0	$F_{exp} < F_{crit}$	0.2	0.74	$t_{cal} < t_{crit}$	6.2	$F_{exp} < F_{crit}$	6.2	0.35	$t_{cal} < t_{crit}$

[a] *F* statistical test to compare population variances.

[b] Experimental *F* value.

[c] Result of the *F*-test, considering a critical *F* value (F_{crit}) of 6.16 for all the PCPs in wastewater and seawater samples (n – 2 degrees of freedom for each calibration and a significance level of 5%, being n the number of calibration levels).

[d] Student's *t* statistical test for equal variances (null hypothesis of the *F*-test accepted).

[e] Variance of the model, estimated as an average of the statistically equal variances of the calibration in aqueous standard and the calibration in water samples.

[f] Calculated *t* value.

[g] Result of the Student's *t*-test, considering a critical *t* value (t_{crit}) of 2.23 for all the PCPs in both water samples ($n_1 + n_2 – 4$ degrees of freedom and a significance level of 5%, being n_1 the number of calibration levels using aqueous standards and n_2 the number of calibration levels in the spiked samples for the calibrations).

REFERENCES

[1] Q. Luo, X. Chen, Z. Wei, X. Xu, D. Wang, and Z. Wang. J. Chromatogr. A 1365 (2014) 45–53.

[2] P.H. Chen, S.D. Richardson, S.W. Krasner, G. Majetich, and G.L. Glish. Environ. Sci. Technol. 36 (2002) 3362–3371.

[3] S. Allard, J.W. Charrois, C.A. Joll, and A. Heitz. J. Chromatogr. A 1238 (2012) 15–21.

[4] P. Araujo and S. Janagap. J. Chromatogr. B 910 (2012) 14–21.

[5] S.L.C. Ferreira, W.N.L. dos Santos, C.M. Quintella, B.B. Neto, and J.M. Bosque-Sendra. Talanta 63 (2004) 1061–1067.

[6] D. Liew, K.L. Linge, C.A. Joll, A. Heitz, and J.W.A. Charrois. J. Chromatogr. A 1241 (2012) 117–122.

[7] I. Kristiana, A. Lethorn, C. Joll, and A. Heitz. Water Res. 59 (2014) 90–98.

[8] E.T. Urbansky. J. Environ. Monitor. 1 (1999) 471–476.

[9] H. Ma, Y. Li, H. Zhang, S.M. Shah, and J. Chen. J. Chromatogr. A 1358 (2014) 14–19.

[10] I. Kristiana, C. Joll, and A. Heitz. J. Chromatogr. A 1225 (2012) 45–54.

[11] R. Maia, M. Correia, I.M.B. Pereira, and V. Beleza. Microchem. J. 112 (2014) 164–171.

[12] J.A. McDonald, N.B. Harden, L.D. Nghiem, and S.J. Khan. Talanta 99 (2012) 146–154.

[13] W. Chu, N. Gao, D. Yin, S.W. Krasner, and M.R. Templeton. J. Chromatogr. A 1235 (2012) 178–181.

[14] E. Malliarou, C. Collins, N. Graham, and M.J. Nieuwenhuijsen. Water Res. 39 (2005) 2722–2730.

[15] Guidelines for Drinking-water Quality, Fourth Edition: Incorporating the First Addendum. World Health Organization (2017).

[16] United States Environmental Protection Agency. Quick reference guide: Stage 1 and 2 Disinfectants and Disinfection Byproducts Rules, https://www.epa.gov/ground-water-and-drinking-water/national-primary-drinking-water-regulations#Byproducts (last accessed: 27th January 2020).

[17] Real Decreto 140/2003 del 7 de febrero de 2003. Criterios sanitarios de la calidad del agua de consumo humano. BOE Nº 45 del 21 de febrero del 2003.

[18] C.V. Antoniou, E.E. Koukouraki, and E. Diamadopoulos. J. Chromatogr. A 1132 (2006) 310–314.

[19] I. Montesinos and M. Gallego. J. Chromatogr. A 1310 (2013) 113–120.

[20] D. Kim, G.L. Amy, and T. Karanfil. Water Res. 81 (2015) 343–355.

[21] Safe Drinking-water from Desalination, WHO/HSE/WSH/11.03. World Health Organization (2011).

[22] E.Y. Companioni-Damas, F.J. Santos, and M.T. Galceran. Talanta 89 (2012) 63–69.

[23] M. Ghidotti, D. Fabbri, and C. Torri. Talanta 195 (2019) 258–264.

[24] C. Rücker and K. Kümmerer. Chem. Rev. 115 (2015) 466–524.

[25] S.L.C. Ferreira, R.E. Bruns, H.S. Ferreira, G.D. Matos, J.M. David, G.C. Brandão, E.G.P. da Silva, L.A. Portugal, P.S. dos Reis, A.S. Souza, and W.N.L. dos Santos. Anal. Chim. Acta 597 (2007) 179–186.

[26] M.A. Bezerra, S.L.C. Ferreira, C.G. Novaes, A.M.P. dos Santos, G.S. Velasques, U.M.F.M. Cerqueira, and J.P.S. Alves. Talanta 194 (2019) 941–959.

[27] M. Bystrzanowska and M. Tobiszewski. Trac-Trends Anal. Chem. 116 (2019) 266–273.

[28] K. Cai, D. Hu, B. Lei, H. Zhao, W. Pan, and B. Song. Anal. Chim. Acta 882 (2015) 90–100.

[29] H. Zhang, S. Bayen, and B.C. Kelly. Sc. Tot. Env. 523 (2015) 219–232.

[30] J.M. Andrade and M.G. Estévez-Pérez. Anal. Chim. Acta 838 (2014) 1–12.

CHAPTER V

Conclusions

Several advanced microextraction methods have been successfully developed in this Doctoral Thesis to determine efficiently an important group of emerging contaminants (30 PCPs and 16 DBPs) in different environmental water samples, thus accomplishing the general purposes initially planned. Among the novel approaches, the liquid-based microextraction and the sorbent-based microextraction techniques, including MOFs as sorbents, were adequately used to improve the extraction efficiencies and the selectivity for the target emerging contaminants. All the developed methods achieved many Green Analytical Chemistry requirements, not only by decreasing the organic solvent consumption, sorbent amounts, residues generated, and analysis times, but also by incorporating novel sustainable MOFs. Furthermore, the optimized and validated methods are characterized for being simple, and some of them even automated.

The main conclusions derived from this Doctoral Thesis are stated below, separated in different sections as a function of the microextraction technique used in the analytical method and in some cases also attending to the materials employed in the microextraction method.

Liquid-phase microextraction applications

1. *A simplified vortex-assisted emulsification microextraction method for determining personal care products in environmental water samples by ultra-high-performance liquid chromatogr*aphy

- The separation of 10 PCPs (7 parabens, 2 UV-filters, and 1 disinfectant) was efficiently performed by UHPLC-UV detection in less than 12 min, achieving adequate precision for the retention times, with RSD values (in %) lower than 0.6% (n = 30).
- The chromatographic calibration curves exhibited excellent linearity with determination coefficient (R^2) higher than 0.997 and LOQ lower than 0.140 mg·L^{-1}. The method was validated with adequate RSD values at three different concentration levels, showing the high repeatability of the chromatographic method.

- The selection of a VAEME method as the extraction stage prior to UHPLC permitted to improve the green characteristics of the existing DLLME methods for emerging contaminants, without the use of organic solvents or surfactants to aid in the emulsification procedure.
- An exhaustive optimization of the entire VAEME procedure (including the study of the extractant solvent, its volume, ionic strength of the aqueous sample, and pH of the aqueous sample) permitted to achieve the following advantages for the optimized method: short analysis time (~10 min for the VAEME procedure and ~12 min for the UHPLC), simplicity in the optimization and development, environmental friendliness (only 200 μL of extractant solvent), and adequate analytical performance even at the low spiked level (3.75 $\mu g \cdot L^{-1}$): in terms of relative recoveries (average value of 112%), enrichment factors (between ~20 and ~100), intra- and inter-day precision (below 10% as RSD), and extraction efficiency (average value of 82.7%).
- The developed VAEME-UHPLC-UV method has been applied for the first time for the determination of PCPs from environmental waters of different nature and complexity, allowing LODs down to 0.79 $\mu g \cdot L^{-1}$.

Sorbent-based microextraction applications

Miniaturized solid-phase extraction applications

1. *Metal-organic frameworks designed for sorbent-based microextraction approaches*

- MOFs based on a pillared-layer structure – termed as CIM-81(Zn), CIM-82(Zn), CIM-83(Zn), CIM-91(Zn), and CIM-92(Zn) – were properly designed with two different ligands (modified or not with -NH_2 groups within a series), to attain a structure yielding larger pores, facilitating this way the diffusion of analytes through the material when these MOFs are used as sorbents in microextraction methods.

- HKUST-1(Cu), MIL-53(Al), and UiO-66(Zr) were the conventional MOFs selected, successfully prepared and characterized, and used to compare with the novel MOFs prepared in this Doctoral Thesis.
- The crystal structures of acetone@CIM-81, DMA@CIM-81, acetone@CIM-91, and DMA@CIM-91, were for the first time obtained with single crystal X-ray diffraction, and their structures were adequately and thoroughly described in this Doctoral Thesis.
- Crystal structure and pores (A-type and B-type) were quite different for CIM-81(Zn) and CIM-83(Zn) compared to CIM-82(Zn), despite presenting same metallic nodes and ligands, with differences only associated to the absence of functionalization or the presence of $-NH_2$ groups in one of the ligands.
- For the CIM-81(Zn) MOF, a thorough computational study using PPB as target analyte showed a preferential adsorption into A-type pores.

2. *Adsorption isotherm studies of CIM-81(Zn), CIM-82(Zn), and CIM-83(Zn)*

- Adsorption isotherm, kinetic, and release studies were successfully performed with the CIM-80s series using as target analyte PPB, as representative emerging contaminant. The maximum uptake obtained for CIM-81(Zn) was 68%, for CIM-82(Zn) was 5%, and for CIM-83 was 65%.
- The faster release was obtained with CIM-81(Zn). For CIM-82(Zn), there was no release, thus indicating that the low amount adsorbed was difficult to liberate. The release obtained for CIM-81(Zn) was also faster than for CIM-83(Zn), indeed CIM-81(Zn) released 75% of the PPB adsorbed after 60 min, whereas CIM-83(Zn) only released 50%. Furthermore, the total release was near 85% for CIM-81(Zn) after 24h, and around 70% for CIM-83(Zn). The release kinetic data were fitted through a non-linear regression with a pseudo-first order model giving a well match for the entire time studied, with R^2 values ranging from 0.96 to 0.98.
- The adsorption capacity of the CIM MOFs follows the trend: CIM-81(Zn) > CIM-83(Zn) > CIM-82(Zn).
- The Langmuir fittings for CIM-81(Zn) and CIM-82(Zn) gave better matchings than the Freundlich model, but this was not the case for CIM-83(Zn). The amino groups in

CIM-83(Zn) seemed to provide another binding point for the adsorbates, and the Freundlich model, which considers multiple adsorption sites, yielded a better result. The maximum adsorption capacity for CIM-81(Zn) from the Langmuir model (350 mg·g^{-1}) was larger than that observed experimentally (280 mg·g^{-1}), as it occurred with CIM-82(Zn). Furthermore, the B parameter in the Langmuir model was larger for CIM-83(Zn), indicating that the amino groups are playing an important role in the adsorption.

3. *Application of a pillared-layer Zn-triazolate metal-organic framework in the dispersive miniaturized solid-phase extraction of personal care products from wastewater samples*

- The as-synthetized and characterized CIM-81(Zn) was tested for the first time as sorbent in a D-µSPE method for a group of 9 PCPs (4 parabens, 4 UV-filters, and 1 disinfectant) in complex wastewaters, demonstrating better analytical performance features than other MOFs already used with success, such as HKUST-1(Cu), MIL-53(Al), and UiO-66(Zr), and also performing better than remaining CIM-80s and CIM-90s, in agreement with the structural and adsorption/release studies.
- The D-µSPE method with CIM-81(Zn) as sorbent, in combination with UHPLC-UV, was adequately optimized, by using firstly a screening and afterwards a Doehlert design. The optimized microextraction method included a number of environmental-friendly characteristics, such as: low amounts of MOF (10 mg), low sample volumes (10 mL), short sample preparation times (8 min for extraction and desorption, and 10 min for the solvent exchange step), and minimization of the organic solvent consumption (1.2 mL of methanol in D-µSPE and ~4 mL of acetonitrile in the chromatographic run). The developed method was sensitive, with limits of detection down to 1.5 ng·mL^{-1}, while fulfilling adequate analytical performance in terms of relative recovery, enrichment factor and intermediate precision, while dealing with complex samples such as wastewaters.
- The promising results achieved with this pillared-layer MOF opened a new line to tailor MOFs in microextraction strategies, particularly considering the simplicity of functionalization of organic ligands in this type of crystalline compounds.

4. *Dispersive miniaturized solid-phase extraction using the CIM-81(Zn) metal-organic framework and gas chromatography–mass spectrometry to determine personal care products in waters*

- The optimum GC-MS separation of the selected 8 PCPs (6 UV-filters, 1 disinfectant, and 1 insect repellent) took less than 14 minutes, with adequate precision for the retention times as RSD (in %), with values lower than 0.07% (n = 40).
- The chromatographic calibration curves exhibited excellent linearity with determination coefficient (R^2) higher than 0.995 and LOQ lower than 4.6 $\mu g \cdot L^{-1}$. The method was validated with adequate RSD values at two different concentration levels, showing the high repeatability of the chromatographic method.
- A D-µSPE method using the CIM-81(Zn) MOF was conveniently optimized in combination with GC-MS for the determination of semi-volatile PCPs.
- The resulting method characterizes for being fast (overall ~8 min for the entire extraction-desorption step), for requiring low amounts of sorbent (10 mg of CIM-81(Zn)), for its low requirements of sample volume (10 mL of water) and low desorption solvent volumes (1.2 mL of methanol), for ensuring simple compatibility with GC (solvent-exchange step reconstituting with 100 µL of cyclohexane:ethyl acetate, 9:1 ratio), while getting adequate precision (<13% as inter-day RSD) and proper sensitivity (LODs down to 0.01 $\mu g \cdot L^{-1}$).
- The reported method ensures a simple adaptation of the D-µSPE approach, previously developed for LC, to GC.
- It is reported for the first time the determination of semi-volatile PCPs with GC-MS using D-µSPE with MOFs.
- The promising CIM-81(Zn) MOF has been successfully used in a dispersive miniaturized solid-phase extraction method combined with GC-MS to determine this group of PCPs in different waters samples (one tap water and two bottled waters), pointing out an almost negligible matrix effect.

Solid-phase microextraction applications

1. *Monitoring trihalomethanes and nitrogenous disinfection by-products in blending desalinated waters using solid-phase microextraction and gas chromatography*

- A HS-SPME-GC-FID method has been adequately optimized for the complete separation of 16 DBPs (4 THMs, 6 HANs, and 6 HNMs) in 9 minutes. The chromatographic retention times together with their reproducibility values under the optimized chromatographic conditions showed the high repeatability of the chromatographic method. The chromatographic separation was achieved in 9 min, and the precision of the retention times, in terms of RSD (in %), was lower than 0.22% (n = 32).
- After the selection of the fiber coating nature, an optimization of the HS-SPME method (to be combined with GC-FID) was adequately carried out by using firstly a screening and afterwards a Doehlert design. A compromising situation was taken to select the optimum values of each variable: 60 minutes for the extraction time, 30% (w/v) of NaCl content for the ionic strength, and 30 ºC for the extraction temperature; thus, pointing out for milder conditions in agreement with Green Analytical Chemistry requirements.
- The optimized HS-SPME-GC-FID method was conveniently validated to analyze blending desalinated waters, which may have higher contents of brominated and iodine-based DBPs (with consequent health issues). Blended waters are important in the Canary Islands because desalinated waters are commonly blended with conventionally treated single or multiple fresh waters drawn from other sources to meet the demands of drinking water and to increase the concentration of some desired ions.
- The method is simple and automated, organic solvent-free, and it presents good linearity (R^2 values above 0.991), adequate precision (inter-day RSD values lower than 9.7% at the low spiked level), and good sensitivity (LOQ down to 3.03 $\mu g \cdot L^{-1}$), particularly if it is considered that FID (cheap and widely available in laboratories worldwide) and not MS has been utilized as detection system.
- Adequate average relative recoveries (~98.2%) were obtained for spiked blending desalinated water samples, demonstrating the successful applicability of the method for

the determination of THMs, HANs, and HNMs in real samples at concentration values lower than the guideline values.

2. *Solid-phase microextraction based on the metal-organic framework CIM-80(Al) to determine volatile methylsiloxanes and musk fragrances in aqueous samples using gas chromatography*

- A total of 13 PCPs (6 methylsiloxanes, and 7 musk fragrances) were conveniently studied with GC-FID. The optimum GC-FID chromatographic conditions allowed the complete separation of the analytes in 45 min with RSD (in %) values lower than 0.23% (n = 30) for the retention times.
- The analytical performance of different commercial SPME fibers was evaluated under the same experimental conditions for the HS-SPME-GC-FID method. The best results were obtained for the novel CIM-80(Al)-based fiber.
- The optimization of the HS-SPME-GC-FID method was successfully carried out using an experimental design, specifically a Box-Behnken design, which indicated the following optimum conditions: 20% (w/v) of NaCl content, 40 minutes of extraction time, 10 minutes of desorption time, and 55 ºC of extraction temperature; thus pointing out milder conditions.
- The validation of the entire method was carried out, with the resulting approach characterized for being simple, organic solvent-free, and for presenting good linearity (R^2 values above 0.992), precision (inter-day RSD values lower than 9.7% at the low spiked level), and sensitivity (LOQ down to 3.03 $\mu g \cdot L^{-1}$).
- The validated method was also successfully applied to the analysis of wastewater and seawater samples, with adequate analytical performance.

GLOSARY

μSPE	miniaturized sorbent-based microextraction
AAS	atomic absorption spectroscopy
ACN	acetonitrile
ANOVA	analysis of variance
BBD	Box-Behnken design
BET	Brunauer, Emmet and Teller
CAR/PDMS	carbonxen/polydimethylsiloxane
CCD	Central Composite Design
CCDC	Cambridge Crystallographic Data Centre
CHN	cyclohexane
CNTs	carbon nanotubes
CTAB	cetyltrimethyl ammonium bromide
CW-PEG	carbowax-polyethylene glycol
D-μSPE	dispersive miniaturized solid-phase extraction
DBPs	disinfection by-products
DFT	Density Functional Theory
DI	direct immersion
DLLME	dispersive liquid-liquid microextraction
DMA	N,N-dimethylacetamide
DMF	N,N-dimethylformamide
DVB/CAP/PDMS	divinylbenzene/carbonxen/polydimethylsiloxane
EA	ethyl acetate
ECD	electron capture detection
E_F	enrichment factor
E_R	extraction efficiency
EU	European Union
FID	flame ionization detection
GAC	Green Analytical Chemistry
GAPI	Green Analytical Procedure Index
GC	gas chromatography
GO	graphene oxide
HAAs	haloacetic acids
HANs	haloacetonitriles
HF-LPME	hollow-fiber liquid-phase microextraction
HNMs	halonitromethanes

HS	headspace
ILs	ionic liquids
IR	infrared
K_{OW}	octanol/water partition coefficient
LC	liquid chromatography
LLE	liquid-liquid extraction
LOD	detection limit
LOQ	quantification limit
LPME	liquid-phase microextraction
MAE	microwave-assisted extraction
M-D-µSPE	magnetic dispersive miniaturized solid-phase extraction
MIPs	molecularly-imprinted polymers
MNPs	magnetic nanoparticles
MOFs	metal-organic frameworks
MTBE	methyl-t-butyl ether
MWCNTs	multi-walled carbon nanotubes
NCI	non-covalent interactions
NEMI	National Environmental Methods Index
NOM	natural organic matter
NPs	nanoparticles
PA	polyacrylate
PCPs	personal care products
PDMS	polydimethylsiloxane
PDMS/DVB	polydimethylsiloxane/divinylbenzene
PILs	polymeric ionic liquids
PLE	pressurized-liquid extraction
PXRD	powder X-ray diffraction
R	correlation coefficient
R^2	determination coefficient
RR	relative recovery
RSD	relative standard deviation
RSM	response surface methodology
RTILs	room temperature ionic liquids
SBSE	stir-bar sorptive extraction
SBU	secondary building unit
SD	standard deviation
SDME	single drop microextraction

SDS	sodium dodecyl sulfate
SEM	scanning electron microscopy
SFE	supercritical-fluid extraction
SFOME	solidified floating organic drop microextraction
SPE	solid-phase extraction
SPME	solid-phase microextraction
SWCNTs	single-walled carbon nanotubes
$S_{y/x}$	standard deviation of the residuals
TDU	thermal desorption unit
TFME	thin-film microextraction
TGA	thermogravimetric analysis
THMs	trihalomethanes
t_R	retention times
UAE	ultrasound-assisted extraction
UHPLC	ultra-high performance liquid chromatography
US	United States
US-EPA	Environmental Protection Agency of United States
VAEME	vortex assisted emulsification microextraction
WHO	World Health Organization
WWTPs	wastewater treatment plants


N
Br
Br
O₂N
Br
Br
Br
Br
Cl
Cl
Cl
Cl
Cl
Cl